A model for Improvement of Water Heating Heat Exchanger Designs for Residential Heat Pump Water Heaters

A thesis presented in fulfillment of the requirement for the degree of
Master of Engineering at Massey University
Palmerston North, New Zealand

Weerawoot Arunwattana

B.Sc. in Applied Physics
M.Sc. in Thermal Technology
2010

ABSTRACT

Heat pump water heaters are a promising technology to reduce energy use and greenhouse gas emissions. A key component is the water heating heat exchanger. Two multi-zone models of the double-wall counter-current flow heat exchanger (condenser and gas cooler models) for residential air-source heat pump water heaters were developed. These models were validated against available data in the open literature. They predicted heat exchanger size within -0.8% for a HFC-134a (with oil) condenser and within -14% for a CO_2 gas cooler. The multi-zone model was significantly more accurate than one and three zone models. The models for a R410A subcritical heat pump and a CO_2 transcritical heat pump were used to investigate the effect of key design parameters by varying water or refrigerant flow channel size for three water heating heat exchanger configurations: circular tube-in-tube, flat tube-on-tube, and twisted tube-in-tube. For the circular tube-in-tube configuration, refrigerant flow in the annulus (case *B*) performed better than refrigerant flow in the inner tube. The optimal flow channels for the circular tube-in-tube configuration case *B* with 0.1 mm thick air gap in the double wall were found to be d_i (inside diameter of the 1st tube) of 8 mm and annulus [D_i (inside diameter of the 3rd tube) $-d_2$ (outside diameter of the 2nd tube)] of 1.5 mm for R410A and d_i of 7 mm and $D_i - d_2$ of 1.0 mm for R744. The optimal flow channels for the flat tube-on-tube configuration with b_{1i} (major length of the refrigerant flow channel) and b_{2i} (major length of the water flow channel) both of 9 mm were found to be a_{1i} (minor length of the refrigerant flow channel) and a_{2i} (minor length of the water flow channel) of 1.5 mm for R410A and a_{1i} of 1 mm and a_{2i} of 1.5 mm for R744. The optimal flow channels for the twisted tube-in-tube configuration were found to be d_i of 7.94 mm and d_1 (original inside diameter of twisted tube) of 12.7 mm for R410A and d_i of 6.35 mm and d_1 of 9.525 mm for R744. At the optimal flow channel size in each configuration, heat exchanger weight of the flat tube-on-tube was lower than the circular tube-in-tube by about 34.4% for R410A and by about 66.6% for R744. This was mainly due to elimination of the air gap resistance with the tube-on-tube configuration. Heat exchanger length, weight, and pumping power of the twisted tube-in-tube with 94% contact were significantly lower than the flat tube-on-tube by about 85%, 62%, and 97% respectively for R410A and by about 65%, 35.7%, and 98% respectively for R744. Overall, the flat tube-on-tube and the twisted tube-in-tube configurations are most promising for the water heating heat exchanger in terms of the lowest investment and running costs respectively.

ACKNOWLEDGMENT

Thanks in particular to my Supervisor Prof. Don Cleland and Dr. Jianfeng Wang (School of Engineering and Advanced Technology (SEAT) Massey University, NZ) for guiding the project.

Thanks to Ministry of Science and Technology, Thailand for supporting a scholarship.

Thanks to Prof. Eckhard A. Groll and Prof. Somchai Wongwises for helping on experimental data.

CONTENTS

LIST OF FIGURES

LIST OF TABLES

CHAPTER 1

INTRODUCTION

Worldwide energy use continues to increase despite limitations in fossil fuel based energy sources. Further, the use of energy generated by fossil fuels contributes to global warming and it is predicted to lead to significant climate change and a large impact to society. As a result, many countries have tried to decrease their energy use. Energy conservation is effective because it decreases total energy use and also it helps extent the life of non-renewable energy sources as well as reducing global warming impact.

Residential energy use is a significant fraction of the total nationwide energy use. More than 25% of total energy use goes on residential energy use in most countries. For instance, the residential energy use in New Zealand is about one-third of the total nationwide energy use (BRANZ, 2009).

The energy used in the hot water heating systems is a major part of the New Zealand's residential energy use (BRANZ, 2009). Mostly, the hot water heaters are either electric water heaters or the gas water heaters. Both types use a lot of energy when compared to alternative hot water systems because they are less than 100% energy efficient. Thus, if alternative systems that use smaller amounts of energy are used, instead of the conventional systems, the total energy use in the residential sector will decline.

Heat pump water heating system is one alternative system that is interesting because it uses about one third of the energy use for the same heating capacity (Ochsner, 2008). Heat pump water heaters can be used for all climates. In mild or hot climates, air-source heat pump water heaters are suitable. On the other hand, ground source heat pump water heaters are suitable for cold climates. In addition, water source heat pump water heaters are available for mild or hot climates; however, these systems are not convenient unless water sources are readily available.

Air-source heat pump water heaters are suitable for New Zealand due to its mild climate. These heaters are able to operate on either a subcritical cycle or transcritical cycle. Both cycles can work either on a one-pass heating system or a multi-pass heating system for domestic applications. The transcritical cycle is most suitable for one-pass heating systems while the subcritical cycle is most suitable for multi-pass heating systems.

Air-source heat pump water heaters are not yet successful on the market for New Zealand because their costs are still high. One contributing factor is that water heating heat exchangers have to prevent refrigerant or oil contaminating the hot water supply if it leaked. As a consequence, double wall heat exchangers are used resulting in larger heat transfer area of the heat exchanger and higher cost compared with single wall designs. In addition, water heating heat exchanger for air-source heat pump water heaters is a relatively new field application, so there is limited design and

manufacturing knowledge. Therefore, these water heating heat exchangers are a priority component to develop for domestic applications.

Any heat exchanger design is a trade off between heat transfer performance, pressure drop, and cost. Heat exchanger configuration is the most important factor affecting heat transfer performance and pressure drop of the system. Experimental investigation of alternative heat exchanger designs is very time consuming and expensive. Further, due to ozone depleting and global warming concerns, a range of refrigerants must be considered for heat pump systems. In such a situation, mathematical modelling is an alternative approach as it allows a wide range of alternative refrigerants and heat exchanger designs to be evaluated in a cost-effective manner.

In this research, models of water heating heat exchangers based on air-source heat pump water heaters will be developed in order to improve water heating heat exchanger designs for domestic applications in New Zealand.

CHAPTER 2

LITERATURE REVIEW

In this review domestic hot water heating requirements, energy uses, hot water supply systems, and types of hot water heaters will be discussed. Heat pump water heaters will be discussed in the terms of types of the system, standards for such systems, operating cycles, and refrigerants used. In addition, heat exchangers commonly used for heat exchange between the refrigerant and the water will be briefly discussed. Finally, available correlations or equations for predicting heat transfer coefficients and pressure drops during single-phase flow region, condensation phase flow region, and transcritical phase flow region of working fluids in tubes will be reviewed.

2.1 Hot Water Heating

2.1.1 Requirements for hot water

Hot water is widely used for many applications such as processes in industry, medical equipments, commercial buildings, hotels etc. Further, it is provided for household applications. The distribution of the household hot water consumption for some parts of the world is shown in the map (Fig. 2.1). It can be seen that the global hot water consumption for household applications is a significant fraction of the total global hot water consumption.

The amount of household hot water consumption is in accordance with the requirement of consumer. In New Zealand, the household hot water requirement is between 40 and 60 litres of hot water per day per people with the water temperature requirement of between 40^{o}C to 80^{o}C, depending on various applications (Williamson, 2001).

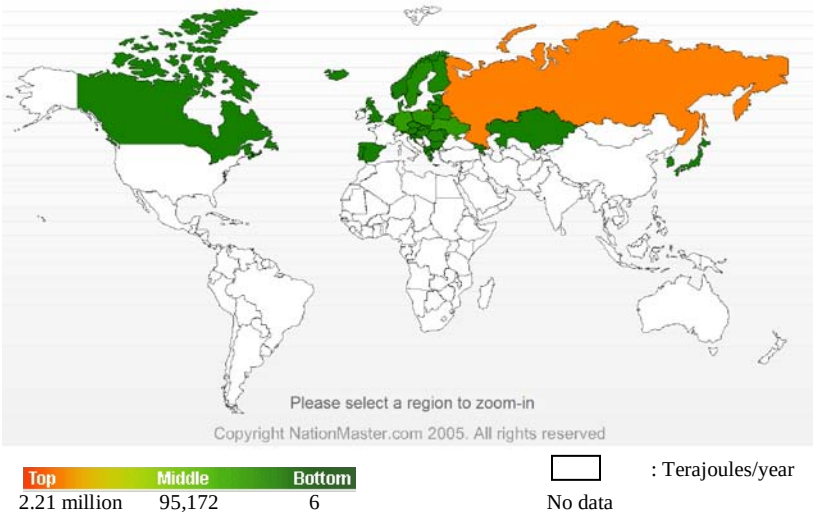

Figure 2.1: Map of hot water consumption by household by country (NationMaster, 2005): Terajoules/year

2.1.2 Energy consumption

The global primary energy consumption continues to increase as shown in Fig. 2.2. Mostly the primary energy sources come from fossil fuels. Increase of fossil fuel consumption is a major cause of global warming. The distribution of the global primary energy supply and carbon dioxide emissions are shown in Fig. 2.3 and 2.4 respectively. Greatest primary energy use is in North America and Asia including China causing large amount of carbon dioxide emissions. On the other hand, the amount of primary use of Latin America, Africa and Middle East are quite small. However, the overall primary energy supply and carbon dioxide emissions are still high.

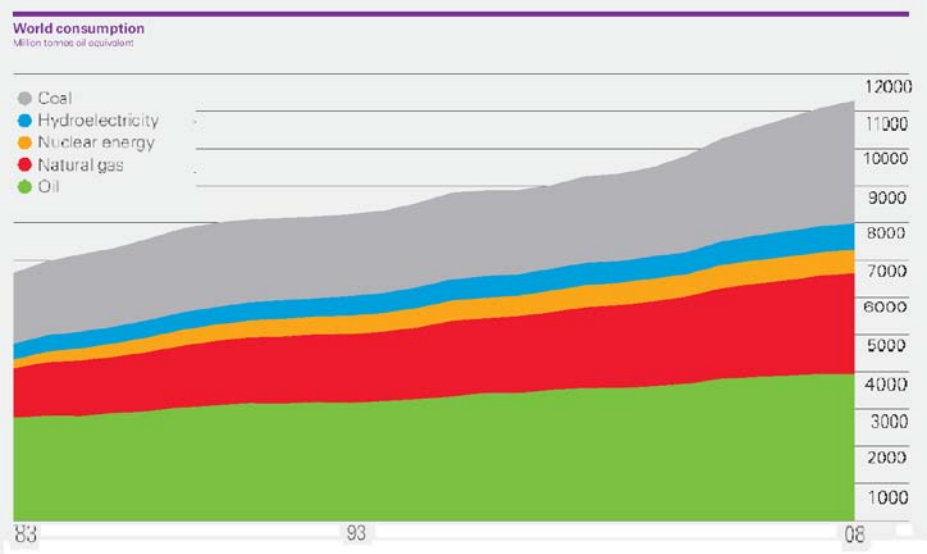

Figure 2.2: Global primary energy consumption (BP, 2009) : Million tonnes oil equivalent

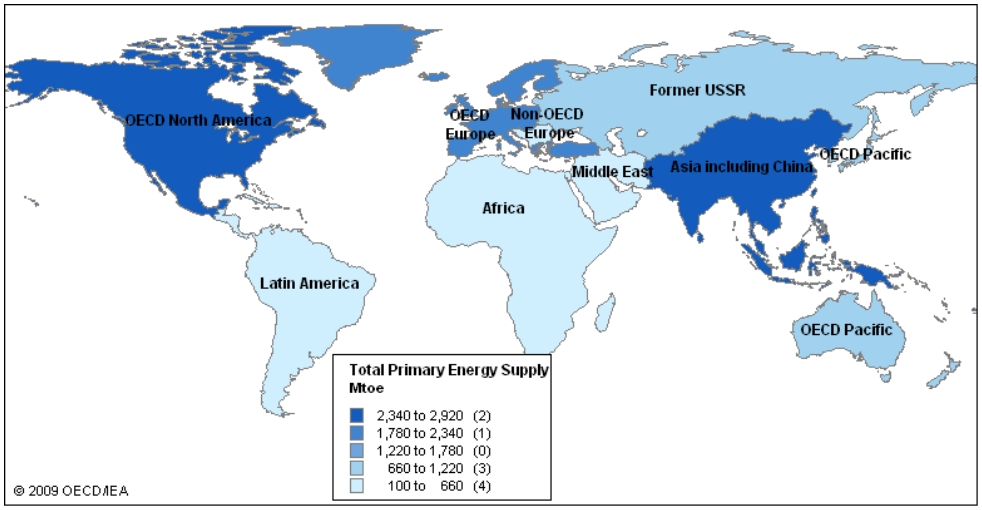

Figure 2.3: Map of global primary energy supply (IEA, 2009): Million tonnes oil equivalent

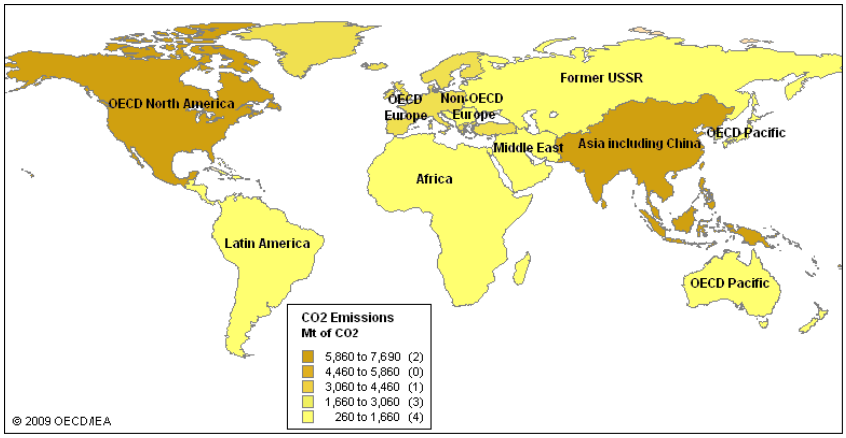

Figure 2.4: The map of the annual CO_2 emissions in 2006 (IEA, 2009): Million tonnes

The residential energy use is significantly relative to the primary energy. The carbon dioxide emission from the residential sector is a very significant fraction of the overall carbon dioxide emissions as shown in Fig. 2.5. In New Zealand, about 69% of the total household energy use by fuel type comes from the electricity (Fig. 2.7). Approximately 32% of nationwide electricity energy use is consumed by the residential sector (Fig. 2.6).

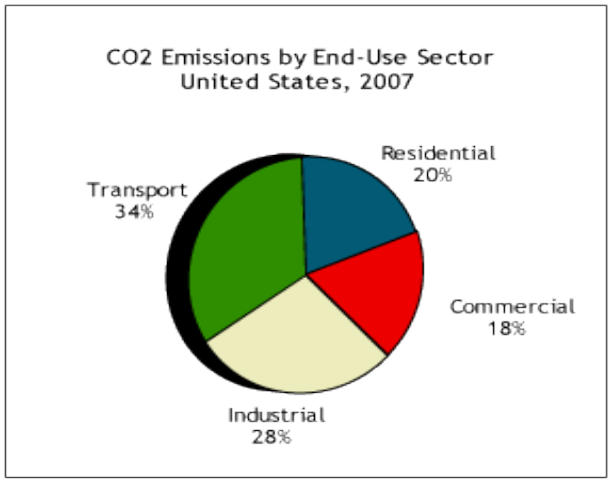

Figure 2.5: CO_2 emissions by sector (DOE, 2007)

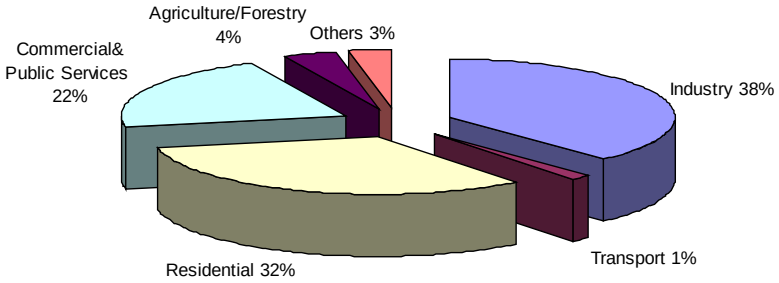

Figure 2.6: The electricity energy use in New Zealand in 2006 (IEA, 2009)

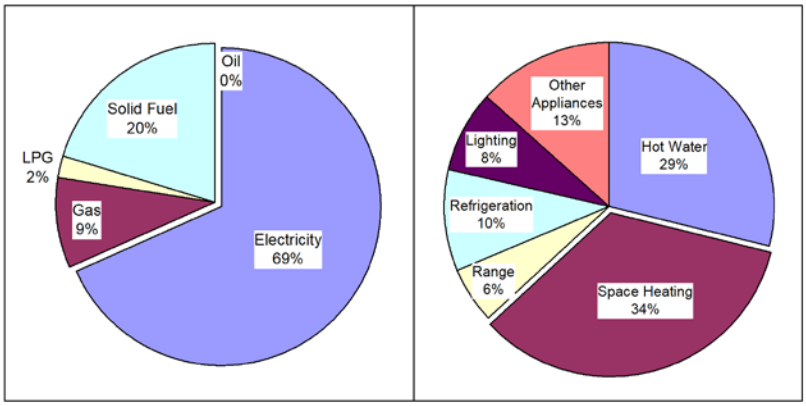

(a) Total energy use by fuel type (b) Total energy use by end-use

Figure 2.7: Energy use in New Zealand households (BRANZ, 2006)

The energy used for heating water is a major part of total energy use in the residential sector. In New Zealand, approximately 29% of an average household's energy end-use goes on water heating (Fig. 2.7) (BRANZ, 2006). About one-third of Australian household energy use is consumed by water heating systems (Kenway, 2008). In South Africa, the hot water production is the largest user of energy in the domestic sector (Meyer, 1997). Further, about 30.7% of household energy consumption in Japan is used for hot water supply (Taira, 2008).

2.1.3 Hot water supply systems

BRANZ (2006) provided an international comparison of the fraction of houses using electric hot water storage systems. New Zealand stood out as having the highest (77%) proportion of such systems.

Generally, hot water supply systems are classified into two main groups: instantaneous systems and storage systems. In instantaneous systems the cold water is heated by the water heater and the hot water produced is supplied directly to the user when required (Fig. 2.8). On the other hand, in a storage system the hot water produced by the heater flows into the hot water cylinder (HWC) in order to store it until delivery to the user (Fig. 2.8). If the temperature of hot water stored in the HWC does not meet the requirement, the hot water is heated in order to increase the temperature until needed.

The heating capacity of hot water heaters for instantaneous systems must be higher than for storage systems at the same water temperature required because they must produce the peak flow required whereas a storage system allows the water heating to occur over a longer period. Further comparison of some characteristics is presented in Table 2.1.

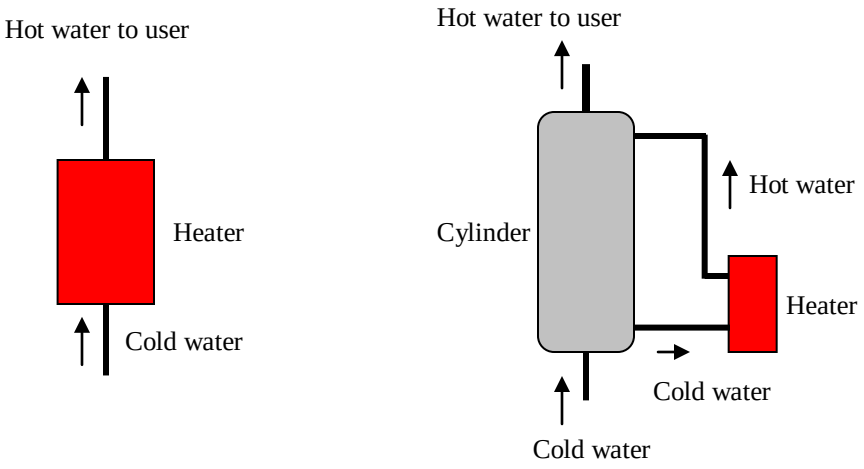

(a) instantaneous system **(b)** storage system

Figure 2.8: Diagram of hot water supply systems

Table 2.1: The comparison of some characteristics between instantaneous and storage systems

Items	Instantaneous system	Storage system
• ability to supply	continuous	limited
• space required in installation	small	large
• start-up delay	long	short
• heat source flexibility	limited	flexible

Energy can be lost in all parts of the hot water supply systems, which can be represented as a Sankey diagram as shown in Fig. 2.9.

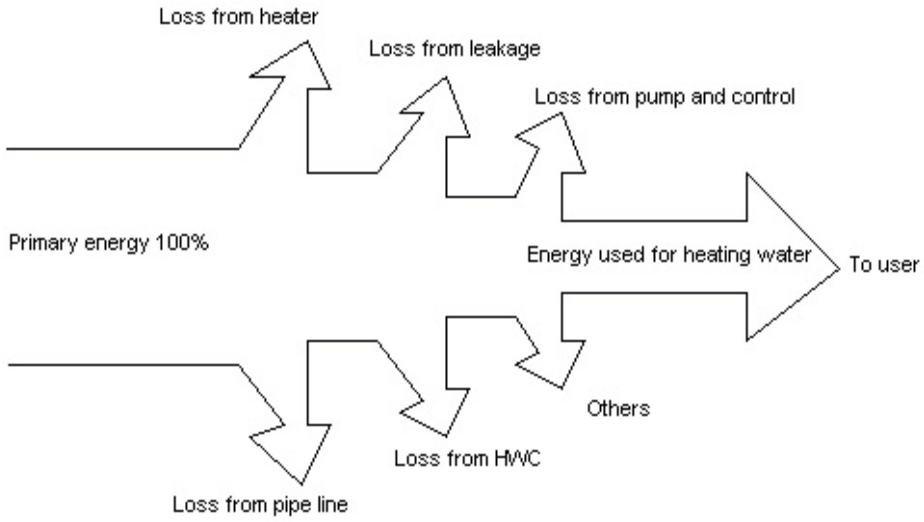

Figure 2.9: Sankey diagram for energy loss in hot water supply system including a hot water cylinder (HWC)

2.2 The Types of Domestic Hot Water Heaters

2.2.1 Conventional storage hot water heaters

At present, most hot water used in New Zealand household applications is produced by electrical hot water heaters. Basically, an electrical hot water heater composes of electrical resistances (elements) submerged inside the HWC, thermostats to control the hot water temperature, and inlet and outlet pipes for cold and hot water as shown in Fig. 2.10.

In addition, some consumers use gas water heaters. These heaters usually use natural gas or propane as a heat source. A gas water heater basically operates as same as the electric water heaters, but its heater is a gas burner, instead of the electrical resistance as presented in Fig. 2.11. The comparison for some characteristics between the electrical hot water heaters and gas hot water heaters is shown in Table 2.2.

Although electrical hot water heaters have almost no loss in the heat transfer from the resistance element to the water, there are standing losses incurred in maintaining the temperature of the stored water. By comparison modern domestic gas storage systems range between 70% and 80% efficient due to heat losses in the flue gas (Williamson & Clark, 2001).

Table 2.2: The comparison of some characteristics between the electrical and gas heaters

Items	Electrical heaters	Gas heaters
• installation & maintenance	easy	more difficult
• venting requirement	no	yes
• supply air	no	yes
• equipment life	acceptable	acceptable
• initial cost	cheap	more expensive
• running cost	expensive	cheaper

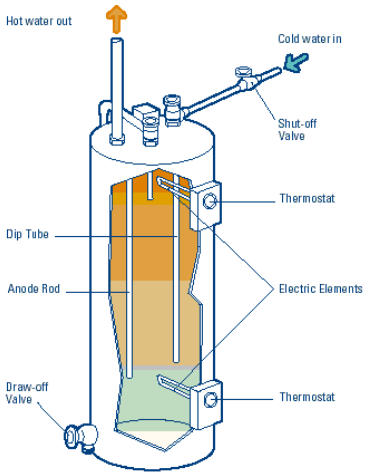

Figure 2.10: An electrical storage hot water heater; no insulation shown (NRC, 2009)

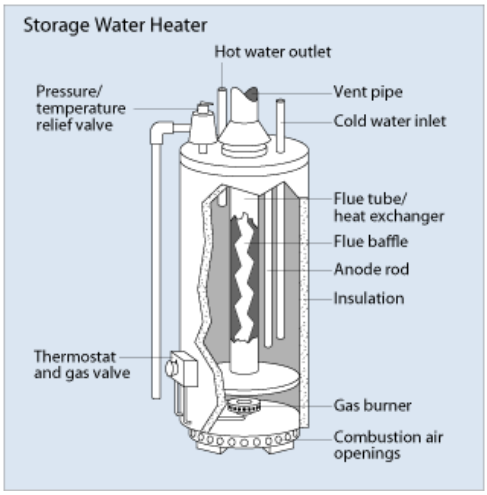

Figure 2.11: A gas storage hot water heater (DOE, 2009)

2.2.2 Alternative hot water heaters

Unfortunately, the traditional hot water systems are less than 100% energy efficient leading to higher energy use and increased global warming.

Alternative hot water heaters are expected to replace the traditional heaters because they are more energy efficient. At present, alternative systems such as solar hot water systems with or without electric or gas backup, or heat pump water heating systems are available for domestic applications. However, these systems are not highly successful on the market because their costs are still high and they are not convenient to use when compared with the traditional heaters. As a consequence, further research and development is required.

In Florida, heat pump water heaters have been developed with a system efficiency roughly twice that of an electrical resistance heater (Merrigan, 1990). Urchueguia (2008) found that a ground source heat pump system is a viable and energy efficient alternative to conventional system for heating and cooling applications in South European regions. For solar systems, Prudhomme and Gillet (1998) found with advanced control technologies that Coefficients of Performance (COPs) of between 1.5 and 1.7 were possible for flat plate solar domestic system in Switzerland. In addition, Biaou and Bernier (2008) compared four systems (a regular electric hot water tank, the desuperheater of a ground source heat pump (GSHP) with electric backup, thermal solar collectors with electric backup, and a heat pump water heater) in terms of energy efficiency. They concluded that heating domestic hot water with thermal solar collectors with an electric back up is the best solution for a zero net energy home (ZNEH) in Canada. Similarly, in Australia, direct solar systems were better performers in the warmer cities (Aye *et al.*, 2002); by contrast, such systems are marginal in the Southern parts of New Zealand in terms of performance (Lloyd & Kerr, 2008).

Anderson *et al.* (1985) measured electrical energy use in New Zealand's domestic hot water heaters. It was found that a heat pump water heater was able to realize annual average saving of 50 – 58% compared with conventional resistance water heaters.

Although the alternative systems have higher energy efficiency resulting in reduced running cost, the investment cost of the systems is still high. Some systems are not convenient to use and not as compact such as the solar systems. Among the alternative systems in terms of the efficiency, the installed cost, and the life-cycle cost (Table 2.3), the heat pump water heater looks promising.

Table 2.3: Comparison of life-cycle costs for different hot water systems (ACEEE, 2007)

Water Heater type	Efficiency (EF)	Installed Cost[1]	Yearly Energy Cost[2]	Life (Years)	Total Cost (Over 13 Years)[3]
Conventional gas storage	0.60	$850	$350	13	$5,394
High-efficiency gas storage	0.65	$1,025	$323	13	$5,220
Condensing gas storage	0.86	$2,000	$244	13	$5,170
Conventional oil-fired storage	0.55	$1,400	$654	8	$11,299
Minimum Efficiency electric storage	0.90	$750	$463	13	$6,769
High-eff. electric storage	0.95	$820	$439	13	$6,528
Demand gas (no pilot)[4]	0.80	$1,600	$262	20	$5,008
Electric heat pump water heater	2.20	$1,660	$190	13	$4,125
Solar with electric back-up	1.20	$4,800	$175	20	$7,072

1. Purchase costs include our best estimates of installation labor and do not include financial incentives.
2. Operating cost based on hot water needs for typical family of four and energy costs of 9.5¢/kWh for electricity, $1.40/therm for gas, $2.40/gallon for oil.
3. Future operating costs are neither discounted nor adjusted for inflation.
4. Estimates for tankless gas water heaters are based on the federal EF rating method, which may over-estimate the efficiency of tankless water heaters in houses.

2.3 Heat Pump Systems

A heat pump system drives heat from the low temperature source to the high temperature sink by input of work into the system (Fig. 2.12). In practice, this system operates as a cycle (Fig. 2.13).

In fact, the system will be charged by a working fluid (refrigerant) in order to absorb heat from the low temperature source and it will be driven to the high temperature sink for rejecting heat. There are many types of heat pump system depending on useful outcome, working fluids, energy input into the system etc.

Heat pump systems are widely used for many applications such as refrigerators, air-conditioners etc. Heat pump water heating is one application of heat pump systems that is currently of interest because of the concern about the energy use and the environmental impact.

Generally, operation of heat pump systems depends on heat source temperatures. As a consequence, air, water, and ground are all often used in as the heat sources.

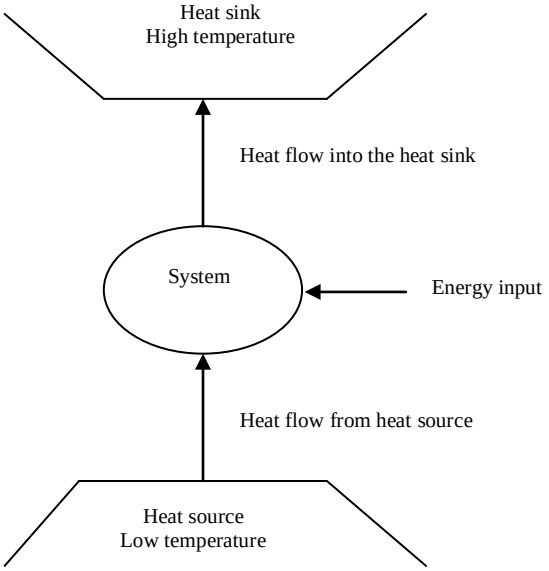

Figure: 2.12: The principle of the heat pump system

2.3.1 Air-source heat pump systems

Air-source heat pump systems use the ambient air as the heat source. A simple air-source heat pump water heater is illustrated in Fig. 2.13. The liquid working fluid at low temperature and low pressure absorbs heat from the air leading to its evaporation to the vapour phase. After that it is compressed to high temperature and high pressure. At this state, the vapourised working fluid is cooled by heat exchange with the water in the heat exchanger (condenser) to become a liquid at high pressure. The high pressure liquid-working fluid is reduced to low side pressure and then flows into the heat exchanger (evaporator) in order to absorb heat from the air once again.

2.3.2 Ground-source heat pump systems

A ground-source heat pump system basically operates as same as the air-source heat pump. It is only different in terms of the heat source used. The ground-source heat pump uses the underground as a heat source. A working diagram is presented in Fig. 2.14.

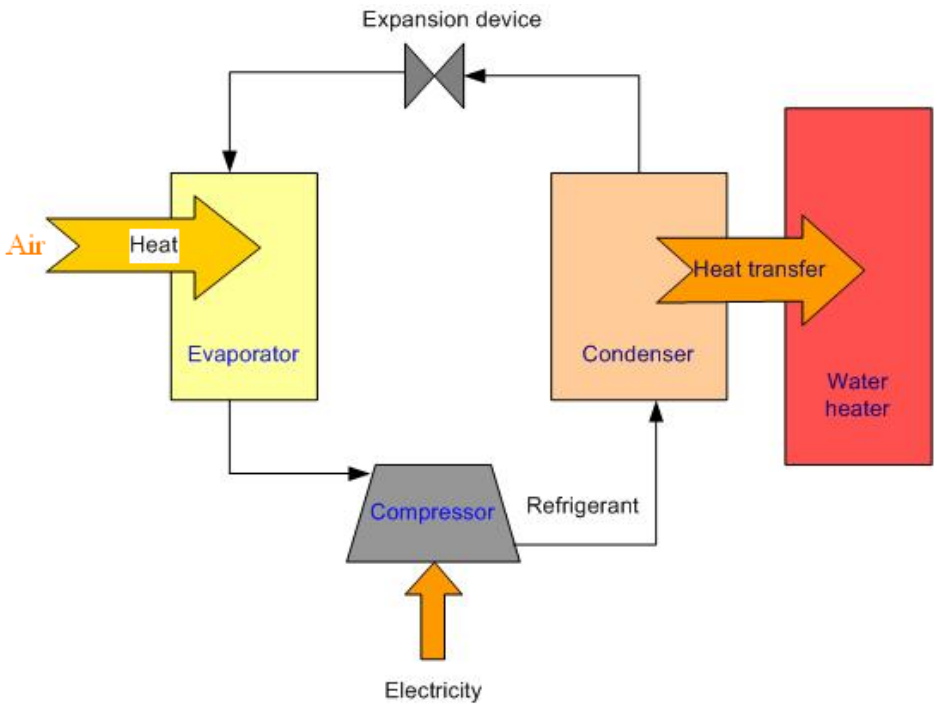

Figure 2.13: A classical air-source vapor compression heat pump system

The advantages and disadvantages of the air-source heat pump system are listed below:

Advantages

- lower in energy use (1/3 to 1/4 of traditional heaters)
- lower in maintenance cost than other types of heat pump system

Disadvantages

- still release the greenhouse gases as primary energy used
- higher in investment cost than traditional heaters
- not suitable for coastal areas (corrosion)
- noisy
- climate impact on performance (frosting)

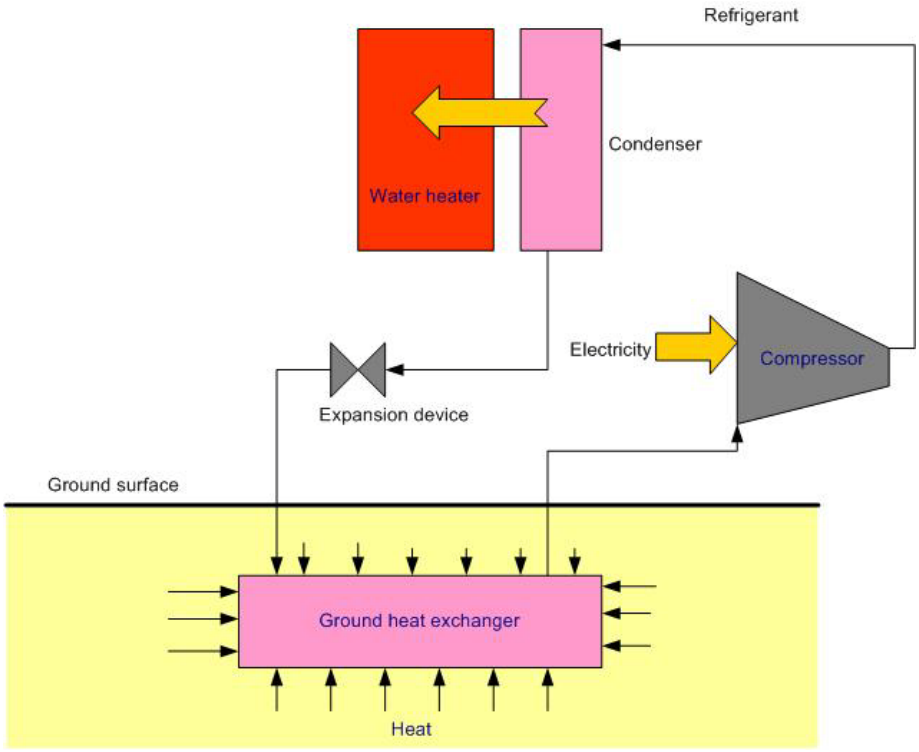

Figure 2.14: A ground-source vapor compression heat pump system

The ground-source heat pump systems are beneficial in many ways compared with air-source heat pumps as listed below:

Advantages

- quieter
- last longer
- lower energy consumption
- need little maintenance
- suitable for the cold climate as almost constant ground source temperature and higher on average than ambient temperature

Disadvantages

- very high investment cost for installation

The key disadvantage is the higher cost of the ground heat exchanger.

2.3.3 Water-source heat pump systems

A water-source heat pump system uses water at the low temperature as the heat source. A classical water-source vapor compression heat pump system is show in Fig 2.15.

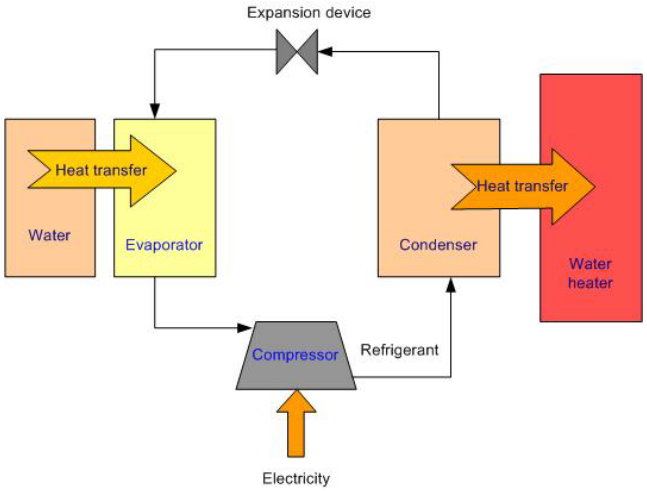

Figure 2.15: A classical water-source vapor compression heat pump system

The advantages and disadvantages of water-source heat pump water heaters are listed below:

Advantages

- lower energy use than the air-source
- available for coastal areas
- very flexible to expand into the new zone

Disadvantages

- higher investment cost than air-source heat pump

2.3.4 Heat pump efficiency

The theoretical energy efficiency of heat pump water heaters can be related to heat sink temperature and heat source temperature according to the COP of the reverse Carnot cycle:

$$COP\big|_{reversible} = \frac{T_H}{T_H - T_L}$$

where T_H = heat sink temperature, K

T_L = heat source temperature, K

Clearly a small temperature difference is desirable. As a consequence, because the heat sink temperature required is high (hot water temperature), heat source temperature should be high as well. Therefore, air-source and water source heat pump water heaters are most suitable for mild and hot climate regions. On the other hand, the ground-source and water source heat pump waters heaters are suitable for cold climate regions because the ground temperature is almost constant for whole year and it is often higher on average than the ambient air temperature. For these reasons, because New Zealand climate is mild, air-source and water source heat pump water heaters are suitable. However, domestically, there is often not a convenient source of water available. Thus, air-source heat pump water heaters are the most suitable type for New Zealand.

2.4 The Types of Air-Source Heat Pump Water Heaters

The types of air-source heat pump water heaters can be characterized by two types: integral and standalone.

2.4.1 Integral unit

All components such as compressor, condenser, evaporator and controller are integrated into the unit which may include a HWC if it is a storage system. Hermetic compressors, finned evaporator, axial or radial fan are often used in the design. Air ducts up to 20 meters in length are acceptable (for radial fans). Optional defrost mechanisms can be used for operation at low outdoor temperatures.

A passive immersed condenser with a cross-flow heat exchanger is usually used for this type. As the body of water will consequently be well-mixed and heat up uniformly, the thermal effectiveness of the condenser will be constrained when the bulk temperature of the storage tank approaches the condensing temperature by less than 5^{o}C (Carrington, 1982)

The advantages of this type they require small space area for installation and have low cost for installation. However, instantaneous integral units are unsuited for domestic applications because of the highly variable hot water flow rates used by most households.

2.4.2 Standalone unit

With standalone (split) hot water units, the heat pump is separate to the hot water storage or hot water cylinder (HWC). A built-in feed pump will circulate water from the heat pump through the HWC. In this way, an existing HWC of any model or capacity can be used.

A condenser with counter-current water and refrigerant flow control is a commonly used design. The use of a counter-current condenser offers the possibility of hot water outlet temperature being higher than the condensation temperature and higher than with a cross-flow or co-current arrangement. Further, counter-current flow also improves cycle efficiency because it is feasible to sub-cool the refrigerant to close to the water inlet temperature (Carrington, 1982).

Heat pump water heaters can produce hot water by two options:

- Water re-circulation (multi-pass)

Water circulates between the heat pump and the hot water cylinder (HWC) until all the water in the HWC is heated to the specified temperature (uniform temperature) as shown in Fig. 2.16.

- One pass heating

The cold water is heated by the heat pump from cold to the specified temperature in one pass and it delivered to the top of the HWC. Because of the decrease in density with

temperature at the top of HWC, the hot water remains above the colder water at the bottom of HWC causing a thermocline in the HWC (stratified storage) as presented in Fig. 2.17.

The one-pass systems can deliver hot water to users immediately after start up while the multi-pass systems do not. One-pass system always operates with high condensing temperature but has high potential for refrigerant sub-cooling; hence, its COP is moderate. Multi-pass system operates at lower condensing temperature; thus, at the beginning heating, its COP is high but at the final heating its COP is low due to low potential for sub-cooling. However, overall COP for both systems may not be significantly different.

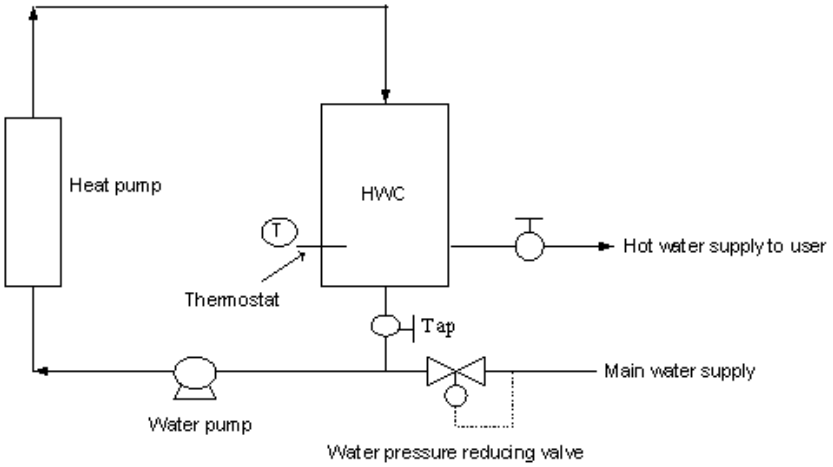

Figure 2.16: Schematic diagram of multi-pass heat pump water heating system

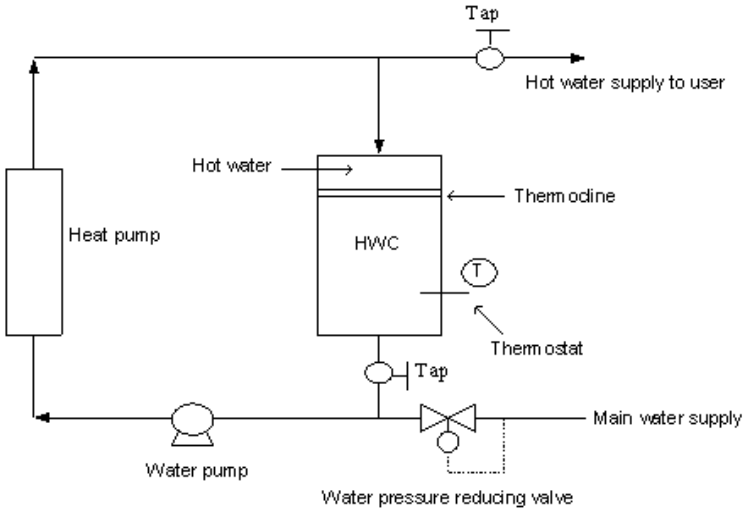

Figure 2.17: Schematic diagram of one-pass heat pump water heating system

2.5 Vapour Compression Cycles

The vapour compression cycle can operate either sub-critical or transcritical.

2.5.1 Subcritical cycles

Subcritical vapor compression cycle is a cycle that operates below the critical point of the refrigerant for both the cooling process (low pressure side) and the heating process (high pressure side) as shown in Fig 2.18. For the cooling process of the cycle (process $6 \rightarrow 1$), a refrigerant evaporates at the evaporator by absorbing heat from the low temperature reservoir (air-source). The refrigerant leaving from the evaporator (state 1) is compressed by the compressor to high pressure side (state 2). Then, the high temperature refrigerant at the high-pressure side will be cooled by the high temperature reservoir (water sink) in the condenser (process $2 \rightarrow 5$). In the heating process (at the condenser), the refrigerant heat flow will occur in three processes, de-superheating (process $2 \rightarrow 3$), condensation (process $3 \rightarrow 4$), and sub-cooling (process $4 \rightarrow 5$). Finally, the pressure of the refrigerant (state 5) will be decreased by an expansion device to the low pressure (state 6).

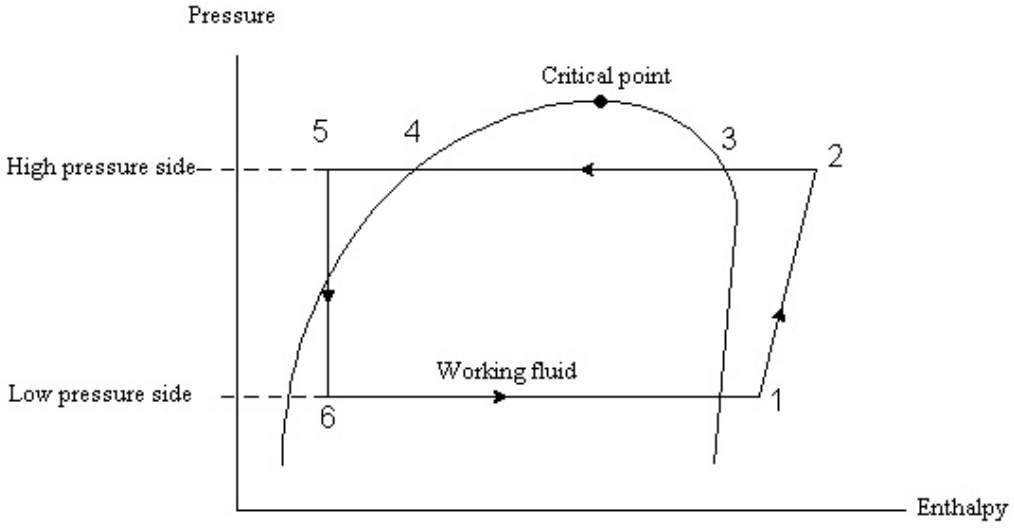

Figure 2.18: Subcritical vapour compression cycle on mollier diagram

In the case of design of water heating heat exchanger (condenser) running on the sub-critical vapour compression cycle, high heat transfer coefficient of refrigerants, a high degree of subcooling of the refrigerant and low pressure ratio between low side and high side of the cycle are required for high energy efficiency. In the heating process (condenser), the heat transfer coefficient of refrigerant side is generally higher during condensation than in super-heating and sub-cooling processes. In order to improve the rate of heat transfer, condensation pressure may be increased but this increases the pressure ratio of the compressor. The condensation pressure is also limited by the critical point and the desired water temperature.

The water temperature required is limited by the critical temperature of refrigerant used in the cycle. Practical cycles are usually designed to condense at 70% to 90% of the critical temperature (on an absolute temperature basis) and, therefore, at corresponding fractions of the critical pressure (Calm & Didion, 1998).

For domestic application, heat pump water heaters can work either on multi-pass or one pass heating. However, for one pass heating, it must produce hot water at the desired temperature leading to use high condensation temperature of refrigerant. This may cause a pinch in heat exchange between the water and refrigerant side at the transition from de-superheating to condensation (Fig. 2.19). In addition, the coefficient of performance of heat pump will be lower due to high pressure ratio of the compressor. For these reasons, multi-pass heating or circulation heating is most suitable for domestic heat pump water heater working on subcritical cycle because this system can operate with low condensation temperature of refrigerant for a large fraction of the time. This allows high coefficient of performance of the system. It can also supply stable hot water temperature to users. However, disadvantages of this system are longer heat pump operating period, the extra cost of the HWC, and slower recovery after a major hot water use.

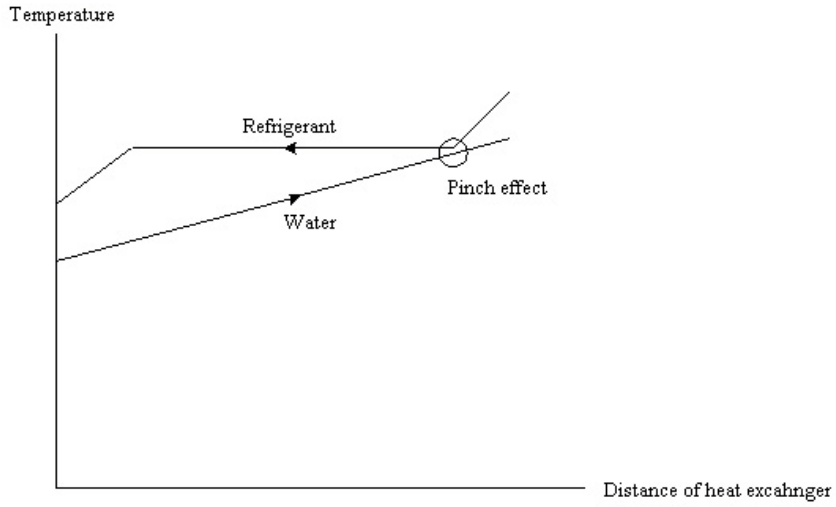

Figure 2.19: Temperature difference profile in a condenser of a subcritical cycle

Single stage

Single stage subcritical cycles which operate with single stage compression require high condensation temperatures in order to produce high hot water temperature. If the heat source temperature is low then the compressor pressure ratio becomes large. Most reciprocating compressors are limited to pressure ratios on the order of 8:1 (Jekel & Reindl, 2008). As a consequence, if the condensation temperature required is high while the evaporation temperature is very low, single stage compression systems have poor energy efficiency.

Multi-stages

Mutiple stages subcritical vapour compression systems are often coupled with multiple stages of liquid expansion and intercooling. Stages of compression represent the number of compression steps required to raise the refrigerant pressure from suction to condensing.

A two-stage system will result in lower compression ratio operation on each individual compressor, which improves compressor efficiency compared to a single stage system. However, more compressors mean more maintenance, more floor space and higher cost etc. These trade-offs are relatively complex and plant-dependent; thus, they will affect the total life-cycle cost of the system (Jekel & Reindl, 2008).

In the case of domestic air-source heat pump water heaters, ambient temperatures of some regions may be low or one-pass heating systems are required. These result in small temperature approach between inlet refrigerant and hot water in condenser. As a consequence, the heat transfer performance of the condenser will be constrained. Further, heat transfer area of condenser used will be large because heat exchange in the de-superheated zone becomes a large fraction of the total for a single stage system. For these reasons, two-stage compression is useful to increase the temperature approach resulting in high heat transfer performance of the condenser.

2.5.2 Transcritical vapour compression cycles

The transcritical cycle operates between subcritical pressure on the low side pressure and supercritical pressure (above critical point) on the high side as shown in the Fig. 2.20. The cycle is similar to the subcritical cycle, but for the heating process (process $2 \rightarrow 3$), the working fluid phase stays in the supercritical phase throughout the heat exchanger (gascooler). Therefore, in the heating process the refrigerant undergoes sensible cooling rather than condensation.

Ordinary synthetic refrigerants are unsuited for use in this cycle because their critical temperature is too high (Table 2.4). Carbon dioxide is a natural refrigerant that has a low critical temperature and good thermal stability; thus, it may suit this cycle.

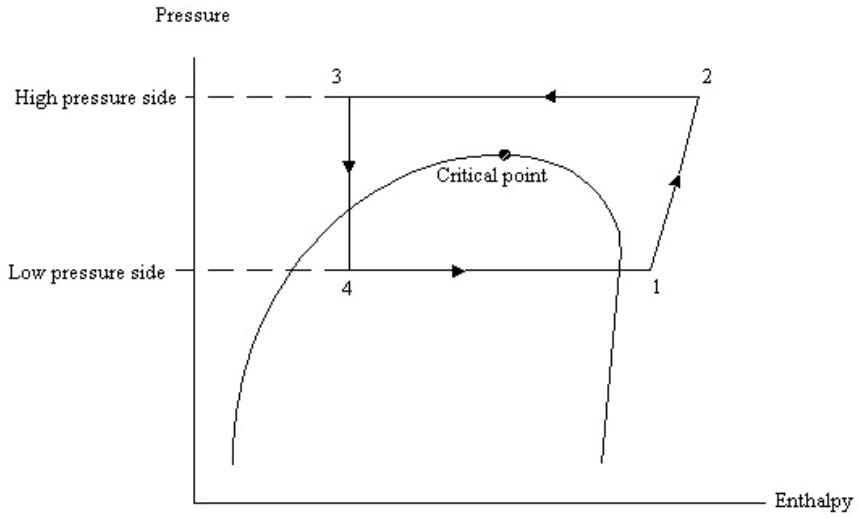

Figure 2.20: Transcritical cycle on mollier diagram

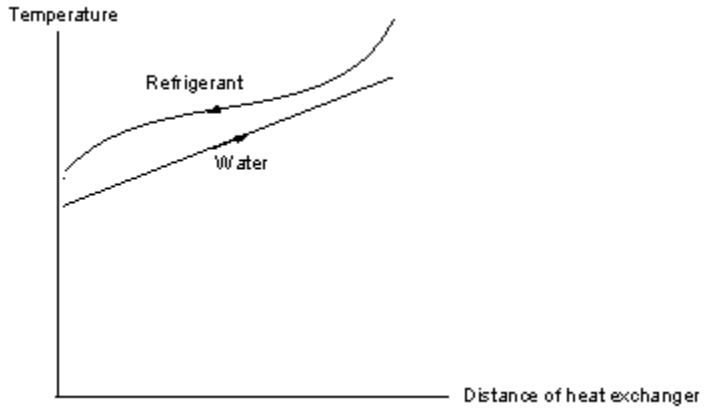

Figure 2.21: Temperature difference profile of gascooler

The CO_2 transcritical vapor compression heat pump systems

Single stage

Generally, the CO_2 transcritical cycle can operate on single stage vapour compression. For the same temperatures CO_2 has much higher evaporation pressures than most other refrigerants. Thus, the transcritical CO_2 system have a smaller components leading to more compact systems than subcritical vapour compression systems. Also the pressure ratio tends to be low for the same temperature range.

On the heating process of the cycle, it runs on above the critical point (35 bar). The hot water temperature and heating capacity can be higher than those of the subcritical vapour compression cycle. Further, the irreversibility loss from heat transfer between the refrigerant side and the water side is lower than that of the heating process of the subcritical vapour compression cycle because the temperature difference between the CO_2 and the water is almost unchanged (see Fig. 2.21). The pinch effect from heat exchange between the refrigerant side and the water side may be avoided because the refrigerant side is single phase in the gascooler. For those reasons, domestic heat pump water heaters working on the transcritical cycle use one pass heating system. These results in reduced extra cost of the HWC, short periods of heat pump operation, and reduced risk of hot water shortage at times of peak demand.

Although, the CO_2 transcritical cycle has many benefits, component cost may be still high due to low sales volumes and the high operating pressure.

In addition, the specific heat capacity of the carbon dioxide near the critical point is not constant, and this can lead to a pinch effect in the middle of refrigerant cooler. This results in reduced heat transfer in this region. The effect of this pinch point can be reduced by increasing the discharge pressure or by increasing the suction temperature by a recuperator (Yarrell, 1998).

Two-stage

Two-stage system may also be essential for transcritical system if the pressure ratio for a single stage system is large.

Table 2.4: The thermodynamic properties of none-ozone depleting potential refrigerants

Refrigerants	Critical pressure (bar)	Critical temperature (^oC)	Saturated pressure at 0 ^oC (bar)
R134a	40.6	101.1	2.9
R410A	49.0	71.4	8.0
R717	113.3	132.3	4.3
R744	73.8	31.0	34.9

2.6 Other Heat Pump Cycles

Absorption heat pump cycle

Basically, an absorption heat pump system operates similarly to the vapour compression system but it is different in energy input into the system and refrigerant used. The absorption system uses the binary-mixture fluids such as LiBr-H_2O, NH_3-H_2O etc. as working fluids in the system. The energy input into the system comes from heat sources such as natural gas combustion, waste heat etc. in order to heat and separate the binary working fluids at the generator. The refrigerant (the fluid having lower boiling point) leaves from the generator at high pressure and temperature to the condenser whereas the weak solution flows into the absorber. The refrigerant is cooled and condensed by the condenser and its pressure is reduced to low side pressure by expansion devices. It flows into the evaporator in order to evaporate. Finally, at the absorber, the weak solution will absorb the refrigerant leaving the evaporator to form a strong solution, and strong solution is then pumped to the generator as shown in Fig. 2.22.

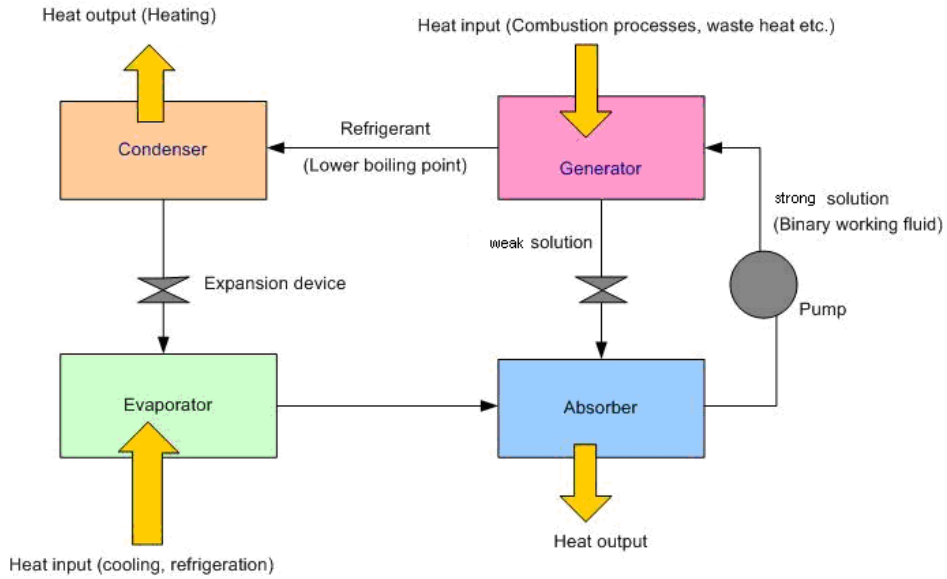

Figure 2.22: An absorption system

The advantage of this system is able to use many heat sources, including waste heat, to operate the system. It can save energy cost. However, it's energy efficiency is lower than that the vapour compression systems. In addition, the components of system are more complex leading to higher cost and more difficult maintenance.

Brayton cycle

A Brayton heat pump system operates as in the vapour compression system but operates completely in the superheated gas phase. A gas is drawn into the compressor at state 1 and compressed to state 2. The hot compressed gas then enters a heat exchanger where it is cooled to state 3, thereby delivering heat to the hot water system. The gas is expanded through the turbine to state 4 in order to produce shaft work, which is delivered directly to the compressor. Finally, the gas flows into the heat source heat exchanger to increase the temperature to state 5 before entering the compressor. The simplified layout of the Brayton heat pump system is presented in Fig. 2.23.

The advantages of the Brayton heat pump system include that refrigerants used in the Brayton heat pump system are abundant such as the air; the cycle is very simple; there are no refrigerant leak problems and there is no requirement for a low-temperature heat exchanger (White, 2009). However, air-cycle devices have a tendency to be bulky due to the low density and thermal capacity of air, and at conditions typical of central heating systems the cycle has a very low work ratio, making it particularly susceptible to irreversibilities (White, 2009).

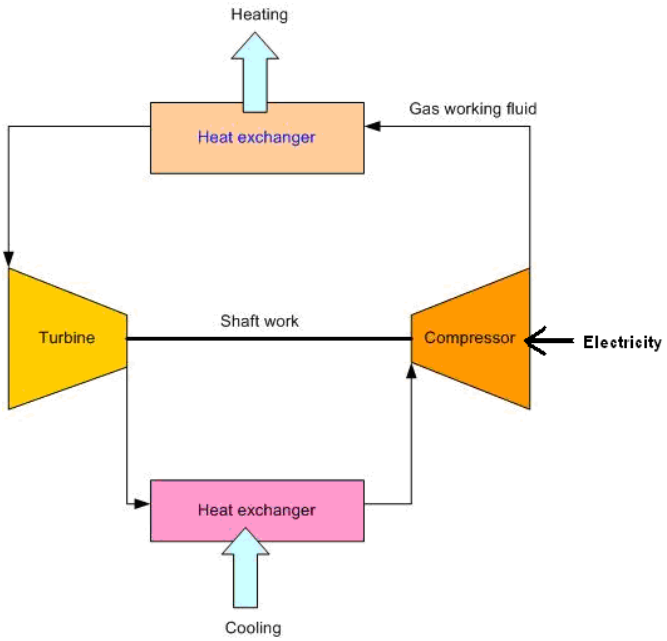

Figure 2.23: Simplified layout of the Brayton heat pump system

2.7 Standards

Standards are a mechanism to ensure system performance can be tested and compared in a consistent manner.

Air source heat pump water heater is a product that is attracting attention for its ability to save energy and reduce greenhouse gas emission. It is expected to replace the traditional water heaters. Therefore, standards for air-source heat pump water heater are being developed.

Standards for air-source heat pump water heaters have been issued in many countries. For examples, standard codes of residential heat pump water heaters of Canada, EU, and Japan are C745-00, EN255-3, and JRA4050 respectively (C745-00, 2000; EN255-3, 1997; JRA4050, 2005).

For New Zealand and Australia, the standard for heat pump water heaters is Australia/New Zealand Standard^{TM} 2712 and 4234 (AS/NZS, 2007).

IEA HPP (Heat Pump Programme) Annex 28 consists of eight counties Australia, Canada, Germany, Japan, Norway, Sweden, and USA. The purpose of the Annex 28 were to elaborate recommendations to standardization organizations concerning for heat pump systems (Wemhoener & Afjei, 2006).

In addition, heat pumps would need to adhere to the generic refrigeration safety standards such as AS/NZS 16771999 or ASHRAE Standard 15 2010.

2.7.1 Standards for the air-source heat pump water heaters

The AS/NZS 2712, covers the following aspects of air source heat pump water heaters design and construction.

- System performance
  - Thermal performance
- Refrigerant
  - Refrigerant type
  - Maximum charge of refrigerant
- Design and construction
  - Materials
  - Over-temperature protection (thermal cut-out)
  - System pressure and temperature
  - Circulating pump construction
  - Controllers for circulating pump and supplementary heating
  - Pressure relief
  - Heat exchangers

- Instruction and Marking
  - Installation instruction
  - Marking

2.7.2 Standards for the heat exchangers

In accordance with the AS/NZS 2712, heat exchangers used in transferring heat from heat pumps to the drinking water supply shall be designed to ensure that the heat transfer fluid does not contaminate the drinking water. The regulations issued for design and construction of heat exchangers are include the following aspects.

- Heat transfer fluid
  - Stability
  - Approvals
  - Indicator colour
- Design and Construction
  - Materials
  - Strength of materials
  - Support
  - Over-pressure test-Internal
  - Facilities for drainage and filling
  - Maintenance of heat transfer fluid level in vented heat exchange systems
- Instruction and marking
  - Pressure information
  - Leakage indication
  - System with non-toxic heat transfer fluids other than water

The key outcome of the standard is that double wall water heating heat exchangers are required to prevent contaminated water supplies by refrigerant or oil if the heat exchanger leaks.

2.8 Refrigerants

The main environmental concerns of refrigerants are their emission into the atmosphere causing ozone depletion and the global warming. The cause of ozone layer depletion is from the emission of chlorinated man-made chemicals into the atmosphere (Rowland & Molina, 1974). As a consequence, an intergovernmental agreements to protect the ozone layer was established in 1987 called “the Montreal Protocol”. Amendments to the Montreal Protocol were followed by the London, Copenhagen, Vienna, Montreal and Beijing in 1990, 1992, 1995, 1997 and 1999 respectively. As a result, production and use of chlorofluorocarbon (CFC) refrigerants used in the refrigeration and heat pump systems were banned in industrialized countries (except for essential applications) (McMullan, 2002); however, they are still used in some developing countries. In addition, Hydro-chlorofluorocarbon (HCFC) refrigerants will be officially phased out in the near future

for industrialized countries. Germany has banned the used of HCFC-22 in new plants after the year 2000 (McMullan, 2002). Eventually all refrigerants releasing chlorinated gases will be replaced by alternative refrigerants.

Climate change or global warming is caused by the increase of carbon dioxide (CO_2) and greenhouse gases in the atmosphere. Normally, the surface of the earth is heated up by about 51% of total incoming solar energy and it is released in the form of infrared radiation, convection and evaporation into the atmosphere. However, the infrared radiation energy can not pass through the atmosphere because it is absorbed by water vapour, carbon dioxide and other infrared absorbers; therefore, heat energy is trapped and the temperature at the surface of the earth is higher than without the insulating blanket of the atmosphere. For that reason, if the atmosphere has an increase of carbon dioxide and other greenhouses gases, the amount of heat trapped will be increased. This causes increase in atmosphere temperatures and consequent long-term climate changes.

Two factors used to measure the impact of a greenhouse gases are Global Warming Potential (GWP) and Total Equivalence Warming Impact (TEWI) (Lucas, 1993). The GWP is based on CO_2 as reference; thus, calculation has to allow for the lifespan of the molecule in the atmosphere. As a consequence, CFCs have a very high global warming impact. For example, one molecule of R-11 will absorb the amount of heat greater than 10,000 times that absorbed by CO_2. TEWI takes into account the direct global warming effect as well as the indirect global warming effect, which depends on the energy used in the process, and thus how much CO_2 is produced by the production of electricity to run the equipment over its life. However, this factor will vary from region to region due to various electricity sources.

Due to environmental concern about the ozone depleting potential (ODP), important candidates for single-compound refrigerants are hydro-fluorocarbon (HFCs) refrigerants (Fig. 2.24). In addition, some blends and natural refrigerants have zero ODP (Table 2.5). Considered both ODP and GWP, the natural refrigerants are most promising as alternatives (Table 2.5). However, heat pump water heaters using hydro-fluorocarbon refrigerants as working fluid will have very small impact to global warming when compared with the conventional hot water heaters in terms of TEWI measurement. Therefore, both the hydro-fluorocarbon refrigerants and the natural refrigerants can be used as alternative refrigerants in heat pump systems.

Beside the environmental data, physical data and safety data should also be considered (Table 2.5).

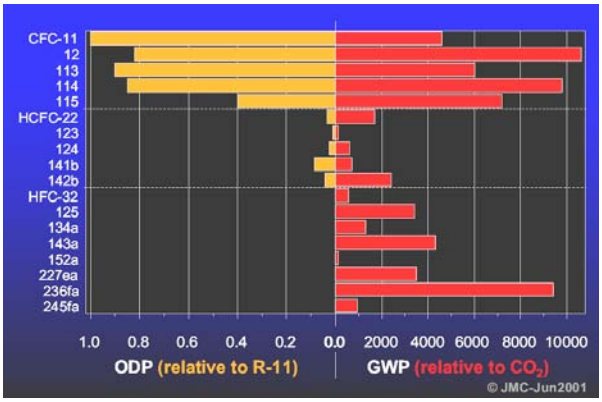

Figure 2.24: Ozone depletion potential (ODP) contrasted to global warming potential (GWP) for key single-compound refrigerants (Calm & Hourahan, 2001)

Table 2.5: Comparison of some characteristics among CFCs, HFCs, and natural Refrigerants (Kim, Pettersen, & Bullard, 2004; Lorentzen, 1994; Tanaka & Kotoh, 2007)

Refrigerants		Synthetic refrigerants				Natural refrigerants				
		CFCs		HFCs						
		R-12	R-22	R-134a	R-410A	CO_2	H_2	NH_3	H_2O	Air
Chemical properties	Toxicity/flammability	∕	∕	∕	∕	∕	×	×	∕	∕
	Material deterioration	∕	∕	∕	∕	∕	∕	×	∕	∕
	Chemical stability	∕	∕	∕	∕	∕	∕	×	∕	∕
Thermophysical properties	Moderate boiling point	∕	∕	∕	∕	×	∕	∕	∕ and ×**	×
	Capacity per unit volume	∕	∕	∕	∕	∕	∕	∕	∕ and ×**	∕
	Theoretical COP	∕	∕	∕	∕	∕ and ×*	∕	∕	∕	×
	Moderate discharge temperature	∕	∕	∕	∕	∕	∕	∕	∕	∕
Global environment properly	Ozone layer	×	×	∕	∕	∕	∕	∕	∕	∕
	Warming	×	×	×	×	∕	∕	∕	∕	∕

* Evaluated with air-conditioners/water heaters
** Evaluated for source-of-heat temperature at low/high

∕ = Acceptable
× = Unacceptable

The thermodynamic properties of the alternative refrigerants used in the heat pump water heaters depend on the operating conditions of the systems. Many properties of refrigerants, such as critical pressure, critical temperatures, freezing point, normal boiling point, specific volume etc. should be considered. In addition, the operating pressures, coefficient of performance (COP), specific heat ratio of the system should be carefully considered.

A positive pressure in the system is preferred to prevent the air and moisture flowing into the system. Because the required condensation temperature is high, the critical temperature of the refrigerant should be high if a subcritical cycle is desired.

In order to produce low temperature in the evaporator at positive pressure, boiling point of the refrigerants should be low although too high pressure can increase cost to prevent system rupture. High pressure (low boiling point) can also help reduce the pressure ratio for a given operating temperature range. The system temperatures should also be higher than freezing point of the refrigerants. In order to improve the compressor life, the specific heat ratio of the refrigerants should be low leading to lower discharge temperature. In addition, an indication of the size of the compressor comes from the volume of suction vapour needed per ton of refrigeration (Mohanraj, Jayaraj, & Muraleedharan, 2009).

Based on these criteria, CO_2 (transcritical), R410A, and R134a appear the most promising refrigerants.

2.9 Heat Exchangers for Domestic Hot Water Heating

Heat exchangers are used for many applications including for water heating. Water heating heat exchangers have many types depending on applications. Common types are tube-in-tube heat exchanger, shell-and-tube heat exchanger, plate heat exchanger, or other compact heat exchangers.

Water heating heat exchangers of the residential heat pump water heater must be carefully designed. The contamination cross of water supply must be avoided, according to the AS/NZS 2712 using a double-wall heat exchanger with small air gap. Double wall plate heat exchangers are available for tube-in-tube, tube-on-tube and plate heat exchanger configuration.

In addition to preventing the cross contamination of water supply, other desirable features are:

- simple construction and manufacturing,
- able to be designed for high temperature (up to 200 ^{o}C) and high pressure (up to 150 bar),
- able to be configured in countercurrent mode (allow greatest water temperature rise), and
- easy to maintain.

Tube-in-tube and tube-on-tube double wall heat exchanger are illustrated in Fig 2.25 and 2.26, respectively.

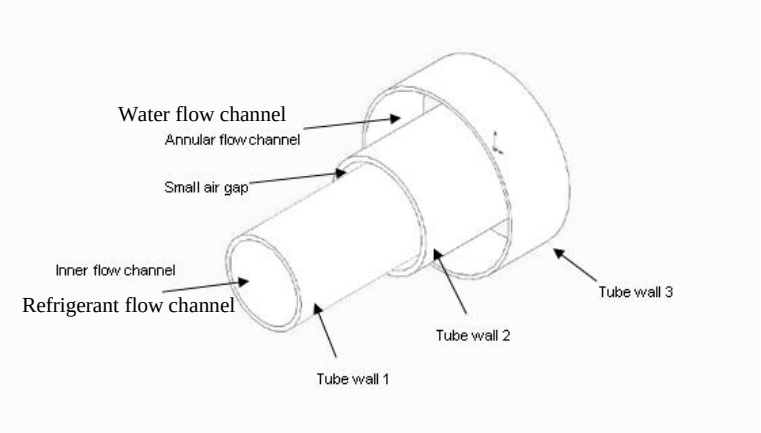

Figure 2.25: A tube-in-tube double wall heat exchanger

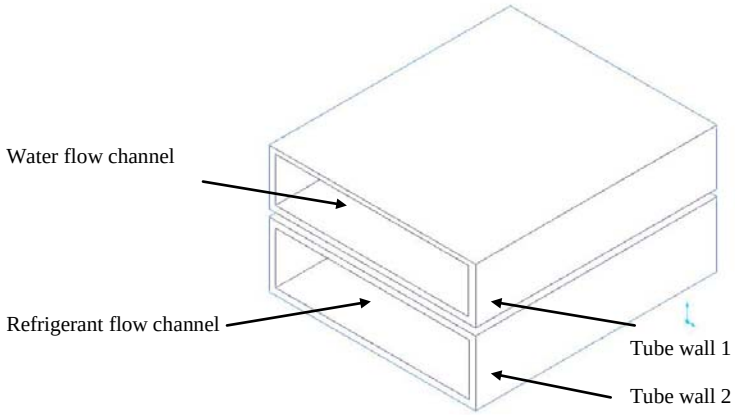

Figure 2.26: A tube-on-tube double wall heat exchanger

For a water heating heat exchanger of a heat pump system, the inlet temperature of refrigerant is relatively high and the mass flow rate is low. In order to heat the water efficiently, the temperature difference between the refrigerant side and water side should be close together along the distance of the heat exchanger (lowest discharge pressure). Also a high water temperature rise is desirable especially for once-through configuration. A heat exchanger operating in countercurrent mode is best as shown in Fig. 2.27 and 2.28.

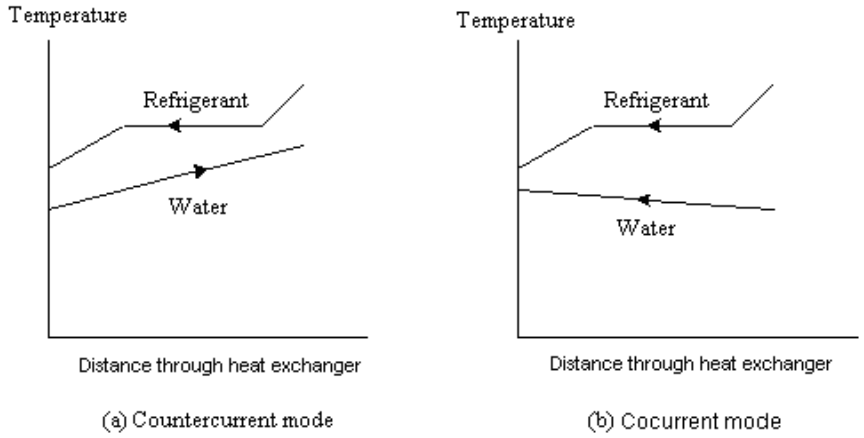

Figure 2.27: Temperature difference between the refrigerant and the water in the condenser for countercurrent and cocurrent configurations

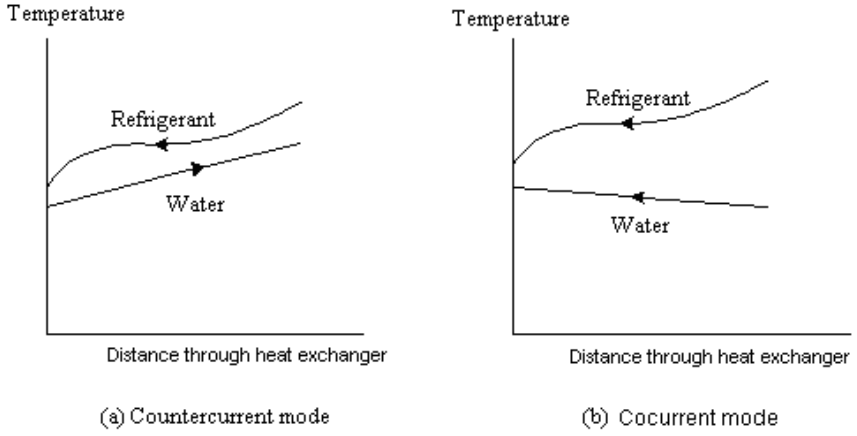

Figure 2.28: Temperature difference between the refrigerant and the water in the gascooler for countercurrent and cocurrent configurations

2.10 Flow Passage

The ideal heat exchanger design provides high heat transfer performance with low pressure drop, compactness, a low cost, and is easy to maintain. However, high heat transfer performance of the heat exchanger is often achieved by causing high pressure drop of the water or refrigerant whereas low pressure drop often leads to low heat transfer performance and less compact design.

Flow passages in the heat exchanger have a most significant effect on heat transfer performance and pressure drop. Therefore, configurations of the heat exchanger must be carefully considered in the design. Basically, the hydraulic diameter of the flow passage is a primary design factor.

In theory, when the hydraulic diameter is decreased, the heat transfer performance will be increased for both sides due to increased mass flux (and therefore increased turbulence) but this will be offset by higher pressure drop for both sides leading to higher pump power for the water side and higher compressor power for the refrigerant side. As a consequence, it is necessary to optimize flow passages for both the refrigerant side and water side based on design conditions.

2.11 Heat Exchanger Optimization

A heat exchanger is designed for its specific application. Basically, heat exchangers designs should be not only workable but also optimal based on consumer requirements. When a consumer requirement is defined quantitatively and it is to be maximized or minimized, it is called *objective function* in a design optimization. However, the objective function depends on many particular requirements such as allowance pressure drop, required heat transfer, limitation on height, weight and/or length of heat exchanger etc. These requirements are called *constraints* in design optimization (Shah & Sekulic, 2001).

In order to investigate the optimal solution in an objective function, many designers search the solutions by many approaches based on their experience. Configuration of geometry and/or operation of heat exchangers is one approach to search the optimal solution in the objective function. However, the objective function and constraints in this approach should be expressed mathematically.

In aiming for an optimized heat exchanger design, two important aspects that can be expressed mathematically are the heat transfer coefficient and pressure drop of working fluids exchanging heat in the heat exchanger. Equations to estimate these aspects are used for evaluation in the optimization (search) technique. However, often these equations have a limitation in use depending on the operating conditions. A methodology for heat exchanger optimization is shown in the Fig. 2.29.

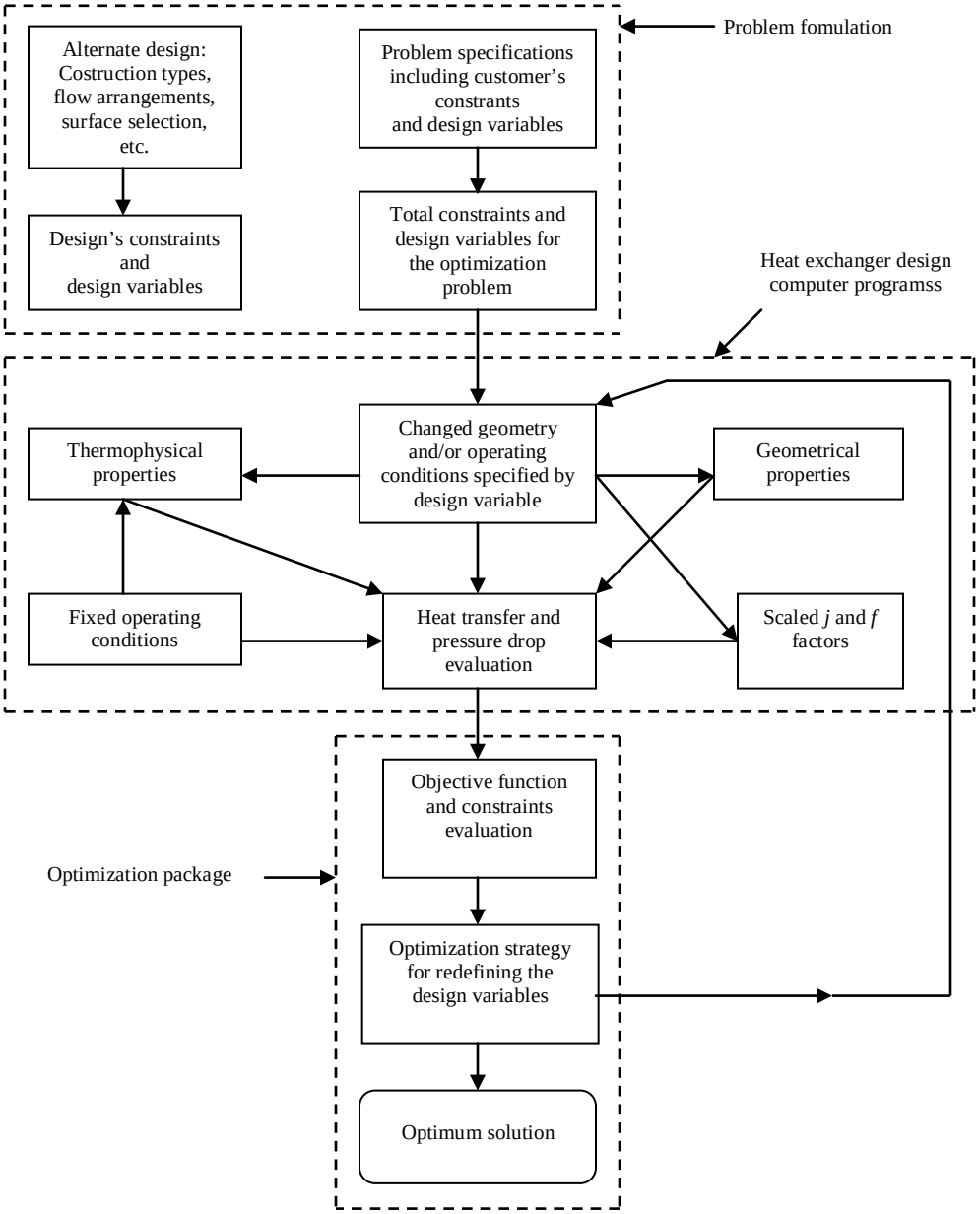

Figure 2.29: Methodology for heat exchanger optimization (Shah *et al.*, 1988)

2.12 Prediction of Heat Transfer Coefficients and Pressure Drops

A heat exchanger design has a trade off between the heat transfer performance and pressure drop. The design needs to be optimized in accordance with the requirements of high heat transfer performance and low pressure drop. If both can be achieved then operating cost and investment cost of the system will be low and the heat exchanger will be also compact. Therefore, in order to search an optimal heat exchanger, the overall heat transfer coefficient and pressure drop of the system must be predicted with high accuracy. This section reviews heat transfer coefficient and pressure drop correlations that might be used for such predictions.

2.12.1 Subcritical cooling processes

Heat transfer between the refrigerant side and the water side in the water heating heat exchanger running on a sub-critical vapour heat pump system can be characterized by three zones as previously mentioned. Generally, however, the proposed correlations of heat transfer coefficient and pressure drop depend on the phase flow in the flow channel. Therefore, the correlations for both single-phase flow and two-phase flow (condensation flow) are reviewed.

2.12.1.1 Single-phase flow regions

2.12.1.1.1 Conventional channels with and without fins

Heat transfer coefficient correlations without oil

Webb and Zhang (1997) surveyed methods to predict heat transfer coefficients for single phase flow inside plain tubes and micro-fin tubes. They recommended that for turbulent flow in circular tubes the equations of Petukhov (1970) are suitable.

Yang (1996) reported R-134a and R-12 data for single phase flow inside extruded aluminium tubes with and without micro-fin. He found that the Petukhov equation reasonably predicted the single-phase heat transfer coefficients.

Brognaux et al. (1997) compared heat transfer coefficients between experimental data and predicted data using the Petukhov equation for single phase flow on a 14.9 mm inside diameter round micro-fin tube. They found that the heat transfer coefficient is over predicted by nearly 30%. In addition, they developed an empirical correlation to account for helix angle of the micro-fins.

Wang *et al*. (1996) compared their test results and prediction values by Dittus-Boelter correlation and Gnielinski correlation (Gnielinski, 1976) for water flow in a smooth tube hydraulic diameter of 7.92 mm. The experimental results for heat transfer data agree very well with the Dittus-Boelter correlation for Reynolds number (Re) greater than 10,000, and show a detectable deviation for Re $\leq$ 9,000 while the Gnielinski correlation,

which correlates the available data over the range of Prandtl number from 0.5 to 2,000 and the Reynolds number from 2300 to 5×10^6, gave the best agreement with their experimental data.

In addition, because the Dittus-Boelter type correlation is valid only for the higher Reynolds numbers, Wang et al. (1996) proposed an approach to predict heat transfer factors using the heat-momentum transfer analogy and compared it with their experimental data for water flow in microfin tubes with nominal diameter of 9.52, 7.94, and 7.0 mm. They summarized that the heat-momentum transfer analogy be used to correlate the single-phase heat transfer data rather than the the Dittus-Boelter type equation. In the range of 2,500 < Re < 40,000, the proposed heat transfer correlation can predict 85% of the microfin data within 10%.

Generally, single phase heat transfer coefficients for micro-fin tubes were higher than that of equivalent smooth tubes from 50 to 100% while a pressure drop increased from 20 to 50% (Schlager *et al.,* 1989).

Pressure drop correlations without oil

Webb and Zhang (1997) surveyed methods to predict pressure drops for single phase flow inside plain tubes and micro-fin tubes. They recommended that for turbulent flow in circular tubes the simple empirical Blasius friction equation is suitable.

Yang (1996) reported pressure drop data of 134a and R-12 during single phase flow inside extruded aluminium tubes with and without micro-fin. He found that the Blasius equations predicted pressure drops during single phase flow reasonably accurately.

Wang *et al*. (1996) compared test result friction factors and predicted values by the Blasius correlation for water flow in a smooth tube having hydraulic diameter of 7.92 mm. They found that the experimental friction factors are in good agreement with the Blasius equation at the Reynolds number from 7,000 to 25,000, and higher by about 8% at a Reynolds number of 40,000.

In addition, as the Blasius correlation is valid only for the higher Reynolds numbers, Wang et al. (1996) proposed an approach to predict friction factors using the roughness Reynolds number correlated as a function of Re and the enhancement dimensions and compared prediction values with their experimental data for water flow in micro-fin tubes with nominal diameter of 9.52, 7.94, and 7.0 mm. They found that, in the range of 2,500 < Re < 40,000, the proposed friction factor correlation can predict 96% of the micro-fin data within 10%.

2.12.1.1.2 Microchannels

Heat transfer coefficient correlations without oil

Reviews of heat transfer correlations for single-phase flow in mini-channel tubes were proposed by Palm (2001); Sobhan and Garimlla (2001); and Morini (2004).

Webb and Zhang (1998) reviewed comparisons between heat transfer data of Zhang and Webb and predicted values by the the Petukhov and Dittus-Boelter equations, as reported by (Incropera & DeWitt, 1990) for liquid R134a flow in a tube having hydraulic diameter of 1.31 mm. The equations predicted the measured Nusselt number accurately and showed good agreement with standard heat transfer correlation. Further, they confirmed that the experimental data of (Horiuchi, 1995) that measured similar data for R-134a in three circular multiport channels having hydraulic diameter of 0.96, 1.45, and 2.13 mm were equally well predicted by the standard correlations.

Adams *et al* (1997) compared experimental data and Nusselt numbers predicted by traditional large channel correlations for single phase forced convection of water in circular microchannels with diameters of 0.76 and 1.09 mm. They found that the Nusselt numbers obtained by the experiments are higher than those predicted by traditional correlations. As a consequence, they developed a new heat transfer correlation based on their experimental data for the tube diameter range of 0.102-1.09 mm, the Reynolds number range of 2600-23000, and the Prandtl number range of 1.53-6.43. With a confidence level of greater than 95%, differences between experimental and predicted Nusselt number values were less ±18.6%.

Celata (2003) showed a general review of research carried out in single phase heat transfer and flow in capillary (micro) pipes. The results obtained by different researchers were analysized in detail for laminar flow and laminar-to-tubulent flow transition in order to clarify the discrepancies. In addition, he proposed new heat transfer experimental data. The results show that heat transfer correlations in laminar and turbulent regimes, developed for conventional (macro) tubes, are not valid for micro tubes.

Chen and Kuo (2004) proposed a numerical procedure which solves the compressible boundary-layer equations to study the heat transfer characteristics of gaseous laminar and turbulent flows in mini and microtubes. The numerical results show that the numerically predicted Nusselt numbers agree with conventional correlations (the Dittus-Boelter correlation) for compressible turbulent flow in larger tubes (D=100 and 50 mm). On the other hand, for compressible turbulent flow in smaller tubes (D=10, 5, and 1 mm), the predicted Nusselt number disagree with the conventional correlation. They summarized that compressibility plays a very important role in the heat transfer characteristics of gaseous flow in long mini/micro tubes, and conventional correlations cannot be used in this area.

Qi *et al.* (2007) measured the average Nusselt numbers for single phase flow of liquid nitrogen in four microtubes with diameters of 1.931, 1.042, 0.834, and 0.531 mm

conducted by the experiments to compare with the correlations for the conventionals and microchannels respectively. The experimental data show that the average Nusselt numbers for the microtubes are higher than those predicted by the correlation for conventional channels (i.e. Dittus and Boelter correlation, Gnielinkski correlation). Therefore, they modified the Gnielinski correlation. This modified correlation predicted the experimental Nusselt numbers with a mean absolute error of 6.4%.

Pressure drop correlations without oil

Reviews of pressure drop correlations for single phase flow in mini channel tubes can be found in Palm (2001); Sobhan and Garimlla (2001); and Morini (2004).

Webb and Zhang (1998) compared the friction data of Zhang and Webb (Zhang & Webb, 1997) and predicted values by the Blasius friction factor equation as reported by White (1994) for liquid R134a flow in a tube having hydraulic diameter of 1.31 mm. The predicted values agree well with the experimental data, consistent with the results of (Horiuchi, 1995).

Qi *et al.* (2007) compared experimental single phase pressure drops and conventional correlations over a Reynold number range 10,000-90,000 for liquid nitrogen flow in four microtubes with diameters of 1.931, 1.042, 0.834, and 0.531 mm. The experimental data show that the friction factor for 1.931 and 1.042 mm tubes agree quite well with the Von Karman Nikuradse (White, 1994) and Colebrook correlations. However, for 0.834 mm tube, the relative surface roughness plays relatively important role on the friction factor. The Colebrook correlation provided satisfactory predicted results, but the agreement with the Von Karman Nikuradse correlation was poor. For the tube with a diameter of 0.531 mm, the friction factor was 20% higher than the Colebrook prediction.

2.12.1.1.3 Curved tubes

Recently, reviews of heat transfer correlations and pressure drop correlations for single phase flow in curved tubes (i.e. helical tubes, spiral tubes) were carried out by Naphon and Wongwises (2006); Vashisth, Kumar, and Nigam (2008).

Heat transfer coefficient correlations without oil

Helical tubes

Guo, Chen, Feng, and Bai (1998) performed preliminary experiments of steady single phase heat transfer of steam in a helical coiled tube having a 6448 mm long, tube of ¢15×2 mm, with helix angle of 4.27°, coil diameter of 256 mm and a pitch of 60 mm. The experimental results showed good agreement with the average heat transfer coefficient correlation of Seban and Melaughlin (1963) for $6000<Re<60000$. However, this correlation did not accurately predict the average heat transfer coefficient for

Re>60000. As consequence, they developed a new correlation to predict the average Nusselt numbers for 6000<Re<180000.

Yildiz, Bicer, and Pehlivan (1995) proposed two heat transfer correlations to predict the Nusselt number for air-flow in helical pipes by using regression analysis of experimental data. Their correlations have an error within ±10%.

Kumar, Saini, Sharma, and Nigam (2006) measured heat transfer coefficients for hot water flow in a tube-in-tube helical heat exchanger having outer tube diameter of 0.0508 m, inner tube diameter of 0.0254 m, inner tube coil diameter of 0.762, and number of turns of 4. The experimental results were compared with their numerical model, and predicted values by Kalb and Seader correlation and Manlapaz and Churchill correlation (Kalb and Seader, 1972; Manlapaz and Churchill, 1981). They found that the numerical results agree fairly well with the measurements with maximum difference of 4%. However, the experimental values were higher than that predicted values in terms of Kalb and Seader and Manlapaz and Churchill correlations.

Sivashanmugam, Nagarajan, and Suresh (2008) proposed an empirical heat transfer correlation based on their experiments for turbulent water flow in through a circular tube fitted with right and left helical screw-tape inserts. An empirical correlation for Nusselt number was developed and found to fit the experimental data within 10%.

Spiral tubes

Naphon and Wongwises (2002) measured the average in-tube heat transfer coefficients of water in a spiral-coil heat exchanger having a steel outer tube with a spirally coiled copper tubes. Each tube was constructed by bending a 9.27 mm diameter straight copper tube into a spiral-coil are 6.77 and 22.76 cm in diameter, respectively. The experimental results were compared with existing heat transfer correlations proposed by Dravid, Kalb and Seader, and Xin and Ebadian (Dravit et al., 1971; Kalb and Seader, 1974; Xin and Ebadian, 1997). It was found that three different correlations poorly matched the experimental data. The data were lie within ±25% for the Dravid correlation, -20% to +30% for the Kalb and Deader correlation, and +50% for the Xin and Ebadian correlation. In addition, they modified the Kalb Seader correlation and found that the majority of the experimental data fall within ±10% of predicted values by the modified correlation.

Pressure drop correlations without oil

Helical tubes

Kumar et al. (2006) measured friction factors for hot water flow in a tube-in-tube helical heat exchanger. The experimental results were compared with their numerical model and predicted values by the White correlation (White, 1979) and Mishra and Gupta correlation (Mishra and Gupta, 1979). They found that the numerical results agree fairly

well with the experimental results and were in good agreement with predicted values by both the White correlation and the Mishra and Gupta correlation.

Sivashanmagam *et al.* (2008) proposed an empirical friction factor relating Reynolds number based on their experimental data for turbulent water flow through a circular tube fitted with right and left helical screw-tape inserts. This empirical friction factor was found to fit the experimental data within 20%.

Summaries of heat transfer and pressure drop correlations for single phase flow proposed by many authors are presented in Table 2.6 and 2.7 respectively.

Table 2.6: Single phase heat transfer correlations without oil

Authors	Conditions	Working fluids	Recommended or proved by	Results
	Conventional smooth tubes			
Petuhov (1970)	Circular tubes Turbulent flow	-	Webb and Zhang (1997)	Acceptable
	Extruded aluminium tubes with and without micro-fin	R-134a, R-12	Yang (1996)	Acceptable
Dittus and Boelter	D_h = 7.92 mm Re > 10,000 Re ≤ 9,000	water	Wang et al. (1996)	Acceptable Not acceptable
	D_i = 100 and 50 mm Compressible flow	gas	Chen and Kuo (2004)	Acceptable
Gnielinski	D_h = 7.92 mm $0.5 \leq Pr \leq 2{,}000$ $2{,}300 \leq Re \leq 5\times10^6$	water	Wang et al. (1996)	Acceptable
	Micro-fin tubes			
Wang et al. (1996) (modified Dittus and Boelter correlation)	D_i = 9.52, 7.94, 7.0 mm $2{,}500 \leq Re \leq 40{,}000$	water-		Deviation of ±10%
	Mini channel tubes			
Dittus and Boelter	Circular D_i = 0.76, 1.09 mm	water	Adams et al. (1997)	Not acceptable
	Smooth tubes D_i = 10, 5, 1 mm	gas	Chen and Kuo (2004)	Not acceptable
	D_i = 1.931, 1.042, 0.834, 0.531 mm	liquid N_2	Qi et al. (2007)	Not acceptable
	D_h = 0.96, 1.45, 2.13 mm	R-134a	Horiuchi (1995)	Acceptable

Table 2.6: Continued

Authors	Conditions	Working fluids	Recommended or proved by	Results
Petuhov (1970)	Circular D_i = 0.76, 1.09 mm	water	Adams et al. (1997)	Not acceptable
	D_h = 1.31	liquid R-134a	Webb and Zhang (1998)	Acceptable
Gnielinski	D_i = 1.931, 1.042, 0.834, 0.531 mm	liquid N_2	Qi et al. (2007)	Not acceptable
	Mini channel tubes (continued)			
Adams et al. (1997)	Circular D_i = 0.102 – 1.09 mm 2,600 ≤ Re ≤ 23,000 1.53 ≤ Pr ≤ 6.43	water	-	Deviation of ±18.6% Acceptable
Qi et al. (2007)	D_i = 1.931, 1.042, 0.834, 0.531 mm	liquid N_2	-	Deviation of ±6.4% Acceptable
	Curved tubes			
Seban and Melaughlin (1963)	Helically coiled tubes 6,000 ≤ Re ≤ 60,000 Re > 60,000	steam	Guo et al. (1998)	Acceptable Not acceptable
Guo et al. (1998)	Helically coiled tubes Re > 60,000	steam	-	Acceptable
Yildiz et al. (1995)	Helically coiled tubes	air	-	Deviation of ±10%
Sivashanmugam et al. (2008)	Circular tube fit with right and left helical screw-tape inserts for turbulent flow	water	-	Deviation of ±10%
Kalb and Seder (1972) **Manlapaz and Churchill (1981)**	Tube in tube helical tube D_i (tube) = 0.0354 m D_i (coil) = 0.762 Number of turns = 4	water	Kumar et al. (2006)	Not acceptable
Dravit et al. (1971)	Intube spirally coiled tubes	water	Naphon and Wongwises (2002)	Deviation of ±25%
Kalb and Seader (1974)	Intube spirally coiled tubes	-	Naphon and Wongwises (2002)	Deviation of -20% to +30%
Xin and Ebadian (1997)	Intube spirally coiled tubes	-	Naphon and Wongwises (2002)	Deviation of +50%
Naphon and Wongwises (2002)	Intube spirally coiled tubes	water	-	Deviation of ±10%

Table 2.7: Single phase pressure drop correlations without oil

Authors	Conditions	Working fluids	Recommended or proved by	Results
	Conventional smooth tubes			
Blasius	Circular tubes Turbulent flow	-	Webb and Zhang (1997)	Acceptable
	Smooth tube D_h = 1.31	R-134a	Webb and Zhang (1997)	Accebtable
	D_h = 0.96, 1.45, 2.13 mm	R-134a	Horiuchi (1995)	Acceptable
	Micro-fin tubes			
Wang et al. (1996)	D_i = 9.52, 7.94, 7.0 mm 2,500 ≤ Re ≤ 40,000	water	-	Deviation of ±10%
	Mini channel tubes			
Nikuradse	D_i = 1.931, 1.042 mm 10,000 ≤ Re ≤ 90,000	liquid N_2	Qi et al. (2007)	Acceptable
	D_i = 0.834, 0.531 mm 10,000 ≤ Re ≤ 90,000	liquid N_2	Qi et al. (2007)	Not acceptable
Colebrook	D_i = 1.931, 1.042 mm 10,000 ≤ Re ≤ 90,000	liquid N_2	Qi et al. (2007)	Acceptable
	D_i = 1.931, 0.531 mm 10,000 ≤ Re ≤ 90,000	liquid N_2	Qi et al. (2007)	Acceptable
	Curved tubes			
White (1979)	tube in tube helical heat exchanger	water	Kumar et al. (2006)	Acceptable
Mishra and Gupta (1979)	tube in tube helical heat exchanger	water	Kumar et al. (2006)	Acceptable
Sivashanmagam et al. (2008)	a circular tube fitted with right and left helical screw-tape inserts	water	-	Deviation of ±20%

2.12.1.2 Condensation (Two phase) flow regions

Condensation heat transfer was first studied by Nusselt (1916) based on a simple balance between gravity and shear on an element of the condensate in a vertical plate. Condensation heat transfer in tubes was found to depend on flow patterns from vapour inlet to outlet (Bell, Taborek, & Fenoglio, 1970; Breber, Palen, & Taborek, 1980; Palen, Breber, & Taborek, 1979). However, it is very difficult to predict heat transfer coefficient in the condensation region; therefore, identification of flow patterns in order to predict heat transfer coefficients and pressure drops during condensation is very important. Most approaches to identify flow patterns are in form of flow maps or graphs (Baker, 1954; Jaster & Kosky, 1976; Soliman & Azer, 1971; Taitel & Dukler, 1976; Tandon, Varma, & Gupta, 1982; Traviss & Rohsenow, 1973; Weisman, Duncan, Gibson, & Crawford, 1979). However, each flow map is only valid for its particular conditions.

2.12.1.2.1 Flow maps

The early studies about flow maps for condensation in horizontal tubes were undertaken by Breber et al. (1980); Soliman and Azer (1974); Tandon et al. (1982). These flow maps have been used and modified by many researchers in order to predict heat transfer coefficients and pressure drops, which are relevant to their applications.

To consider for fundamental flow regimes in horizontal two phase flow (Fig. 2.30) as described by Dobson et al. (1994), the vapor-shear controlled flow and the gravity controlled flow are the main factors that have most influence on condensation flow in horizontal tube. If the vapor velocity is low, the flow pattern is dominated by the gravity controlled flow. As a consequence, the vapor condenses primarily on the top portion of the tube and condensate flows downward into a liquid pool which is driven out axially partly by the vapor flow and partly by a gravitational head. Classification of flow regimes is also defined in the terms of void fraction which is a measure of the void space in a material, and is a ratio of the volume of voids to the total volume. For high void fractions, flow pattern is sub-divided by five flow regimes: stratified flow, wavy flow, wavy annular flow, annular flow, and annular-mist flow. In the other hand, at low void fractions, flow patterns include slug, plug, and bubbly flow. For the high void fraction flow patterns, stratified flow and wavy flow are dominated by gravity; wavy annular flow is dominated by both gravity and vapor shear while annular flow and annular-mist flow are dominated by vapor shear. The three flow regimes in the low void fraction flow pattern are formed such that the transition from one flow regime to the next corresponds to an increase in the liquid inventory.

The early flow map to predict flow patterns during condensation in horizontal tube for high density components as refrigerants was proposed by Taitel and Dukler (1976). The map includes five flow regimes: stratified smooth, stratified wavy, annular, intermittent (plug and slug), and dispersed bubble (Fig. 2.31). However, this map is valid for a limited range of diameter of horizontal tubes.

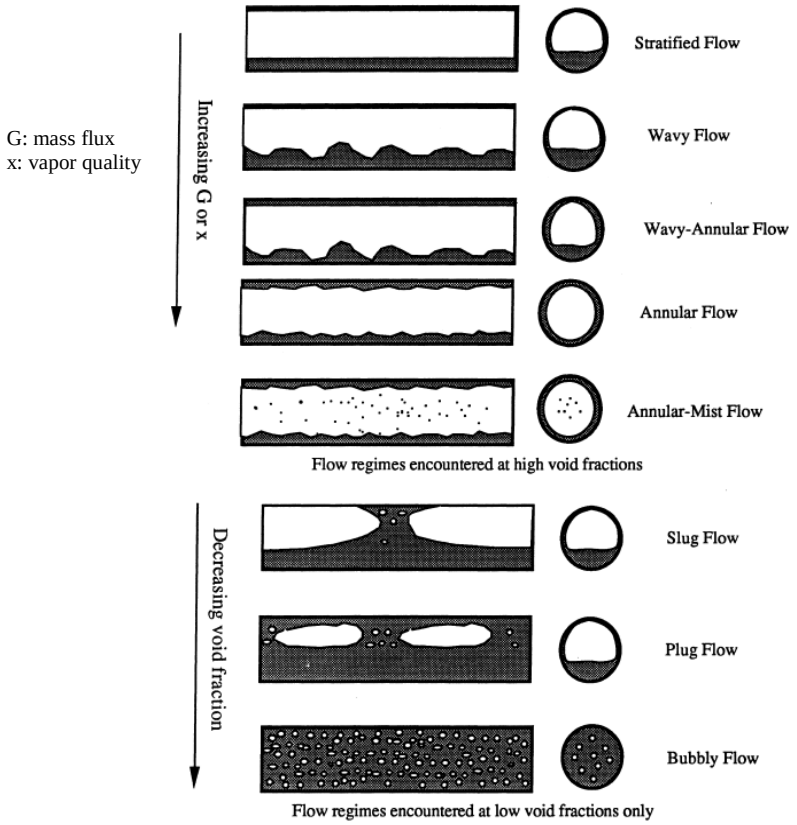

Figure 2.30: Flow regimes typically encountered in condensation processes (Dobson *et al.*, 1994)

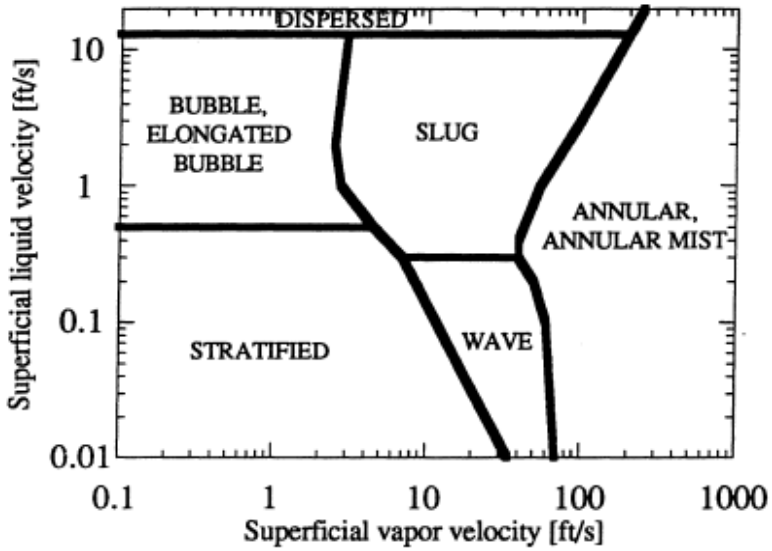

Figure 2.31: The flow regime map of Mandhane *et al.* (1974)

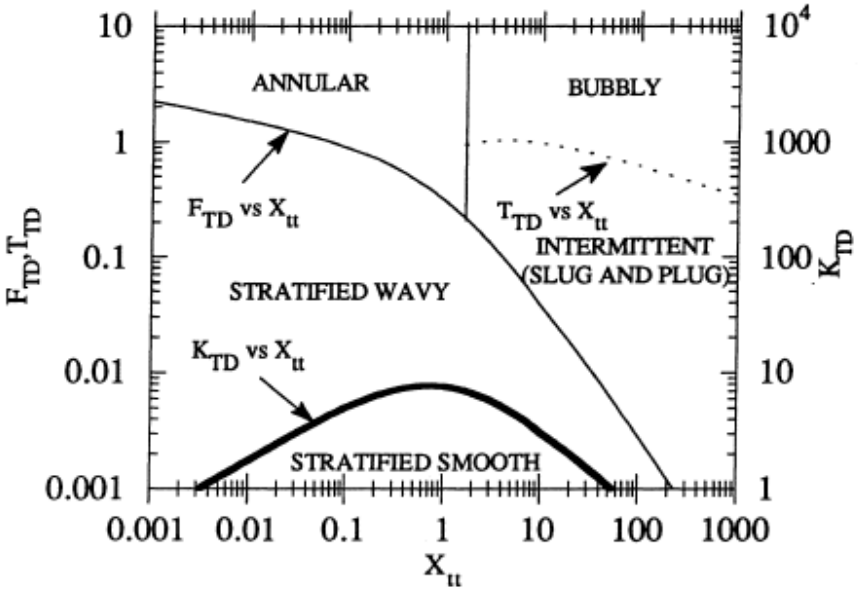

Figure 2.32: Flow regime map of Taitel-Dukler (1976) for horizontal flow with both phases flowing turbulently

2.12.1.2.2 Heat Transfer and pressure drop correlations without oils

Generally, prediction of heat transfer coefficients is in the form of heat transfer correlations based on the Nusselt correlation (Nusselt, 1916), which is valid for each flow regime. Most correlations proposed are based on gravity force or shear stress in analysis. Heat transfer coefficients during condensation dominated by gravity force is for stratified, wavy, and slug flow regions while that dominated by shear stress is usually for annular flow regions.

Some early heat transfer correlations during condensation in horizontal tubes for the gravity-driven flow were proposed by Chato (1962); Jaster and Kosky (1976); Rosson and Meyers (1965); Tien, Chen, and Peterson (1988). For the shear flow regimes, heat transfer correlations are usually based on three approaches: two-phase multiplier approaches (Cavallini & Zecchin, 1974; Shah, 1979), shear-based approaches (Chen, Gemer, & Tien, 1987; Soliman, 1986), and boundary layer approaches (Dukler, 1960; Traviss, Rohsenow, & Baron, 1973).

Recently, Dalkilic and Wongwises (2009) reviewed condensation heat transfer and pressure drop correlations inside smooth and enhanced tubes proposed by many authors. In addition, an intensive review of heat transfer and pressure drop correlations of refrigerants inside horizontal enhanced tubes was presented by Cavallini *et al.* (2000).

2.12.1.2.2.1 Conventional channels

Heat transfer correlations

Dobson and Chato (1998) developed heat transfer correlations during condensation in smooth horizontal tubes with diameters ranging from 3.14 mm to 7.04 mm for R-12, R-22, R-134a, and near-azeotropic blends of R-32/R-125 with 50/50 and 60/40 compositions with a saturation temperature range of 35 to 45^{o}C. Heat transfer correlations in both the gravity-dominated flow regimes and the shear-dominated flow regimes successfully predicted data from several other sources. In addition, they found that heat transfer coefficients in this regime were independent of temperature difference between wall and refrigerants but very dependent on mass flux and quality.

Cavallini *et al* (2001) measured heat transfer coefficients during condensation inside a smooth tube for pure HFC refrigerants (R134a, R125, R236ea, R32) and the near azeotropic HFC refrigerant blend R410A in order to compare with predictions from the Kosky and Staub's correlation (Kosky & Staub, 1971) for the annular flow regimes and the Jaster and Kosky's correlation (Jaster & Kosky, 1976) for the gravity-dominated flow regimes. The experimental runs were carried out at a saturation temperature ranging between 30^{o}C and 50^{o}C, and mass velocities varying from 100 to 750 kg/(m^{2} s), over the vapour quality range 0.15-0.85. They concluded that the Kosky and Staub' correlation and the Jaster and Kosky' s correlation are valid for the annular flow regimes and the gravity-dominated flow regimes and can accurately predict condensation heat transfer coefficients even for the new high pressure HFC fluids.

Jung, Song, Cho, and Kim (2003) modified Dobson and Chato's correlation in order to predict condensation heat transfer coefficients on a horizontal plain copper tube for R12, R22, R32, R123, R125, R134a, and R142b with an outside diameter of 9.52 mm and 1 m length with a fixed saturation temperature of 40^{o}C. Their new correlation showed a mean deviation of 10.7% for all pure halogenated refrigerants' data obtained in this study.

Kim and Shin (2005) measured condensation heat transfer coefficients for R-22 and R-410A refrigerants flowing inside a 9.52 mm outer diameter smooth tube in order to compare (only R-22) with the Dobson and Chato correlation, the Shah correlation and the Akers *et al.* correlation. The measured heat transfer coefficients are in agreement with the Shah correlation within the absolute mean deviation of 15.6%. In addition, they found that the temperature profile of R-22 during condensation was similar to that of R-410A.

Cavallini *et al* (2006) proposed a new heat transfer correlation during condensation in a smooth tube having inside diameter more than 3 mm based on a simple flow regime. The flow regime is considered by two regions: ΔT independent involved with wavy and annular flow and ΔT dependent involved with stratified flows. Predicted values were compared with experimental data obtained from many authors. They found good agreement except for R-410A refrigerant.

Pressure drop correlations

Webb and Zhang (1997) surveyed methods to pressure drop predictions during condensation in plain tubes. They found that Moser, Webb, and Na (1998) have developed a condensation correlation described as the "equivalent Reynolds number concept" and used the Friedel correlation to predict the two-phase friction pressure gradient for single, round tubes having of 3.14 to 20 mm inside diameter. Moser et al. results showed that local and average condensation data were predicted within 14%. In addition, Webb and Zhang (1997) used the "equivalent single-phase Reynolds number model" with the pressure gradient predicted by Friedel equation in order to predict pressure drops during condensation flow of the R134a at 40 and 65^{o}C on three different tubes with port diameters of 0.96, 1.45, and 2.13 mm. They suggest that the Friedel equation does not accurately predict R-134a pressure gradient at high saturation temperature (65^{o}C) for round tube diameters below 2.13 mm.

Cavallini *et al.* (2001) compared experimented pressure drop values with predictions by the Friedal correlation (the single-phase friction factor is estimated from Blausius equation and the Friedel equation is applied by using the correction of Mickley, Ross, Squyers, and Stewart (1954) during condensation flow inside a horizontal tube (8 mm in diameter) for HFC refrigerants (R134a, R125, R236ea, R32, R410A) at a saturation temperature ranging between 30 and 50^{o}C, and mass velocities varying from 100 to 750 kg/(m^{2} s), over the vapour quality range 0.15 – 0.85. They found that the Friedel correlation seems to slightly overestimate the experimental pressure drop for high pressure fluids and underestimate it for low pressure fluids at high mass velocities.

Ould Didi, Kattan, and Thome (2002) measured two-phase pressure drop for evaporation in two horizontal test sections of 10.92 and 12 mm diameter for five refrigerants (R-134a, R-123, R-402A, R-410A and R-502) over mass velocities from 100 to 500 kg/m^{2}.s and vapour qualities from 0.04 to 1.0. Their experimental data were compared against the predicted values obtained by seven two-phase frictional pressure drop correlations. They found that the best available correlation for annular flow was the Muller-Steinhagen and Heck correlation (Muller-Steinhagen & Heck, 1986) whereas the best correlation for intermittent and stratifiedwavy flows was Gronnerud (1979).

2.12.1.2.2.2 Micro-fin channels

Heat transfer correlations

In order to increase heat transfer performance of heat exchangers, increasing the area of conventional smooth tubes by adding fins may be successful. Many authors showed enhancement of heat transfer coefficient when adding micro-fins in conventional smooth tubes (Fujie et al., 1977; Schlager, Pate, & Bergles, 1989; Chamra, Webb, & Randlett, 1996; Wijaya & Spatz, 1994; Dunn, 1996; Uchida *et al.*, 1996; Nualboonrueng *et al.*, 2003; Kim & Shin, 2005). Mostly, micro-fin tubes gave heat transfer coefficients higher than equivalent smooth tubes at the same operating conditions from 80 to 180% while a

pressure drop increase from 20 to 80% (Cavallini *et al.*, 2000). Generally, micro-fin tube have an outside diameter between 4 and 15 mm having a single set of 50-70 spiral fins with spiral angle between 6^o and 30^o and a height between 0.1 and 0.25 mm (Han & Lee, 2005). As a consequence, heat transfer correlations for micro-fin tubes were often based on extensions of smooth-tube correlations.

Many authors have proposed heat transfer correlations to predict condensation heat transfer coefficients for refrigerants condensing inside micro-fin tubes (Luu & Begles, 1980; Cavallini *et al*., 1995; Yu & Koyama, 1998; Shikazono *et al.*, 1998; Wang et al., 2002)

Wang and Honda (2003) studied about condensation heat transfer coefficients of refrigerants flowing inside micro-fin tubes. The heat transfer coefficients calculated by Luu and Bergless (1980), Cavallini *et al*. (1995), Yu and Koyama (1998), Shikazono *et al.* (1998) and Wang *et al.* (2002) correlations were compared to the experimental data for six different micro-fin tubes and five refrigerants (R11, R123, R134a, and R410A). The results showed that the root mean square error (r.m.s) for all tubes and all refrigerants decreased in the order of the correlations proposed by Luu & Begles (1980), Cavallini *et al.* (1995); Yu & Koyama (1998); Shikazono *et al.* (1998); Wang *et al.* (2002).

Cavallini *et al.* (2009) proposed a new simple model for prediction of heat transfer coefficient to be applied to condensation in horizontal micro-fin tubes of halogenated and natural refrigerants, pure fluids or nearly azeotropic mixtures. The model has been developed from an extensive analysis of experimental heat transfer data points and it is considered in two regions similar to the previous work (Cavallini *et al.*, 2006): ΔT independent and ΔT dependent. In order to validate their model, the predicted values were compared with the experimental data from several independent laboratories. The results showed that an average deviation, an absolute mean deviation, and a standard deviation are 3.2%, 16.5%, and 21.9% respectively.

Pressure drop correlations

Pressure drop correlations for micro-fin tubes were often based on extensions of smooth-tube correlations. A review of two-phase pressure drop correlations was presented by Newell and Shah (2001).

Han and Lee (2005) investigated the pressure drop penalty factors during condensation flow inside four micro-fin tubes for three refrigerants (R-134a, R-22 and R-410A). The pressure drop factors are the pressure drop ratio of the micro-fin tube to the smooth tube at the same maximum inside diameter and operating condition. The Muller-Steinhagen and Heck correlation was used to evaluate the corresponding smooth tube pressure drop. Based on the experimental data, in addition, they proposed a correlation for the four tested micro-fin tubes with the heat momentum relation.

2.12.1.2.2.3 Micro channels

Heat transfer correlations

Micro-channel heat exchangers are now of interest in many applications in industry including heat exchangers for heat pump water heaters as they are more compact and lighter weight; furthermore, they are effective in heat transfer compared to normal tube heat exchangers. However, existing flow maps and heat transfer correlations may be invalid for condensation flow in micro-channel tubes. As a consequence, few papers have been proposed to predict flow regimes and heat transfer correlations during condensation flow in the micro-channel tubes based on existing flow regimes and heat transfer correlations.

Wang, Radcliff, and Christensen (2002) showed comparison between existing heat transfer correlations and their experimental data for condensation flow of HFC-134a inside a horizontal rectangular multi-port aluminium condenser tube of 1.46 mm hydraulic diameter. They found that the Akers and Rosson correlation (Akers & Rosson, 1960) provided reasonable predictions at high mass flux whereas the correlations proposed by Azer, Abis, and Soliman (1972); Cavallini and Zecchin (1974); Chen, Gemer, and Tien (1987); Dobson and Chato (1998); Shah (1979); Traviss and Rohsenow (1973) did not accurately predict. Likewise, only the Jaster and Kosky (1976) correlation gave an acceptable prediction at low mass fluxes.

Wang *et al.* (2002) also observed condensation flow regimes for comparison with the flow maps of Breber and Soliman transitions. They found that Breber's criteria predicted the wavy and slug flows fairly well; however, the transition from stratified to annular flow was observed to occur at superficial velocity (j_v^*) of 0.24 m/s instead of the 0.46 m/s predicted. They reasoned that the small cross-section may draw the condensate liquid into the corners, forming an annular liquid film at lower vapour velocity than in the large-diameter round tubes that were the basis of the Breber's map. For Soliman's map, the transition between stratified and annular flow was well predicted at qualities higher than 30%; however, at lower qualities the transition occurred at a smaller mass flux than that predicted by Soliman. They reasoned that this is generally consistent with the comparison of the data with the Breber model, presumably for the same reason. Further, they also observed that the transition from annular to mist flow did not appear in the presented data.

Bandhauer, Agawal, and Garimella (2006) measured heat transfer coefficients during condensation of refrigerant R134a in horizontal microchannels having hydraulic diameter of between 0.506 and 1.524 mm with 0 to 100% vapour quality and 150 to 750 kg/m^2 s mass flux. They summarized that heat transfer coefficient increases between 10% and 40% for more than 45% vapour quality as a hydraulic diameter is reduced from 1.524 mm to 0.506 mm. This effect is more prominent for a decrease in hydraulic diameter from 0.761 mm to 0.506 mm. In addition, they compared heat transfer coefficients measured with predictions from available correlations. Comparison with correlations based on two phase multiplier approaches: modified from Dittus-Boelter equation

(Cavallini & Zecchin, 1974; Shah, 1979) and a modified version of the equivalent Reynolds number analysis by Akers *et al.* (Moser, Webb, & Na, 1998), showed that the Moser *et al.* correlation does a reasonably good job of predicting the present data (14% deviation). When compared with correlations based on the homogeneous flow (annular flow) they observed that the homogeneous flow correlation of (Boyko & Kruzhilin, 1967) and the mist flow correlation of (Soliman, 1986) are better at predicting the current data (13% and 23% average deviation, respectively). Further, they also showed a comparison of the data with the predictions of shear-dominated flow correlations using boundary layer treatments. The Soliman et al. correlation (Soliman, Schuster, & Berenson, 1968) and the Chen and Kocamustafaogullari (Chen & Kocamustafaogullari, 1987) are acceptable with average deviation of 18% and 13% respectively while the Traviss *et al.* correlation (Traviss *et al.*, 1973) and Traviss and Rohsenow correlation (Traviss & Rohsenow, 1973) showed the largest average deviation (38%).

Pressure drop correlations

Cavallini *et al.* (2005) showed measured pressure drops during condensation flow of HFC refrigerants (R236ea, R134a and R410A) in a 1.4 hydraulic diameter multiport minichannel tube at 40^{o}C saturation temperature, mass velocities ranging from 200 to 1400 kg/(m^2 s), and three values of vapour quality (0.25, 0.5, and 0.75 with variations of 0.01-0.02) in order to compare with prediction values by available pressure drop correlations: (Lockhart & Martinelli, 1949), (Friedel, 1979), Chen *et al.* (2001), (Zhang & Webb, 2001), (Mishima & Hibiki, 1996), (Yang & Lin, 1999), and (Muller-Steinhagen & Heck, 1986). They concluded that the correlations by Friedel *et al.*, Zhang and Webb, Mishima and Hibiki, and Mueller-Steinhagen and Heck are in good agreement with the R-134a experimental data. The R236ea data are in good agreement with the predictions by Mueller-Steinhagen and Heck. For the R410A data, all the correlations tend to overpredict the experimental values. Among the models, the correlation by Zhang and Webb had the lowest deviation.

Summaries of two-phase heat transfer and pressure drop correlations for refrigerants without oils proposed by many authors are presented in Table 2.8 and 2.9 respectively.

2.12.1.2.3 Effect of lubricating oil

In practice, the compressor normally uses oil for lubricating, cooling and sealing purposes. When the compressor discharges the refrigerant, small amounts of lubricating oil is also discharged along with the refrigerant. As a consequence, this oil flows through condenser, expansion device, and evaporator and finally returns to the compressor. Therefore, small amounts of lubricating oil may affect the heat transfer performance during flow through heat exchangers.

Many authors data confirm that refrigerant with small amounts of oils can reduce heat transfer coefficients during condensation inside tubes (Tichy, Macken, & Duval, 1985; Schlager, Pate, & Bergles, 1990; Sur and Azer, 1991)

Shao and Granryd (1995) reported the results of condensation heat transfer and pressure drop from tests with pure and oil contaminated refrigerant HFC134a in a horizontal tube having 10 m length and 6 mm inside diameter. They concluded that the condensation heat transfer coefficients of oil-refrigerant mixture based on the mixture saturation temperature are reduced by on average 10-20%, depending on oil concentrations, compared with pure refrigerant. However, if the pure refrigerant is used to determine the saturation temperature, the heat transfer coefficients of oil-refrigerant mixture are not found to be reduced significantly, compared with pure refrigerant. The pressure drop of oil-HFC134a is increased by approximately 20% in comparison with pure HFC134a according to the results in their investigation.

Further, Shao and Granryd (1995) compared the experimental and predicted heat transfer coefficients. They summarized that Tandon *et al.* correlation (Tandon, Varma, and Gupta, 1995) and modified Tandon *et al.* correlation (Shao and Granryd, 1995) predict very well for pure refrigerant while the oil-refrigerant mixture can be predicted fairly well by their proposed correlations.

Bassi and Bansal (2003) showed a comparative study of the condensation heat transfer coefficients in a smooth tube having 3.125 mm inside diameter and 3.5 mm outside diameter with pure refrigerant R134a and its mixture with lubricant oil (synthetic polyol ester oil). Two concentrations of R134a-oil mixtures of 2% and 5% oil (by mass) were used for a range of saturation temperature of refrigerant R134a between 35^{o}C and 45^{o}C, a vapour quality varying between 1.0 and 0, and a constant mass flow rate of 1 g/s. The contamination of R134a with the lubricant oil resulted in a decrease in the in-tube condensation heat transfer coefficient. The coefficient decreased respectively by 5% and 10% when R134a was mixed with 2% and 5% oil (by mass).

In addition, Bassi and Bansal (2003) showed a comparison of the experimental and predicted heat transfer coefficients from earlier models (Shah, 1979; Cavallini and Zecchin, 1974; Traviss et al., 1972; Dobson and Chato, 1998). They found that the model of Cavallini and Zecchin was the best and predicted the in-tube condensation heat transfer coefficient for pure R134a to within 8%. Models of Shah and Dobson disagreed by up to 20% with the experimental values. Finally, they developed two models for predicting condensation heat transfer coefficients for pure R134a and for a mixture of refrigerant R134a with the oil, which predict the heat transfer coefficients to within 3-13% and 2-11% respectively.

Table 2.8: Two phase heat transfer correlations without oil

Correlations	Conditions	Working fluids	Recommended or proved by	Results
	Conventional smooth tubes			
Akers et al. (1959)	D_o = 9.52 mm 0.1 $\leq x \leq$ 0.9 156 $\leq x \leq$ 0.9 kg/m^2.s Tsat = 45 ^{o}C	R-22	Kim and Shin (2005)	Deviation of –16.4%
Kosky and Staub (1971)	30 ^{o}C $\leq T_{sat} \leq$ 50 ^{o}C 100 $\leq m'' \leq$ 750 kg/(m^2.s) 0.15 $\leq x \leq$ 0.85 For annular flow regime	R-134a, R-125, R-238ea, R-32, R-410A	Cavallini et al. (2001)	Acceptable
Jaster and Kosky (1976)	30 ^{o}C $\leq T_{sat} \leq$ 50 ^{o}C 100 $\leq m'' \leq$ 750 kg/(m^2.s) 0.15 $\leq x \leq$ 0.85 For the gravity dominated flow regime	R-134a, R-125, R-238ea, R-32, R-410A	Cavallini et al. (2001)	Acceptable
Shah (1979)	D_o = 9.52 mm 0.2 $\leq x \leq$ 0.9 156 $\leq x \leq$ 0.9 kg/m^2.s Tsat = 45 ^{o}C	R-22	Kim and Shin (2005)	Deviation of 15.6%
Dobson and Chato (1998)	3.14 mm $\leq D_i \leq$ 7.04 mm 35 ^{o}C $\leq T_{sat} \leq$ 45 ^{o}C	R-12, R-22, R-134a, R-32/R-125	-	Acceptable
	D_o = 9.52 mm 0.3 $\leq x \leq$ 0.9 156 $\leq x \leq$ 0.9 kg/m^2.s Tsat = 45 ^{o}C	R-22	Kim and Shin (2005)	Deviation of 19.8%
Jung et al. (2003)	D_o = 9.52 mm L = 1 m T_{sat} = 40 ^{o}C	R-12, R-22, R-32, R-123 R-125, R-134a, R-142b	-	Deviation of ±10.7%
Cavallini et al. (2006)	D_i > 3 mm ΔT independent or ΔT dependent flow $P_{RED} \leq$ 0.8	HCFCs, HFCs, HCs, CO_2, NH_3, H_2O	-	Deviation of 14% (Mean)

Table 2.8: (Continued)

Correlations	Conditions	Working fluids	Recommended or proved by	Results
	Micro-fin tubes			
Luu and Bergles (1980)		R-134a		Deviation of 40.25%
		R-410A		Deviation of 49.6
Cavallini et al. (1995)		R-134a		Deviation of 16.1%
		R-410A		Deviation of 37%
Yu and Koyama (1998)	$6.49 \leq D_i \leq 8.88$ mm $0.16 \leq$ fin height ≤ 0.24 mm $0.34 \leq$ fin picth ≤ 0.53 mm $12^o \leq$ helix angle $\leq 20^o$ $94 \leq G \leq 459$ kg/m^2.s	R-134a	Wang and Honda (2003)	Deviation of 16.3%
		R-410A		Deviation of 16%
Shikazono et al. (1998)		R-134a		Deviation of 32.2%
		R-410A		Deviation of 25%
Kedzierski and Goncalves (1980)		R-134a		Deviation of 26%
		R-410A		Deviation of 13.7%

Table 2.8: (Continued)

Correlations	Conditions	Working fluids	Recommended or proved by	Results
	Micro-fin tubes (continued)			
Wang et al. (2002)	$6.49 \leq D_i \leq 8.88$ mm $0.16 \leq$ fin height ≤ 0.24 mm $0.34 \leq$ fin picth ≤ 0.53 mm $12^o \leq$ helix angle $\leq 20^o$ $94 \leq G \leq 459$ kg/m^2.s	R-134a		Deviation of 10.2%
		R-410A	Wang and Honda (2003)	Deviation of 17.1%
Cavalini et al. (2009)	$h/D < 0.04$ $0^o \leq$ helix angle $\leq 30^o$ $0.1 \leq P_{RED} \leq 0.67$	HCFCs, HFCs, CO_2,	-	Deviation of 14% (Mean)
	Mini-channel tubes			
Azer et al. (1997)	Horizontal rectangular multi-port Aluminium tube, $D_h = 1.46$ mm	R-134a	Wang et al. (2002)	Not acceptable
Cavallini and Zecchin (1974)				Not acceptable
Chen et al. (1987)				Not acceptable
Donson and Chato (1998)				Not acceptable
Shah (1979)				Not acceptable
Traviss and Rohsenov (1973)				Not acceptable
Akers and Rosson (1960)	Horizontal rectangular multi-port Aluminium tube, $D_h = 1.46$ mm For high mass flux	R-134a	Wang et al. (2002)	Acceptable
Jaster and Kosky (1976)	For low mass flux	R-134a	Wang et al. (2002)	Acceptable

Table 2.8: (Continued)

Correlations	Conditions	Working fluids	Recommended or proved by	Results
	Mini-channel tubes (continued)			
Cavallini et al. (1979)	$0.506\ mm \leq D_h \leq 1.524\ mm$ $0 \leq x \leq 1$ $150 \leq G \leq 750\ kg/(m^2.s)$	R-134a	Bandhauer et al. (2006)	Not acceptable
Moser et al. (1998)				Deviation of ±14%
Boyko and Kruzhilin (1967)				Deviation of ±13%
Soliman (1986)				Deviation of ±23%
Soliman et al. (1968)				Deviation of ±18%
Chen and Kocamustafaogullari (1987)				Deviation of ±18%
Traviss and Rohsenov (1973)				Deviation of ±38%

Table 2.9: Two phase pressure drop correlations without oil

Correlations	Conditions	Working fluids	Recommended or proved by	Results
	Conventional smooth tubes			
Moser et al. (1997)	Plain tubes 3.14 mm $\leq D_i \leq$ 20 mm	-	Webb and Zhang (1997)	Deviation of ±14%
Friedel (1979) **Using correction** **by Mickley et al. (1954)**	D_i = 8 mm 30 $^oC \leq T_{sat} \leq$ 50 ^oC $100 \leq G \leq 750$ kg/(m^2.s) $0.15 \leq x \leq 0.85$	R-134a, R-125, R-236ea, R-32, R-410A	Cavallini et al. (2001)	at high mass velocity slightly overestimate for high pressure fluid and high underestimate for low pressure
Friedel (1979)				Deviation of 12.79% (average)
Lockhart and Martinelli (1949)	D_i = 10.92 mm $100 \leq G \leq 500$ kg/(m^2.s) (boiling flow)	R-134a, R-123, R-402A, R-404A, R-502	Ould Didi et al. (2002)	Deviation of 63.44%
Chriholm (1973)	$0.04 \leq x \leq 1.0$			Deviation of 91.36
Gronnerrud (1979)				Deviation of –10.25%
Muller-Steinhagen and Heck (1986)				Deviation of –14.67%
	Micro-fin tubes			
Choi et al. (1999)				Deviation of 45.3% (r.m.s)
Nozu et al. (2000)				Deviation of 130.8% (r.m.s)
Haraguchi et al. (1993)				Deviation of 96.9% (r.m.s)
Kedzierski and Goncalves (1997)	$D_{i,max}$ = 8.92, 6.46, 5.1, 4 mm	R-134a, R-22, R-410A	Han and Lee (2005)	Deviation of 49.9% (r.m.s)
Nozu et al. (2000)				Deviation of 36.4% (r.m.s)
Haraguchi et al. (1993)				Deviation of 34.8% (r.m.s)
Kedzierski and Goncalves (1997)				Deviation of 32% (r.m.s)
Han and Lee (2005)				Deviation of 33.7% (r.m.s)

Table 2.9: (Continued)

Correlations	Conditions	Working fluids	Recommended or proved by	Results
	Mini-channel tubes			
Friedel (1979)	Multiport mini channel tube D_h = 1.4 mm T_{sat} = 40 ^oC 200 ≤ G ≤ 1400 kg/(m^2.s) 0.25 ≤ x ≤ 0.75	R-134a	Cavallini et al. (2005)	Acceptable
Webb and Zhang (1997)	Plain tubes D_i = 0.96, 1.45, 2.13 mm T_{sat} = 40 – 65 ^oC (equivalent single phase Re)	R-134a	-	Not acceptable
Chen et al. (2001)	Multiport mini channel tube D_h = 1.4 mm T_{sat} = 40 ^oC 200 ≤ G ≤ 1400 kg/(m^2.s) 0.25 ≤ x ≤ 0.75	R-134a	Cavallini et al. (2005)	Acceptable
Zhang and Webb (2001)	Multiport mini channel tube D_h = 1.4 mm T_{sat} = 40 ^oC 200 ≤ G ≤ 1400 kg/(m^2.s) 0.25 ≤ x ≤ 0.75	R-134a	Cavallini et al. (2005)	Acceptable
Mishima and Hibiki (1996)	Multiport mini channel tube D_h = 1.4 mm T_{sat} = 40 ^oC 200 ≤ G ≤ 1400 kg/(m^2.s) 0.25 ≤ x ≤ 0.75	R-134a	Cavallini et al. (2005)	Acceptable
Yan and Lin (1999)	Multiport mini channel tube D_h = 1.4 mm T_{sat} = 40 ^oC 200 ≤ G ≤ 1400 kg/(m^2.s) 0.25 ≤ x ≤ 0.75	R-134a	Cavallini et al. (2005)	Acceptable
Muller-Steinhagen and Heck (1986)	Multiport mini channel tube D_h = 1.4 mm T_{sat} = 40 ^oC 200 ≤ G ≤ 1400 kg/(m^2.s) 0.25 ≤ x ≤ 0.75	R-134a R-236ea	Cavallini et al. (2005)	Acceptable

2.12.2 Transcritical cooling processes

In the last decade, heat pump water heaters using the CO_2 transcritical cycle has been researched. However, few researchers have proposed heat transfer correlations and pressure drop correlations during heat transfer in the water heating heat exchanger. Most used pure CO_2 as the working fluid for investigation.

2.12.2.1 CO_2 cooling processes without oil

A few studies on heat transfer coefficient and pressure drop correlations of carbon dioxide as refrigerant during cooling process (transcritical process) in tube with oil-free have been proposed in the last decade. Most correlations were developed based on experiment data so they are limited in the range of conditions they cover.

A critical literature review for heat transfer pressure drop correlations of carbon dioxide during cooling process in tube without oil was made by Pitla, Robinson, Groll, and Ramadhyani (1998). A few heat transfer coefficient correlations for supercritical carbon dioxide under cooling processes in single tubes of different diameter and multi-port channels were reviewed by Spindler (2006).

Transcritical single phase heat transfer coefficients and pressure drop for an enhanced tube (small size grooved tube) were twice that of a smooth tube with the same mean inner diameter (Dang *et al.*, 2008).

In the transcritical process for heating, the temperature gradient of carbon dioxide as it pass through the heat exchanger is not constant and it is very sensitive to other thermodynamic properties of the carbon dioxide, especially near the critical point. Therefore, gas-phase heat transfer correlations using bulk temperature of the carbon dioxide to calculate other parameters in the equations may be unsuited. In this case, using not only the bulk temperature of the carbon dioxide but also the wall temperature to calculate the other parameters may be more accurate. Many others (Krasnoshchekov et *al.*, 1970; Petrov & Popov, 1985; Pitla et *al.*, 2002; Fang et *al*, 2001; Yoon et *al.*, 2003; Son & Park, 2006; Liao & Zhao, 2002) proposed heat transfer correlations based on the wall temperature and/or the bulk temperature of the carbon dioxide. Most of them were modified from the single-phase correlations based on the bulk temperature proposed by Dittus and Boelter or Gnielinski equations.

As for the heat transfer correlations based on the wall temperature effect, the friction factors may be calculated by the equations proposed by Petrov and Popov (1985). However, some studies (Dang & Hihara, 2004; Son & Park, 2006) confirmed that the Blasius correlation can predict friction values well when compared with their experimental data.

In addition, Kato et *al.*, (2008) proposed empirical heat transfer and pressure drop correlations for a new microchannel heat exchanger for a hot water supply with S-shaped

fins, using supercritical carbon dioxide as the heating medium. Experiments were carried out under pressures of 9.5 to 12.5 MPa, flow rates of 25 to 70 kg/h, and inlet temperatures of 100 to 120°C for the S-CO_2 side, and flow rates of 20 to 50 kg/h and inlet temperatures of 7 to 25°C for the water side. They showed that their correlations have standard deviations of $\pm 2.3\%$ and 5.8 for the overall heat transfer coefficient and pressure drop respectively.

Dang *et al* (2008) presented experimental heat transfer coefficient and pressure drop values of supercritical carbon dioxide cooled inside a small size grooved tube at pressures in the range of 8 to 10 MPa and mass fluxes in the range of 400 to 1200 kg/m^2s. They found that the results for grooved tube are similar to the variation in heat transfer coefficients with bulk-temperature, pressure and mass flux observed for smooth tubes, which are proposed by previous authors (e.g. Dang & Hihara, 2004). In addition, these experimental results were compared with prediction models. The heat transfer coefficient model was adapted from the model for the smooth tube (Dang & Hihara, 2004) by incorporating the area enlargement ratio in the equation and with no effect of helix angle. The prediction of pressure drop was derived from the Filonenko equation (Gnielinski, 1976) by incorporating an area enlargement ratio in the equation. It was observed that the predicted results agreed with the experimental results. In the case of predicted heat transfer coefficients, approximately 97% of the 103 valid experimental data are within the ±20% accuracy limits, while in the case of predicted pressure drops, approximately 96% of experimental data have a deviation of less than ±20%.

Summaries of heat transfer and pressure drop correlations for CO_2 transcitical cooling process without oils are presented in Table 2.10 and 2.11 respectively.

2.12.2.2 Effect of lubricating oil

Dang, Iino, Fukuoka, and Hihara (2007) reviewed effects of lubricating oil on cooling heat transfer of supercritical carbon dioxide conducted by some authors (Zingerli & Groll, 2000; Gao & Honda, 2002; Mori, Onishi, Shimaoka, Nakanishi, & Kimoto, 2002; Kaneko, Ikeda, Tokiai, Yoshii, & Suto, 2006;).

The small amount of lubricant oils mixed in the pure refrigerants were shown to reduce the heat transfer coefficients significantly (Zinggerli and Groll, 2000; Kaneko et al., 2006; Gao & Honda, 2002; Mori et al. 2002)

Chaobin Dang, Koji Iino, Ken Fukuoka, and Eiji Hihara (2007) gave the experimental results of the cooling heat transfer coefficient and the pressure drop of supercritical CO_2 with the entrainment of a small amount of PAG-type lubricating oil. The inner diameter of the test tubes ranged from 1 to 6 mm. The experiments were conducted at oil concentrations from 0 to 5%, pressures from 8 to 10 MPa, mass fluxes from 200 to 1200 kg $m^{-2}s^{-1}$, and heat fluxes from 12 to 24 kW m^{-2}. From their experiments, they made four main conclusions. First, the flow pattern varies with the temperature, mass flux, and tube diameter. For a 2 mm ID tube at a low temperature, the oil flows in the bulk region with a

thickness from 50 to 100 μm. With an increase in the temperature, an oil-rich layer is observed in the near-wall region. For a 6 mm ID, the flow pattern was a separated wavy flow at a low mass flux, and it transformed into an annular-dispersed flow at a high mass flux. Second, for a large-sized tube with a mass flux lower than 400 kg $m^{-2}s^{-1}$, no significant difference in the heat transfer coefficient was observed until the oil concentration reach 1%. A sharp decrease occurred at an oil concentration approximately between 1 and 3%. A further increase in the oil concentration above 3% did not decrease the heat transfer coefficient significantly. Third, for small-sized tubes, the heat transfer coefficient dropped at lower oil concentrations. At an oil concentration of 1%, the heat transfer coefficient was 60% and 50% of that at the oil-free concentration for the 2 and 1 mm ID tubes, respectively. Fourth, the pressure drops for the 2 and 1 mm ID tubes did not increase significantly at an oil concentration of 1%. For the 2 mm ID tube, there was no difference between the pressure drops for the oil concentrations of 5% and 3%. However, for the 1 mm ID tube, the pressure drop increased monotonously with an increase in the oil concentration.

Dang, Iino, and Hihara (2008) proposed two-phase flow patterns of supercritical carbon dioxide with entrained PAG-type lubricating oil in a gas cooler by using a high-speed camera. The experiments were conducted with lubricating oil concentrations of 1 and 5 wt%, pressures between 8 and 10 MPa, and mass fluxes between 200 and 1200 kg $m^{-2}s^{-1}$. They concluded that for a 2 mm ID tube, mist flow, annular-dispersed flow and annular flow are observed. The flow pattern changes with the temperature. The mist-flow pattern occurs at low temperature. In the pseudocritical-temperature area, with an increase in temperature, the flow pattern seems change from an annular-dispersed flow to an annular flow. For a 6 mm ID tube at a low mass flux of 200 $kgm^{-2}s^{-1}$ wavy-dispersed flow and wavy flow are observed. At a high mass flux of 800 $kgm^{-2}s^{-1}$, usually, an annular-dispersed flow pattern is observed. In addition, they compared the flow pattern observations with the previous heat transfer measurements (Chaobin Dang, Koji Iino, K Fukuoka, & E Hihara, 2007). They found that the mechanism behind the heat transfer performance drop is mainly due to the formation of an oil film along the inner wall, and the oil droplets do not contribute significantly to the heat transfer deterioration.

Table 2.10: Transcritical heat transfer correlations without oil

Authors	Conditions	Working fluids	Recommended or used by	Results
Krasnoshchekov *et al.* (1969)	$9 \times 10^4 \leq Re_b \leq 3.2 \times 10^5$ $6.3 \times 10^4 \leq Re_w \leq 2.9 \times 10^5$	CO_2		
Petrov and Popov (1985)	$3.1 \times 10^4 \leq Re_b \leq 8 \times 10^5$ $1.4 \times 10^4 \leq Re_w \leq 7.9 \times 10^5$ $-350 \leq q_w \leq -29$ J/kg	CO_2		
Pitla *et al.* (2002)	Nu_b and Nu_w calculated by Gnielinski (1976) correlation	CO_2		
Fang *et al.* (2001)	$3500 \leq Re_w \leq 2.5 \times 10^4$ $-115 \leq q_w \leq -3$ J/kg	CO_2		
Liao and Zhao (2002)	$7.4 \leq P \leq 120$ MPa $20 \leq T_b \leq 110\ ^{O}C$ $20 \leq T_b - T_w \leq 110\ ^{O}C$ $0.02 \leq m \leq 0.2$ kg/min $10^{-5} \leq Gr/Re_b^2 \leq 10^{-2}$ $0.5 \leq D \leq 2.16$ mm for horizontal	CO_2		
Kato *et al.* (2008)	Microchannel tubes 9.5 MPa $\leq P \leq$ 12.5 MPa 100 ^{o}C $\leq T_{inlet} \leq$ 120 ^{o}C 25 kg/h $\leq m \leq$ 70 kg/h	CO_2	-	Deviation of 2.3%
Dang and Hihara (2004)	Small size grooved tubes 8 MPa $\leq P \leq$ 10 MPa 400 $\leq$ m" $\leq$ 1,200 kg/(m^2.s)	CO_2	Dang et al. (2008)	Deviation of 20%

Table 2.11: Transcritical pressure drop correlations without oil

Authors	Conditions	Working fluids	Recommended or used by	Results
Petrov and Popov (1985)	$3.1 \times 10^4 \leq Re_b \leq 8 \times 10^5$ $1.4 \times 10^4 \leq Re_w \leq 7.9 \times 10^5$ $-350 \leq q_w \leq -29$ J/kg	CO_2		
Kato et al. (2008)	Microchannel tubes 9.5 MPa ≤ P ≤ 12.5 MPa 100 $^oC \leq T_{inlet} \leq 120$ ^oC 25 kg/h ≤ m ≤ 70 kg/h	CO_2	-	Deviation of 5.8%
Gnielinski (1976) Derived from Filonenko equation	Small size grooved tubes 8 MPa ≤ P ≤ 10 MPa 400 ≤ m" ≤ 1,200 kg/(m^2.s)	CO_2	Dang et al. (2008)	Deviation of 20%
Blasius	Macro-scale channels	CO_2	Dang and Hihara (2004), Son and Park (2006)	Acceptable
	Micro-scale channels	CO_2	Pettersen et al. (2000)	Acceptable

2.13 Conclusions

Energy used in domestic hot water heaters is a major fraction of total energy used in New Zealand. In New Zealand, residential energy use is about 32% of total energy use and approximately 29% of residential energy use is used for hot water systems. Most hot water heaters in New Zealand are electrical heaters. These heaters are less than100% in energy efficiency.

Heat pump water heaters can be about 2-3 time more energy efficient than conventional hot water heaters. For this reason, they are a promising technology to use in domestic applications not only for energy saving but also for breaking an increased amount of CO_2 emission into the atmosphere based on fossil fuels used.

Air-source heat pump water heaters are suited for New Zealand due to the mild climate. These heaters are able to operate on either subcritical or transcritical cycles depending on alternative refrigerant used. HFCs, blends, and some natural refrigerants can be used in subcritical cycle as working fluids. CO_2 refrigerant is well suited for transcritical cycle for domestic applications.

When both cycles are compared it was found that the transcritical cycle can produce higher heating capacity and higher water temperature. Hot water temperature produced by subcritical cycle is limited by the critical temperature and condensation temperature of the refrigerant used. As a consequence, heat pump water heaters based on the transcritical cycle could operate well for instantaneous hot water supply systems. However, both cycles are suitable for domestic applications where the required hot water temperature is below 65^{o}C.

Instantaneous heat pump hot water supply systems are unsuited for domestic applications due to the variable hot water flowrates required. Standalone air-source heat pump water heaters are suitable for domestic applications combined with HWC. Stratified storage (one pass heating system) is suitable for heat pump water heaters running on the transcritical process. Heat pump water heaters using the subcritical process can work well on multi-pass heating mode. In the one pass heating mode they might not work as well because they are constrained by condensation temperature of refrigerant used.

Air-source heat pump water heaters with one-stage compression using the subcritical cycle are suitable in mild or hot climate and multi-pass heating system. At low ambient temperatures, air-source heat pump water heaters with two-stage compression might be required.

Air-source heat pump water heaters require more research and development, as they have experienced limited success in the marketplace due to high initial cost. Water heating heat exchangers (condenser or gascooler) are a high priority because they are not a well established technology.

According to AS/NZ 2712, double wall water heating heat exchangers are required for domestic applications because they can prevent refrigerant or oil contaminating the hot water supply if there is a leak. Further, water heating heat exchangers running on counter current flow mode are preferred because the temperature difference

between the refrigerant side and the water side is maximized along the whole length of the heat exchanger. This is particularly relevant for heating water from low temperature to high temperature while limiting the refrigerant condensation temperature and operating with low mass flow rate.

Heat exchanger configurations significantly affect heat transfer performance and pressure drop. Two aspects that are most important to heat exchanger optimization are heat transfer coefficient and pressure drop correlations for fluid flow in channels.

For single phase flow in conventional tubes without fin, the heat transfer correlation proposed by Petuhov (1970), Dittus and Boelter, and Gnielinski (1976) are available for turbulent flow while the Blasius equation is available for predicting the friction factor.

For single phase-flow in enhanced tubes, predicted heat transfer coefficient values by conventional correlations are lower than experimental values. The friction factors calculated by the conventional correlations are higher than values from experiments for gas-flow in tubes. In the case of liquid-flow in tubes, the experimental values will be higher than the values calculated by the conventional correlations. Most correlations for enhanced tubes were modified from the conventional correlations to fit experimental data. Therefore, the use of these correlations should be careful.

In order to accurately predict heat transfer coefficient and pressure drop for condensation flow in tubes of refrigerants, flow maps are necessary. However, very few flow maps of condensing refrigerant flow have been proposed.

Most heat transfer and pressure drop correlations cannot accurately predict over the entire range of condensation flow in tubes. Each correlation may be valid for a flow regime. For the annular flow regime (often occurred in water heating heat exchanger) in conventional channels, many correlations are available for such specific conditions (Table 9 and 10); by contrast, these correlations may not predict for enhanced channels such as micro-fin tubes and mini or micro channels. Very few correlations of heat transfer and pressure drop predict as well for condensation flow in enhanced channels. In addition, the range of vapour qualities of refrigerant used in the prediction of heat transfer and pressure drop is mostly 0.2 to 0.9 for conventional channels but 0.25 to 0.75 for mini or micro channels.

Recently, Cavallini *et al*. (2006) proposed a heat transfer procedure to predict heat transfer coefficient over the entire flow maps for condensation flow in tubes having diameter more than 3 mm. Further, Cavallini *et al*. (2009) proposed a heat transfer procedure to predict heat transfer coefficient over the entire range for condensation flow in micro-fin tubes. Although, their correlations can predict over the entire flow regimes based on their experimental data, these correlations still need to be validated by other authors.

For CO_2 transcritical processes, the generalized heat transfer and pressure drop correlations for carbon dioxide flow in tube have not yet been developed. Large data sets with high accuracy are required in order to validate the correlations previously proposed. Thus, the use of these correlations for design of heat exchangers should be cautious.

Small amount of oil mixed into refrigerants significantly degrade heat transfer performance of those refrigerants flowing in tube or channels for both condensation and transcritical processes.

CHAPTER 3

OBJECTIVES

The overall aim of the research is to improve water heating heat exchangers through modeling the heat transfer and fluid flow for domestic applications based on vapour compression heat pump cycles.

The discussion of Sections 2.1 to 2.9 suggest that for domestic water heating the focus should be on double wall heat exchangers with a counter current configuration of the refrigerant and water being heated. Both condensers (water heating by a sub-critical heat pump cycle) and gas coolers (water heating by a transcritical heat pump cycle, partially using CO_2) should be considered. Further, due to the desire for high water temperature rise; and the target of a heat pump linked to HWC with storage capacity, the flow rate of both water and refrigerant will be low.

Therefore, the specific objectives of the project are to:

3.1 Review heat transfer and fluid flow in heat exchanger configurations likely to used for such heat pumps..
3.2 Develop mathematical models of processes occurring in water heating heat exchangers.
3.3 Validate the models with the experimental data from the open literature
3.4 Use the model to investigate the effect of key design parameters on heat exchanger performance
3.5 Use the model to investigate alternative water heating heat exchanger configurations
3.6 Recommend at least two of the most promising water heating heat exchanger designs
3.7 Recommend system improvements and tasks for further research.

CHAPTER 4

MODELING

4.1. Multi-Zone Model of Water Heating Heat Exchangers

In this research, configurations of double wall counter-current flow heat exchangers will be investigated based on a general steady-state multi-zone model of the cross sectional flow channel on both the refrigerant and water side.

4.1.1 General zone model

A general zone in the multi-zone model of the double-wall counter-current flow heat exchanger with air gap is shown in the Fig. 4.1. Zone *i* extends from node *i* on the right hand side to node *i + 1* on the left hand side.

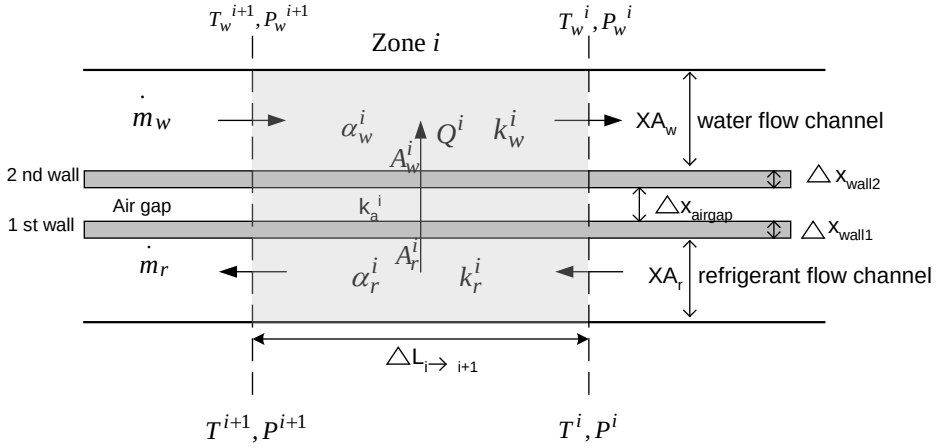

Figure 4.1: A general zone in the multi-zone model of a double wall heat exchanger

Assumptions for the general zone are:

- Flow rates of both refrigerant and water are steady;
- Operating conditions are constant;
- Heat transfer from refrigerant side to water side occurs in one dimension only;
- Heat losses from the system or heat gains into the system are negligible;
- The effects from radiation heat transfer are negligible;
- Due to very small air gap, heat transfer through the air gap is dominated by the conduction;
- Temperature change and pressure drops are sufficiently low; across a zone that the effect of pressure and temperature on thermal and physical properties in a zone can be ignored.

By using mass and energy balances for each zone at steady state, the heat transfer for zone *i* can be defined by the following equations.

The equation for heat transfer in zone *i* is given by:

$$Q^i = (UA)^i \, \Delta T^i_{LMTD} \tag{4.1}$$

$$\Delta T^i_{LMTD} = \frac{(T^i - T^i_w) - (T^{i+1} - T^{i+1}_w)}{\ln((T^i - T^i_w)/(T^{i+1} - T^{i+1}_w))} \tag{4.2}$$

where Q^i = heat transfer rate for zone *i*, kW

$(UA)^i$ = product of overall heat transfer coefficient and area of heat transfer for zone *i*, kW/K

ΔT^i_{LMTD} = log-mean temperature difference for zone *i*, ^oC

T^i = refrigerant temperature for node *i*, ^oC

T^i_w = water temperature for node *i*, ^oC

T^{i+1} = refrigerant temperature for node *i+1*, ^oC

T^{i+1}_w = water temperature for node *i+1*, ^oC

The heat transfer of zone *i* can also be calculated by refrigerant side or water side balances:

$$Q^i = \dot{m}_r (h^i - h^{i+1}) = \dot{m}_w \, c^i_{pw} (T^i_w - T^{i+1}_w) \tag{4.3}$$

where $\dot{m}_r$ = mass flow rate of refrigerant, kg/s

$\dot{m}_w$ = mass flow rate of water, kg/s

h^i = enthalpy of refrigerant at the node *i*, kJ/kg

h^{i+1} = enthalpy of refrigerant at the node *i+1*, kJ/kg

c^i_{cpw} = specific heat of water at the node *i*, kJ/kgK

Pressure drop of refrigerant side ($\Delta P_{r,i \to i+1}$) and water side ($\Delta P_{w,i+1 \to i}$) in the zone *i* are given by:

$$P^{i+1}_r = P^i - \Delta P_{r,i \to i+1} \tag{4.4}$$

$$P_w{}^{i+1} = P_w{}^i + \Delta P_{w,i+1 \to i} \tag{4.5}$$

where P^{i+1} = absolute pressure of refrigerant side at node *i+1*, kPa

P^{i+1}_w = absolute pressure of water side at node *i+1*, kPa

P^i = absolute pressure of refrigerant side at node *i*, kPa

P^i_w = absolute pressure of water side at node *i*, kPa

The overall heat transfer coefficient of each zone *i* is given by:

$$\frac{1}{U^i A^i_{mean}} = R^i_{convect,r} + R^i_{F,r} + R^i_{conduct,wall1} + \frac{1}{\frac{\%contact}{100} \times \frac{A^i_{wall,gap}}{R^i_{contact}} + \frac{100-\%contact}{100} \times \frac{1}{R^i_{airgap}}} + R^i_{conduct,wall2} + R^i_{convect,w} + R^i_{F,w} \tag{4.6}$$

$$R^i_{convect,r} = \frac{1}{\alpha^i_r A^i_{wall1,in}} \tag{4.7}$$

$$R^i_{convect,w} = \frac{1}{\alpha^i_w A^i_{wall2,out}} \tag{4.8}$$

$$R^i_{conduct,wall1} = \frac{\Delta x_{wall1}}{k_{wall1} A^i_{wall1}} \tag{4.9}$$

$$R^i_{conduct,wall2} = \frac{\Delta x_{wall2}}{k_{wall2} A^i_{wall2}} \tag{4.10}$$

$$R^i_{airgap} = \frac{\Delta x_{airgap}}{k^i_a A^i_{wall,gap}} \tag{4.11}$$

$$\%contact = \frac{A^i_{contact}}{A^i_{wall,gap}} \times 100 \tag{4.12}$$

$$A^i_{wall,gap} = A^i_{airgap} + A^i_{contact} \tag{4.13}$$

$$A^i_{wall,gap} = \frac{A^i_{wall1,out} + A^i_{wall2,in}}{2} \tag{4.14}$$

$$A^i_{mean} = \frac{A^i_{wall1,in} + A^i_{wall2,out}}{2} \tag{4.15}$$

$$A^i_{wall1,in} = B^i_{wall1,in} \Delta L_{i \to i+1} \tag{4.16}$$

$$A^i_{wall1,out} = B^i_{wall1,out} \Delta L_{i \to i+1} \tag{4.17}$$

$$A^i_{wall2,in} = B^i_{wall2,in} \Delta L_{i \to i+1} \tag{4.18}$$

$$A^i_{wall2,out} = B^i_{wall2,out} \Delta L_{i \to i+1} \tag{4.19}$$

$$A^i_{wall1} = \frac{A^i_{wall1,in} + A^i_{wall1,out}}{2} \tag{4.20}$$

$$A^i_{wall2} = \frac{A^i_{wall2,in} + A^i_{wall2,out}}{2} \tag{4.21}$$

where U^i = overall heat transfer coefficient based on the mean heat transfer surface area of zone *i*, kW/m^{2}K

$R^i_{convect,r}$ = thermal convection resistance of refrigerant side for zone *i*, K/kW

$R^i_{convect,w}$ = thermal convection resistance of water side for zone *i*, K/kW

$R^i_{conduct,wall1}$ = thermal conduction resistance of the first wall for zone *i*, K/kW

$R^i_{conduct,wall2}$ = thermal conduction resistance of the second wall for zone *i*, K/kW

R^i_{airgap} = thermal conduction resistance of the air gap for zone *i*, K/kW

$R^i_{contact}$ = thermal contact resistance for zone *i*, Km^2/kW

$R^i_{F,r}$ = thermal fouling resistance in refrigerant flow channel for zone *i*, K/kW

$\%contact$ = a fraction of the heat transfer surface of the contact between the first and the second walls to the total heat transfer surface (the heat transfer surface of the contact combined with the heat transfer surface of the air gap, %

$R^i_{F,w}$ = thermal fouling resistance in water flow channel for zone *i*, K/kW

A^i_{mean} = mean heat transfer surface area of zone *i*, m^2

$A^i_{wall1,in}$ = inside heat transfer surface of the first wall for zone *i*, m^2

$A^i_{wall1,out}$ = outside heat transfer surface of the first wall for zone *i*, m^2

$A^i_{wall2,in}$ = inside heat transfer surface of the second wall for zone *i*, m^2

$A^i_{wall2,out}$ = outside heat transfer surface of the second wall for zone *i*, m^2

A^i_{wall1} = mean heat transfer surface of the first wall for zone *i*, m^2

A^i_{wall2} = mean heat transfer surface of the second wall for zone *i*, m^2

A^i_{airgap} = mean heat transfer surface of the air gap for zone *i*, m^2

$B^i_{wall1,in}$ = inside perimeter of the first wall, m

$B^i_{wall1,out}$ = outside perimeter of the first wall, m

$B^i_{wall2,in}$ = inside perimeter of the second wall, m

$B^i_{wall2,out}$ = outside perimeter of the second wall, m

Δx_{wall1} = thickness of the first wall, m

Δx_{wall2} = thickness of the second wall, m

Δx_{airgap} = thickness of the air gap, m

k_{wall1} = thermal conductivity of the first wall, kW/mK

k_{wall2} = thermal conductivity of the second wall, kW/mK

k^i_a = thermal conductivity of the air for zone *i*, kW/mK

$\Delta L_{i\rightarrow i+1}$ = the length of the heat exchanger for zone *i*, m

α^i_r = heat transfer coefficient of pure refrigerant flow in or on smooth tube for zone *i*, kW/m^{2}K

α^i_w = heat transfer coefficient of water flow in or on smooth tube for zone *i*, kW/m^{2}K

4.1.2 Boundary zones

The overall heat exchanger is divided into I zones with equal water temperature change.

$$I = \frac{T_{w,out} - T_{w,in}}{\Delta T_w} \tag{4.22}$$

$$\Delta T_w = T_w^i - T_w^{i+1} \tag{4.23}$$

where ΔT_w = water temperature increase for each zone, ^oC

Thus, boundaries conditions are given by:

at i = 1: $T^i = T_{r,inlet}$, $P^i = P_{r,inlet}$ and $T_w^i = T_{w,outlet}$

at $i = I + 1$: $T^{i+1} = T_{r,outlet}$, $T_w^{i+1} = T_{w,inlet}$ and $P_w^{i+1} = P_{w,inlet}$

4.1.3 Prediction of heat transfer coefficients and pressure drops of fluid flow without oil in or on smooth tubes

4.1.3.1 Refrigerant side

4.1.3.1.1 Sub-critical process

For a sub-critical process, the flow of refrigerant through the heat exchanger occurs in three regions: de-superheating, condensing, and sub-cooling. As a consequence, in the multi-zone model for the subcritical process is separated into three regions by two transition zones: transition between de-superheating and condensing and transition between condensing and sub-cooling.

4.1.3.1.1.1 De-superheating region

The zone will be de-superheating when:

$$h^{i+1} > h_g^{i+1} \tag{4.24}$$

where h_g^{i+1} = enthalpy of saturated vapor refrigerant at node i+1, kJ/kg

Enthalpy of refrigerant for node $i+1$ is calculated at the pressure and temperature of node i+1 while the enthalpy of saturated vapor refrigerant for node i+1 is calculated at the pressure of node i +1 and vapor quality of 100%.

Heat transfer coefficient of pure refrigerant for de-superheating is given by:

$$\alpha_r^i = \frac{Nu_r^i k_r^i}{D_{h,r}} \tag{4.25}$$

$$D_{h,r} = \frac{4XA_r}{B_r^i} \tag{4.26}$$

where Nu_r^i = the Nusselt number of refrigerant side of zone *i*

k_r^i = conductivity of refrigerant of zone *i*, kW/mK

$D_{h,r}$ = hydraulic diameter of refrigerant flow channel, m

XA_r = cross section flow area of refrigerant side, m^2

B_r^i = perimeter of refrigerant side for zone *i*, m

The conductivity of refrigerant for zone *i* is evaluated at the average pressure (P_{ave}^i) and temperature (T_{ave}^i) using the in-built functions in *EES* (Engineering Equation Solver) program. Average pressure drop and temperature for zone *i* are given by:

$$P_{ave}^i = \frac{P^i + P^{i+1}}{2} \tag{4.27}$$

$$T_{ave}^i = \frac{T^i + T^{i+1}}{2} \tag{4.28}$$

The Nusselt number of zone *i* can be predicted by the Petukhov equation (Petukhov, 1970) because this equation had been proved to accurately predicted for single-phase refrigerant flow in both smooth and micro-fin tubes (see Section 2.11.1.1.1):

$$Nu_r^i = \frac{\frac{f_{r,\alpha}^i}{8} \times \mathrm{Re}_r^i \times \mathrm{Pr}_r^i}{b_r^i + 12.7 \times \left[\frac{f_r^i}{8}\right]^{0.5} \times (\mathrm{Pr}_r^{i\,2/3} - 1)} \tag{4.29}$$

$$b_r^i = 1.07 + \frac{900}{\mathrm{Re}_r^i} - \frac{0.63}{1 + 10\,\mathrm{Pr}_r^i} \tag{4.30}$$

Friction factor of zone *i* ($f_{r,\alpha}^i$) used for calculating the Nusselt number (in Equation 4.29) and is determined by Filonenko's equation:

$$f_{r,\alpha}^i = \frac{1}{(0.79 \ln \mathrm{Re}_r^i - 1.64)^2} \tag{4.31}$$

Prandtl number (Pr_r^i) and Reynold number (Re_r^i) of zone *i* are determined by:

$$\mathrm{Pr}_r^i = \frac{\mu_r^i c_{pr}^i}{k_r^i} \tag{4.32}$$

$$\mathrm{Re}_r^i = \frac{\rho_r^i u_r^i D_{h,r}}{\mu_r^i} = \frac{G_r^i D_{h,r}}{\mu_r^i} \tag{4.33}$$

where μ_r^i = dynamic viscosity of refrigerant at zone *i*, N s m^{-2}

c_{pr}^i = specific heat of refrigerant at zone *i*, kJ/kg K

ρ_r^i = density of refrigerant at zone *i*, kg/m^3

$$u_r^i = \frac{\dot{m}_r}{\rho_r^i X A_r}$$

u_r^i = velocity of refrigerant at zone *i*, m/s

$G_r^i = \rho_r^i u_r^i$

G_r^i = mass flux of refrigerant at zone *i*, kg/m^2 s

The refrigerant properties for zone *i* are all calculated at the average pressure and temperature of zone *i* as defined in Equation 4.27 and 4.28.

Pressure drop on the refrigerant side in zone *i* for de-superheating is given by:

$$\Delta P_{r,i\to i+1} = \frac{f_{r,p}^i \rho_r^i u_r^{i\,2} \Delta L_{i\to i+1}}{2D_{h,r}} = \frac{f_{r,p}^i G_r^{i\,2} \Delta L_{i\to i+1}}{2\rho_r^i D_{h,r}} \tag{4.34}$$

The friction factor value used in the Equation (4.34) is calculated by Blasius's equation as proved by many authors (see Section 2.11.1.1.1):

$$f_{r,p}^i = \frac{0.316}{\mathrm{Re}_r^{i\,0.25}} \tag{4.35}$$

4.1.3.1.1.2 Transition between de-super heating and condensing

The transition from de-superheating to condensing will occur when:

$$h^{i+1} < h_g^{i+1} \text{ and } \quad h^i > h_g^{i+1} \tag{4.36}$$

The heat transfer coefficient and pressure drop for such transition zones are calculated assuming the whole zone is desuperheating (Section 4.1.3.1.1.1). Because condensing heat transfer coefficients tend to be higher than for de-superheating, this approach should be conservative in terms of the heat exchanger size.

4.1.3.1.1.3 Condensing region

The zone will be in the condensing region when $h^i < h_g^i$ *and* $h^{i+1} > h_f^{i+1}$.

<u>*Condensation heat transfer coefficient*</u>

Heat transfer coefficient of pure refrigerant side in zone *i* is given by:

$$\alpha_r^i = \frac{Nu_r^i k_{lr}^i}{D_{h,r}} \tag{4.37}$$

where k_{lr}^i = conductivity of saturated liquid refrigerant at zone *i*, kW/m K

The conductivity of saturated liquid refrigerant at zone *i* is calculated at the average condensing temperature of zone *i* and vapor quality of 0%.

The Nusselt number in zone *i* can be predicted by the model described by Dobson and Chato (1998) because this equation accurately predicted for alternative refrigerants especially near azeotropic blends as reviewed in Section 2.11.1.3.2.1.

$$Nu_r^i = \frac{0.23\,\mathrm{Re}_{vr}^{0.12}}{1+1.11 X_{tt}^{i\,0.58}} \left[\frac{Ga_r^i \,\mathrm{Pr}_{lr}^i}{Ja_{lr}^i} \right]^{0.25} + (1-\theta_l^i/\pi) Nu_{r,\,fored}^i \tag{4.38}$$

Prandtl number (Pr_{lr}^i) and Reynold number (Re_{vr}^i) of zone *i* are given by:

$$\mathrm{Pr}_{lr}^i = \frac{\mu_{lr}^i c_{plr}^i}{k_{lr}^i} \tag{4.39}$$

$$\mathrm{Re}_{lr}^i = \frac{G_r^i D_{h,r}}{\mu_{vr}^i} \tag{4.40}$$

where μ_{lr}^i = dynamic viscosity of saturated liquid refrigerant at zone *i*, N s m^{-2}

c_{plr}^i = specific heat of saturated liquid refrigerant at zone *i*, kJ/kg K

μ_{vr}^i = dynamic viscosity of saturated vapor refrigerant at zone *i*, N s m^{-2}

The refrigerant properties are all calculated at the average condensing temperature and vapor quality of 100% for saturated vapor and vapor quality of 0% for saturated liquid.

The Lockhart Martinelli parameter of zone *i* (X_{tt}^i) is given by:

$$X_{tt}^i = \left[\frac{\rho_{vr}^i}{\rho_{lr}^i} \right]^{0.5} \times \left[\frac{\mu_{lr}^i}{\mu_{vr}^i} \right]^{0.1} \times \left[\frac{1-x_{ave}^i}{x_{ave}^i} \right]^{0.9} \tag{4.41}$$

where ρ_{vr}^{i} = density of saturated vapor refrigerant at zone *i*, kg/m^3

μ_{vr}^{i} = dynamic viscosity of saturated vapor refrigerant at zone *i*, N s m^{-2}

$$x_{ave}^{i} = \frac{x^{i} + x^{i+1}}{2}$$

$$x^{i} = \frac{h^{i} - h_f^{i}}{h_v^{i} - h_f^{i}}$$

$$x^{i+1} = \frac{h^{i+1} - h_f^{i+1}}{h_v^{i+1} - h_f^{i+1}}$$

x_{ave}^{i} = average vapor quality for zone *i*, fraction

x^{i} = vapor quality at node *i*, fraction

x^{i+1} = vapor quality at node *i+1*, fraction

h_f^{i} = enthalpy of saturated-liquid refrigerant at node *i*, kJ/kg

h_v^{i} = enthalpy of saturated-vapor refrigerant at node *i*, kJ/kg

h_f^{i+1} = enthalpy of saturated-liquid refrigerant at node *i*+1, kJ/kg

h_v^{i+1} = enthalpy of saturated-vapor refrigerant at node *i+1*, kJ/kg

The Galileo number at segment *i* (Ga_r^{i}) is defined by:

$$Ga_r^{i} = \frac{g\rho_{lr}^{i}(\rho_{lr}^{i} - \rho_{vr}^{i})(\sqrt{\varepsilon_r^{i}}D_{h,r})^3}{\mu_{lr}^{i\,2}} \tag{4.42}$$

where g = acceleration due to gravity, m/s^2

ε_r^{i} = void fraction of refrigerant at zone *i*

The Jakob number of liquid (Ja_{lr}^{i}) is given by:

$$Ja_{lr}^{i} = \frac{c_{plr}^{i}(T_{sat}^{i} - T_s^{i})}{h_{fg}^{i}} \tag{4.43}$$

where $T_{sat}^{i} = \frac{T^{i} + T^{i+1}}{2}$

$$T_s^{i} = T_{sat}^{i} - \frac{Q^{i}}{1/R_{convect,r}^{i}}$$

T_{sat}^{i} = condensing temperature for zone *i*, ^{o}C

T_s^{i} = surface temperature of the tube wall at zone *i*, ^{o}C

h_{fg}^{i} = enthalpy of vaporization of zone *i*, kJ/kg

θ_l^{i} is angle subtended from the top of the tube to the liquid level, which is geometrically related to the void fraction by the following formula if the area occupied by the thin condensation film is neglected:

$$\varepsilon_r^{i} = \frac{\theta_l^{i}}{\pi} - \frac{\sin(2\theta_l^{i})}{2\pi} \tag{4.44}$$

ε_r^i is void fraction of refrigerant at zone i calculated by the void fraction correlation of Zivi (1964) as given by:

$$\varepsilon_r^i = \left[1 + \frac{1-x_{ave}^i}{x_{ave}^i}\left(\frac{\rho_{vr}^i}{\rho_{lr}^i}\right)^{2/3}\right]^{-1} \tag{4.45}$$

Finally, the forced-convective Nusselt number ($Nu_{r,\,forced}^i$) is given by:

$$Nu_{r,\,forced}^i = 0.0195\,\mathrm{Re}_{lr}^{i\ 0.8}\,\mathrm{Pr}_{lr}^{i\ 0.4}\,\phi_l^i(X_{tt}^i) \tag{4.46}$$

$$\phi_l^i(X_{tt}^i) = \sqrt{1.376 + \frac{c1}{X_{tt}^{i\ c2}}} \tag{4.47}$$

For $0 < Fr_l \le 0.7$,

$$c1 = 4.172 + 5.48Fr_l - 1.564Fr_l^2 \tag{4.48}$$

$$c2 = 1.773 - 0.169Fr_l \tag{4.49}$$

For $Fr_l > 0.7$

$$c1 = 7.242 \tag{4.50}$$

$$c2 = 1.655 \tag{4.51}$$

The Froude number (Fr_l) is given by:

$$Fr_l = \frac{G_r^{i\ 2}}{\rho_{lr}^{i\ 2} g D_{h,r}} \tag{4.52}$$

Condensation pressure drop

The pressure drop in condensation zones can be calculated using the frictional multiplier (ϕ_{LO}) of Zhang and Webb correlation (Zhang and Webb, 2001) multiplied by single phase pressure drop equation (see Table 2.9).

$$\Delta P_{r,i\to i+1} = \phi_{LO}^{i\,2} f_{LO}^i \frac{G_r^{i\,2}\Delta L_{i\to i+1}}{2D_{h,r}\rho_{lr}^i} \tag{4.53}$$

$$\phi_{LO}^{i\,2} = (1-x_{ave}^i)^2 + 2.87(x_{ave}^i)^2\left(\frac{P_{sat}}{P_{crit}}\right)^{-1} + 1.68(x_{ave}^i)^{0.8}(1-x_{ave}^i)^{0.25}\left(\frac{P_{sat}}{P_{crit}}\right)^{-1.64} \tag{4.54}$$

$$f_{LO}^i = 0.316\left(\frac{G_r^i D_{h,r}}{\mu_{lr}^i}\right)^{-0.25} \tag{4.55}$$

where P_{crit} = critical pressure of refrigerant, kPa

f_{LO}^i = friction factor for only liquid phase at zone i

4.1.3.1.1.4 Transition between condensing and sub-cooling

The transition from condensing zone to sub-cooling will occur when:

$$h^{i+1} < h_f^{i+1} \text{ and } \quad h^i > h_f^{i+1} \tag{4.56}$$

where h_f^{i+1} = enthalpy of saturated liquid refrigerant for node *i+1*, kJ/kg

In practice, the location of the transition will also depend on the configuration of the condenser and refrigerant charge. Often condensers are configured to ensure a liquid seal must form part way along the condenser heat transfer surface so that the rest of the condenser acts to sub-cool the refrigerant.

The heat transfer coefficient and pressure drop for such transition zones are calculated using subcooled liquid properties (Section 4.1.3.1.1.5). Because sub-cooling heat transfer coefficients tend to be lower than for condensing, then this approach should be conservative in terms of heat exchanger size.

4.1.3.1.1.5 Subcooling region

Subcooling occurs when $h^i < h_f^i$.

Heat transfer coefficient of pure refrigerant side in each zone *i* is given by:

$$\alpha_r^i = \frac{Nu_r^i k_r^i}{D_{h,r}} \tag{4.57}$$

The Nusselt number of zone *i* can be predicted by the the Petukhov's equation Eq. (4.29) (Section 4.1.3.1.1.1).

Pressure drop of refrigerant side in each zone *i* for sub-critical cooling zone is given by:

$$\Delta P_{r,i\to i+1} = \frac{f_{r,p}^i \rho_r^i u_r^{i\,2} \Delta L_{i\to i+1}}{2D_{h,r}} = \frac{f_{r,p}^i G_r^{i\,2} \Delta L_{i\to i+1}}{2\rho_r^i D_{h,r}} \tag{4.58}$$

The friction factor value is calculated by Blasius's equation detailed in Section 4.1.3.1.1.1.

4.1.3.1.2 Supercritical cooling process

Heat transfer coefficient of pure refrigerant for each zone *i* in the supercritical zone is given by:

$$\alpha_r^i = \frac{Nu_r^i k_{rb}^i}{D_{h,r}} \tag{4.59}$$

where k_{rb}^i = conductivity of refrigerant at bulk temperature of zone *i*, kW/m K

The Nusselt number of zone *i* can be predicted by the equation proposed by Pitla *et al*. (2002) because this equation included wall temperature effect:

$$Nu_r^i = \left[\frac{Nu_{rw}^i + Nu_{rb}^i}{2}\right] \times \frac{k_{rw}^i}{k_{rb}^i} \tag{4.60}$$

Nusselt numbers based on thermophysical properties at the wall temperature (Nu_{rw}^i) and at the bulk temperature (Nu_{rb}^i) can be calculated by Gnielinski's equation:

$$Nu_{rw}^i = \frac{\frac{f_{rw}^i}{8} \times (\mathrm{Re}_{rw}^i - 1000) \times \mathrm{Pr}_{rw}^i}{1.07 + 12.7 \times \left[\frac{f_{rw}^i}{8}\right]^{0.5} \times (\mathrm{Pr}_{rw}^{i\ 2/3} - 1)} \tag{4.61}$$

$$Nu_{rb}^i = \frac{\frac{f_{rb}^i}{8} \times (\mathrm{Re}_{rb}^i - 1000) \times \mathrm{Pr}_{rb}^i}{1.07 + 12.7 \times \left[\frac{f_{rb}^i}{8}\right]^{0.5} \times (\mathrm{Pr}_{rb}^{i\ 2/3} - 1)} \tag{4.62}$$

Prandtl number (Pr_{rw}^i) and Reynold number (Re_{rw}^i) at the wall temperature of zone *i* can be determined by:

$$\mathrm{Pr}_{rw}^i = \frac{\mu_{rw}^i c_{prw}^i}{k_{rw}^i} \tag{4.63}$$

$$\mathrm{Re}_{rw}^i = \frac{\rho_{rw}^i u_r^i D_{h,r}}{\mu_{rw}^i} \tag{4.64}$$

where μ_{rw}^i = dynamic viscosity at wall temperature of zone *i*, N s m^{-2}

c_{prw}^i = specific heat at wall temperature of zone *i*, kJ/kg K

k_{rw}^i = conductivity at wall temperature of zone *i*, kW/m K

ρ_{rw}^i = density of refrigerant at zone *i*, kg/m^3

The wall temperature of zone *i* is given by:

$$T_{wall1,in}^i = T_{ave}^i - \frac{Q^i}{1/R_{convect,r}^i} \tag{4.65}$$

Prandtl number (Pr_{rb}^i) and Reynold number (Re_{rb}^i) at bulk temperature of zone *i* can be determined by:

$$\mathrm{Pr}_{rw}^i = \frac{\mu_{rb}^i c_{prb}^i}{k_{rb}^i} \tag{4.66}$$

$$\mathrm{Re}_{rb}^{i} = \frac{\rho_{rb}^{i} u_{r}^{i} D_{h,r}}{\mu_{rb}^{i}} \tag{4.67}$$

where μ_{rb}^{i} = dynamic viscosity at wall temperature of zone *i*, N s m^{-2}
c_{prb}^{i} = specific heat at wall temperature of zone *i*, kJ/kg K
ρ_{rb}^{i} = density of refrigerant at zone *i*, kg/m^3

The refrigerant properties are all calculated at the average pressure and temperature of zone *i* using the in-built property functions in *EES*.

The friction factors at wall temperature (f_{rw}^{i}) and at bulk temperature (f_{rb}^{i}) can be calculated by Filonenko's equation:

$$f_{rw}^{i} = \frac{1}{(0.79 \ln \mathrm{Re}_{rw}^{i} - 1.64)^2} \tag{4.68}$$

$$f_{rb}^{i} = \frac{1}{(0.79 \ln \mathrm{Re}_{rb}^{i} - 1.64)^2} \tag{4.69}$$

Pressure drop of refrigerant side in zone *i* ($\Delta P_{r,i\to i+1}$) is determined by:

$$\Delta P_{r,i\to i+1} = \frac{f_{rb}^{i} \rho_{r}^{i} u_{r}^{i\,2} \Delta L_{i\to i+1}}{2 D_{h,r}} = \frac{f_{rb}^{i} G_{r}^{i\,2} \Delta L_{i\to i+1}}{2 \rho_{r}^{i} D_{h,r}} \tag{4.70}$$

4.1.3.2 Water side

For the water side the following heat transfer coefficient and pressure drop correlations can be used for all zones for both condensers and gas coolers.

Heat transfer coefficient of zone *i* (α_{w}^{i}) can be determined by:

$$\alpha_{w}^{i} = \frac{Nu_{w}^{i} k_{w}^{i}}{D_{h,w}} \tag{4.71}$$

$$D_{h,w} = \frac{4 XA_{w}}{B_{w}^{i}} \tag{4.72}$$

where k_{w}^{i} = conductivity of water at zone *i*, kW/m K
$D_{h,w}$ = hydraulic diameter of water flow channel, m
XA_{w} = cross section flow area of water side, m^2
B_{w}^{i} = perimeter of water side for zone *i*, m

The Nusselt number of zone *i* can be predicted by the Petukhov equation (Petukhov, 1970) as recommended by Webb and Zhang (1997):

$$Nu_w^i = \frac{\frac{f_w^i}{8} \times \mathrm{Re}_w^i \times \mathrm{Pr}_w^i}{b_w^i + 12.7 \times \left[\frac{f_w^i}{8}\right]^{0.5} \times (\mathrm{Pr}_w^{i\,2/3} - 1)} \tag{4.73}$$

$$b_w^i = 1.07 + \frac{900}{\mathrm{Re}_w^i} - \frac{0.63}{1 + 10\,\mathrm{Pr}_w^i}$$

The friction factor value is calculated by Filonenko's equation:

$$f_w^i = \frac{1}{(0.79 \ln \mathrm{Re}_w^i - 1.64)^2} \tag{4.74}$$

Prandtl number (Pr_w^i) and Reynold number (Re_w^i) of zone *i* can be determined by:

$$\mathrm{Pr}_w^i = \frac{c_{pw}^i \mu_w^i}{k_w^i} \tag{4.75}$$

$$\mathrm{Re}_w^i = \frac{\rho_w^i u_w^i D_{h,w}}{\mu_w^i} = \frac{G_w^i D_{h,w}}{\mu_w^i} \tag{4.76}$$

$$u_w^i = \frac{\dot{m}_w}{\rho_w^i X A_w} \tag{4.77}$$

where μ_w^i = dynamic viscosity of water at zone *i*, N s m^{-2}

c_{pw}^i = specific heat of water at zone *i*, kJ/kg K

ρ_w^i = density of water at zone *i*, kg/m^3

u_w^i = velocity of water at zone *i*, m/s

G_w^i = mass flux of water, kg/m^{2}s

The water properties are all calculated at the average pressure and temperature of zone *i* using the in-built property functions in *EES*.

Pressure drop of water side in each zone is given by:

$$\Delta P_{w,i+1\to i} = \frac{f_{w,p}^i \rho_w^i u_w^{i\,2} \Delta L_{i\to i+1}}{2 D_{h,w}} = \frac{f_w^i G_w^{i\,2} \Delta L_{i\to i+1}}{2 \rho_w^i D_{h,w}} \tag{4.78}$$

where $f_{w,p}^i$ is friction factor used for pressure drop equation, which is calculated by Blasius's equation:

$$f_{w,p}^i = \frac{0.316}{\mathrm{Re}_w^{i\,0.25}} \tag{4.79}$$

4.1.4 Prediction of heat transfer coefficients and pressure drops of fluid flow with oil or on enhanced tubes

Enhanced tubes improve the heat transfer by increasing the heat transfer surface area of smooth tube and providing greater fluid turbulence. The improvement is commonly quantified by a combination of a heat transfer area enhancement factor and/or a heat transfer coefficient enhancement factor. The heat transfer surface enhancement factor is given by:

$$\varepsilon = \frac{A_{enhanced}}{A_{smooth}} \tag{4.80}$$

where ε = heat transfer surface enhancement factor
$A_{enhanced}$ = heat transfer surface of enhanced tube, m^2
A_{smooth} = heat transfer surface of equivalent smooth-tube, m^2

There are two methods to predict heat transfer coefficient and friction factor for enhanced tube. One is direct calculation by a correlation developed for enhanced tubes and another is by using heat transfer enhancement factors and friction penalty factors for correlation without enhancement, which are determined from experiments.

No general equations to predict their factors for enhanced tube were found in the literature (Chapter 2); thus, in this study prediction of heat transfer coefficients and friction factors were determined using heat transfer enhancement factors and friction penalty factors.

In order to calculate heat transfer coefficient for enhanced tubes, heat transfer coefficients based on the equivalent smooth-tube (in the above model) were multiplied by a heat transfer enhancement factor. The heat transfer enhancement factor is defined by:

$$Heat\ transfer\ enhancement\ \ factor,\ E = \frac{Heat\ transfer\ coefficient\ of\ \ enhanced\ tube}{Heat\ transfer\ coefficient\ of\ \ smooth\ tube} \tag{4.81}$$

Pressure drop of fluid flow in enhanced tube will be increased. As a consequence, friction factors based on the equivalent smooth-tube (in the above model) will be multiplied by friction penalty factor due to enhanced heat transfer surface.

The friction penalty factor, F is defined by:

$$Friction\ \ penalty\ \ factor,\ F = \frac{Friction\ \ factor\ of\ \ enhanced\ tube}{Friction\ \ factor\ of\ \ smooth\ tube} \tag{4.82}$$

The review of heat transfer coefficients and pressure drop correlations (Chapter 2) found that sub-critical single phase, condensation (two phase) and transcritical single phase flows in enhanced tubes gave heat transfer coefficients higher than equivalent smooth tubes at the same operating conditions while pressure drop increased. The values of E and F used were an average of those reviewed in Chapter 2.

Subcritical single phase:	$E = 1.75$	$F = 1.35$
Condensation (two-phase)	$E = 2.3$	$F = 1.5$
Transcritical single phase	$E = 2$	$F = 2$

4.1.5 Effect of oil

Small amounts of oil in the refrigerant impact on the heat transfer performance and pressure drop of refrigerant. As a consequence, the heat transfer coefficient of refrigerant used in the above model based on pure refrigerant without oil were multiplied by a heat transfer degradation factor due to oil. In addition, in order to calculate the pressure drop the friction factor used in the above model will be multiplied by friction penalty factor due to oil.

The review of heat transfer coefficients and pressure drop correlations (Chapter 2) found that both subcritical single-phase and condensation (two-phase) small amount of oil (less than 5% by mass) degraded heat transfer coefficient about 15% and increased pressure drop by about 20% for both smooth and enhanced tubes. For transcritical single phase, the effect of oil degrades heat transfer coefficient and increases pressure drop about 50% on average so these were used as the basis for the penalty factors.

4.1.6 Configurations of double wall heat exchanger

In this study, three configurations of double wall counter current heat exchanger will be investigated as illustrated below:

Parameters needed in the model are cross section flow area (*XA*), wetted perimeter (*B*), and hydraulic diameter D_h for each of the refrigerant and water sides.

4.1.6.1 Configuration *I*: Smooth circular tube-in-tube with small air gap

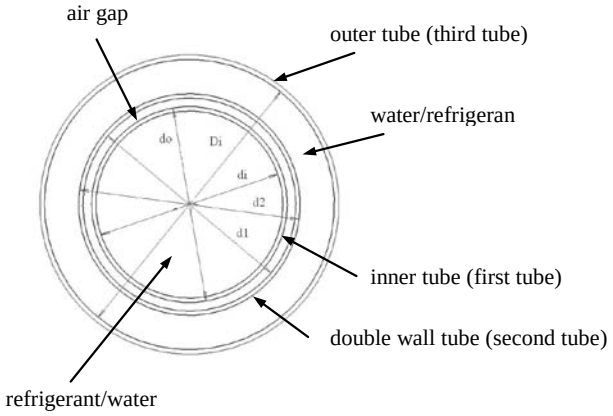

Figure 4.2: Circular tube-in-tube with small air gap

This configuration (Fig. 4.2) consists of three tubes: first tube (inner tube), second tube, and third tube (outer tube). Refrigerant can flow either inside the inner tube or in the annulus between the second and the third tubes while water can flow either in the annulus or inside the inner tube in the countercurrent direction. The small air gap between the first wall and the second wall means that the first wall and the second wall do not contact each other perfectly (%contact = 0). This gap allows refrigerant or oil to flow out of the system if it leaks.

For configuration *I*:

$$XA_{inner} = \pi d_i^2 / 4 \tag{4.83}$$

$$XA_{annulus} = \frac{\pi}{4}(D_i^2 - d_2^2) \tag{4.84}$$

$$B_{wall1,in} = \pi d_i \tag{4.85}$$

$$B_{wall1,out} = \pi d_o \tag{4.86}$$

$$B_{wall2,in} = \pi d_1 \tag{4.87}$$

$$B_{wall2,out_2} = \pi d_2 \tag{4.88}$$

$$B_{inner} = B_{wall1,in} \tag{4.89}$$

$$D_{h,inner} = \frac{4XA_{inner}}{B_{inner}} \tag{4.90}$$

$$D_{h,annulus} = \frac{D_i^2 - d_2^2}{D_i + d_2} \tag{4.91}$$

4.1.6.2 Configuration *II*: Flat tube-on-tube

In addition to tube-in-tube water heating heat exchanger, tube-on-tube water heating heat exchangers were investigated. In this study, flat tube-on-tube was selected because they are easier to manufacture rather than rectangular tube-on-tube because it can be manufactured by flattening circular tube. This configuration is shown in Fig. 4.3.

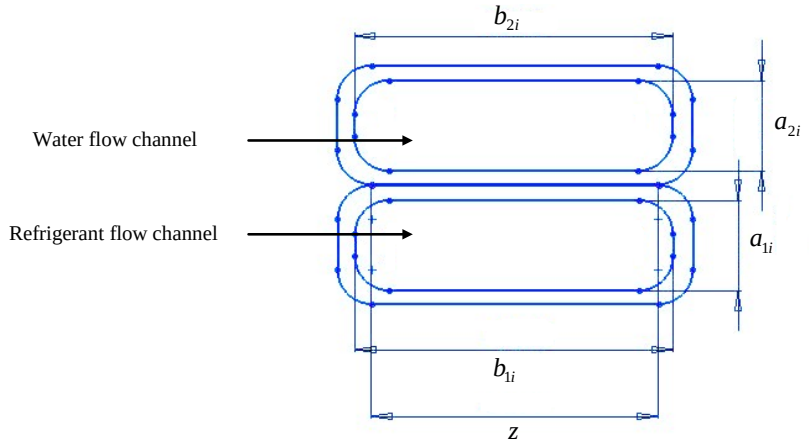

Figure 4.3: Flat tube-on-tube

In this study tube ends were assumed to be semi-circles. Thus, the radius of the ends is equal to $\frac{1}{2}a_{1i}$ for the refrigerant flow channel and it is equal to $\frac{1}{2}a_{2i}$ for the water flow channel. To investigate for this configuration, parameters needed in the model are:

$$XA_1 = \frac{\pi a_{1i}^2}{4} + a_{1i}(b_{1i} - a_{1i}) \tag{4.92}$$

$$XA_2 = \frac{\pi a_{2i}^2}{4} + a_{2i}(b_{2i} - a_{2i}) \tag{4.93}$$

$$B_{wall1,in} = z \tag{4.94}$$

$$B_{wall1,out} = z \tag{4.95}$$

$$B_{wall2,in} = z \tag{4.96}$$

$$B_{wall2,out} = z \tag{4.97}$$

$$B_1 = \pi a_{1i} + 2(b_{1i} - a_{1i}) \tag{4.98}$$

$$B_2 = \pi a_{2i} + 2(b_{2i} - a_{2i}) \tag{4.99}$$

$$D_{h,1} = \frac{4XA_1}{B_1} \tag{4.100}$$

$$D_{h,2} = \frac{4XA_2}{B_2} \tag{4.101}$$

In this study, b_{1i} was assumed to be equal b_{2i}. Thus, contact distance (z) can be defined by:

1. $z = b_{1o} - a_{1o}$ when $a_{1o} \geq a_{2o}$ (4.101*a*)
2. $z = b_{1o} - a_{2o}$ when $a_{1o} < a_{2o}$ (4.101*b*)

4.1.6.3 Configuration *III*: Twisted tube-in-tube with small air gap

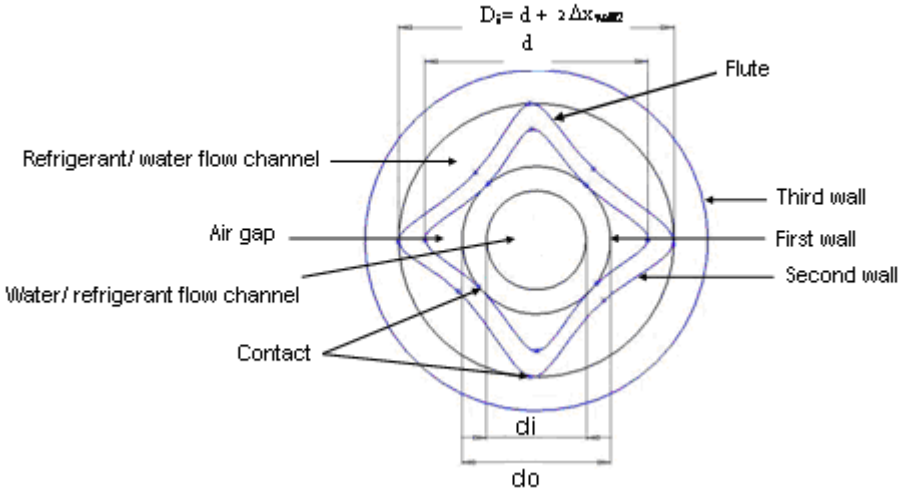

Figure 4.4: Twisted tube-in-tube with small air gap

Potential limitations of circular tube-in-tube (Configuration *I*) are:

- high water pumping power and low COP due to high water pressure drop if water flow channel is reduced,
- not as strong as the third tube is not attached to the other tube except at the end of the tube length.

A common approach to improve performance is to twist the inner two tubes together (Fig. 4.4 to 4.6). The twists provide a number of potential benefits:

- increased heat transfer coefficient for both refrigerant side and water side due to greater turbulence generation;
- reduced water pressure drop for the same heat transfer performance;
- given air gap between inner tubes needed for refrigerant venting; and
- strength due to tube-to-tube contact.

The outside tube (3rd tube) should be a tight fit to the outside of the twisted 2nd tube. This means low bypass of water/refrigerant over the heat transfer surface and effectively smaller flow channels (flows in the channels formed between the flutes formed by the twisting). Further, the tube to tube contact provides strength to the structure.

There are many possible combinations of tube size, tightness of twist (pitch between flutes), size of flute, number of flutes per circumference, angle of flute, %contact between 1st and 2nd tube etc. Relative size of the 1st and 2nd tube affects size of flute, %contact, and the degree of enhancement of the 1st tube. A small difference in size tends to provide less air gap and less enhancement of the 1st tube (Fig. 4.5) while big differences in size tends to provide larger air gaps and more enhancement of the 1st tube (Fig. 4.6). Time did not allow the full range of combinations to be investigated.

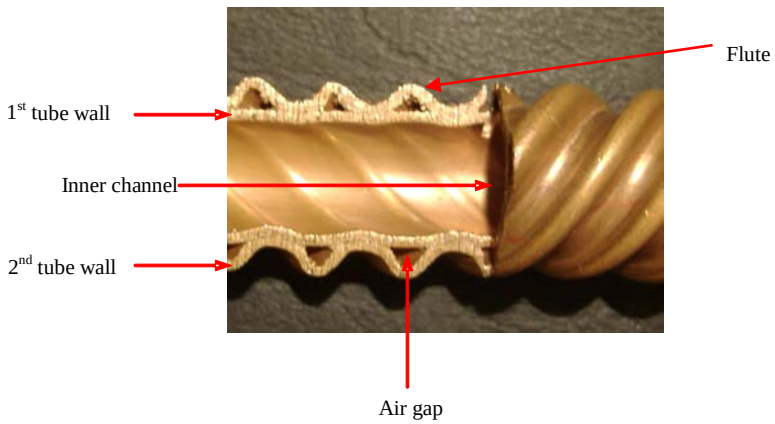

Figure 4.5: Possible twisted tube if small difference in size between the 1st and 2nd tubes

Figure 4.6: Possible twisted tube if big difference in size between the 1st and 2nd tubes

In this study, only the case of a small difference between the 1st and 2nd tubes (Fig. 4.5) was investigated. Further, it was assumed that:
- the inner tube (1st tube) was unaffected by twisting (no enhancement);
- the inner tube size chosen was the optimum for configuration *I* (Section 6.3); and
- the outer tube (3rd tube) touches the extremity of the middle tube (2nd tube) (*i.e.* $D_i = d$).
- the outside diameter of the 2nd (twisted) tube (d) was smaller than the original diameter of the untwisted tube;
- there are four flutes/twists per circumference;
- the inside circumference of the twisted tube was the same as the circumference of the original tube;

The net effect of these assumptions is that the distance between the tops of adjacent flutes equals quarter of the original circular tube circumference.

Given these constraints, %contact and d are interrelated and depend on the tightness of twisting. One extreme is that d equals the original inside diameter of the tube before twisting. In this case, the %contact is minimized but the best case is when the flute is shaped as shown in Fig. 4.7.

Another extreme is when the %contact is close to 100% and the flute shape is as shown in Fig. 4.8. In this case d must be less than the original diameter so that the 2nd tube surface can follow the profile of the 1st tube. The two cases can be analysed to describe a relationship between d and % contact.

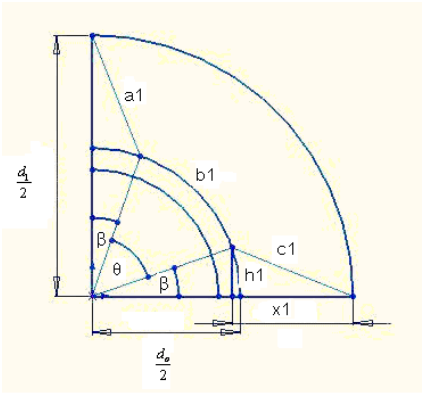

Figure 4.7: Dimension of twisted tube ($d = d_1$)

From Fig. 4.7 the following geometric relationship can be formulated:

$$\frac{1}{4}\pi d_1 = a_1 + b_1 + c_1 \tag{4.102}$$

$$a_1 = c_1 \tag{4.103}$$

$$b_1 = \frac{\theta}{360} \times \pi d_o \tag{4.104}$$

$$c_1 = \sqrt{x^2 + h^2} \tag{4.105}$$

$$h_1 = \frac{d_o}{2}\sin(\beta) \tag{4.106}$$

$$x_1 = \frac{d_1}{2} - \frac{d_o}{2}\cos(\beta) \tag{4.107}$$

$$\beta = \frac{1}{2}(90 - \theta) \tag{4.108}$$

Eq. (4.102) to (4.108) can be solved for θ using *EES* and the %contact is determined by:

$$\%contact(d = original\ diameter) = \frac{\theta}{90} \times 100 = CT \tag{4.109}$$

For example, if d_1 = 10 mm and d_o = 5 mm then θ = 56^o and % contact = 62%.

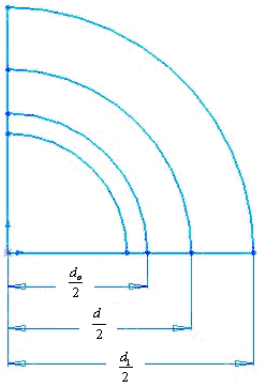

Figure 4.8: Dimension of twisted tube with 100% contact

In the other case, %contact is 100% (θ = 90**).** As for the above equations, inside diameter of twisted tube (d at θ = 90) can be determined by:

$$d(\theta = 90) = \frac{1}{4}\pi(d_1 - d_o) + d_o \tag{4.110}$$

For example, if d_1 = 10 mm, d_o = 5 mm, and θ = 90 (%contact = 100) and then d = 8.9 mm.

The relationship between the %contact and inside diameter of twisted tube between the two cases was assumed to be linear (Fig. 4.9). The relationship can be expressed by:

$$\%contact = \left(\frac{100 - CT}{0.215(d_o - d_1)}\right)d - \left(\frac{100 - CT}{0.215(d_o - d_1)}\right)d_1 + CT \tag{4.111}$$

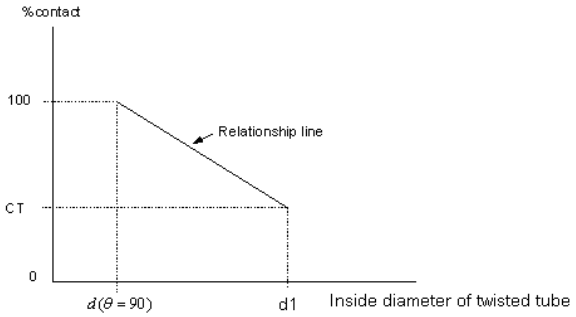

Figure 4.9: Relationship between inside radius of twisted tube and %contact

The parameters needed in the model namely $B_{wall1,in}$, $B_{wall1,out}$, $B_{wall2,in}$, and B_{wall2,out_2} were determined using similar equations in configuration *I* based on original tubes. Thickness air gap (Δx_{airgap}), cross section flow area in each subchannel and hydraulic diameter were calculated by the following equations based on the geometry shown in Fig. 4.10.

Thickness air gap was given by:

$$\Delta x_{airgap} = \frac{1}{4}(d - d_o) \tag{4.112}$$

Cross section flow area in each subchannel was calculated by:

$$XA_{subchannel} = \left(\frac{1}{4}\pi\left(\frac{d}{2} + \Delta x_{wall2}\right)^2\right) - \left(2\left(\frac{1}{2}h_2 x_2\right)\right) - \left(2\left(\frac{1}{2}(\frac{d_o}{2} + \Delta x_{wall2})h_2\right)\right) - \left(\frac{\theta}{360} \times \pi(\frac{d_o}{2} + \Delta x_{wall2})^2\right) \tag{4.113}$$

where $$h_2 = (\frac{d_o}{2} + \Delta x_{wall2})\sin(\beta) \tag{4.114}$$

$$x_2 = \left(\frac{d}{2} + \Delta x_{wall2}\right) - (\frac{d_o}{2} + \Delta x_{wall2})\cos(\beta) \tag{4.115}$$

And hydraulic diameter in each sub-channel is determined by:

$$D_{h,subchannel} = \frac{4XA_{subchannel}}{B_{subchannel}} \tag{4.116}$$

where $$B_{subchannel} = \frac{1}{4}\pi d_1 + \frac{1}{4}\pi(d + 2\Delta x_{wall2})) \tag{4.117}$$

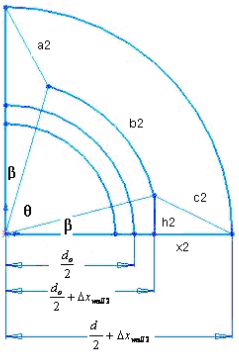

Figure 4.10: Dimension of twisted tube for outside wall

4.2 Vapor Compression Heat Pump Cycle Model

Two available vapor compression heat pump cycles for producing hot water are the vapor compression cycle and the transcritical vapor compression cycle. The basic components for both cycles are most the same, but only differ in terms of the heating process for the cycles. Therefore, most component models for both cycles are the same except for the water heating heat exchanger model (see Section 4.1).

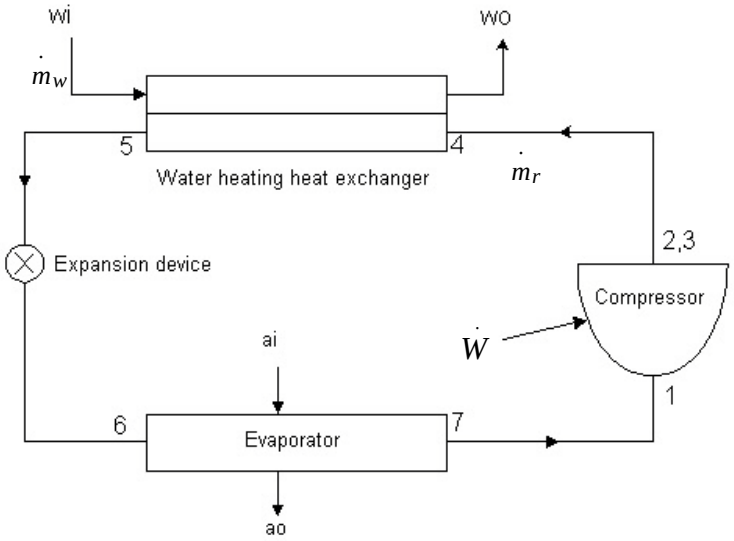

Figure 4.11: Vapor compression heat pump cycle model

4.2.1 Compressor Model

The compressor work rate can be determined by:

$$W_{12} = \dot{m}_r (h_2 - h_1) \tag{4.118}$$

where W_{12} = compressor work rate, kW

$\dot{m}_r$ = refrigerant mass flow rate, kg/s

h_1 = refrigerant enthalpy at the compressor suction, kJ/kg

h_2 = refrigerant enthalpy at the compressor discharge assuming no heat losses, kJ/kg

The mass flow rate of refrigerant and the suction volume flow rate can be determined by:

$$\dot{m}_r = \rho_1 \eta_v \dot{V}_1 \tag{4.119}$$

where ρ_1 = refrigerant density at the compressor suction, kg/m^3

η_v = compressor volume efficiency, fraction

$\dot{V}_1$ = compressor displacement volume, m^3/s

The isentropic efficiency ($\eta_{is,c}$) and volumetric efficiency (η_v) equations were related to the pressure ratio (PR) based on published data for a hermetic compressor used in space heating heat pump equipment (model RN104V produced by Siam Compressor Industry Co., Ltd):

$$\eta_{is,c} = 0.0069PR^3 - 0.0987PR^2 + 0.4274PR + 0.072 \quad (4.120)$$

$$\eta_v = 0.003PR^3 - 0.0441PR^2 + 0.1796PR + 0.6803 \quad (4.121)$$

The pressure ratio is given by:

$$PR = \frac{P_2}{P_1} \quad (4.122)$$

where P_1 = refrigerant pressure at the compressor suction, kPa
P_2 = refrigerant pressure at the compressor discharge, kPa

Refrigerant enthalpy at the compressor discharge without heat losses is given by:

$$h_2 = \frac{h_{is,2} - h_1}{\eta_{is,c}} + h_1 \quad (4.123)$$

where $h_{is,2}$ = isentropic enthalpy at the compressor discharge, kJ/kg

If compressor heat loss occurs (Q_{12}), refrigerant enthalpy at the compressor discharge with heat losses (h_3) will be:

$$h_3 = h_2 - \frac{Q_{12}}{\dot{m}_r} \quad (4.124)$$

And heat compressor heat loss is estimated by:

$$Q_{12} = FH \times W_{12} \quad (4.125)$$

where FH = heat loss factor for the compressor, fraction

4.2.2 Discharge line model

The heat loss from the discharge line (Q_{34}) can be calculated by:

$$Q_{34} = \dot{m}_r (h_3 - h_4) \quad (4.126)$$

where h_4 = condenser/gascooler inlet refrigerant enthalpy, kJ/kg

And pressure drop of discharge line (ΔP_{24}) is:

$$\Delta P_{24} = P_2 - P_4 \tag{4.127}$$

In this case, Q_{34} and ΔP_{24} were assumed to be negligibly small.

4.2.3 Expansion model

It was assumed that the heat loss, kinetic energy difference, and potential energy difference of the expansion valve are negligible. Therefore, the enthalpy of refrigerant flowing through the expansion valve is constant:

$$h_5 = h_6 \tag{4.128}$$

h_5 is calculated by:

$$h_5 = h_4 - \frac{Q_{45}}{\dot{m}_r} \tag{4.129}$$

where h_5 = condenser/gascooler outlet enthalpy, kJ/kg
h_6 = evaporator inlet enthalpy, kJ/kg
Q_{45} = heating capacity of the water heating heat exchanger, kW

4.2.4 Evaporator model

The type of evaporator is a fined tube air-coil cross flow heat exchanger. Sensible only cooling of the air was assumed (air-off humidity ratio equal air-on humidity ratio). The cooling capacity of evaporator (Q_{67}) can be calculated by:

For refrigerant side:

$$Q_{67} = \dot{m}_r (h_7 - h_6) \tag{4.130}$$

For air side:

$$Q_{67} = \dot{m}_a (h_{ai} - h_{ao}) \tag{4.131}$$

For heat exchanger:

$$Q_{67} = (UA)_{67} \Delta T_{LM,67} \tag{4.132}$$

$$\Delta T_{LM,67} = \frac{(T_6 - T_{ai}) - (T_7 - T_{ao})}{\ln \frac{T_6 - T_{ai}}{T_7 - T_{ao}}} \tag{4.133}$$

where h_7 = outlet evaporator refrigerant enthalpy, kJ/kg

$\dot{m}_a$ = air mass flow rate, kg/s

h_{ai} = inlet evaporator air enthalpy, ^oC

h_{ao} = outlet evaporator air enthalpy, ^oC

UA_{67} = product of overall heat transfer coefficient and area of heat transfer for evaporator, kW/K

$\Delta T_{LM,67}$ = log-mean temperature difference for evaporator, ^oC

T_6 = inlet evaporator refrigerant temperature, ^oC

T_7 = outlet evaporator refrigerant temperature, ^oC

T_{ai} = inlet evaporator air temperature, ^oC

T_{ao} = outlet evaporator air temperature, ^oC

h_{ai} was determined for the air-on temperature and humidity and h_{ao} was determined by Eq. (4.131).

Pressures drop in evaporator are illustrated by:

For refrigerant side:

$$\Delta P_{67} = P_6 - P_7 \tag{4.134}$$

where ΔP_{67} = evaporator refrigerant pressure drop, kPa

P_6 = inlet evaporator refrigerant pressure, kPa

P_7 = outlet evaporator refrigerant pressure, kPa

In this study, ΔP_{67} value was assumed to be negligibly small.

4.2.5 Suction line model

The suction refrigerant temperature (T_1) can be calculated by:

$$T_1 = T_7 + \Delta T_{71} \tag{4.135}$$

And suction refrigerant pressure (P_1) is:

$$P_1 = P_7 - \Delta P_{71} \tag{4.136}$$

where ΔT_{71} = superheated refrigerant temperature, ^oC

ΔP_{71} = suction line pressure drop, kPa

In this study, ΔT_{71} and ΔP_{71} were assumed to be negligibly small.

4.2.6 Coefficient of performance (COP) and water pump power

The heating *COP* of heat pump water heaters and water pump power (*EP*) are given by:

$$COP = \frac{Q_{45}}{EP + W_{12} + W_{fans}} \tag{4.137}$$

$$EP = \frac{\Delta P_w \dot{m}_w}{\rho_w \eta_{pump}} \tag{4.138}$$

where EP = power transmitted to the water by the pump, kW
W_{fans} = fan power in evaporator, kW
ΔP_w = total pressure drop of water side, kPa
ρ_w = water density, kg/m^3
η_{pump} = pump efficiency of water pump, fraction

4.2.7 Water pump effect

The water pump affects the water inlet temperature to the condenser/gas cooler. Assuming all the pump power is converted to heat immediately:

$$T_{w,in} = T_{w,\text{sup}\,ply} + \frac{EP}{\dot{m}_w c_{pw}} \tag{4.139}$$

where $T_{w,in}$ = inlet condenser/gascooler water temperature, ^{o}C
$T_{w,\text{sup}\,ply}$ = supply cold water temperature, ^{o}C
c_{pw} = water specific heat, kJ/kg K

4.3 Calculation Procedure

The input data are $\dot{V}_c$, η_{pump}, $T_E(T_7)$, T_C (for condenser), P_2 (for gascooler), ΔT_{71}, ΔP_{71}, ΔP_{67}, ΔP_{24}, Q_{45} (heating capacity), Q_{12}, Q_{34}, ΔT_w, $T_{w,in}$ $T_{w,out}$, $P_{w,out}$, T_{ai}, $\dot{m}_a$, XA_w, XA_r, Δx_{wall1}, Δx_{wall2}, k_{wall1}, k_{wall2}, $B_{wall1,in}$, $B_{wall1,out}$, $B_{wall2,in}$, $B_{wall2,out}$, $\%contact$, $R_{contact}$, $R_{F,r}$, and $R_{F,w}$.

And then calculation procedure are:

1. calculate $\dot{m}_w$, $\dot{m}_r$, $T_{r,in}(T_4)$, $P_{r,in}(P_4)$ using the heat pump model (Section 4.2);
2. calculation of the multi-zone condenser/gascooler model sequentially from zone *1* to zone *I*. The procedure of calculation in each zone *i* are:

2.1 calculate the heating capacity of zone *i* using Eq. (4.3);

2.2 calculate h^{i+1} and calculate T^{i+1} (assume $P^i = P^{i+1}$) and then calculate ΔT^i_{LMTD};

2.3 calculate $(UA)^i$ using Eq. (4.1);

2.4 calculate heat transfer coefficient for both refrigerant side and water side of zone *i* and then calculate thermal resistances of zone *i;*

2.5 calculate the length of zone *i* ($\Delta L_{i\to i+1}$) and then calculate A^i_{mean}, $A^i_{wall1,in}$, $A^i_{wall1,out}$, $A^i_{wall2,in}$, $A^i_{wall2,out}$, A^i_{airgap}, A^i_{wall1}, A^i_{wall2};

2.6 calculate the pressure drop for both refrigerant side and water side and then calculate P^{i+1} and P^{i+1}_w;

2.7 calculate T^{i+1} by:

$T^{i+1} = f(R, P^{i+1}, h^{i+1})$ for single phase flow (de-super heating, sub-cooling, and supercritical cooling

$T^{i+1} = f(R, P^{i+1}, x^{i+1})$ for two phase flow (condensing) and;

2.8 Repeat 2.1 to 2.7 for the next zone *i* until $T^{i+1}_w \le T_{w,in}$

3. calculate total lengths, total areas, total weight, refrigerant and water pressure drops of condenser/gascooler;
4. calculate EP (water pump power) and COP.

Model Implementation

The models were programed and implemented in a EES software program called "*tool*". The EES code is listed in Appendix. The tools used in this study consist of three parts: heat pump cycle, condenser, and gascooler tools. The heat pump cycle tool (model in Section 4.2 implemented in EES) is used to estimate refrigerant mass flow, inlet condenser/ gascooler temperatures while condenser and gascooler tools (model in Section 4.1 and linked to heat pump cycle model implemented in EES) are used for design water heating heat exchangers.

Heat pump cycle tool

This tool is necessary to estimate primary parameters for water heating heat exchanger design because design conditions depend on consumer requirement, ambient air temperature and cold water temperature. As a consequence, input data into this tool consist of:

- Heating capacity of water heating heat exchanger
- Refrigerant type
- Refrigerant condensing temperature for subcritical cycle
- Discharge refrigerant pressure for supercritical cycle
- Outlet refrigerant temperature from water heating heat exchanger
- Inlet and outlet water temperatures from water heating heat exchanger
- Refrigerant evaporation temperature based on ambient air temperature
- Heat losses or heat gain from discharge and suction lines
- Pressure drop of evaporator, water heating heat exchanger, suction and discharge lines
- Heat loss from compressor
- Displacement volume of compressor
- Isentropic and volume efficiencies of compressor

Finally, this tool will estimate inlet refrigerant temperature and pressure of water heating heat exchanger, refrigerant and water mass flow rates.

Condenser and gascooler tools

These tools are used for design water heating heat exchangers. Input data into these tools consist of:

- Inlet and outlet water temperature from water heating heat exchanger
- Outlet water pressure from the condenser or gascooler
- Refrigerant and water mass flow rates (estimated from heat pump cycle tool)
- Inlet refrigerant temperature and pressure of water heating heat exchanger (estimated from heat pump cycle tool)
- Outlet refrigerant temperature from water heating heat exchanger
- Water temperature difference in each zone i (ΔT_w)
- Conductivities of tube walls
- Wall and air gap thicknesses
- Cross section areas of water and refrigerant sides
- Inside and outside perimeters of the 1^{st} and 2^{nd} walls

Finally, these tools will estimate water pumping power, coefficient of performance (COP), mean heat transfer surface, length, and weight of water heating heat exchanger. These parameters will be used to evaluate alternative designs and configurations of water heating heat exchangers. In addition, these tools can estimate all thermodynamic property changes across the multi-zones means that process understanding can be gained by using these tools for a range of design parameters.

4.4 Three Zone Model of Condenser

Three zone model of condenser consists of one zone model of de-superheating, condensing, and sub-cooling (Fig. 4.12). Pressure drop for both refrigerant and water side was not predicted and assumed negligibly small.

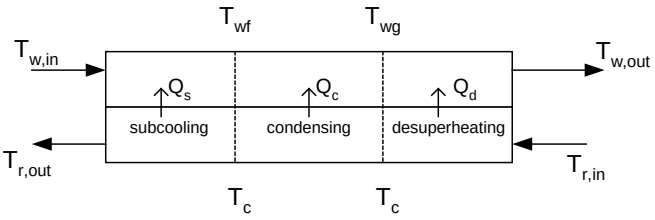

Figure 4.12: Three zone model of condenser

Heat transfer in each zone is given by:

Refrigerant side:

$$Q_d = \dot{m}_r (h_{r,in} - h_g) \tag{4.140}$$

$$Q_c = \dot{m}_r (h_g - h_f) \tag{4.141}$$

$$Q_s = \dot{m}_r (h_f - h_{r,out}) \tag{4.142}$$

Water side:

$$Q_d = \dot{m}_w c_{pw} (T_{w,out} - T_{wg}) \tag{4.143}$$

$$Q_c = \dot{m}_w c_{pw} (T_{wg} - T_{wf}) \tag{4.144}$$

$$Q_s = \dot{m}_w c_{pw} (T_{wf} - T_{w,in}) \tag{4.145}$$

Condenser:

$$Q_d = U_d A_d \Delta T_{LMTD,d} \tag{4.146}$$

$$Q_c = U_c A_c \Delta T_{LMTD,c} \tag{4.147}$$

$$Q_s = U_s A_s \Delta T_{LMTD,s} \tag{4.148}$$

$$\Delta T_{LMTD,d} = \frac{(T_{r,in} - T_{w,out}) - (T_c - T_{wg})}{\ln \frac{T_{r,in} - T_{w,out}}{T_c - T_{wg}}} \tag{4.149}$$

$$\Delta T_{LMTD,c} = \frac{(T_c - T_{wg}) - (T_c - T_{wf})}{\ln \frac{T_c - T_{wg}}{T_c - T_{wf}}} \tag{4.150}$$

$$\Delta T_{LMTD,s} = \frac{(T_c - T_{wf}) - (T_{r,out} - T_{w,in})}{\ln \frac{T_c - T_{wf}}{T_{r,out} - T_{w,in}}} \tag{4.151}$$

where Q_d = heat transfer rate in de-superheating zone, kW
Q_c = heat transfer rate in condensing zone, kW
Q_s = heat transfer rate in sub-cooling zone, kW
$h_{r,in}$ = inlet condenser refrigerant enthalpy, kJ/kg

$h_{r,out}$ = outlet condenser refrigerant enthalpy, kJ/kg

h_g = saturated vapor enthalpy, kJ/kg

h_f = saturated liquid enthalpy, kJ/kg

T_{wg} = water temperature at the saturated refrigerant vapor, ^oC

T_{wf} = water temperature at the saturated refrigerant liquid, ^oC

A_d = mean heat transfer surface in desuperheating zone, m^2

A_c = mean heat transfer surface in condensing zone, m^2

A_s = mean heat transfer surface in subcooling zone, m^2

U_d = overall heat transfer coefficient in desuperheating zone, kW/m^2K

U_c = overall heat transfer coefficient in condensing zone, kW/m^2K

U_s = overall heat transfer coefficient in subcooling zone, kW/m^2K

$\Delta T_{LMTD,d}$ = log-mean temperature difference in desuperheating zone, ^oC

$\Delta T_{LMTD,c}$ = log-mean temperature difference in condensing zone, ^oC

$\Delta T_{LMTD,s}$ = log-mean temperature difference in subcooling zone, ^oC

The overall heat transfer coefficient of each zone is given by:

$$\frac{1}{U_d A_d} = R_{convect,rd} + R_{F,rd} + R_{conduct,wall1d} + \frac{1}{\frac{\%contact}{100} \times \frac{A_{wall,gapd}}{R_{contact}} + \frac{100-\%contact}{100} \times \frac{1}{R_{airgap,d}}} + R_{conduct,wall2d} + R_{convect,wd} + R_{F,wd} \tag{4.152}$$

$$\frac{1}{U_c A_c} = R_{convect,rc} + R_{F,rc} + R_{conduct,wall1c} + \frac{1}{\frac{\%contact}{100} \times \frac{A_{wall,gapc}}{R_{contact}} + \frac{100-\%contact}{100} \times \frac{1}{R_{airgap,c}}} + R_{conduct,wall2c} + R_{convect,wc} + R_{F,wc} \tag{4.153}$$

$$\frac{1}{U_s A_s} = R_{convect,rs} + R_{F,rs} + R_{conduct,wall1s} + \frac{1}{\frac{\%contact}{100} \times \frac{A_{wall,gaps}}{R_{contact}} + \frac{100-\%contact}{100} \times \frac{1}{R_{airgap,s}}} + R_{conduct,wall2s} + R_{convect,ws} + R_{F,ws} \tag{4.154}$$

$$R_{airgap,d} = \frac{\Delta x_{airgap}}{k_{ad} A_{wall,gapd}} \tag{4.155}$$

$$R_{airgap,c} = \frac{\Delta x_{airgap}}{k_{ac} A_{wall,gapc}} \tag{4.156}$$

$$R_{airgap,s} = \frac{\Delta x_{airgap}}{k_{as} A_{wall,gaps}} \tag{4.157}$$

$$R_{conduct,wall1d} = \frac{\Delta x_{wall1}}{k_{wall1} A_{wall1d}} \tag{4.158}$$

$$R_{conduct,wall1c} = \frac{\Delta x_{wall1}}{k_{wall1} A_{wall1c}} \tag{4.159}$$

$$R_{conduct,wall1s} = \frac{\Delta x_{wall1}}{k_{wall1} A_{wall1s}} \tag{4.160}$$

$$R_{conduct,wall2d} = \frac{\Delta x_{wall2}}{k_{wall2} A_{wall2d}} \tag{4.161}$$

$$R_{conduct,wall2c} = \frac{\Delta x_{wall2}}{k_{wall2} A_{wall2c}} \tag{4.162}$$

$$R_{conduct,wall2s} = \frac{\Delta x_{wall2}}{k_{wall2} A_{wall2s}} \tag{4.163}$$

$$R_{convect,rd} = \frac{1}{\alpha_{rd} A_{wall1,ind}} \tag{4.164}$$

$$R_{convect,rc} = \frac{1}{\alpha_{rc} A_{wall1,inc}} \tag{4.165}$$

$$R_{convect,rs} = \frac{1}{\alpha_{rs} A_{wall1,ins}} \tag{4.166}$$

$$R_{convect,wd} = \frac{1}{\alpha_{wd} A_{wall2,outd}} \tag{4.167}$$

$$R_{convect,wc} = \frac{1}{\alpha_{wc} A_{wall2,outc}} \tag{4.168}$$

$$R_{convect,ws} = \frac{1}{\alpha_{ws} A_{wall2,outs}} \tag{4.169}$$

$$A_{wall,gapd} = \frac{A_{wall1,outd} + A_{wall2,ind}}{2} \tag{4.170}$$

$$A_{wall,gapc} = \frac{A_{wall1,outc} + A_{wall2,inc}}{2} \tag{4.171}$$

$$A_{wall,gaps} = \frac{A_{wall1,outs} + A_{wall2,ins}}{2} \tag{4.172}$$

$$A_{d} = \frac{A_{wall1,ind} + A_{2,outd}}{2} \tag{4.173}$$

$$A_{c} = \frac{A_{wall1,inc} + A_{2,outc}}{2} \tag{4.174}$$

$$A_{s} = \frac{A_{wall1,ins} + A_{2,outs}}{2} \tag{4.175}$$

where $R_{convect,rd}$ = thermal convection resistance of refrigerant for desuperheating, K/kW

$R_{convect,rc}$ = thermal convection resistance of refrigerant for condensing, K/kW

$R_{convect,rs}$ = thermal convection resistance of refrigerant for subcooling, K/kW

$R_{conduct,wall1d}$ = thermal conduction resistance of the 1st tube for desuperheating, K/kW

$R_{conduct,wall1c}$ = thermal conduction resistance of the 1st tube for condensing, K/kW

$R_{conduct,wall1s}$ = thermal conduction resistance of the 1st tube for subcooling, K/kW

$R_{conduct,wall2d}$ = thermal conduction resistance of the 2nd tube for desuperheating, K/kW

$R_{conduct,wall2c}$ = thermal conduction resistance of the 2nd tube for condensing, K/kW

$R_{conduct,wall2cs}$ = thermal conduction resistance of the 2nd tube for subcooling, K/kW

$A_{wall1,ind}$ = inside heat transfer surface of the 1st tube for desuperheating, m^2

$A_{wall1,inc}$ = inside heat transfer surface of the 1st tube for condensing, m^2

$A_{wall1,ins}$ = inside heat transfer surface of the 1st tube for subcooling, m^2

$A_{wall2,outd}$ = outside heat transfer surface of the 2nd tube for desuperheating, m^2

$A_{wall2,outc}$ = outside heat transfer surface of the 2nd tube for condensing, m^2

$A_{wall2,outs}$ = outside heat transfer surface of the 2nd tube for subcoolig, m^2

α_{rd} = refrigerant heat transfer coefficient in desuperheating zone, kW/m^2K

α_{rc} = refrigerant heat transfer coefficient in condensing zone, kW/m^2K

α_{rc} = refrigerant heat transfer coefficient in subcooling zone, kW/m^2K

α_{wd} = water heat transfer coefficient in superheating zone, kW/m^2K

α_{wc} = water heat transfer coefficient in condensing zone, kW/m^2K

α_{ws} = water heat transfer coefficient in subcooling zone, kW/m^2K

All heat transfer coefficients are estimated using the same Equations predicted in Section 4.1.3. For example, for the subcooling and desuperheating zones the water and refrigerant properties were estimated at the average water or refrigerant temperature in the zone. For the condensing zone average vapor quality used in the prediction of α_{rc} was 0.5.

4.5 One-Zone Model of Gascooler

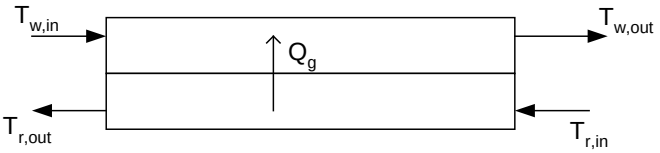

Figure 4.13: One zone model of gas cooler

Heat transfer in gascooler is given by:

Refrigerant side:

$$Q_g = \dot{m}_r (h_{r,in} - h_{r,out}) \tag{4.176}$$

Water side:

$$Q_d = \dot{m}_w c_{pw}(T_{w,out} - T_{w,in}) \tag{4.177}$$

Gascooler:

$$Q_g = U_g A_g \Delta T_{LMTD,g} \tag{4.178}$$

$$\Delta T_{LMTD,g} = \frac{(T_{r,in} - T_{w,out}) - (T_{r,out} - T_{w,in})}{\ln \frac{T_{r,in} - T_{w,out}}{T_{r,out} - T_{w,in}}} \tag{4.179}$$

$$\frac{1}{U_g A_g} = R_{convect,rg} + R_{F,r} + R_{conduct,wall1} + \frac{1}{\frac{\%contact}{100} \times \frac{A_{wall,gap}}{R_{contact}} + \frac{100 - \%contact}{100} \times \frac{1}{R_{airgap}}} + R_{conduct,wall2} + R_{convect,w} + R_{F,w} \tag{4.180}$$

$$R_{convect,rg} = \frac{1}{\alpha_{rg} A_{wall1,in}} \tag{4.181}$$

where Q_g = heat transfer rate in gascooler, kW

$h_{r,in}$ = inlet gascooler refrigerant enthalpy, kJ/kg

$h_{r,out}$ = outlet gascooler refrigerant enthalpy, kJ/kg

A_g = mean heat transfer surface in gascooler, m^2

U_g = overall heat transfer coefficient in gascooler, kW/m^2K

$\Delta T_{LMTD,g}$ = log-mean temperature difference in gascooler, ^oC

α_{rg} = refrigerant heat transfer coefficient in gascooler, kW/m^2K

All thermodynamic properties used to calculate heat transfer coefficient were determined at the average temperature in the gascooler ($T_{r,average} = \frac{T_{r,in} + T_{r,out}}{2}$). Otherwise the same equation predicted in Section 4.1.3.1.2 were used to estimate α_{rg} *and* α_w.

4.6 Number of Zones and Accuracy

Multi-zone models should be more accurate than three or one-zone models. However, more zones take a longer time to calculate. Further, as the number of zones is increased, accuracy will ultimately reach a value that is almost constant as shown in Fig. 4.14. The trade-off between accuracy and calculation time means that *optimum number of zone* depends on the relative cost of calculation and the benefit of greater accuracy.

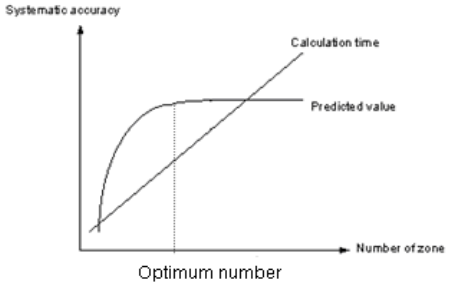

Figure 4.14: The systematic accuracy of calculation

In this study, the optimal number of zone was first determined for both multi-zone subcritical and super-critical cooling models. The model was run for a range of numbers of zone for a typical operating condition. The optimal number of zones for subcritical-cooling was evaluated as illustrated in Fig. 4.15. It was found that the optimal number was approximately 90 zones. At higher zones, there was insignificant change in the predicted values of the overall pressure drop and heat exchanger size. In the same way, the optimal number of zone for supercritical-cooling model is about 90 zones as illustrated in Fig. 4.16.

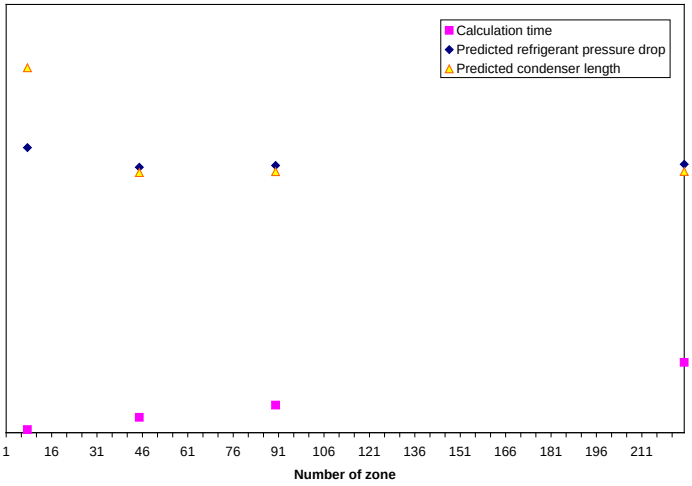

Figure 4.15: Accuracy and calculation time for the subcritical cooling model as a function of number of zones: *R410A, T_C = 60 °C, T_E = 5 °C $T_{r,in}$ = 98.41 °C, $T_{r,out}$ = 25 °C, $T_{w,in}$ = 15 °C, $T_{w,out}$ = 60 °C, d_i=6 mm,$D_{in} - d_2$ =1 mm, $d_1 - d_o$ =0.2 mm and 0%contact*

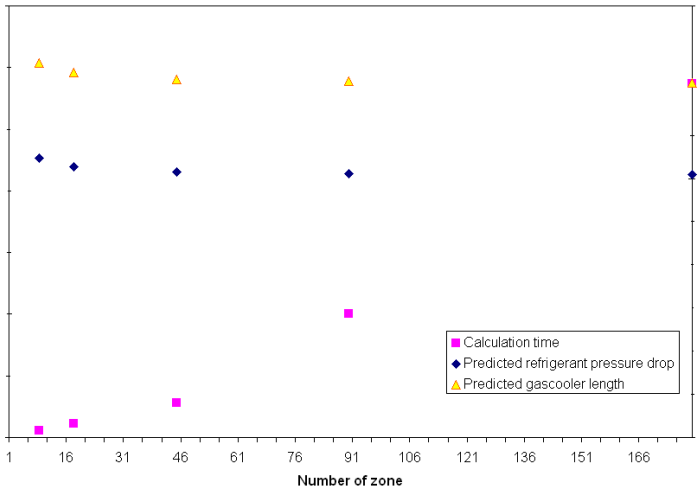

Figure 4.16: Accuracy and calculation time for the super-critical cooling model as a function of number of zones: *CO_2, $P_{r,in}$ = 12 MPa, T_E = 5 °C, $T_{r,in}$ = 100.2 °C, $T_{r,out}$ = 25 °C, $T_{w,in}$ = 15 °C, $T_{w,out}$ = 60 °C, d_i=4 mm, $D_{in} - d_2$ =1 mm, $d_1 - d_o$ =0.2 mm and 0%contac*

CHAPTER 5

MODEL VALIDATION

5.1 Introduction

The system model must be shown to be accurate in order to predict useful results. Therefore, the system model was validated against experimental data. There are a lot of parameters in the water heating heat exchanger model and each parameter has a complex relationship to many other parameters. However, two parameters that are most influential on water heating heat exchanger design are heat transfer coefficients and pressure drop of fluid flows. In the model these parameters are predicted by heat transfer and pressure drop correlations for three situations: single-phase flow under the critical point, condensation flow, and single-phase flow above the critical point.

Experimental data of heat transfer coefficient and pressure drop of fluids flow in or on tubes are available in the open literature. The heat transfer correlations proposed by Petukhove, and the associated Filonenko correlation for friction are widely used to predict heat transfer coefficient for single phase turbulent-flow under the critical point in horizontal smooth-tubes and the simple empirical Blasius friction equation is also suitable for predicting pressure drop. Those correlations have been validated extensively with experimental data and they are proven for alternative refrigerants as recommended by Webb (1994). They are also applicable for non-circular tubes if the hydraulic diameter concept is used. Therefore, further validation of these correlations was not performed.

There is extensive experimental data for condensation flow in or on tubes for traditional refrigerants and existing correlations are capable of predicting heat transfer coefficient and pressure drop. Unfortunately, few experimental data exist for alternative refrigerants such as R410A which is promising for heat pump water heaters. As a consequence, condensation heat transfer and pressure drop correlations of pure refrigerants flow in horizontal smooth tube used in the water heating heat exchanger model will be validated with the experimental data in the available open literature for R410A.

In the last two decade, experimental data has become been available for single-phase flow of CO_2 above the critical point. Unfortunately, measurements at this condition are difficult and low measurement accuracy has often occurred.

Therefore, heat transfer correlations used in the model for condensation (two phase) and above the critical point will be validated against with the experimental data for R-410A and R-744 respectively. The available experimental data of condensation heat transfer and pressure drop are summarized in Table 5.1 and 5.2 respectively. Experimental data of supercritical heat transfer and pressure drop are summarized in Table 5.3.

Table 5.1: Specification of test tubes for condensation heat transfer in/on smooth tube

Authors	**Configurations**	**Fluids**	T_c[°C]	G[kg/m^2 s]	ΔT[°C]	q [kW/m^2]	x
Cavallini *et al.* (2001)	Copper tube	R 22	40	100 – 750	5 – 15	-	0.21 – 0.84
	Smooth in-tube,	***R 134a***	30 – 60	100 – 750	2.5 – 13	-	0.25 – 0.82
	D_i = 8 mm, L = 1 m	R 236ea	30 – 51	100 – 600	3 – 9	-	0.15 – 0.85
		R 125	30 – 52	100 – 750	3.5 – 12	-	0.23 – 0.82
		R 32	30 – 50	100 – 600	3.6 – 14	-	0.22 – 0.86
		R 410A	28 – 50	100 – 750	4.6 – 13	-	0.15 – 0.88
Son and Lee (2009)	Copper tube, smooth in-tube	R 22	40	200 – 400	-	-	0.04 – 0.94
	D_i = 1.77, 3.36, 5.35 mm,	***R 134a***					
	L = 1.22, 2.66, 3.62 m	***R 410A***					
Kim and Shin (2005)	Copper tube, smooth in-tube,	R 22	45	186.9 – 373.8	-	11	0.9 – 0.1
	D_i = 8.7 mm, L = 9.20 m	***R410A***					

D_o = outside diameter, D_i = inside diameter, L =length of tube, T_c = condensation temperature, G = mass flux, q = heat flux, x = vapor quality, $\Delta T = T_b - T_{wall}$
T_b = bulk temperature of fluid, T_{wall} = surface wall temperature

Table 5.1 *Continued*

Authors	Configurations	Fluids	T_c[°C]	G[kg/m^2 s]	ΔT[°C]	q [kW/m^2]	x
Jung *et al.* (2004)	Copper tube, smooth in-tube, D_i = 8.82 mm, L = 1 m	R22	40	100 – 300		7.7 – 7.9	-
		R134a					
		R407C					
		R410A					
Boissieux *et al.* (2000)	Copper tube, smooth in-tube, D_i = 9.525 mm, L = 4.0 m	Isceon 59	31.5 – 35.7	207 – 386	-	17.5 – 36.8	-
		R407C	15.7 – 29.8	199 – 393	-	20.7 – 38.1	-
		R404A	24.3 – 27.5	153 – 410	-	11 – 28.6	-
Miyara *et al.* (2000)	Copper, smooth in-tube, D_i = 6.4 mm, L = 4.0 m	R22	40	100 – 400	-	-	0.1 – 0.9
		R410A					
Nuzo and Honda (2000)	Copper tube, smooth in-tube, D_i = 8.18 mm, L = 3.2 m	R11, R12	40	80 – 460	-	-	-
		R134a,					
		R123					
Ferreira *et al.* (2003)	Copper tube, smooth in-tube, D_o = 9.52 mm, L = 1 m	***R410A***	40	200-400	-	-	-
		R410A/oil					
Lee and Son (2010)	Copper tube, smooth in-tube, D_i = 5.8, 6.54, 7.73, 10.07 mm L = 0.5 m	R290	40	35.5 – 210.4	-	-	-
		R600a					
		R134a					
		R22					

Table 5.2: Specification of test tubes for condensation pressure drop in/on smooth tube

Authors	Configurations	Fluids	T_c[^{o}C]	G[kg/m^2 s]	ΔT[^{o}C]	[kW/m^2]	x
Cavallini *et al.* (2001)	Copper tube	R 22	40	100 – 750	5 – 15	-	0.21 – 0.84
	Smooth in-tube,	***R 134a***	30 – 60	100 – 750	2.5 – 13	-	0.25 – 0.82
	D_i = 8 mm, L = 1 m	R 236ea	30 – 51	100 – 600	3 – 9	-	0.15 – 0.85
		R 125	30 – 52	100 – 750	3.5 – 12	-	0.23 – 0.82
		R 32	30 – 50	100 – 600	3.6 – 14	-	0.22 – 0.86
		R 410A	28 – 50	100 – 760	4.6 – 13	-	0.15 – 0.88
Cavallini *et al.* (2005)	Aluminum tube						
	Muti-port mini-channel	R236a	40	200 – 600	-	-	0.25 – 0.75
	D_h = 1.4 mm, L = 1.8 m	***R134a***	40	400 – 1000	-	-	0.25 – 0.75
		R410A	40	600 – 1400	-	-	0.25 – 0.75
Coleman (2004)	Micro-channel D_h = 0.83 mm	***R134a***	-	185 – 785	-	-	0.0 – 1.0
	L = 5 mm						
Cavallini *et al*. (2009)	Copper tube						
	Mini-in tube D_i = 0.96 mm	***R134a***	39 – 41	400 – 800	-	-	0.0 – 1.0
	L = 0.2285 m	R32		200 – 1000	-	-	
Lee and Son (2010)	Copper tube, smooth in-tube						
	Smooth in-tube,	R290	40	35.5 – 210.4	-	-	-

Table 5.3: Specification of test tubes for cooling heat transfer and pressure drop of supercritical carbon dioxide

Authors	Configurations	Fluids	P[MPa]	G[kg/m2 s]	T_d[oC]	q [kW/m2]
Yoon *et al.* (2003)	Horizontal smooth copper tube D_i = 7.73 mm L = 0.47 m	CO_2	7.5 – 8	225 – 450	50 – 80	-
Dang and Hihara (2004)	Horizontal smooth copper tube D_i = 1, 2, 4, 6 mm L = 0.5 m	CO_2	8 – 10	200 – 1200	-	6 - 33
Son and Park (2006)	Horizontal smooth Stainless steel tube D_i = 7.75 mm	CO_2	7.5 – 10	200 – 400	90 – 100	-
Huai *et al.* (2007)	Horizontal multi-port Minichannel (10 circular copper channel) D_i = 1.31 mm L = 0.5 m	CO_2	7.4 – 8.5	113.7 – 418.6	22 – 53	-

P = pressure, T_d = CO_2 temperature inlet

Finally, in order to ensure that the overall water heating heat exchanger model is accurate or not, the sizes and temperature profiles of water heating heat exchangers predicted by the model will also be compared with experimental values of water heating heat exchangers proposed by authors in the open literature. This will validate the model as a whole and not just the refrigerant or water correlations.

5.2 Condensation Flow in Horizontal Smooth Tube of Pure Alternative Refrigerants

5.2.1 Heat transfer correlation validation

In this study, the experimental condensation heat transfer coefficients measured by Cavallini et *al.* (2001) for R410A were selected to compare with predicted values because they experimented with wide range of condensation temperatures and mass fluxes. In addition, accuracy for sensors and parameter of their experiment are acceptable as shown in Table 5.4.

Fig. 5.1 to 5.3 present comparison of experimental condensation heat transfer coefficients of pure R-410A flow in horizontal smooth tube and prediction values by means of three authors: Shah's correlation (Shah, 1979), Dobson's correlation (Dobson and Chato,1998) and Cavallini's correlation (Cavallini *et al.*, 2006) at the mass fluxes of 200, 400, and 750 kg/m^{2}s respectively. At the low mass flux (200 kg/m^{2}s), predicted values by means of the Dobson's correlation are close to experimental values while the other correlations predict poorly. However, heat transfer coefficients predicted by the Dobson correlation are different from the experimental values with an average deviation of about 25.6%.

At the medium and high mass fluxes (400 and 750 kg/m^{2}s), predicted heat transfer coefficients by means of the Dobson correlation agree very well with the experimental values with average deviation of 2.8% and 5.3% respectively. However, at the high vapor quality the predicted values are quite different from the experimental values.

Overall, the Dobson's correlation was deemed to provide adequate prediction accuracy across the full range of conditions for R410A refrigerant and its use in the model is justified.

Table 5.4: Accuracy for sensors and parameters (Cavallini *et al*., 2001)

Temperature	± 0.05 ^{o}C	Temperature difference	± 0.03^{o}C
Refrigerant flow rate	± 0.4%	Absolute pressure	± 0.1% f.s.
Water flow rate	± 1%	Differential pressure	± 0.06 kPa
Vapor quality	± 0.05	Heat flow rate	± 4.5%
Heat transfer coefficient	± 5.0%		

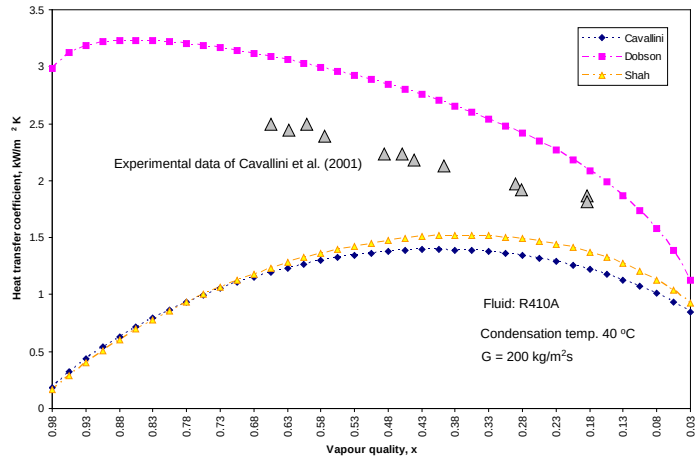

Figure 5.1: Predicted heat transfer coefficients against with the experimental data at G = 200 kg/m^{2}s

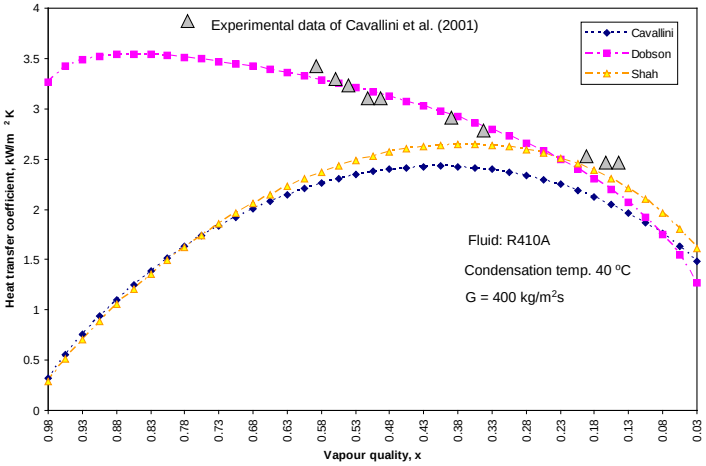

Figure 5.2: Predicted heat transfer coefficients against with the experimental data at G = 400 kg/m^{2}s

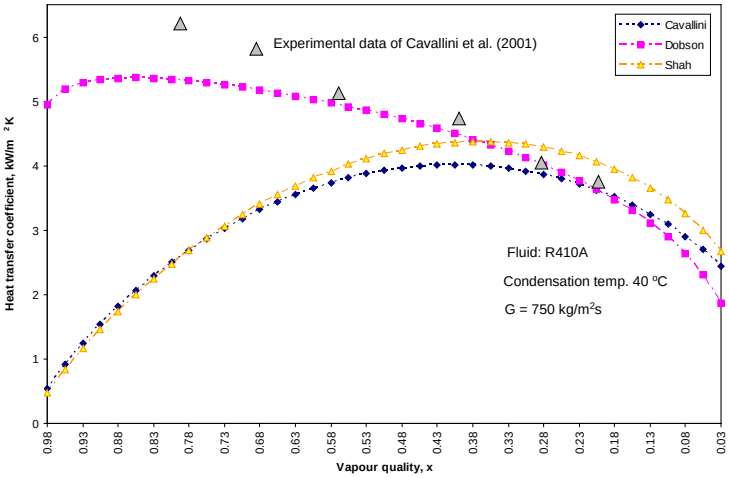

Figure 5.3: Predicted heat transfer coefficients against with the experimental data at G = 750 kg/m^{2}s

5.2.2 Pressure drop correlation validation

Fig. 5.4 presents comparisons between predicted and experimental pressure drops. It was found that predicted values by means of the Zhang and Webb's correlation agrees with the experimental with the mean difference of 7.14%, 8.8%, and 10.8% for mass flux of 200 kg/m^{2}s, 400 kg/m^{2}s, and 750 kg/m^{2}s respectively. At the high mass flux and high vapor quality the predictions are less accurate but still adequate.

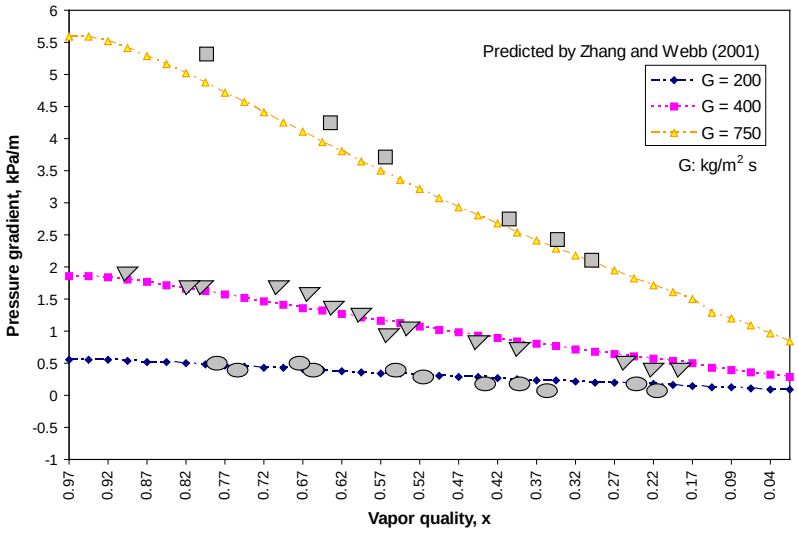

Figure 5.4: Predicted pressure gradient by Zhang and Webb's correlation against with the experimental data

5.3 Supercritical Flow in Horizontal Smooth Tubes for CO_2

Some experimental data for supercritical heat transfer coefficients and pressure drops are summarized in Table 5.3. The experimental data of Dang and Hihara (2004) were selected to compare with predicted data by means of Pitla *et al.* equation (Pitla *et al.*, 2001) used in the model. The accuracy for sensors and parameters of their experiment are presented in Table 5.5.

Table 5.5: Accuracy for sensors and parameters (Dang and Hihara, 2004)

Temperature	± 0.1^{o}C
Refrigerant flow rate	± 0.1 % F.S.
Water flow rate	± 0.5 % F.S.
Heat transfer coefficient	± 8.2% to ±30.4%
Absolute pressure	±0.001 MPa
Pressure drop	± 0.13.3 % to ±29.7%

5.3.1 Heat transfer correlation validation

Fig. 5.5 to Fig. 5.7 present comparison of measured heat transfer coefficients and predicted values using the Pitla *et al.* equation (Pitla *et al.*, 2001) at mass fluxes of 200, 400, and 800 kg/m^{2}s respectively. At all mass fluxes, the trend of predicted values agreed with the trend of the experimental values. At low mass flux (200 kg/m^{2}s) the prediction are slightly poorer than at high mass flux. For a discharge pressure at 10 MPa, the predicted values are just as accurate as shown in Fig. 5.8.

Overall, the Pitla *et al.* correlation was deemed to provide adequate prediction accuracy across the full range of conditions for R744 refrigerant and its use in the model is justified.

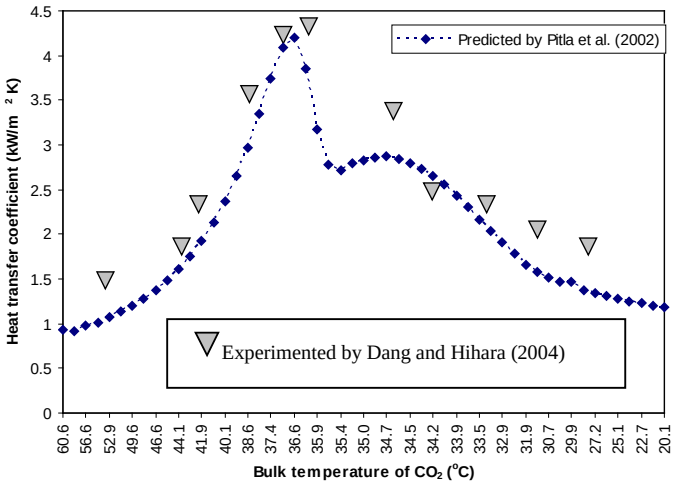

Figure 5.5: Predicted heat transfer coefficient against with the experimental data at G = 200 kg/m^2 s, P = 8 MPa, d_i = 6 mm

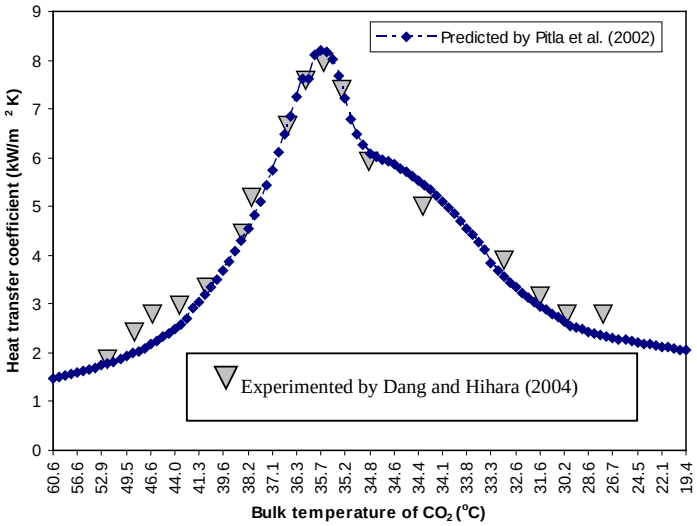

Figure 5.6: Predicted heat transfer coefficient against with the experimental data at G = 400 kg/m^2 s, P = 8 MPa, d_i = 6 mm

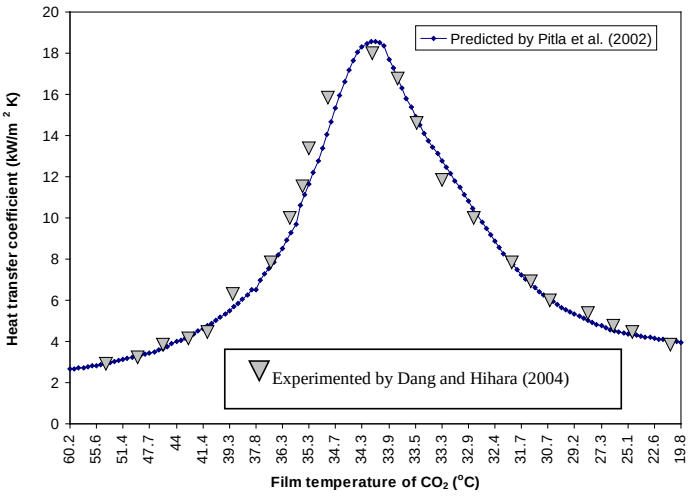

Figure 5.7: Predicted heat transfer coefficient against with the experimental data at G = 800 kg/m^2 s, P = 8 MPa, d_i = 4 mm

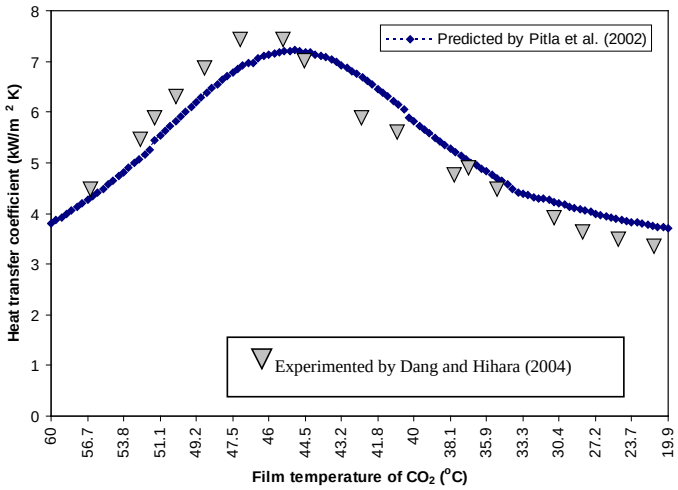

Figure 5.8: Predicted heat transfer coefficient against with the experimental data at G = 800 kg/m^2 s, P = 10 MPa, d_i = 4 mm

5.3.2 Pressure drop correlation validation

Fig. 5.9 presents comparison of experimental pressure drops and values predicted by means of three correlations at mass flux of 800 kg/m^{2}s. The methods were: *(1)* friction factor is calculated by Blasius's equation; *(2)* friction factor is replaced by modified friction factor calculated from Petrov and Propov equation and combined with Fang *et al.* equation (Fang *et al*., 2001); *and (3)* friction factor is calculated by Filonenko's equation. The methods *(1)* and *(3)* gave good agreement with the experimental data while *(2)* predicted very poorly. Therefore, the decision to use correlation *(3)* in the heating heat exchanger model is justified.

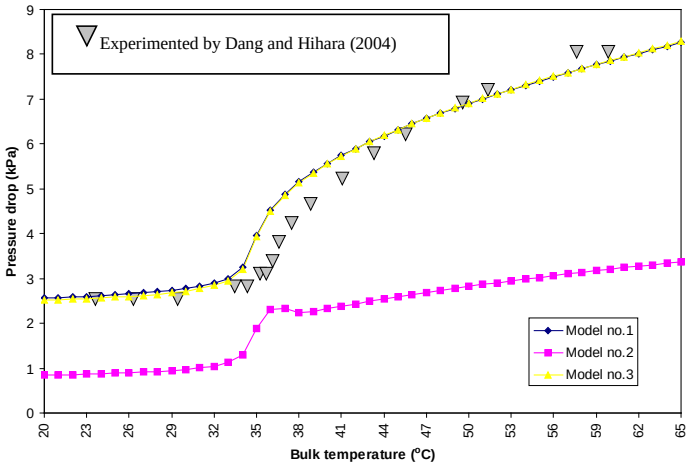

Figure 5.9: Predicted pressure drop against with the experimental data at G = 800 kg/m^2 s, P = 8 MPa, d_i = 2 mm

5.4 Validation of Water Heating Heat Exchanger Models

5.4.1 Available data

Some available configurations of water heating heat exchangers in the open literature are summarized in Table 5.6.

Table 5.6: Available configuration of water heating heat exchanger in the open literature

Authors	Single wall countercurrent heat exchanger		Fluid flow	
	Inner tube	Annulus tube	Inner tube	Annulus tube
Bukasa *et al.* (2004)	*C1:* smooth *C2:* inside-spiral fin	*C1:* smooth *C2:* smooth	R22, R134a	water
Lee *et al.* (2006)	*C3:* smooth	*C3:* smooth	R290, R600a, R1270, R22	water
Laohalertdecha and Wongwises ((2010)	*C4:* smooth *C5:* inside-corrugated	*C4:* smooth *C5:* smooth	R134a	water
Shao and Granryd (1995)	*C6:* smooth	*C6:* smooth	R134a/oil	water
Pitla *et al.* (2000)	*C7:* smooth	*C7:* smooth	CO_2	water

C: Configuration

Unfortunately, data supplied for *C1* to *C5* (Table 5.6) were incomplete so they could not be used for validation. The measurements with complete data that could be used for validation are available for *C6* and *C7*. The details are summarized below.

Configuration 6 (*C6*):

Fluid flow:	Countercurrent
Length:	10 m (considered only in condensation)
Inner tube:	Copper
- Inside diameter (smooth wall)	6 mm
- Outside diameter (smooth wall)	8 mm
- Working fluid	R134a with oil (SW2, 3.6% bulk mass)
- Mass flux	122 kg/m^2s
- Saturation temperature (refrigerant)	30 ^oC
Annulus tube: Copper	
- Inside diameter (smooth wall)	12.6 mm
- Outside diameter (smooth wall with complete insulation)	- mm
- Working fluid	water
- Water temperature outlet	29^oC
- Water temperature inlet	25 ^oC

Configuration 7 (*C7*):

Fluid flow:	Countercurrent
Length:	3.1 m
Inner tube:	stainless steel
- Inside diameter (smooth wall)	4.72 mm
- Outside diameter (smooth wall)	6.35 mm
- Working fluid	CO_2
- Mass flow rate	0.0274 kg/s
- Inlet temperature (refrigerant)	126
- Outlet temperature (refrigerant)	31.72
- Inlet pressure	11.19 MPa
- Outlet pressure	10.873 MPa
Annulus tube:	Copper tube
- Inside diameter (smooth wall)	15.748 mm
- Working fluid	water
- Mass flow rate	0.040497 kg/s
- Water temperature outlet	68.27^oC
- Water temperature inlet	24.1^oC

5.4.2. Condenser model validation

The experimental data of Shao and Granryd (1995) was used to validate the multi-zone and three zone models. As the experiment measured only condensation, the multi-zone model predicted from x = 0.99 until x = 0.0001 while three zone model (one-zone in condensation) predicted at $\bar{x}$ = 0.5. The data was for a single wall countercurrent heat exchanger. Therefore, the thermal conduction resistance of the second wall, thermal contact resistance, and thermal conduction resistance of air gap (Eq. 4.6) were set to zero. Input data into the model consisted of refrigerant mass flux, refrigerant condensation temperature, inlet and outlet water temperature, the first wall thickness, and inside diameter of inner and annulus tube as shown in Configuration 6.

Fig. 5.10 presents comparison of temperature profiles along the condenser. It was found that the predicted temperature profiles of refrigerant and water agreed well with the experimental temperature profiles. The predicted wall temperatures were slightly different from the experimental data. It may be caused by the measurement uncertainty.

The size of condenser predicted by the multi zone model and the one-zone model are given in Table 5.7. The multi-zone model is the best with very small deviation of -0.8%, while the one-zone model predicted with a deviation of -9.8%. The predicted length of condenser is less than the experimental length because in the multi-zone model heat loss was assumed negligible.

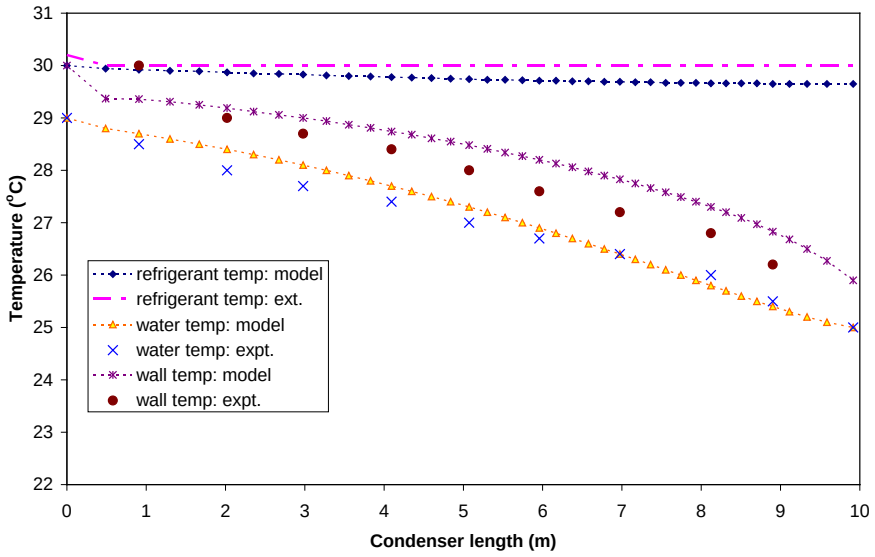

Figure 5.10: Temperature profiles along the condenser

Table 5.7: Comparison of experimented and the predicted lengths of condenser (% difference from experiment in bracket)

Experiment	One-zone model	Multi-zone model
10 m	9.017 (-9.8%)	9.917 m (-0.8%)

5.4.3 Gas cooler validation

Experimental data conducted by *Pitla et al.* (2000) was selected to validate the gas cooler multi-zone and one-zone models. The heat transfer test section (Fig. 5.11) consists of eight sub sections of counter current flow tube-in-tube heat exchanger. The first five sections were 1.8 m long heat exchanger and the remaining three were 1.3 m long.

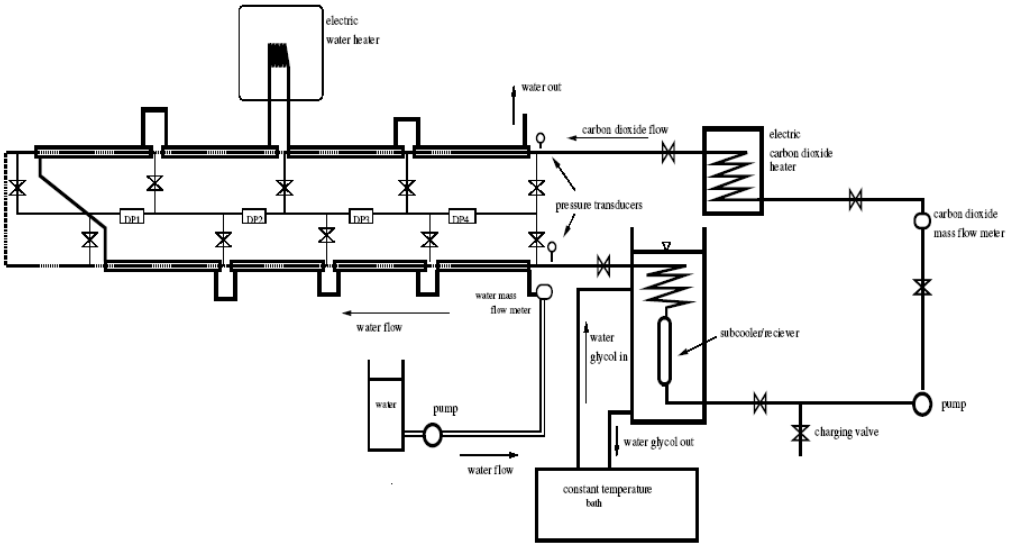

Figure 5.11: Schematic of the test apparatus (Pitla *et al.*, 2000)

As in the water loop the water was heated by the electrical heater, calculation of multi-zone and one-zone models was divided into two parts. The first part consisted of two sub heat exchangers (the 7^{th} and 8^{th} sub heat exchangers) and another part consists of six sub heat exchangers. The data was for a single wall countercurrent heat exchanger so the thermal conduction resistance of the second wall, thermal contact resistance, and thermal conduction resistance of air gap (Eq. 4.6) were assumed to be zero. Input data into the model consisted of mass flow rate of refrigerant and water, inlet refrigerant temperature, inlet refrigerant pressure, outlet water temperature, the first wall thickness, and inside diameter of inner and annulus tubes as shown in Configuration 7. The multi-zone model started to predict at the inlet refrigerant temperature until predicted water temperature was equal to outlet water temperature.

Table 5.8: Comparison of experimented and the predicted lengths of gascooler (% difference from experiment in bracket)

Experiment	One zone-model	Multi-zone model
3.1 m	3.32 m (+7.1%)	2.67m (-13.9%)

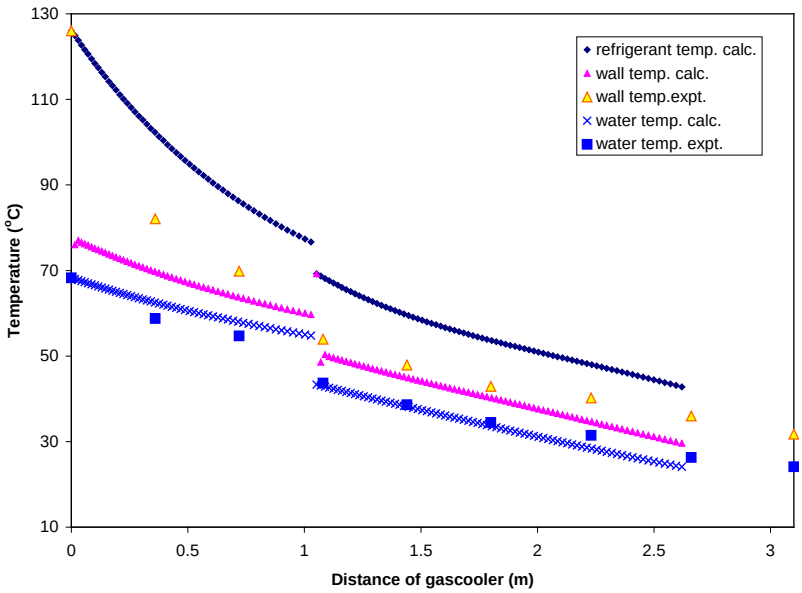

Figure 5.12: Temperature profiles along the gascooler

When temperature profiles along the gascooler were considered (Fig. 5.12), it was found that the predicted water temperatures agree with the experimental water temperatures along the gascooler. The predicted wall temperatures at CO_2 temperature above 90°C and at the below 50°C are quite different from the experimental wall temperatures. This may be caused by two things; first, it may be caused by heat loss as in the multi-zone model heat loss is negligible, and second it may be caused by the error of calculating CO_2 thermodynamic properties used in the model. For CO_2 temperature between 50°C and 90°C there was good agreement.

The predicted lengths from the multi-zone model deviated by -13.9%, while the one-zone model predicted poorly. As the model assumption heat losses were ignored, the predicted length should be lower than the experimental length.

The percent deviation of predicted length for gascooler model is higher than that of predicted length for condenser model because heat losses in gascooler might be higher than that in the condenser due to higher refrigerant temperature.

In conclusion, considering both the condenser and the gas cooler predictions, the multi-zone model for design water heating countercurrent heat exchanger (both condenser and gascooler) was deemed more accurate than the one-zone model.

CHAPER 6

HEAT EXCHANGER DESIGN USING THE MODEL

6.1 Design Conditions

The design focus was a heat exchanger for a once-through heat pump that would be connected to a stratified hot water cylinder. In this study, two alternative refrigerants, R-410A and R-744 (CO_2), were investigated because the environmental, physical, and safety data of these refrigerants are acceptable (see Table 2.5). Further, the R-410A refrigerant is suitable for subcritical cycle as a high pressure refrigerant and the R-744 refrigerant is suitable for transcritical cycle due to lower critical temperature combined with high pressure.

The heating capacity of the water heating heat exchanger should be high enough to allow rapid recovery of water temperature after water use but it should not have too high system and running costs. In addition, running time should not be too short with average hot water use. For that reasons, the heating capacity of water heating heat exchanger was designed to be 3 kW. Based on annual average cold water temperature in New Zealand, the inlet water temperature was assumed to be 15^{o}C and to avoid the growth of *Legionella* the outlet water temperature was assumed to be 60^{o}C. The outlet heat exchanger water pressure was assumed to be 101.3 kPa. As the annual ambient air temperature in New Zealand is between 10 and 15^{o}C, the refrigerant evaporation temperature was assumed to be 5^{o}C (that is an evaporator design temperature difference of 5 to 10^{o}C). As a consequence, in order to prevent too larger pinch effect in the heat exchanger, and too high discharge temperature, yet give reasonably COP of the system, the condensing temperature was assumed to be 64^{o}C for R-410A and the inlet gascooler refrigerant pressure was assumed to be 11 MPa for R-744. In both systems the refrigerant was assumed to be sub cooled to 25^{o}C which is a 10^{o}C approach to the water inlet temperature.

At the above conditions, the inlet refrigerant temperatures, refrigerant mass flow rates, and water flow rate were predicted by the overall heat pump model. Compressor heat loss was assumed to be 10% of compressor work rate. Heat losses or gain from discharge and suction lines were assumed negligible and refrigerant pressure drops in discharge and suction lines were also assumed negligible. As a consequence, the predicted inlet refrigerant temperatures to the condenser/gascooler were 98.4^{o}C for R-410A and 92.4^{o}C for R-744. The predicted R-410A and R-744 mass flow rates were 0.01247 kg/s and 0.01311 kg/s respectively, and the predicted water flow rate was 0.01594 kg/s.

6.2 Criteria for Comparison of Heat Exchanger Design

The criteria for comparison of different designs consisted of water pumping power (*EP)*, coefficient of performance (*COP*), mean heat transfer surface area (*HTA*) of heat exchanger, length and weight of heat exchanger, heat transfer coefficient for both refrigerant and water sides, and average log-mean temperature difference (*LMTD*).

- *EP* is the energy use by the water pump. A high *EP* means high operating cost of the system and lower *COP*.
- *COP* is an indicator of energy efficiency of the system. A high *COP* means reduced energy use and operating cost saving.
- *HTA* is an indicator of heat transfer performance of a heat exchanger. A low *HTA* means high heat transfer performance leading to shorter heat exchanger length and lower heat exchanger weight.
- Heat exchanger length is an indicator of compactness of a heat exchanger. It may also affect ease of manufacture and cost.
- Heat exchanger weight is an indicator of material cost. A low heat exchanger weight means low material cost.
- *LMTD* is an indicator of potential for heat transfer and the effect of refrigerant pressure drop on heat exchanger design. If refrigerant pressure drop is high, *LMTD* will be lower leading higher *HTA*.

6.3 Configuration *I* Design

6.3.1 Effects of flow channel dimensions

This section analyses the effect of flow channel for configuration *I* using the model. The %contact and air gap thickness were chosen to be 0% and 0.1 mm respectively. A This gap size is the minimum so that refrigerant or oil can leave from the system if it leaks yet keeps thermal resistance from the air gap small. All tube used in this investigation were copper tubes. For R-410A, tube wall thickness was chosen to be 0.8128 mm (Table 6.1) for all tubes because they are standard tubes used in the industry. For R-744, tube wall thicknesses were 0.9 mm for the first tube due to higher operating pressure and 0.8128 mm for the second and the third tubes. The design was considered by two cases:

1. Case *A*: The refrigerant flows in the inner tube while the water countercurrent flows in the annulus tube.
2. Case *B*: The water flows in the inner tube while the refrigerant countercurrent flows in the annulus tube.

Table 6.1 Copper tube standard for TATMB 280 Copper Tube-ACR

Inside diameter	Wall thickness
3.175 – 6.35 mm	0.762 mm
7.9375 – 12.7 mm	0.8128 mm
15.875 – 19.05 mm	0.889 mm

6.3.1.1 Configuration *I* design for case *A*

6.3.1.1.1 Water flow channel dimensions

The refrigerant flow channel (d_i) was chosen to be 9.525 mm for both R410A and R744 systems while the water flow channel ($D_i - d_2$) was varied from 0.5 mm to 3 mm.

Predicted results for water flow channel effect on water pressure and heat transfer coefficient were presented in Fig. 6.1. The results showed that there is a trade-off between water pressure drop and water heat transfer coefficient for both R410A system and R744 system. When water flow channel ($D_i - d_2$) was decreased, water heat transfer coefficient increased significantly while water pressure drop slowly increased (Fig. 6.1). For $D_i - d_2 < 1$ mm, both water pressure drop and heat transfer coefficient dramatically increased.

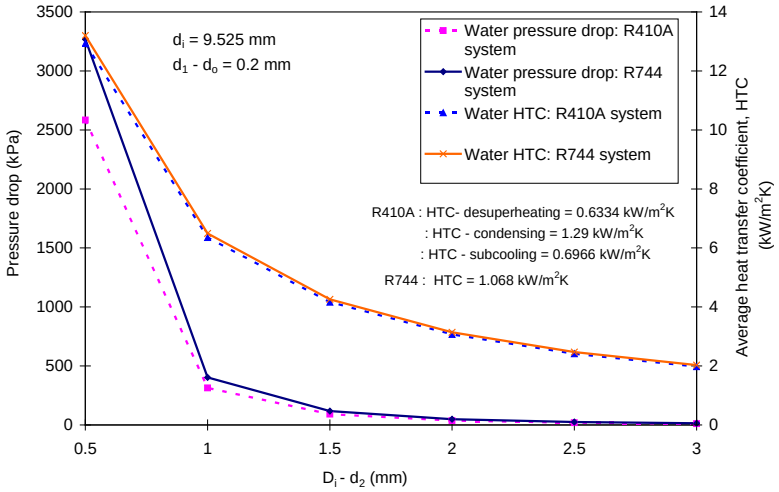

Figure 6.1: Water flow channel effect of configuration *I* on pressure drop and heat transfer coefficient for case *A*

As water heat transfer coefficient significantly increased when water flow channel decreased with constant refrigerant flow channel (constant refrigerant heat transfer coefficient), length and mean heat transfer surface decreased for both systems (Fig. 6.2) and weight of heat exchanger also decreased (Fig. 6.3). Length, mean heat transfer surface and weight were less for R410A system than the R744 system because the average log-mean temperature of the R410A system was higher than the R744 system due to the higher discharge temperature.

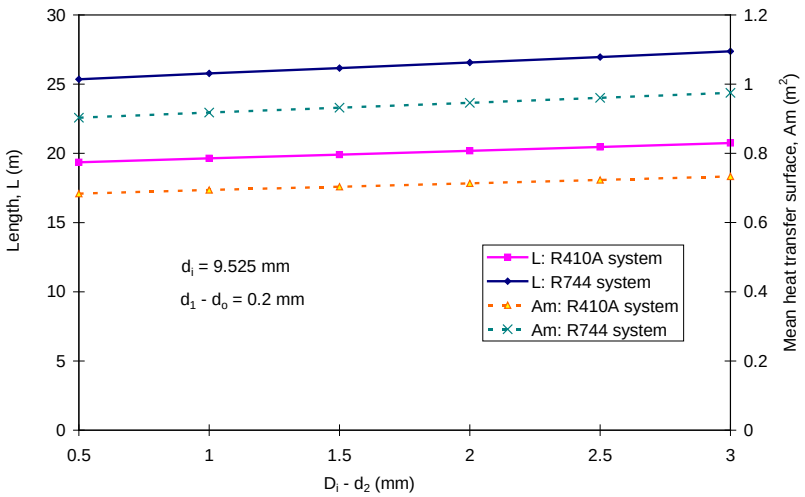

Figure 6.2: Water flow channel effect of configuration *I* on length and heat transfer surface of heat exchanger for case *A*

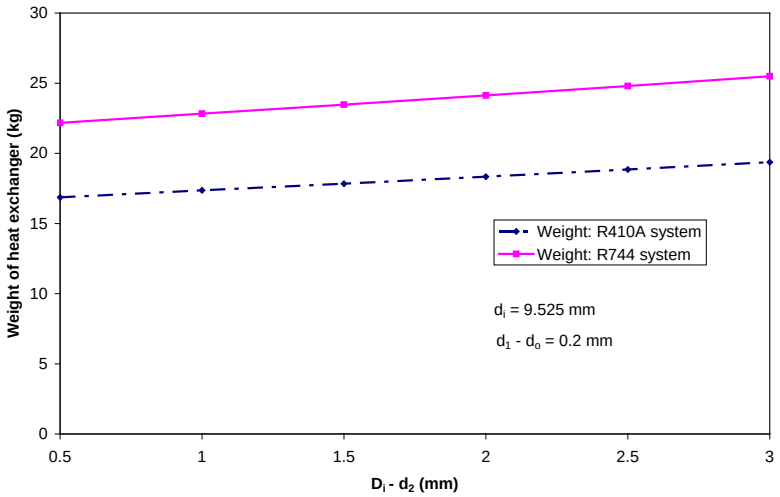

Figure 6.3: Water flow channel effect of configuration *I* on weight of heat exchanger for case *A*

Decreased water flow channel led to increased water pumping power due to higher water pressure drop while *COP* of the system decreased (Fig. 6.4). The effect on water pumping power and *COP* was only significant for water flow channels less than 1 mm. As a consequence, the optimal water flow channel was deemed to be between 1 and 2 mm. This corresponds to a water-side cross-sectional area for flow of between 0.00001563 and 0.00003283 m^2.

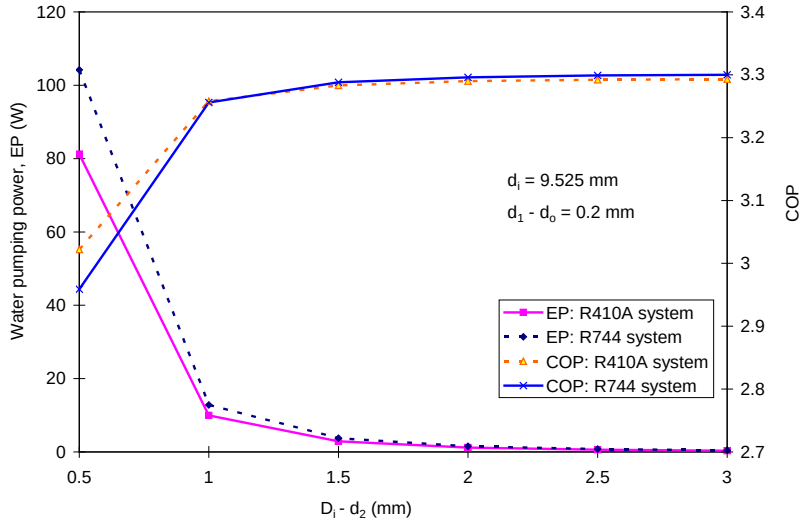

Figure 6.4: Water flow channel effect of configuration *I* on pumping power and *COP* of the system for case *A*

6.3.1.1.2 Refrigerant flow channel dimensions

In this investigation, cross-sectional area of water was fixed at 0.00002304 m^2 (based on optimal water flow channel) while the refrigerant flow channel (d_i) was varied from 4 to 9 mm for R410A and from 2.5 to 8 mm for R744.

Predicted results for refrigerant flow channel effect on refrigerant pressure drop and heat transfer coefficient are shown in Fig. 6.5 for R410A system and in Fig 6.6 for R744 system. The results showed that there is a trade-off between the refrigerant pressure drop and refrigerant heat transfer coefficient similar to the water flow channel effect. However, decreased refrigerant flow channel reduced average log-mean temperature difference (*LMTD*) due to higher pressure drop as shown in Fig 6.7 and 6.8. There was significant decrease of average *LMTD* when the refrigerant flow channel was less than 5 mm for R410A (Fig. 6.7) and less than 4 mm for R744 (Fig. 6.8). In a range of insignificant decrease of average *LMTD* (low refrigerant pressure drop), mean heat transfer surface area of heat exchanger was dominated by increased refrigerant heat transfer coefficient. As a consequence, mean heat transfer surface area significantly decreased as refrigerant heat transfer coefficient increased when refrigerant flow channel decreased to 5 mm for R410A (Fig. 6.9) and to 4 mm for R-744 (Fig 6.11). This corresponded to decrease heat exchanger weight for both R-410A (Fig. 6.10) and R744 (6.12). By contrast, in a range of significant decrease of average *LMTD* (high refrigerant pressure drop), mean heat transfer surface area of heat exchanger was dominated by *LMTD* drop rather than increased refrigerant heat transfer coefficient when refrigerant flow channel decreased. Therefore, mean heat transfer surface area increased as average *LMTD* decreased when refrigerant flow channel was less than 5 mm for R410A system (Fig. 6.9) and less than 4 mm for R-744 (Fig 6.11). This corresponded to increase heat exchanger weight for both R-410A (Fig. 6.10) and R744 (6.12).

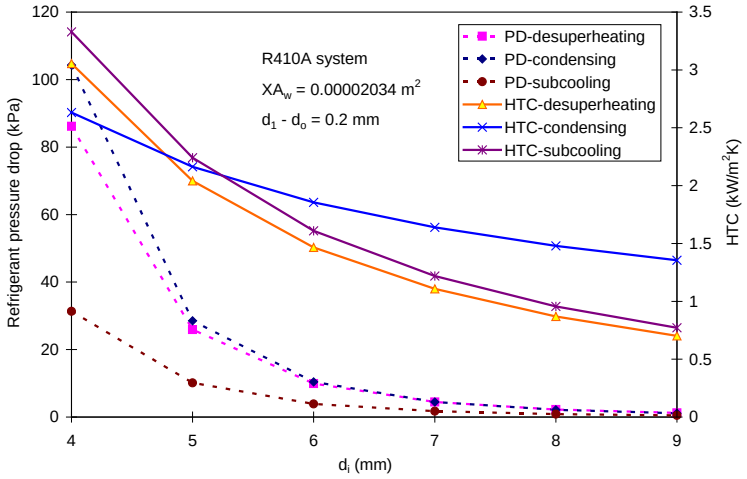

Figure 6.5: Refrigerant flow channel effect of configuration *I* on refrigerant pressure drop and heat transfer coefficient for R410A case *A*

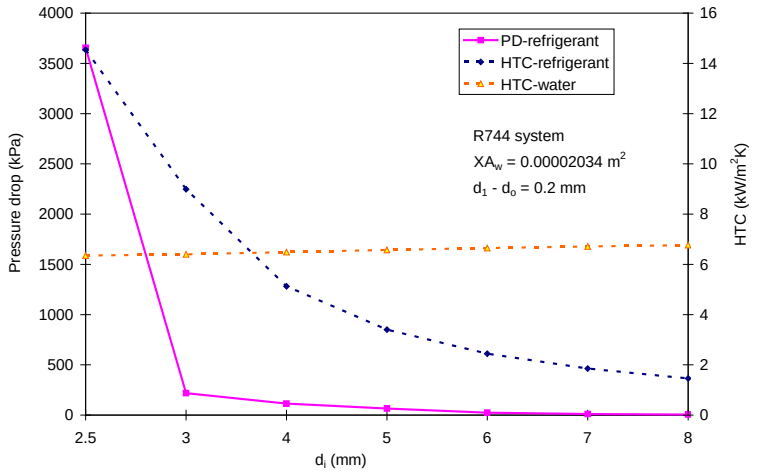

Figure 6.6: Refrigerant flow channel effect of configuration *I* on refrigerant pressure drop and heat transfer coefficient for R744 case *A*

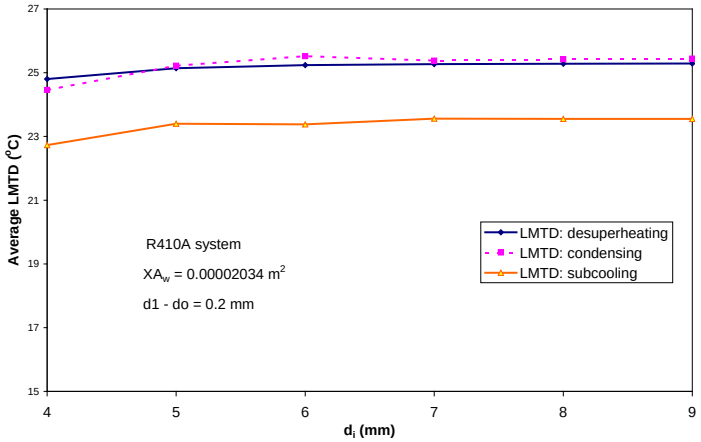

Figure 6.7: Refrigerant flow channel effect of configuration *I* on *LMTD* for R410A case *A*

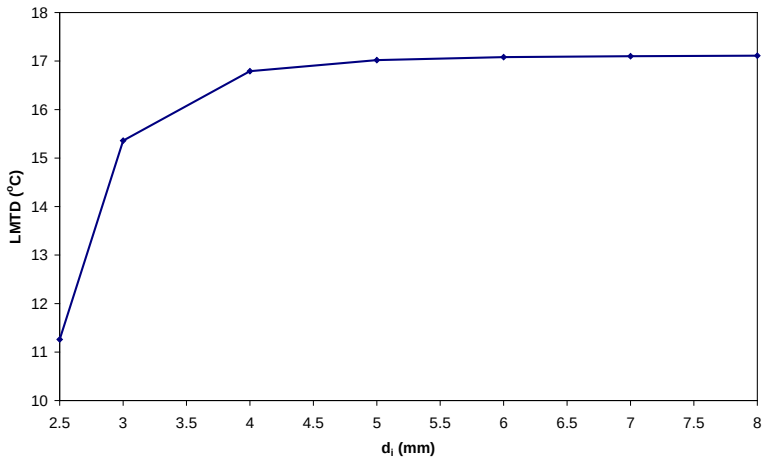

Figure 6.8: Refrigerant flow channel effect of configuration *I* on *LMTD* for R744 case *A*

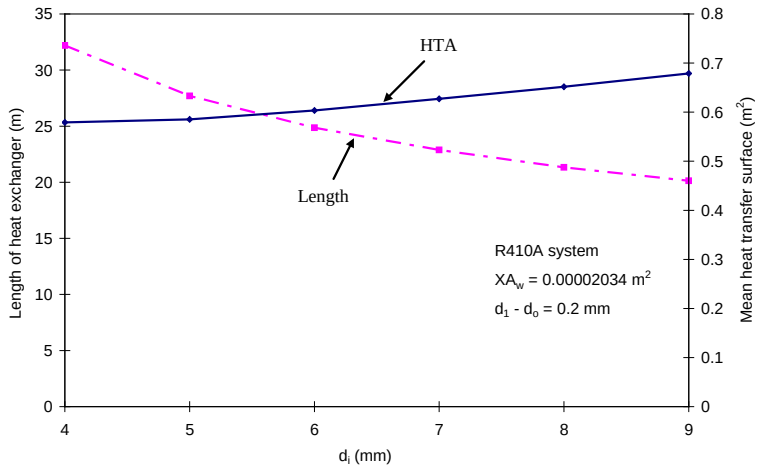

Figure 6.9: Refrigerant flow channel effect of configuration *I* on length and heat transfer surface of heat exchanger for R410A case *A*

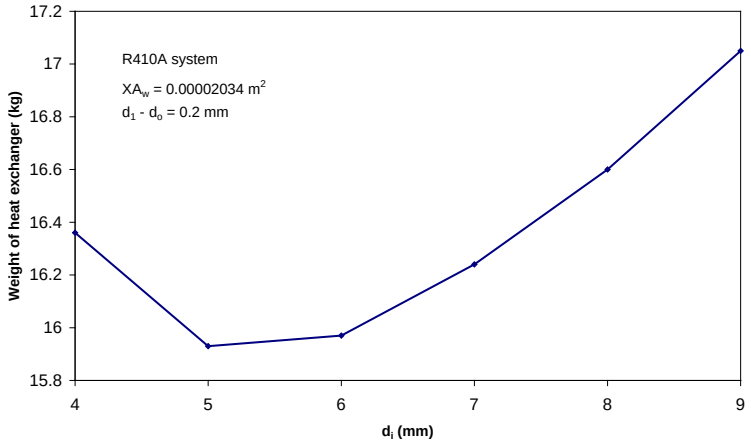

Figure 6.10: Refrigerant flow channel effect of configuration *I* on weight of heat exchanger for R410A case *A*

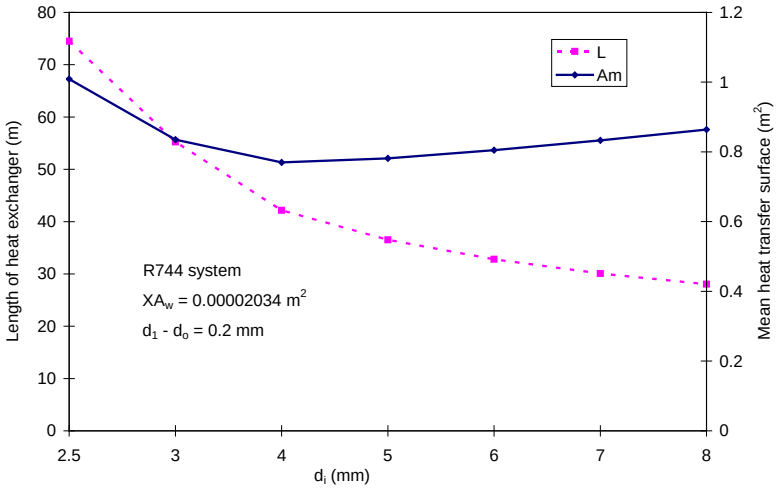

Figure 6.11: Refrigerant flow channel effect of configuration *I* on length and heat transfer surface of heat exchanger for R744 case *A*

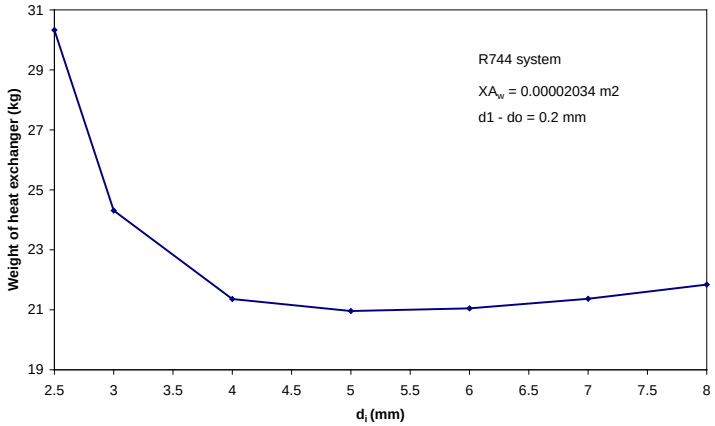

Figure 6.12: Refrigerant flow channel effect of configuration *I* on weight of heat exchanger for R744 case *A*

The effect of refrigerant flow channel on water pumping power and *COP* of the system for both R410A and R744 was insignificant because water pressure drop was not significantly changed (Fig. 6.13 and 6.14). As a consequence, the optimal refrigerant flow channel was determined to be between 5 and 6 mm for R410A and between 4 and 5 mm for R744.

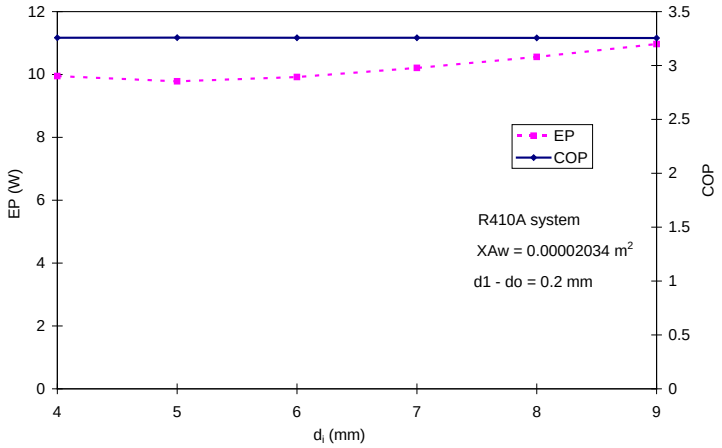

Figure 6.13: Refrigerant flow channel effect of configuration *I* on pumping power and *COP* for R410A case *A*

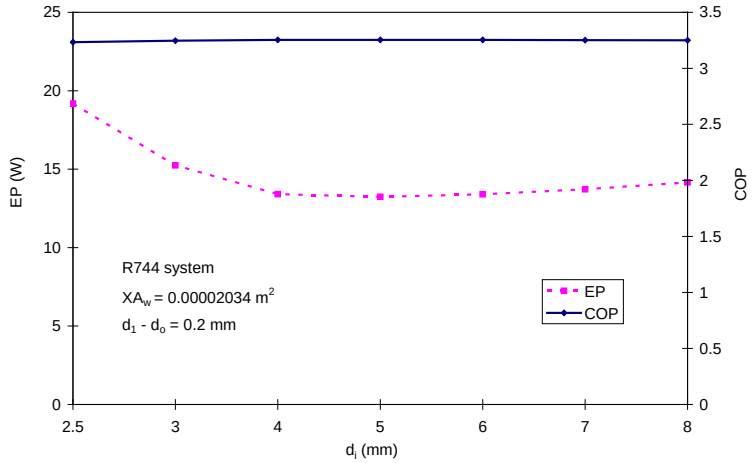

Figure 6.14: Refrigerant flow channel effect of configuration *I* on pumping power and *COP* for R744 case *A*

In conclusion, the optimal configuration *I* for R410A case *A* with d_i of 6 mm, $d_1 - d_o$ of 0.2 mm, and $D_i - d_2$ of 1.5 mm has a length of 27.5 m, a weigth of 16.2 kg, a mean *HTA* of 0.6 m^2, a pumping power of 28.6 W, and a *COP* of 3.3.

For the optimal configuration *I* for R744 case *A* with d_i of 5 mm, $d_1 - d_o$ of 0.2 mm, $D_i - d_2$ of 1.5 mm has a length of 41.6 m, a weigth of 21 kg, a mean *HTA* of 0.78 m^2, a pumping power of 24.4 W, and a *COP* of 3.3.

6.3.1.2 Configuration *I* design for case *B*

6.3.1.2.1 Water flow channel dimensions

In this investigation, cross-sectional flow area for refrigerant (XA_r) was fixed at 0.00004 m^2 for both R410A and R744 while the water flow channel (d_i) was varied from 5 mm to 9 mm.

The water flow channel effect on water pressure drop and water heat transfer coefficient are presented in Fig. 6.15. The results showed that there is a trade-off between water pressure drop and water heat transfer coefficient for both R410A and R744. The water heat transfer coefficient for both R410A and R744 has the same trend.

In addition, the water flow channel effect on heat exchanger length and mean heat transfer surface area are shown in Fig. 6.16. It was found that there is a trade-off between heat exchanger length and mean heat transfer surface area for both R410A and R744 because outside perimeter of the 1st and the 2nd tubes changed as water flow channel changed. When water flow channel decreased, heat exchanger length increased but mean heat transfer surface area decreased due to increased water heat transfer coefficient (Fig. 6.15). The net effect on predicted heat exchanger weight as presented in Fig. 6.17. Predicted heat exchanger weight increased when water flow channel was lower than or greater than 8 mm for R410A and 7 mm for R744 (Fig. 6.17) but the difference were not large.

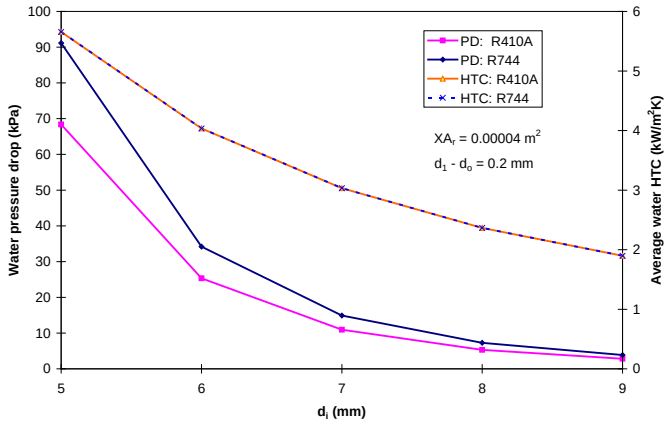

Figure 6.15: Water flow channel effect of configuration *I* on pressure drop and heat transfer coefficient for case *B*

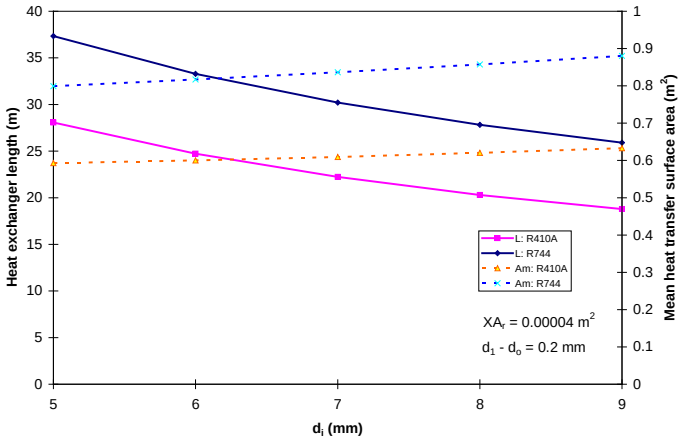

Figure 6.16: Water flow channel effect of configuration *I* on length and heat transfer surface of heat exchanger for case *B*

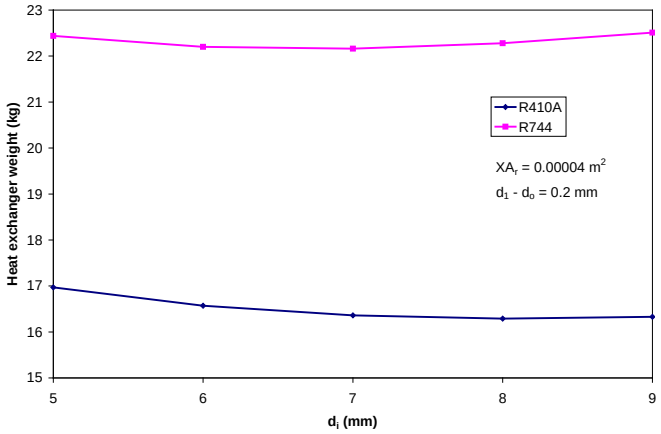

Figure 6.17: Water flow channel effect of configuration *I* on weight of heat exchanger for case *B*

The water flow channel effect on pumping power and coefficient of performance (*COP*) is significant. However, a range of water flow channel used in this investigation was not significant to increase water pumping power and to decrease *COP* as shown in Fig. 6.18.

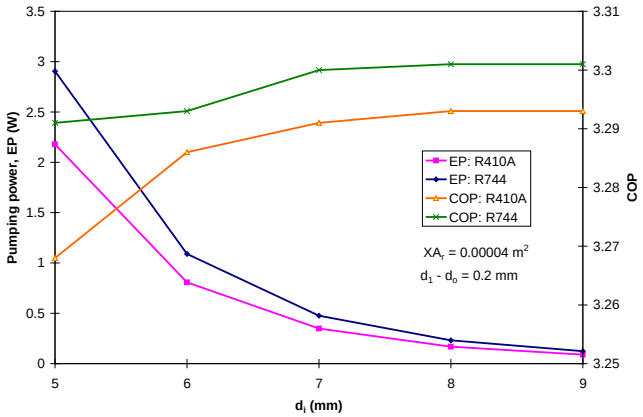

Figure 6.18: Water flow channel effect of configuration *I* on pumping power and *COP* for case *B*

Therefore, the optimal flow channel (d_i) for configuration *I* case *B* is 8 mm for R410A and 7 mm for R744.

6.3.1.2.2 Refrigerant flow channel dimensions

In this investigation, cross-sectional flow area for water was fixed at d_i = 8 mm for R410A and at d_i = 7 mm for R744 (based on optimal water flow channel) while the refrigerant flow channel ($D_i - d_2$) was varied from 1 to 2.5 mm for R410A and was varied from 0.5 to 2.5 mm for R744.

The refrigerant flow channel effect on refrigerant pressure drop and heat transfer coefficient was shown in Fig. 6.19 for R410A and Fig. 6.20 for R744. As similar to case *A* there is a trade-off between refrigerant pressure drop and refrigerant heat transfer coefficient for both R410A and R744 for case *B*.

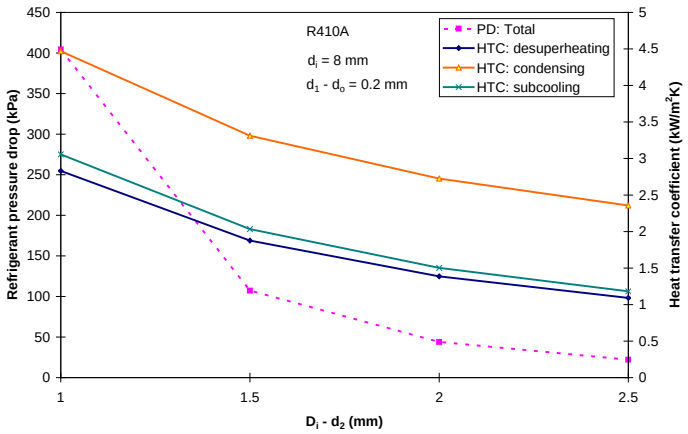

Figure 6.19: Refrigerant flow channel effect of configuration *I* on refrigerant pressure drop and heat transfer coefficient for R410A case *B*

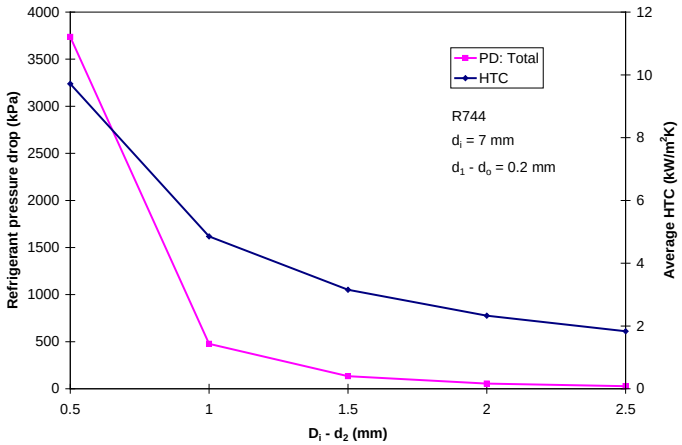

Figure 6.20: Refrigerant flow channel effect of configuration *I* on refrigerant pressure drop and heat transfer coefficient for R744 case *B*

Refrigerant pressure drop significantly increased when refrigerant flow channel (D_i – d_2) was less than 1.5 mm for R410A (Fig. 6.19) and was less than 1 mm for R744 (Fig. 6.20). The high pressure drop caused decreased average *LMTD* for both R410A and R744 as shown in Fig. 6.21 and 6.22 respectively.

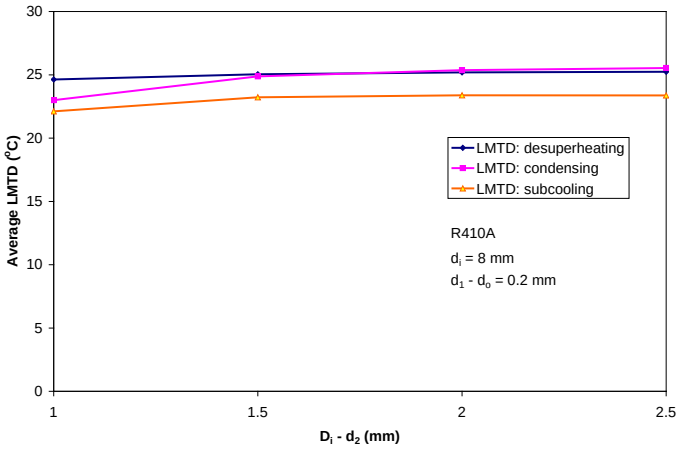

Figure 6.21: Refrigerant flow channel effect of configuration *I* on *LMTD* for R410A case *B*

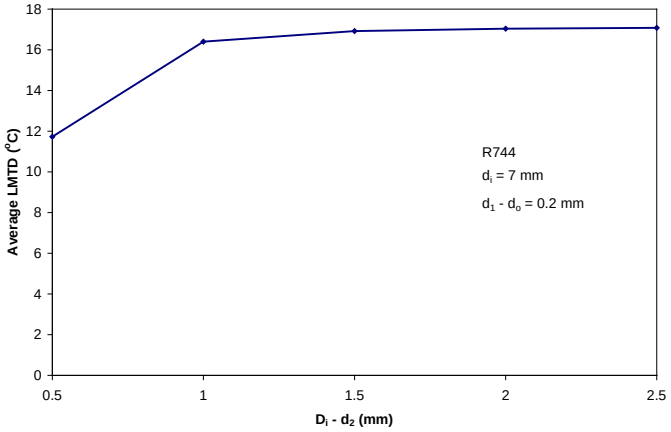

Figure 6.22: Refrigerant flow channel effect of configuration *I* on *LMTD* for R744 case *B*

A decrease of *LMTD* was significant to increase mean heat transfer surface area for both R410A and R744 (Fig. 6.23 and 6.24) while an increase of refrigerant heat transfer coefficient with low pressure drop (no effect on *LMTD*) was significant to decrease mean heat transfer surface area for R410A (Fig. 6.23) and was small significant to decrease mean heat transfer surface area for R744 (Fig. 6.24). As a consequence, heat exchanger length and weight increased when refrigerant flow channel was lower than or greater than 1.5 mm for R410A (Fig. 6.23 and 6.25) and 1 mm for R744 (Fig. 6.24 and 6.26).

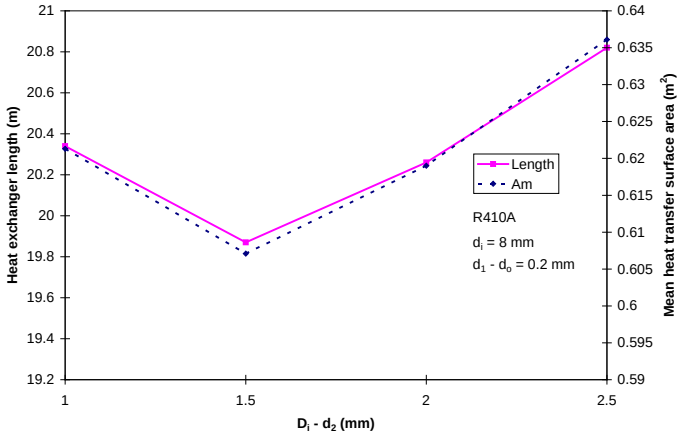

Figure 6.23: Refrigerant flow channel effect of configuration *I* on length and heat transfer surface of heat exchanger for R410A case *B*

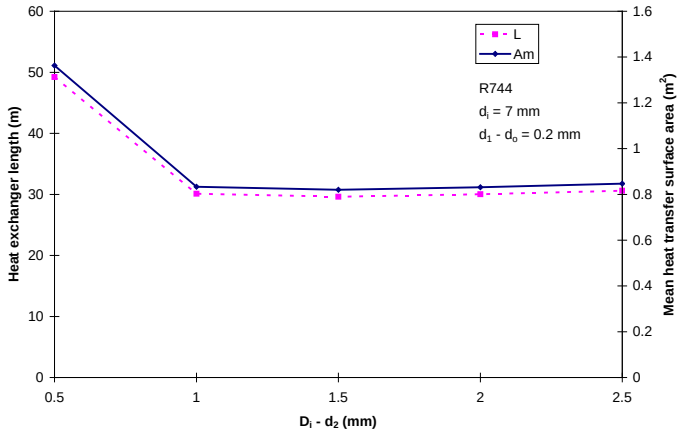

Figure 6.24: Refrigerant flow channel effect of configuration *I* on length and heat transfer surface of heat exchanger for R744 case *B*

The refrigerant flow channel effect on water pumping power and *COP* was insignificant for both R410A and R744 as shown in Fig. 6.27 and 6.28 respectively.

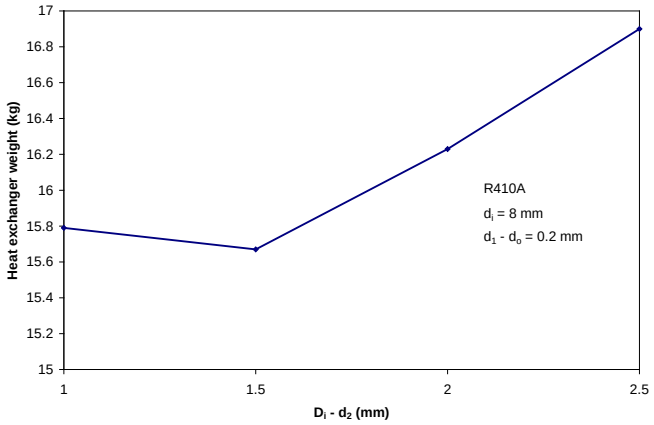

Figure 6.25: Refrigerant flow channel effect of configuration *I* on weight of heat exchanger for R410A case *B*

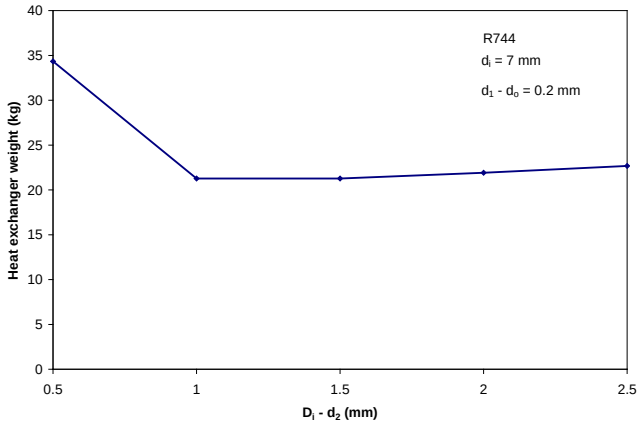

Figure 6.26: Refrigerant flow channel effect of configuration *I* on weight of heat exchanger for R744 case *B*

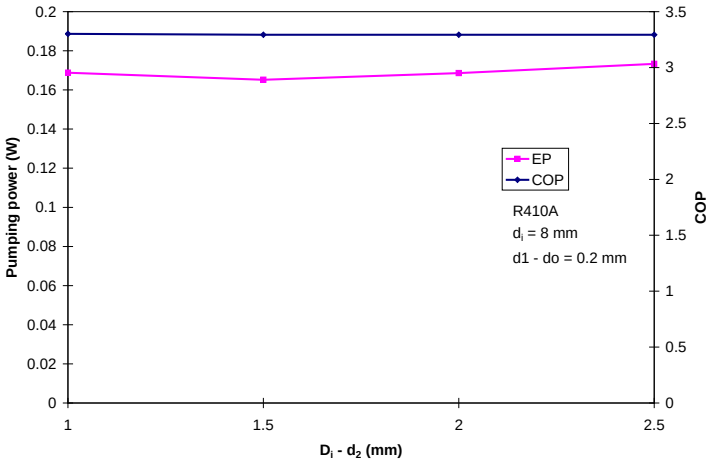

Figure 6.27: Refrigerant flow channel effect of configuration *I* on pumping power and *COP* for R410A case *B*

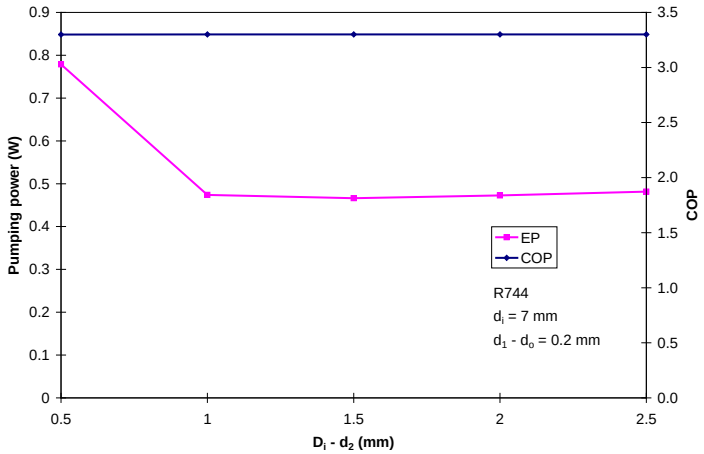

Figure 6.28: Refrigerant flow channel effect of configuration *I* on pumping power and *COP* for R744 case *B*

In conclusion, the optimal configuration *I* for R410A case *B* with d_i of 8 mm, $d_1 - d_o$ of 0.2 mm, and $D_i - d_2$ of 1.5 mm has a length of 20 m, a weigth of 16 kg, a mean *HTA* of 0.60 m^2, a pumping power of 0.2 W, and a *COP* of 3.3.

The optimal configuration *I* for R744 case *B* with d_i of 7 mm, $d_1 - d_o$ of 0.2 mm, $D_i - d_2$ of 1 mm has a length of 30 m, a weigth of 21 kg, a mean *HTA* of 0.82 m^2, a pumping power of 0.5 W, and a *COP* of 3.3.

Clearly, configuration *I* case *B* was performed better than case *A* for both R410A and R744.

Further, when thermal resistances in the optimal configuration *I* case *B* for both R410A and R744 were compared (Table 6.2), it was found that the resistance of air gap was the largest resistance for both R410A and R744 and it was much greater than other resistances. The resistance of water side was slightly higher than the refrigerant side for both R410A and R744. Therefore, in order to improve this configuration, the air gap should be improved first followed by both water and refrigerant flow channels for both R410A and R744.

Table 6.2: Average thermal resistance in optimal configuration *I* case *B* (based on mean *HTA*)

Thermal resistance (Km^2/kW)	R410A	R744
1. Refrigerant side ($R_{convect,r}$)	0.35	0.26
2. Water side ($R_{convect,w}$)	0.48	0.41
3. Air gap and contact ($R_{airgap} + R_{contact}$)	3.60	3.61
4. Tube wall conduction ($R_{wall1} + R_{wall2}$)	0.0042	0.0041
5. ***Total***	***4.43***	***4.28***

6.4 Configuration *II* Design

For this configuration, major length and wall thickness for both channels were assummed to be equal ($b_{1i} = b_{2i}$). The wall thickness was chosen to be 0.8128 mm for R410A and 0.9 mm for R744. All tubes were made from copper.

6.4.1 Effects of flow channel dimensions

6.4.1.1 Water flow channel dimensions

The R410A system was used to investigate water flow channel effect. The refrigerant flow channel was assumed to be constant (b_{1i} = 9 mm and a_{1i} = 4 mm) while the water flow channel minor length (a_{2i}) was varied from 0.5 to 4 mm with constant major length (b_{2i}). Therefore, contact distance (z) was determined by:

$$z = b_{1o} - a_{1o} \quad \text{when} \quad a_{2i} \le 4\ mm \quad \text{and} \quad z = b_{1o} - a_{2o} \quad \text{when} \quad a_{2i} > 4\ mm$$

Predicted results for the effect of water flow channel on water pressure drop, heat transfer coefficient, mean *HTA*, length of heat exchanger, weight of heat exchanger, *LMTD*, water pumping power and *COP* are shown in Fig. 6.29 to 6.32. It can be seen that the trends were similar to the predicted results for configuration *I* (see Section 6.2.1.1). Therefore, the optimal flow channel for configuration *II* a_{2i} was deemed to be between 1 and 1.5 mm based on the trade-off between *COP* and *EP* (Fig. 6.32).

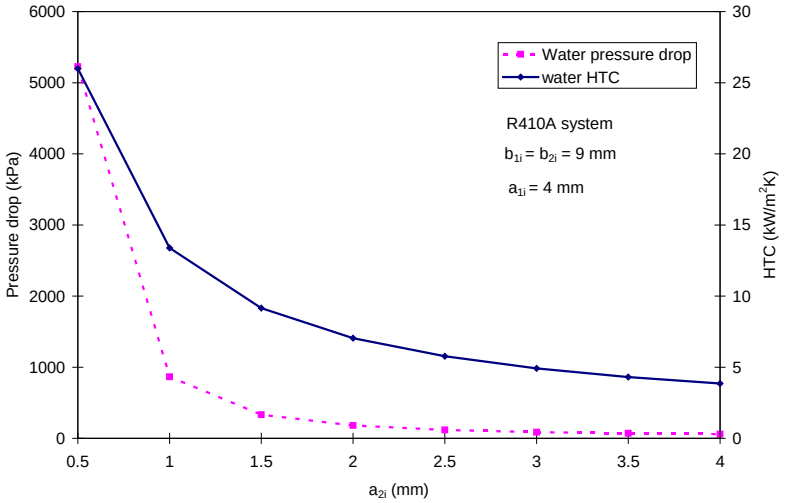

Figure 6.29: Water flow channel effect of configuration *II* on pressure drop and average *HTC* for R410A

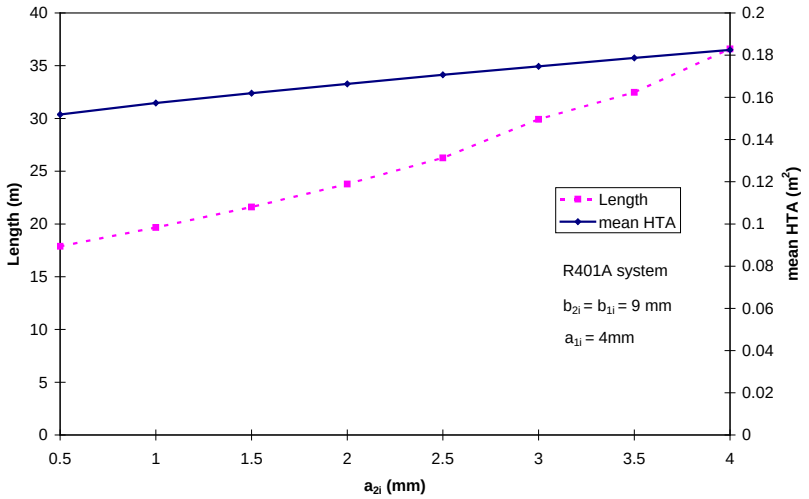

Figure 6.30: Water flow channel effect of configuration *II* on length and mean *HTA* for R410A

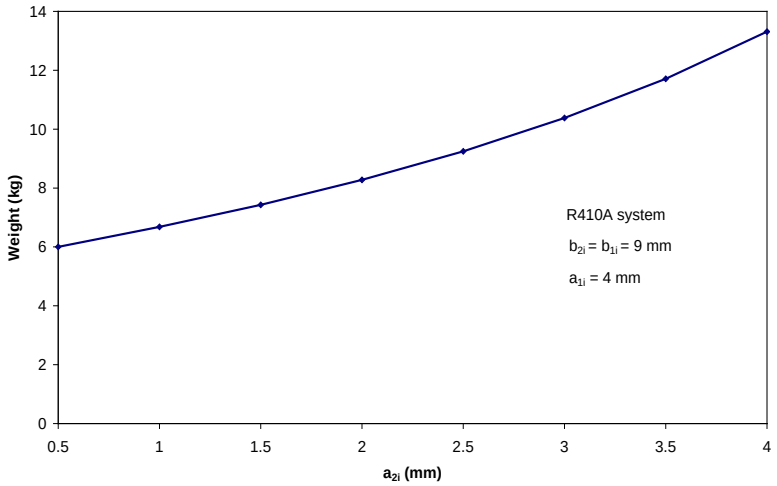

Figure 6.31: Water flow channel effect of configuration *II* on weight of heat exchanger for R410A

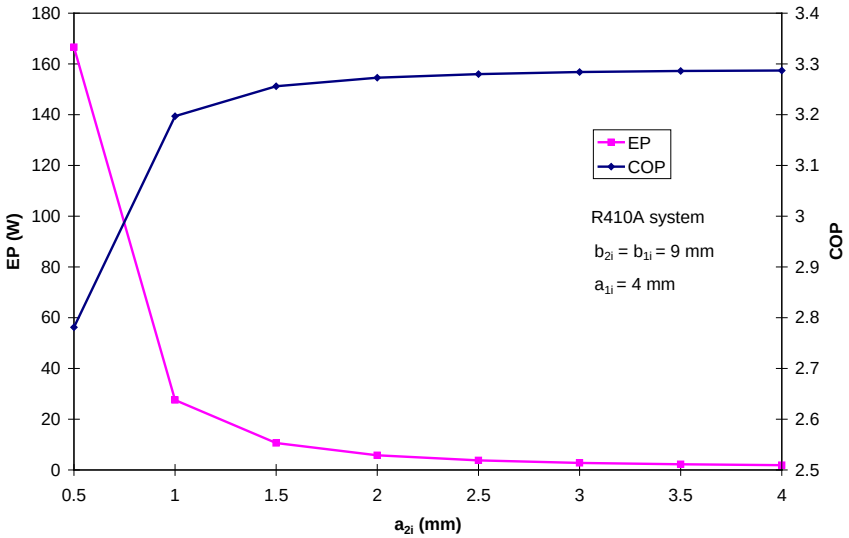

Figure 6.32: Water flow channel effect of configuration *II* on pumping power and *COP* of the system for R410A

6.4.1.2 Refrigerant flow channel dimensions

Both the R410A and R744 systems were used to investigate refrigerant flow channel effect. The water flow channel was assumed to be constant (b_{2i} = 9 mm and a_{2i} = 1.5 mm) based on the previous section while the refrigerant flow channel minor length (a_{1i}) was varied from 1 to 6 mm for R410A and from 0.7 to 4 mm for R744 with constant major length (b_{1i}). Therefore, contact distance for both R410A and R744 (z) was determined by:

$$z = b_{2o} - a_{2o} \quad \text{when} \quad a_{1i} \le 1.5\ mm \quad \text{and} \quad z = b_{2o} - a_{1o} \ \text{when} \ \ a_{1i} > 1.5\ mm$$

Predicted refrigerant flow channel effect on refrigerant pressure drop and heat transfer coefficient are shown in Fig. 6.33 for R410A and Fig. 6.34 for R744.

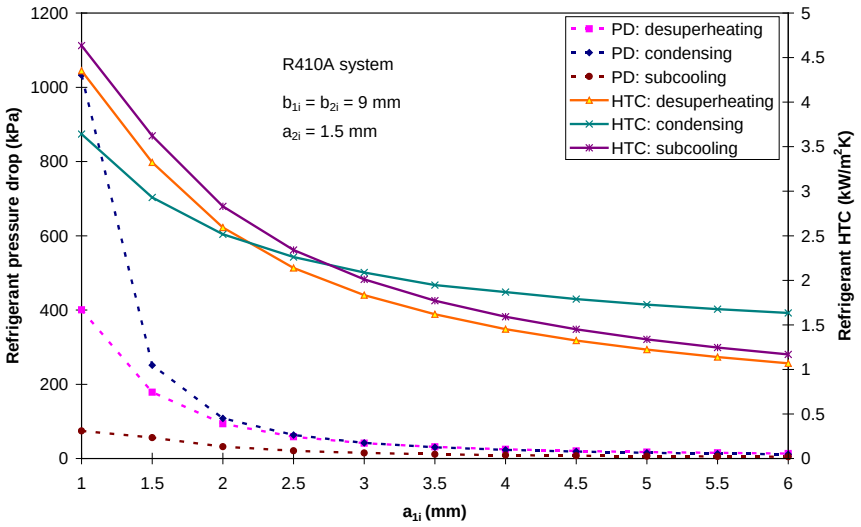

Figure 6.33: Refrigerant flow channel effect of configuration *II* on pressure drop and average *HTC* for R410A

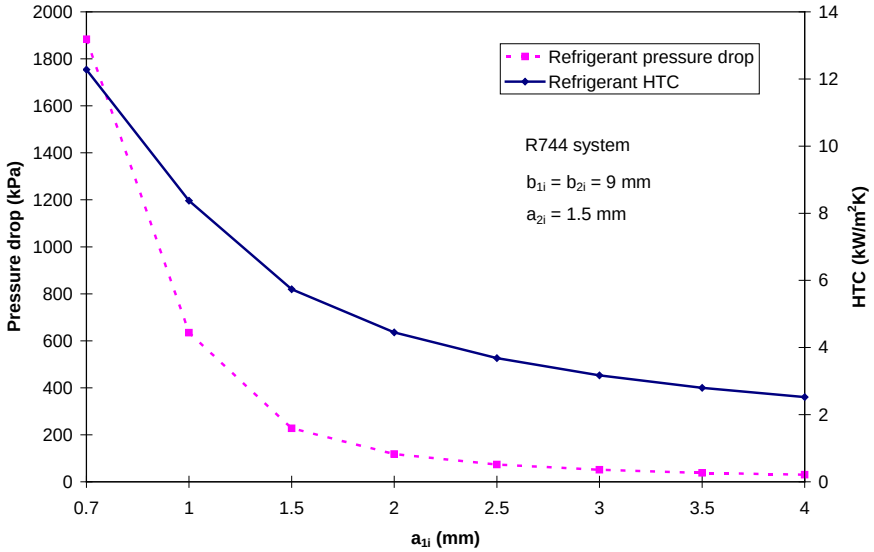

Figure 6.34: Refrigerant flow channel effect of configuration *II* on pressure drop and average *HTC* for R744

It can be seen that as a_{1i} decreased, refrigerant pressure drop increased and heat transfer coefficient increased for both systems similarly to configuration *I* (Fig. 6.33 and Fig. 6.34). For R410A system, when a_{1i} was less than 2 mm, the increase in refrigerant pressure drop was significant giving a large decrease log-mean temperature difference (*LMTD*) (Fig. 6.35) leading to increase in length, mean *HTA*, and weight of heat exchanger rather than decreases as at higher size (Fig. 6.37 and 6.39). For R744 the trends were similar but the transition occurred at about 1 mm rather than 2 mm (Fig. 6.36, Fig. 6.38, and Fig. 6.40).

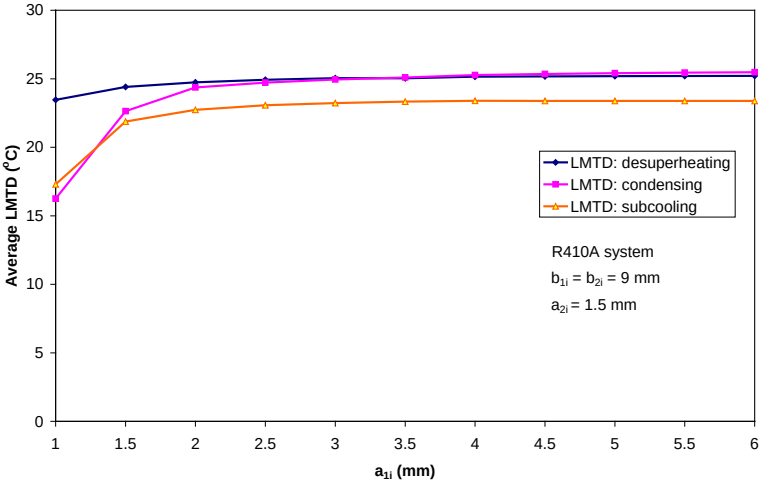

Figure 6.35: Refrigerant flow channel effect of configuration *II* on *LMTD* for R410A

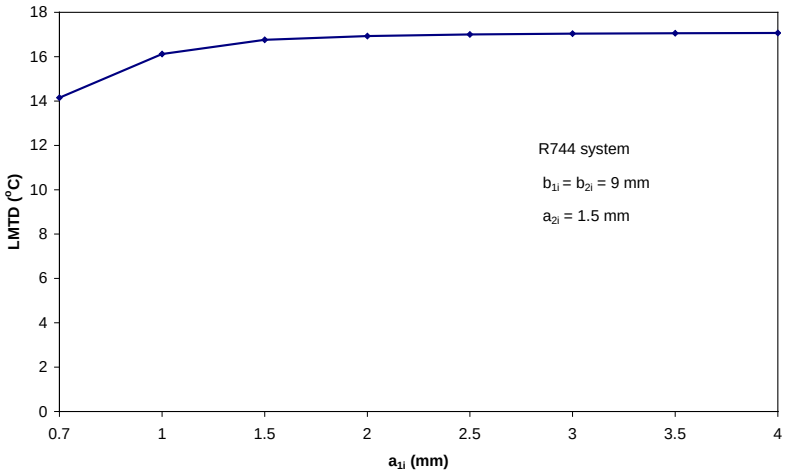

Figure 6.36: Refrigerant flow channel effect of configuration *II* on *LMTD* for R744

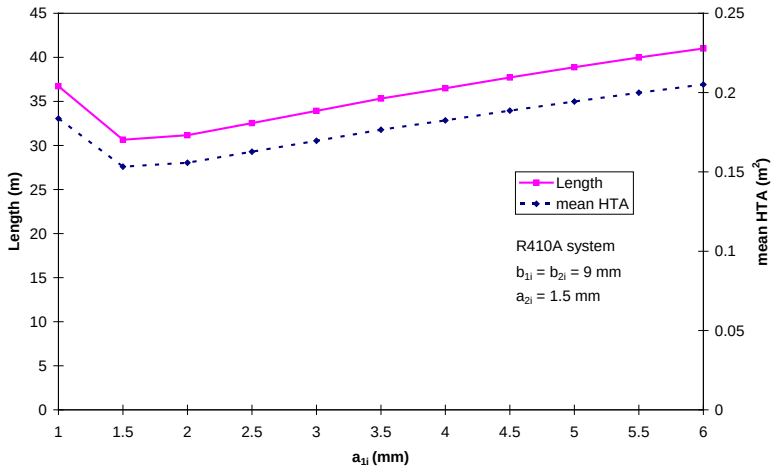

Figure 6.37: Refrigerant flow channel effect of configuration *II* on length and mean *HTA* for R410A

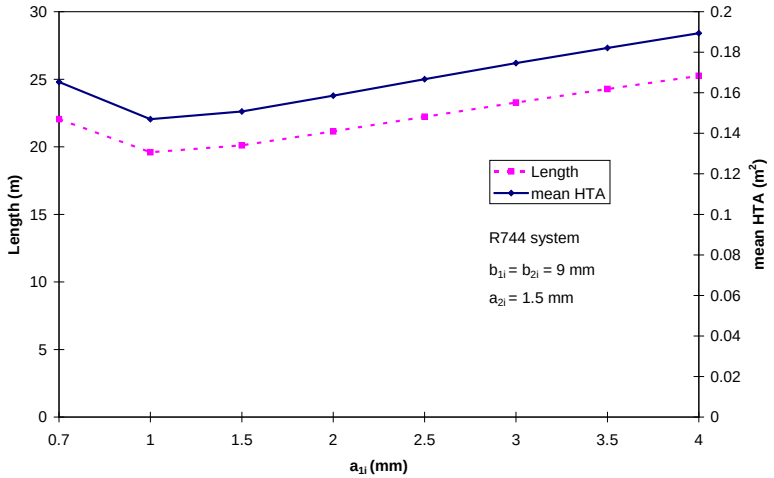

Figure 6.38: Refrigerant flow channel effect of configuration *II* on length and mean *HTA* for R744

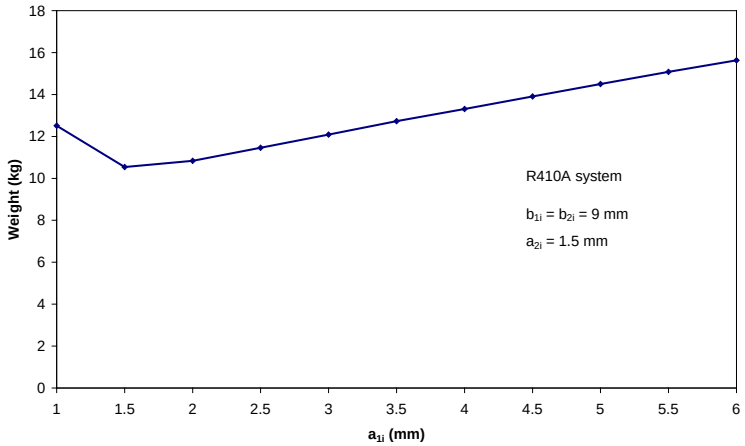

Figure 6.39: Refrigerant flow channel effect of configuration *II* on weight of heat exchanger for R410A

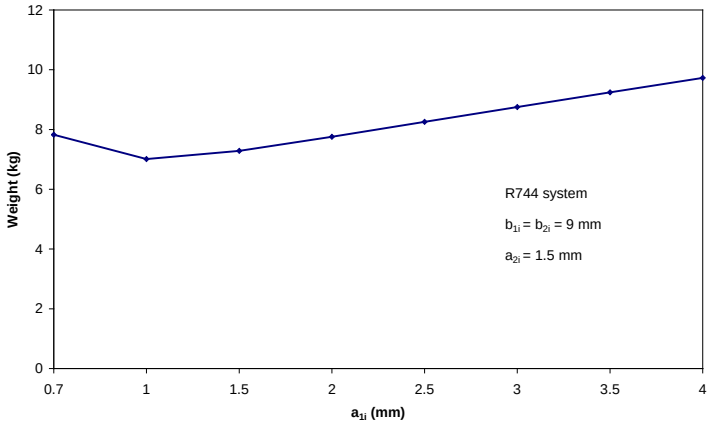

Figure 6.40: Refrigerant flow channel effect of configuration *II* on weight of heat exchanger for R744

Similarly as configuration *I*, the effect of refrigerant flow channel for configuration *II* on water pumping power and *COP* of the system was insignificant for both R410A and R744 as shown in Fig. 6.41 and 6.42 respectively.

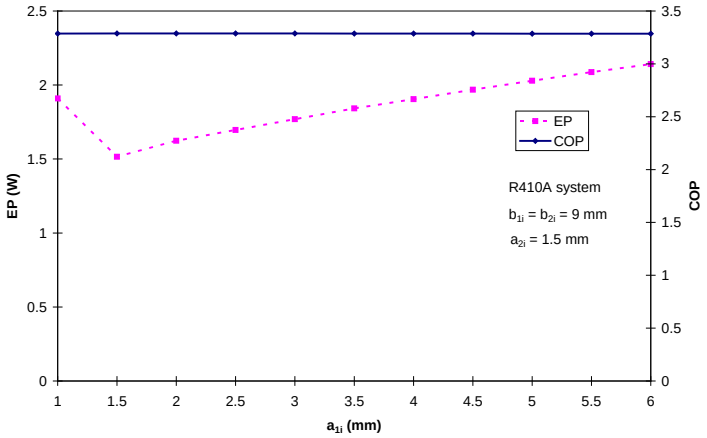

Figure 6.41: Refrigerant flow channel effect of configuration *II* on pumping power and *COP* for R410A system

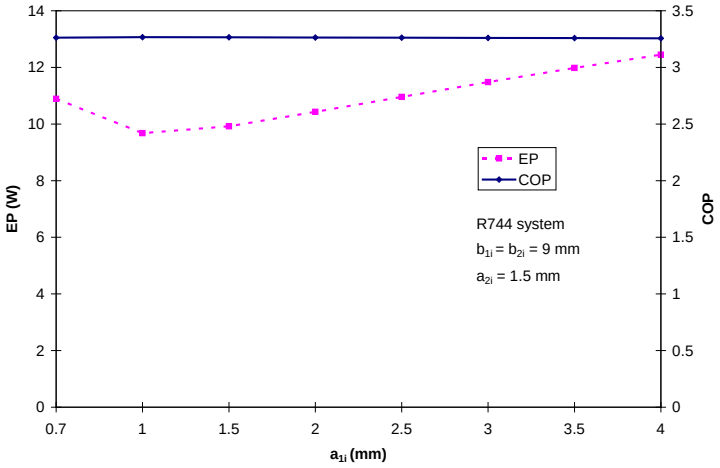

Figure 6.42: Refrigerant flow channel effect of configuration *II* on pumping power and *COP* for R744 system

In conclusion, the optimal configuration *II* for R410A with $a_{1i} = a_{2i} = 1.5$ mm and $b_{1i} = b_{2i}$ 9 mm has a length of 30.6 m, a weight of 10.5 kg, a mean *HTA* of 0.15 m^2, a pumping power of 1.5 W, and a *COP* of 3.3.

The optimal configuration *II* for R744 with $a_{1i} = 1$ mm, $a_{2i} = 1.5$ mm and $b_{1i} = b_{2i}$ 9 mm has a length of 19.6 m, a weight of 7.0 kg, a mean *HTA* of 0.15 m^2, a pumping power of 9.7 W, and a *COP* of 3.3

Table 6.3 Average thermal resistance in optimal configuration *II* (based on mean *HTA*)

Thermal resistance (Km^2/kW)	R410A	R-744
1. Refrigerant side ($R_{convect,r}$)	0.31	0.12
2. Water side ($R_{convect,w}$)	0.11	0.11
3. Air gap and contact ($R_{airgap} + R_{contact}$)	0.52	0.51
4. Tube wall conduction ($R_{wall1} + R_{wall2}$)	0.0042	0.0045
5. ***Total***	***0.94***	***0.75***

For configuration *II* air gap resistance is significantly smaller compared with configuration *I*. As a consequence, the heat exchanger is smaller compact and will probably be cheaper to manufacture. In order to improve this configuration contact between the 1st and 2nd tubes should be improved first for both R410A and R744 due to largest thermal contact resistance (see Table 6.3). The refrigerant flow channel should be following improved for R410A due to higher thermal resistance than water side while both refrigerant or water flow channels should be improved for R744.

6.5 Configuration *III* Design

As previously mentioned, the configuration *I* case *B* was optimal for both R410A and R744. However, the optimal configuration *I* is still not promising because it still has much more heat exchanger weight than the optimal configuration *II*. The main cause is from the critical thermal resistance of the air gap (see Table 6.2). Therefore, in order to improve the configuration *I* case *B* thermal resistance of the air gap must be reduced as much as possible. Configuration *III* heat exchanger is one alternative heat exchanger that can improve the configuration *I* (see Section 4.1.6.3). The configuration *III* is not only to reduce thermal resistance of the air gap but also to reduce thermal resistance of the refrigerant side due to enhanced flow channel shape.

6.5.1 R-410A design

Based on the optimal flow channels for configuration *I* case *B* and standard copper tubes, the inside diameter of the first tube (d_i) was chosen to be 7.9375 mm. The original inside diameter of the 2nd tube (d_1) used for investigation was chosen to be 12.7, or 15.875 mm. The relationship between %contact and inside diameter of the twisted tube (d) for original inside diameter of the twisted tube of 12.7 and 15.875 mm are given in Fig. 6.43 and Fig. 6.44 respectively based on the calculation method given in Section 4.1.6.3.

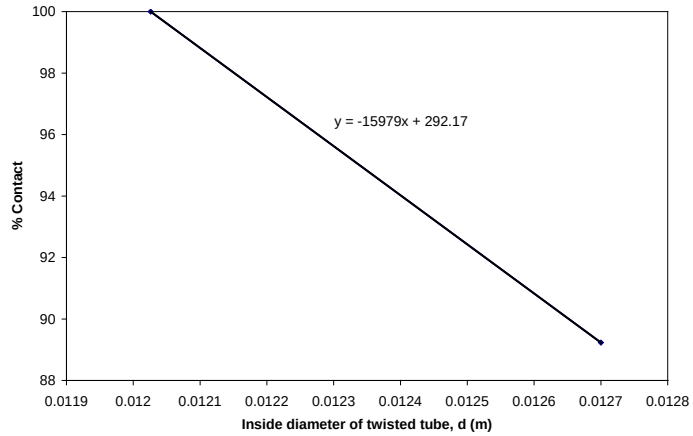

Figure. 6.43: Relationship between %contact and inside diameter of twisted tube having d_1 = 12.7 mm for R410A

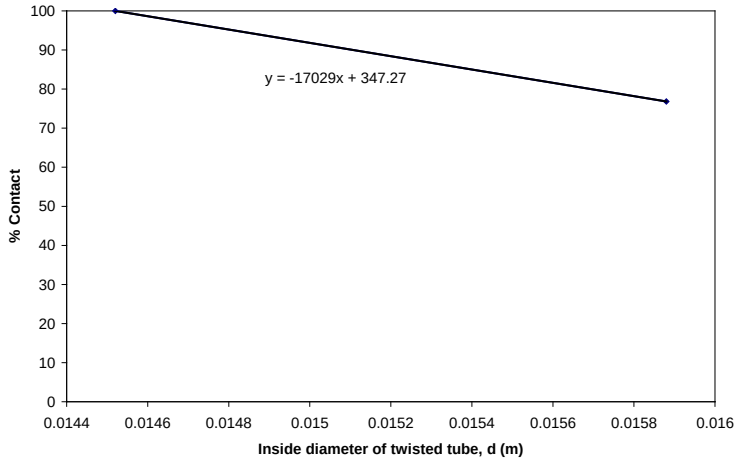

Figure 6.44: Relationship between %contact and inside diameter of twisted tube having d_1 = 15.875 mm for R410A

Given the strong effect of air gap on overall heat transfer resistance, the range of investigation were from 90 to 100%. The predicted results are shown in Fig. 6.45 to 6.49.

Fig. 6.45 gives the effect of %contact on heat exchanger length and mean heat transfer surface area and Fig 6.46 gives the effect of %contact on heat exchanger weight. It was found that when %contact increased from 90% to 100%, heat exchanger length, mean heat transfer surface area, and weight decreased for both original tube size (d_1 and d_2). The heat exchanger length, mean heat transfer surface area, and weight of the smaller tube (d_1 = 12.7 mm) were less than the larger tube (d_1 = 15.875 mm) due to smaller air gap and higher refrigerant heat transfer coefficient (Fig. 6.47) with a small decrease of average *LMTD* partially in condensing region due to small pressure drop (Fig. 6.48).

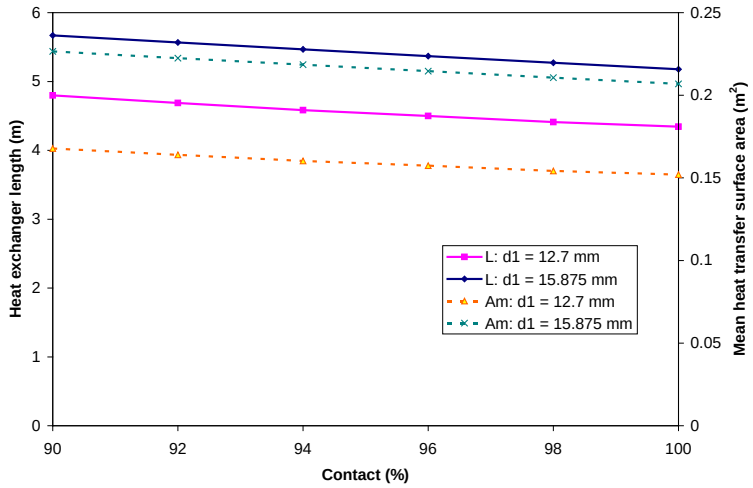

Figure 6.45: %contact effect on heat exchanger length and mean heat transfer surface area for R410A

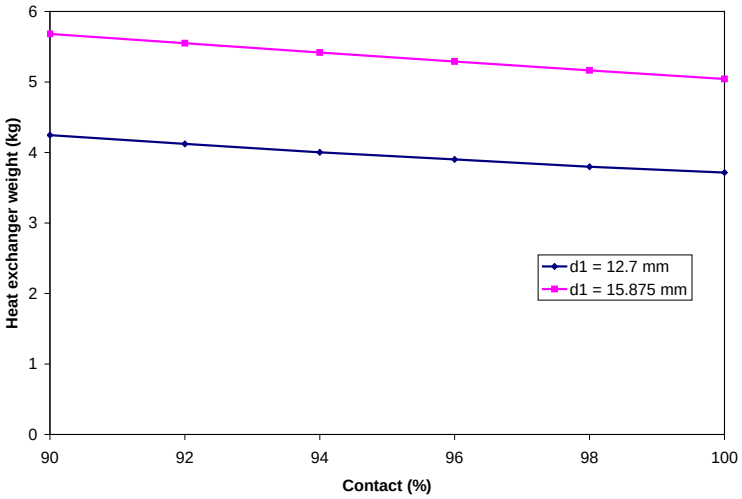

Figure 6.46: %contact effect on heat exchanger weight for R410A

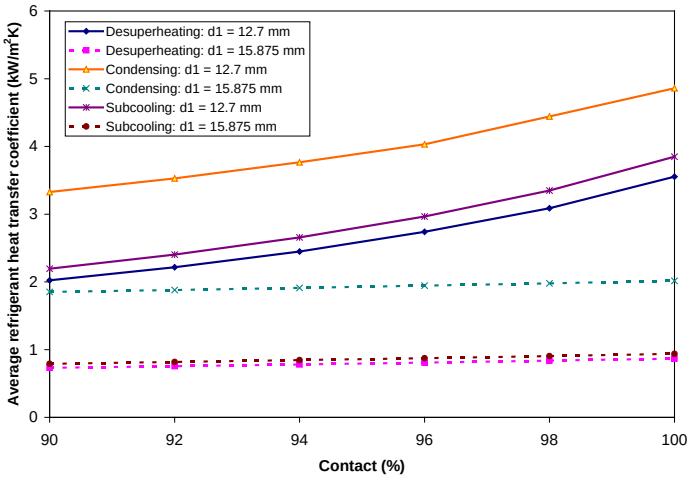

Figure 6.47: %contact effect on refrigerant heat transfer coefficient for R410A

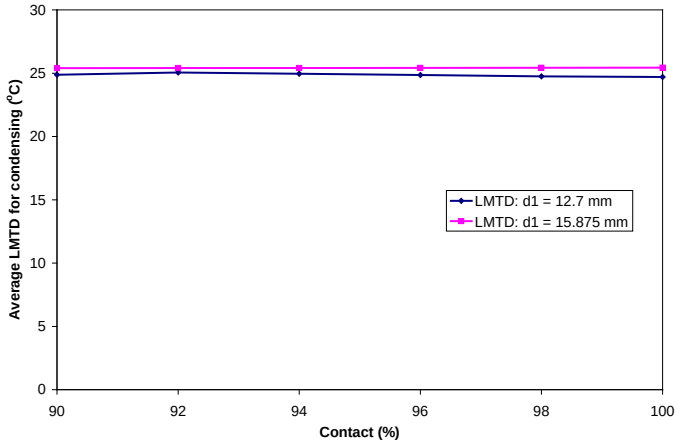

Figure 6.48: %contact effect on average *LMTD* for R410A

Therefore, an increase of %contact from 90 to 100% and a decrease of inside diameter of original tube from 15.875 to 12.7 mm not only reduced thermal resistance of the air gap but also increased refrigerant heat transfer coefficient leading to significantly reduced heat exchanger length, mean *HTA*, and heat exchanger weight.

The effect of %contact on pumping power and *COP* of the system was insignificant for both original tube sizes as shown in Fig. 6.49.

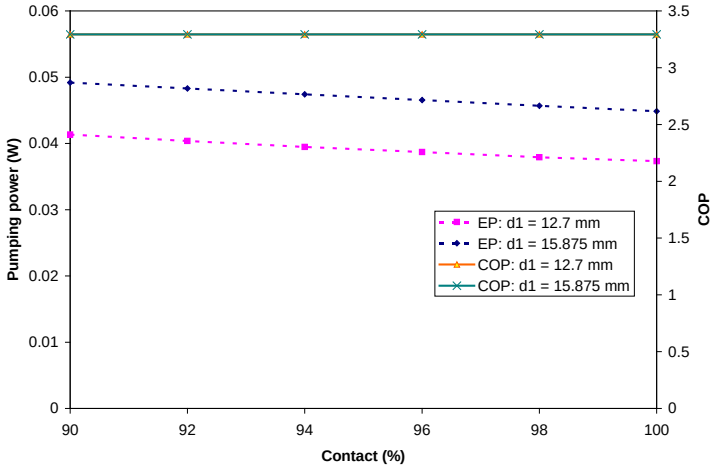

Figure 6.49: %contact effect on pumping power (*EP*) and *COP* for R410A

In conclusion, 100% contact gave the best results in terms of heat exchanger length mean *HTA*, and heat exchanger weight for both original tube sizes. However, at 100% contact there has no air gap for venting and it is difficult to manufacture to get tube profile needed to achieve the keep of contact. A %contact of 94% was considered the practical maximum that could be achieved. As a consequence, for d_1 = 12.7 mm this configuration at 94% contact has a length of 4.6 m, a mean *HTA* of 0.16 m^2, a heat exchanger weight of 4.0 kg, a pumping power of 0.04 *W*, and a *COP* of 3.3. The heat exchanger for a larger original tube size (d_1 = 15.875 mm) was predictably performed less full to be larger in size.

6.5.2 R-744 design

Based on the best flow channels in configuration *I* case *B* and standard copper tubes, the inside diameter of the first tube (d_i) was chosen to be 6.35 mm. The original inside diameter of the 2nd tube (d_1) used was chosen to be 9.525 or 12.7 mm. The relationship between %contact and inside diameter of the twisted tube (d) for original inside diameter of the 2nd tube of 9.525 mm and of 12.7 mm are presented in Fig. 6.50 and Fig. 6.51 respectively.

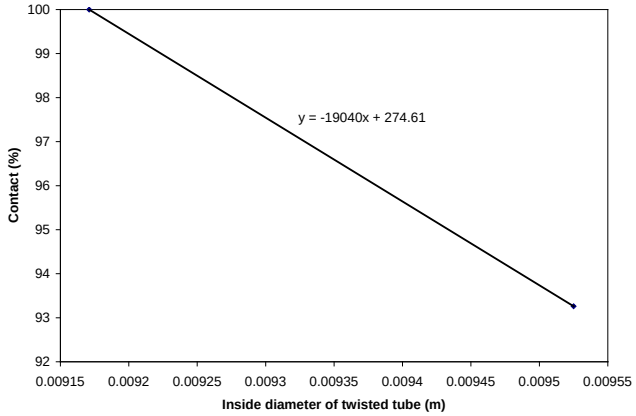

Figure 6.50: Relationship between %contact and inside diameter of twisted tube having d_1 = 9.525 mm for R744

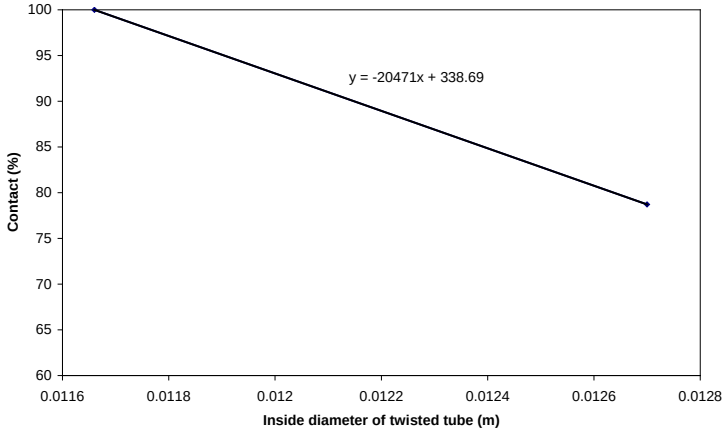

Figure 6.51: Relationship between %contact and inside diameter of twisted tube having d_1 = 12.7 mm for R744

As for R744 the key design parameters investigated were %contact from 94 to 100% for both d_1 = 9.525 mm and d_1 = 12.7 mm. The predicted results are shown in Fig. 6.52 to 6. 55.

Figure 6.52 and 6.53 present the predicted heat exchanger length and mean heat transfer surface area, and heat exchanger weight respectively when %contact was varied from 94 to 100%. The trends were similar to R410A. The heat exchanger length, mean heat transfer surface area, and weight for d_1 = 9.525 mm were lower than that values for d_1 = 12.7 mm due to smaller air gap and higher refrigerant heat transfer coefficient (Fig. 6.54) with very small difference in average *LMTD* (Fig. 6.55).

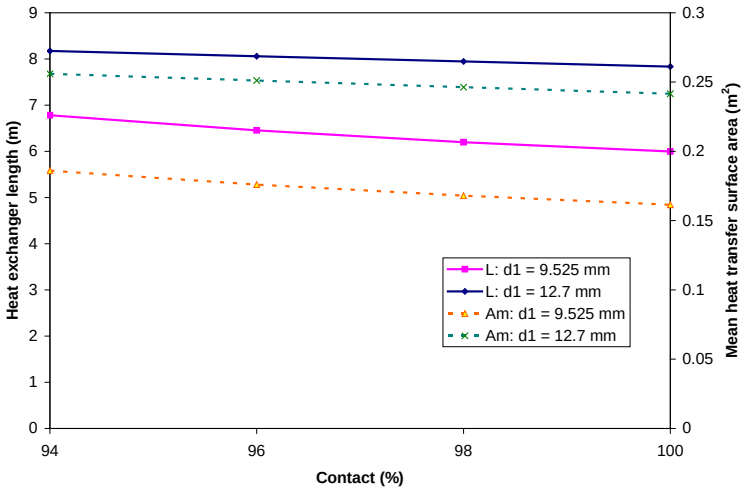

Figure 6.52: %contact effect on heat exchanger length and mean heat transfer surface area for R744

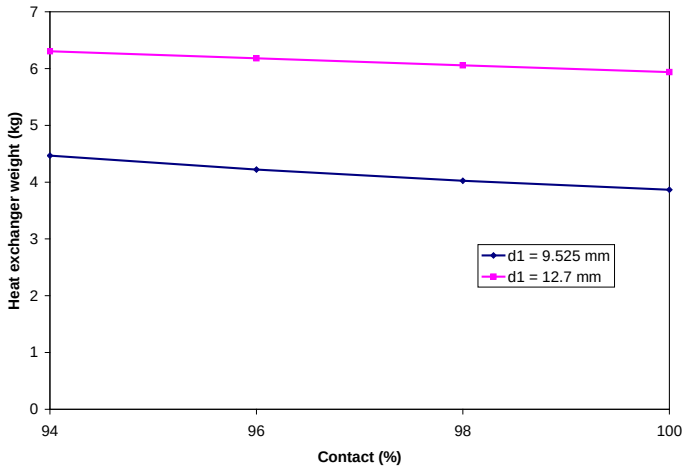

Figure 6.53: %contact effect on heat exchanger weight for R744

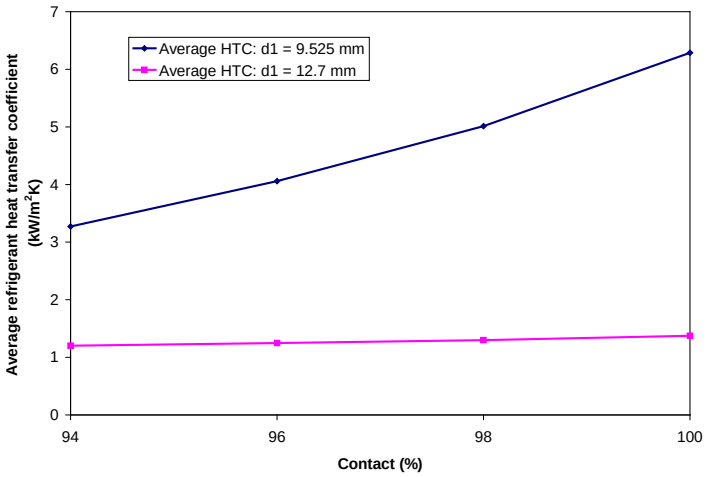

Figure 6.54: %contact effect on refrigerant heat transfer coefficient for R744

Similarly as R410A, the effect of %contact for R744 on pumping power and *COP* of the system was insignificant for both original tube sizes as shown in Fig. 6.56.

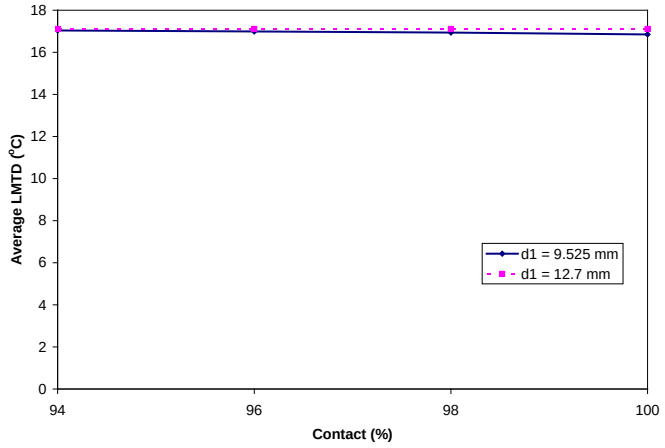

Figure 6.55: %contact effect on average *LMTD* for R744

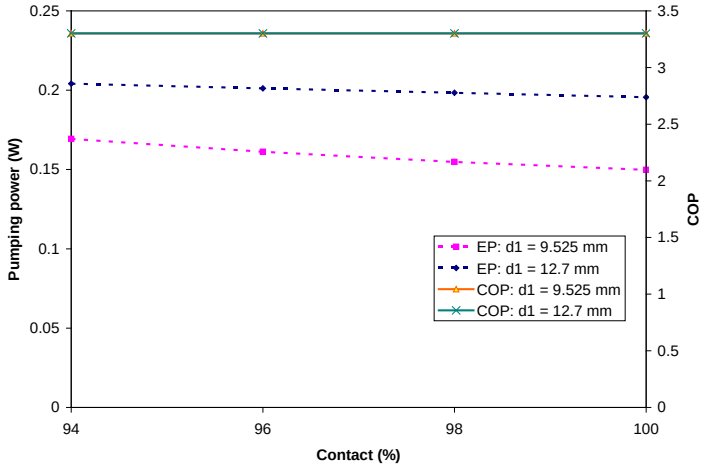

Figure 6.56: %contact effect on pumping power (*EP*) and *COP* for R744

In conclusion, at the 94% contact the configuration *III* for R744 with d_1 = 9.525 mm has a length of 6.9 m, a mean *HTA* of 0.19 m^2, a heat exchanger weight of 4.5 kg, a pumping power of 0.2 W, and a *COP* of 3.3. The heat exchanger for a larger original tube size (d_1 = 12.7 mm) was predictably performed less full to be larger in size as similar to R410A.

Table 6.4 showed that the configuration *III* significantly decreased thermal resistance of the air gap and the contact (*No. 3)* in the configuration *II* (see Table 6.3) for both R410A and R744. It could also reduce thermal resistantace of refrigerant side for only R410A. However, thermal resistance of water side was higher than the configuration *II*. Thus, the water flow channel should be improved for the configuration *III*.

Table 6.4 Average thermal resistance in optimal configuration *III*
(based on mean *HTA*)

Thermal resistance (Km^2/kW)	R410A	R-744
1. Refrigerant side ($R_{convect,r}$)	0.26	0.24
2. Water side ($R_{convect,w}$)	0.58	0.39
3. Air gap and contact ($R_{airgap} + R_{contact}$)	0.36	0.22
4. Tube wall conduction ($R_{wall1} + R_{wall2}$)	0.0042	0.0041
5. ***Total***	***1.20***	***0.85***

6.6 Summary

Characteristics for best water heating heat exchangers for the three configurations are summarized in Table 6.5. Among three configurations, configuration *II* and *III* were most promising for air-source heat pump water heaters. The R410A was significantly better than the R744 in terms of length, weight, and mean *HTA* for configuration *III*. By contrast, the R744 was significantly better than R410A in term of length and weight for configuration *II*. When the material cost and the running cost were considered, it was found that the configuration *III* was significantly better than configuration *II* for both R410A and R744 due to lower heat exchanger weight and lower water pumping power. However, due to more difficult manufacture for configuration *III* the investment cost might be higher than configuration *II* for both R410A and R744.

Table 6.5: Summary of characteristics for three best water heating heat exchanger configurations

Heat exchanger	Length (m)	Weight (kg)	mean *HTA* (m^2)	*EP* (W)	*COP*
Configuration I					
$d_1 - d_o$ = 0.2 mm, $D_i - d_2$ = 1.5 mm					
Case A:					
R410A system	27.5	16.2	0.60	28.6	3.3
d_i = 6 mm					
R744 system	41.6	21	0.78	24.4	3.3
d_i = 5 mm					
Case B:					
R410A system	20	16	0.60	0.2	3.3
d_i = 6 mm					
R744 system	30	21	0.82	0.5	3.3
d_i = 5 mm					
Configuration II					
$b_{1i} = b_{2i}$					
R410A system	30.6	10.5	0.15	1.5	3.3
a_{1i} = 1.5 mm					
a_{2i} = 1.5 mm					
R744 system	19.6	7.0	0.15	9.7	3.3
a_{1i} = 1 mm					
a_{2i} = 1.5 mm					
Configuration III					
At 94% contact					
R410A system					
d_i = 7.9375 mm					
For d_1 = 12.7 mm	4.6	4.0	0.16	0.04	3.3
R744 system					
d_i = 6.35 mm					
For d_1 = 9.525 mm	6.9	4.5	0.19	0.2	3.3

CHAPTER 7

CONCLUSION AND RECOMMENDATION

Two multi-zone models of the double-wall counter-current heat exchanger: gas cooler and condenser models were developed to design different heat exchanger configurations based on available existing heat transfer and friction correlations in the open literature. In addition, air-source heat pump water heater models for both subcritical and transcritical cycles were developed for predicting overall performance of the system, refrigerant and water mass flow rates, inlet condenser/gas cooler conditions, water pumping power etc. The refrigerant and water properties in the models were all calculated by using the in-built property function in *EES* and the models were also programmed and implemented by *EES*. For multi-zone calculations, water temperature difference in each zone was assumed to be constant and the optimal number of zone was investigated. The optimal number of zone was 90 zones for both condenser and gas cooler models.

The heat exchanger models were validated against available experimental data (only single-wall heat exchangers). It was found that the condenser model closely predicted the size of the condenser (difference of -0.8%) and the gas cooler model predicted the size of gas cooler with an acceptable deviation of -14%. The multi-zone model was significantly more accurate than one and three zone models.

Three double wall water heating heat exchanger configurations: the circular tube-in-tube with a small air gap (Configuration *I*), the flat tube-on-tube (Configuration *II*), and the twisted tube-in-tube with a small air gap (Configuration *III*) were investigated using the models. Two alternative refrigerants (R410A for condenser and R744 for gas cooler) were considered. Heating capacity, inlet and outlet water temperatures were assumed to be 3 kW, 15^{o}C, and 60^{o}C respectively. For the R410A, refrigerant condensation temperature was assumed to be 64^{o}C and for the R744, refrigerant discharge pressure was assumed to be 11 MPa. Refrigerant was assumed to be sub-cooled to 25^{o}C and refrigerant evaporation temperature was assumed to be 5^{o}C for both R410A and R744. The criteria for comparison of different water heating heat exchanger configurations consisted of pressure drop and heat transfer coefficient for refrigerant and water, average temperature difference between refrigerant and water, heat exchanger length and weight, mean heat transfer surface area of the heat exchanger, water pumping power, and coefficient of performance of the system.

The model was used to investigate the effect of key design parameters for each configuration. To investigate the optimal water flow channel size the refrigerant flow channel was fixed while the water flow channel was varied and to investigate the optimal refrigerant flow channel size the water flow channel was fixed while the refrigerant flow channel was varied. The predicted trends of the criteria by using the models showed that the configuration *I* case *B* (refrigerant flow in the annulus) performed better than case *A* (refrigerant flow in the inner tube). The optimal flow channels for configuration *I* case *B* with a 0.1 mm thick air gap were found to be d_i = 8 mm and $D_i - d_2$ = 1.5 mm for R410A and d_i = 7 mm and $D_i - d_2$ = 1.0 mm for R744.

The optimal flow channels for the configuration *II* with $b_{1i} = b_{2i} = 9$ mm were found to be $a_{1i} = a_{2i} = 1.5$ mm for R410A and $a_{1i} = 1$ mm and $a_{2i} = 1.5$ mm for R744. The optimal flow channels for configuration *III* were found to be $d_i = 7.94$ mm and $d_1 = 12.7$ mm for R410A and $d_i = 6.35$ mm and $d_1 = 9.53$ mm for R744. At the optimal flow channel size for both the refrigerant and water sides for configuration *I* case *B* for R410A the heat exchanger had a length of 20 m, a weight of 16 kg, a mean *HTA* of 0.60 m^2, a pumping power of 0.2 W, and a *COP* of 3.3 while for R744 had a length of 30 m, a weigth of 21 kg, a mean *HTA* of 0.82 m^2, a pumping power of 0.5 W, and a *COP* of 3.3. The best configuration *II* heat exchanger for R410A had a length of 30.6 m, a weight of 10.5 kg, a mean *HTA* of 0.15 m^2, a pumping power of 1.5 W, and a *COP* of 3.3 while for R744 had a length of 19.6 m, a weight of 7.0 kg, a mean *HTA* of 0.15 m^2, a pumping power of 9.7 W, and a *COP* of 3.3. The best configuration *III* heat exchanger with 94% contact for R410A had a length of 4.6 m, a mean *HTA* of 0.16 m^2, a heat exchanger weight of 4.0 kg, a pumping power of 0.04 *W*, and a *COP* of 3.3 while for R744 had a length of 6.9 m, a mean *HTA* of 0.19 m^2, a heat exchanger weight of 4.5 kg, a pumping power of 0.3 W, and a *COP* of 3.3.

Among three double wall heat exchangers, the twisted tube-in-tube and the flat tube-on-tube were most promising to use in the air-source heat pump water heaters. The twisted tube-in-tube gave the smallest heat exchanger length, weight and water pumping power than the flat tube-on-tube. However, the investment cost for the twisted tube-in-tube might be higher than the flat tube-on-tube due to more difficult manufacture.

The models should be more fully validated against more experimental data particularly for double wall heat exchanger and a wider range of configurations because they were only validated with available data from the open literature for single wall heat exchanger for both condensing and gas cooling.

REFERENCES

ACEEE. (August, 2007). Consumer guide to home energy savings: water Heating. from http://www.aceee.org/Consumerguide/waterheating.htm#lcc

Adams, T. M., Abdel-Khalik, S. I., Jeter, S. M., & Qureshi, Z. H. (1997). *An experimental investigation of single-phase forced convection in microchannels.* Paper presented at the 32nd National Heat Transfer Conference, Baltimore.

Anderson, J. A., Bradford, R. A., & Carrington, C. G. (1985). Assessment of a heat pump water heater. *Energy Research, 9*, 77-89.

AS/NZS2712. (2007). *Solar and heat pump water heaters-design and construction*. Wellington: Australia/New Zealand Standard.

Aye, L., Charters, W. W. S., & Chaichana, C. (2002). Solar heat pump systems for domestic hot water. *Solar Energy 73*, 169–175.

Baker, O. (1954). Simultaneous flow of oil and gas. *Oil and Gas J., 53*, 185-195.

Bandhauer, T. M., Agarwal, A., & Garimella, S. (2006). Measurement and modelling of condensation heat transfer coefficients in circular microchannels. *J. Heat Transfer, Trans. ASME, 128*, 1050-1058.

Bassi, R., & Bansal, P. K. (2003). In-tube condensation of mixture of R134a and ester oil: empirical correlations. *International Journal of Refrigeration, 26*, 402–409.

Bell, K. J., Taborek, J., & Fenoglio, F. (1970). Interpretation of horizontal intube condensation heat transfer correlations with a two-phase flow regime map. *CEP Symp. Ser., 66*(102), 159-165.

Biaou, A. L., & Bernier, M. A. (2008). Achievement total domestic hot water production with renewable energy. *Building and Environment, 43*, 651-660.

Boissieux, X., Heikal, M. R., & Johns, R. A. (2000). Two-phase heat transfer coefficients of three HFC refrigerants inside a horizontal smooth tube, part II: condensation. *International Journal of Refrigeration, 23*, 345-352.

Boyko, L. D., & Kruzhilin, G. N. (1967). Heat transfer and hydraulic resistance during condensation of steam in a horizontal tube and in a bundle of tubes. *J. Heat Transfer, Trans. ASME, 10*(3), 361-373.

BP. (2009). Statistical review of world energy. from http://www.bp.com/productlanding.do?categoryId=6929&contentId=7044622

BRANZ. (2006). *Energy use in New Zealand households: report on the year 10 analysis for the household energy end-use project (HEEP)* (No. SR155): BRANZ.

Breber, G., Palen, J. W., & Taborek, J. (1980). Prediction of horizontal tubeside condensation of pure components using flow regime criteria. *Trans ASME, 102*, 471-476.

Brognaux, L., Webb, R. L., & Chamra, L. M. (1997). Single-phase heat transfer in micro-fin tubes. *International Journal of Heat and Mass Transfer, 40*(18), 4345-4357.

Bukasa, J. P., Liebenberg, L., & Meyer, J. P. (2005). Influence of spiral angle on heat transfer during condensation inside spiralled micro-fin tubes. *Heat Transfer Engineering, 26*(7), 11-21.

C745-00. (2000). *Energy efficiency of electric storage tank water heaters and heat pump water heaters*: Canadian Standards Association.

Calm, J. M., & Didion, D. A. (1998). Trade-off in refrigerant selections-past, present, and future. *International Journal of Refrigeration, 21*(4), 308-321.

Calm, J. M., & Hourahan, G. C. (2001). Refrigerant data summary. *Engineering systems, 18*(11), 74-88.

Carrington, C. G. (1982). Use of controlled water circulation in tap water heat pumps. *Energy Research, 6*, 233-240.

Cavallini, A., Censi, G., Col, D. D., & Doretti, L. (2001). Experimental investigation on condensation heat transfer and pressure drop of new HFC refrigerants. *International Journal of Refrigeration, 24*, 73-87.

Cavallini, A., Censi, G., Col, D. D., Doretti, L., Longo, G. A., & Rossetto, L. (2001). Experimental investigation on condensation heat transfer and pressure drop of new HFC refrigerants (R134a, R125, R32, R410A, R236ea) in a horizontal smooth tube. *International Journal of Refrigeration, 24*, 73-87.

Cavallini, A., Col, D. D., Doretti, L., Longo, G. A., & Rosssetto, L. (2000). Heat transfer and pressure drop during condensation of refrigerants inside horizontal enhanced tubes. *International Journal of Refrigeration, 23*, 4-25.

Cavallini, A., Col, D. D., Doretti, L., Matkovic, M., Rossetto, L., & Zilio, C. (2005). Two-phase frictional pressure gradient of R236ea, R134a and R410A inside multi-port mini-channels. *Experimental Thermal and Fluid Science, 29*, 861-870.

Cavallini, A., Col, D. D., Matkovic, M., & Rossetto, L. (2009). Frictional pressure drop during vapor-liquid flow in minichannels: modelling and experimental evaluation. *International Journal of Heat and Fluid Flow, 30*, 131-139.

Cavallini, A., DelCol, D., Longo, G. A., & Rossetto, L. (2000). Heat transfer and pressure drop during condensation of refrigerants inside horizontal enhanced tubes. *International Journal of Refrigeration, 23*, 4-25.

Cavallini, A., DelCol, D., Mancin, S., & Rossetto, L. (2009). Condensation of pure and near-azeotropic refrigerants in microfin tubes: a new computational procedure. *International Journal of Refrigeration, 32*, 162-174.

Cavallini, A., Doretti, L., Klammsteiner, N., Longo, L. G., & Rossetto, L. (1995). *Condensation of new refrigerants inside smooth and enhanced tubes* Paper presented at the Proc. 19th Int. Cong. Refrigeration Hague, The Netherlands.

Cavallini, A., Doretti, L., Matkovic, M., & Rossetto, L. (2006). Update on condensation heat transfer and pressure drop inside minichannels. *Heat Transfer Engineering, 27*(4), 74-87.

Cavallini, A., & Zecchin, R. (1974). *A dimensionless correlation for heat transfer in forced convective condensation.* Paper presented at the Proceedings of the Fifth International Heat Transfer Conference, Japan.

Celata, G. P. (2003). *Single-phase heat transfer and fluid flow in micropipes.* Paper presented at the First International Conference on Microchannels and Minichannels Rochester, NY.

Chamra, L. M., & Webb, R. L. (1996). Advanced micro-fin tubes for condensation. *International Journal of Heat Mass Transfer, 39*(9), 1839-1846.

Chato, J. C. (1962). Laminar condensation inside horizontal and inclined tubes. *ASHRAE Journal, 4*, 52-60.

Chen, C. S., & Kuo, W. J. (2004). Heat transfer characteristics of gaseous flow in long mi-ni micro tubes. *Numerical Heat Transfer, Part A, 46*, 497–514.

Chen, I. Y., & Kocamustafaogullari, G. (1987). Condensation heat transfer studies for stratified , cocurrent two-phase flow in horizontal tubes. *Int. J. Heat Mass Transfer, 30*(6), 1133-1148.

Chen, I. Y., Yang, K. S., Chang, Y. J., & Wang, C. C. (2001). Two-phase pressure drop of air-water and R-410A in small horizontal tubes. *Int. J. Multiphase flow, 27*, 1293-1299.

Chen, S. L., Gemer, F. M., & Tien, C. L. (1987). General film condensation correlations. *Experimental Heat Transfer, 1*, 93-107.

Dalkilic, A. S., & Wongwises, S. (2009). Intensive literature review of condensation inside smooth and enhanced tubes. *International Journal of Heat and Mass Transfer, 52*, 3409-3426.

Dang, C., & Hihara, E. (2004). In-tube cooling heat transfer of supercritical carbon dioxide-part 1: experimental measurement. *International Journal of Refrigeration, 27*, 736-747.

Dang, C., & Hihara, E. (2004). In-tube cooling heat transfer of supercritical carbon dioxide: part 1. experimental measurement. *International Journal of Refrigeration, 27*, 736-747.

Dang, C., Iino, K., Fukuoka, K., & Hihara, E. (2007). Effect of lubricating oil on cooling heat transfer of supercritical carbon dioxide. *International Journal of Refrigeration, 30*, 724-731.

Dang, C., Iino, K., & Hihara, E. (2008). Study on two-phase flow pattern of supercritical carbon dioxide with entrained PAG-type lubricating oil in a gas cooler. *International Journal of Refrigeration, 31*, 1265-1272.

Dobson, M. K., & Chato, J. C. (1998). Condensation in smooth horizontal tubes. *J. Heat Transfer, Trans. ASME, 120*, 193-213.

Dobson, M. K., Chato, J. C., Wattelet, J. P., Gaibel, J. A., Ponchner, M., Kenney, P. J., et al. (1994). *Heat transfer and flow regimes during condensation in horizontal tubes*. Illinois: Air Conditioning and Refrigeration Center, University of Illinoiso. Document Number)

DOE. (2007). CO_2 emission by end-use sector united states. from http://www.energy.gov/

DOE. (2009, March 24, 2009). Conventional storage water heaters. from http://www.energysavers.gov/your_home/water_heating/index.cfm/mytopic=12980

Dravid, A. N., Smith, K. A., Merrill, E. W., & Brian, P. L. T. (1971). Effect of secondary fluid on laminar flow heat transfer in helically coiled tubes. *AICHE J., 17*, 1114-1122.

Dukler, A. E. (1960). Fluid mechanics and heat transfer in vertical falling film systems. *Chemical Engineering Progress Symposium Series, 56*(30), 1-10.

Dunn, B. (1996). *Condensation inside tube* (No. EPRI TR-106016-V2): University of Illinois o. Document Number)

EN255-3. (1997). *EN 255-3 Air conditioners, liquid chilling packages and heat pumps with electrically driven compressors heating mode part 3: testing and requirements for making sanitary hot water units*. Brusselso. Document Number)

Fang, X., Bullard, C. W., & Hrnjak, P. S. (2001). Heat transfer and pressure drop of gas cooling. *ASHRAE Journal, 107*(Part 1), 255-266.

Ferreira, C. A. I., Newell, T. A., Chato, J. C., & Nan, X. (2003). R404A condensing under forced flow conditions inside smooth, microfin and cross-hatched horizontal tubes. *International Journal of Refrigeration, 26*, 433-441.

Friedel, L. (1980). Pressure drop during gas/vapor-liquid flow in pipes. *Int. Chem. Eng., 20*, 325-367.

Fujie, K., Itoh, N., Kimura, H., Nakayama, N., & Yanugidi, T. (1977). *Heat transfer pipe* (No. US Patent 4044797): Hitachi Ltd.o. Document Number)

Gao, L., & Honda, T. (2002). *Experiments on heat transfer characteristics of heat exchanger for CO_2 heat pump system.* Paper presented at the Asian Conference on Refrigeration and Air Conditioning, Kobe, Japan.

Gnielinski, V. (1976). New equation for heat and mass transfer in turbulent pipe and channel flow. *Int. Chem. Eng., 16*, 359-368.

Gronnerud, R. (1979). Investigation of liquid hold-up, flow-resistance and heat transfer in circulation type evaporators, part IV: two-phase flow resistance in boiling refrigerants. *Annexe 1972-1, Bull. de l'Inst. de Froid*.

Guo, L., Chen, X., Feng, Z., & Bai, B. (1998). Transient convective heat transfer in a helical coiled tube with pulsatile fully developed turbulent flow. *International Journal of Heat and Mass Transfer, 41*, 2867-2875.

Han, D., & Lee, K. J. (2005). Experimental study on cndensation heat transfer enhancement and pressure drop penalty factors in four microfin tubes. *International Journal of Heat and Mass Transfer, 48*, 3804-3816.

Horiuchi, H. (1995). *Test report on extruded aluminum tubes*: Penn State Universityo. Document Number)

Huai, X. L., Koyama, S., & Zhao, T. S. (2005). An experimental study of flow and heat transfer of supercritical carbon dioxide in multi-port mini channels under cooling conditions. *Chemical Engineering Science, 60*, 3337-3345.

IEA. (2009). Electricity and heat in New Zealand in 2006. from http://www.iea.org/stats/electricitydata.asp?COUNTRY_CODE=NZ

Incropera, F. P., & DeWitt, D. P. (1996). *Fundamentals of heat and mass transfer* (4 ed.). New York Wiley.

Jaster, H., & Kosky, P. G. (1976). Condensation heat transfer in a mixed flow regime. *Int. J. Heat Mass Transfer, 19*, 95-99.

Jekel, T. B., & Reindl, D. T. (2008). Single-or two-stage compression. *ASHRAE Journal.*, 46-51.

JRA. (2005). *JRA450-Standard for residential heat pump water heaters*. Japano. Document Number)

Jung, D., Chae, S., Bae, D., & Oho, S. (2004). Condensation heat transfer coefficients of flammable refrigerants. *International Journal of Refrigeration, 27*, 314-317.

Jung, D., Song, K., Cho, Y., & Kim, S. (2003). Flow condensation haet transfer coefficients of pure refrigerants. *International Journal of Refrigeration, 26*, 4-11.

Kalb, C. E., & Seader, J. D. (1972). Heat and mass transfer phenomena for viscous flow in curved circular pipe. *International Journal of Heat and Mass Transfer, 15*, 801–817.

Kalb, C. E., & Seader, J. D. (1974). Fully developed viscous-flow heat-transfer in curved circular tubes with uniform wall temperature *AICHE J., 20*(2), 340-346.

Kaneko, M., Ikeda, H., Tokiai, T., Yoshii, A., & Suto, H. (2006). *The development of PGA refrigerations for automotive A/C with CO_2.* Paper presented at the JSAE Automotive Air-Conditioning Conference, Tokyo, Japan.

Kato, Y., Ngo, T., Nikitin, K., & Utamura, M. (2008). *Empirical heat transfer and pressure drop correlations for new microchannel heat exchanger between carbon dioxide and water.* Paper presented at the The 8th IIR Gustav Lorentzen Conference on Natural Working Fluids, Copenhagen.

Kenway, S. J., Priestley, A., Cook, S., Seo, S., Inman, M., Gregory, A. (2008). *Energy use in the provision and consumption of urban water in Australia and New Zealand*: CSIRO Water For a Healthy Country National Research Flagshipo. Document Number)

Kim, M.-H., & Shin, J.-S. (2005). Condensation heat transfer of R22 and R410A in horizontal smooth and microfin tubes. *International Journal of Refrigeration, 28*, 949-957.

Kim, M. H., Pettersen, J., & Bullard, C. W. (2004). Fundamental process and system design issues in CO_2 vapor compression system. *Progress In Energy And Combustion Science, 30*, 119-174.

Kim, M. H., & Shin, J. S. (2005). Condensation heat transfer of R-22 and R-410A in horizontal smooth and microfin tubes. *International Journal of Refrigeration, 28*, 949-957.

Kosky, P. G., & Staub, F. W. (1971). Local condensing heat transfer coefficients in the annular flow regime. *AICHE J., 17*.

Krasnoshechekov, E. A., Kuraeva, I. V., & Protopopov, V. S. (1970). Local heat transfer of carbondioxide at supercritical pressure under cooling conditions. *Teplofizika Vysokikh Temperatur, 7*(5), 922-930.

Kumar, V., Saini, S., Shama, M., & Nigam, K. D. P. (2006). Pressure drop and heat transfer study in tube-in-tube helical heat exchanger. *Chemical Engineering Science, 61*, 4403 – 4416.

Laohalertdecha, S., & Wongwises, S. (2010). The effects of corrugation pitch on the condensation heat transfer coefficient and pressure drop of R-134a inside horizontal corrugated tube. *International Journal of Heat and Mass Transfer, 53*, 2924-2931.

Lee, H. S., Yoon, J. I., Kim, J. D., & Bansal, P. K. (2006). Characteristics of condensing and evaporating heat transfer using hydrocarbon refrigerants. *Applied Thermal Engineering, 26*, 1054-1062.

Liao, S. M., & Zhao, T. S. (2002). Measurements of heat transfer coefficients from supercritical carbon dioxide flowing in horizontal mini/micro channels. *Journal of Heat Transfer, 124*, 413-420.

Lloyd, C. R., & Kerr, A. S. D. (2008). Performance of commercially available solar and heat pump water heaters. *Energy Policy, In press*.

Lockhart, R. W., & Martinelli, R. C. (1949). Proposed correlation of data for isothermal two-phase two-component flow in pipes. *Chem. Eng. Prog., 45*(1), 39-48.

Lorentzen, G. (1994). *Natural refrigerants: a complete solution.* Paper presented at the Proceedings of Meetings of International Institute of Refrigeration Commissions B1, B2, E1, E2, Padova.

Lucas, L. (1993). *A new challenge: from the ozone layer to the greenhouse effect.* Paper presented at the Energy Efficiency in Refrigeration and Global Warming Impact: Proceeding of Meetings of International Institute of Refrigeration Commission B1/2.

Luu, M., & Bergles, A. E. (1980). Enhancement of horizontal in-tube condensation of refrigerant-113. *ASHRAE Trans., 86*(pt I), 293-312.

Mandhane, J. M., Gregory, G. A., & Aziz, K. (1974). A flow pattern map for gas-liquid flow in horizontal pipes. *Int. J. Multiphase flow, 1*, 537-553.

Manlapaz, R. L., & Churchill, S. W. (1981). Fully developed laminar convection from a helical coil. *Chemical Engineering Communications, 97*, 185–200.

McMullan, J. T. (2002). Refrigeration and the environment: issues and strategies for the future. *International Journal of Refrigeration, 25*, 89-99.

Merrigan, T., & Parker, D. (1990). *Electrical use, efficiency, and peak demand of electric resistance, heat pump, desuperheater, and solar hot water systems.* Paper presented at the American Council for an Energy Efficient Economy, Asilomar Conference Centre, Pacific Grove. .

Meyer, J. P., & Tshimankinda, M. (1997). Domestic hot-water consumption by South African developing communities *International Journal of Energy Research, 21*, 667-673.

Mishima, K., & Hibiki, T. (1996). Some characteristics of air-water two-phase flow in small diameter vertical tubes. *int. J. Multiphase Flow, 22*, 703-712.

Mishra, P., & Gupta, S. N. (1979). Momentum transfer in curved pipes, 1.Newtonian Fluids; 2. *Non-Newtonian Fluids Industrial & Engineering Chemical Process Design and Development, 18*, 130–142.

Miyara, A., Nonaka, K., & Taniguchi, M. (2000). Condensation heat transfer and flow pattern inside a herringbone-type micro-fin tube. *International Journal of Refrigeration, 23*, 141-152.

Mohanraj, M., Jayaraj, S., & Muraleedharan, C. (2009). Environment friendly alternatives to halogenated refrigerants- A review. *International Journal of Greenhouse Gas Control, 3*, 108-119.

Mori, K., Onishi, J., Shimaoka, H., Nakanishi, S., & Kimoto, H. (2002). *Cooling heat transfer characteristics of CO_2 and CO_2-oil mixture at supercritical pressure conditions.* Paper presented at the Asian Conference on Refrigeration and Air Conditioning Engineers, Kobe, Japan.

Morini, G. L. (2004). Single-phase convective heat transfer in microchannels: a review of experimental results. *International Journal of Thermal Sciences, 43*, 631–651.

Moser, K. W., Webb, R. L., & Na, B. (1998). A new equivalent Reynols number model for condensation in smooth tubes. *J. Heat Transfer, Trans. ASME, 120*, 410-417.

Muller-Steinhagen, H., & Heck, K. (1986). A simple friction pressure drop correlation for two-phase flow in pipes. *Chem. Eng. Process, 20*, 297-308.

Naphon, P., & Wongwises, S. (1993). An experimental study on the in-tube convective heat transfer coefficients in a spiral coil heat exchangers. *Int. Comm. Heat Mass Transfer, 29*(6), 797-809.

Naphon, P., & Wongwises, S. (2002). An experimental study on the in-tube convective heat transfer coefficients in a spiral coil heat exchangers. *Int. Comm. Heat Mass Transfer, 29*(6), 797-809.

Naphon, P., & Wongwises, S. (2006). A review of flow and heat transfer characteristics in curved tubes. *Renewable & Sustainable Energy Reviews, 10*, 463-490.

NationMaster. (2005). Energy statistics: steam and hot water consumption by household by country
from http://www.nationmaster.com/red/graph/ene_ste_and_hot_wat_con_by_hou-steam-hot-water-consumption-households&b_map=1

Newell, T. A., & Shah, R. K. (2001). An assesment of refrigerant heat transfer, pressure drop, and viod fraction effects in microfin tubes. *Int. J. HVA&R Res., 7*(2), 125-153.

Nozu, S., & Honda, H. (2000). Condensation of refrigerants in horizontal, spirally grooved, microfin tubes: numerical analysis of heat transfer in the annular flow regime. *Heat Transfer, 122*, 80-91.

NRC. (2009, April, 2009). Water heaters: energy considerations. from http://oee.nrcan.gc.ca/residential/personal/water-heater-oil-electric.cfm?attr=4#electric

Nualboonrueng, T., Kaewon, J., & Wongwises, S. (2003). Two-phase condensation heat transfer coefficients of HFC134a at high mass flux in smooth and micro-fin tubes. *Int. Comm. Heat Mass Transfer, 30*, 577-590.

Nusselt, W. (1916). Die Oberflachenkondensation des Wasserdamfes. *Z. VDI, 60*, 541.

Ochsner, K. (2008). *Geothermal heat pumps: a guide for planning and installing*. London: Earthscan.

OuldDidi, M. B., Kattan, N., & Thome, J. R. (2002). Prediction of two-phase pressure gradients of refrigerants in horizontal tubes. *International Journal of Refrigeration, 25*, 935-947.

Palen, J. W., Breber, G., & Taborek, J. (1979). Prediction of flow regimes in horizontal tubeside condensation. *Heat Transfer Eng., 1*(2), 47-57.

Palm, B. (2001). Heat transfer in microchannels. *Microscale Thermophysical Engineering, 5*, 155–175.

Petrov, N. A., & Popov, V. N. (1985). Heat transfer and resistance of carbon dioxide being cooled in the supercritical region. *Thermal Engineering, 32*(3), 131-134.

Petukhov, B. S. (1970). Heat transfer and friction in turbulent pipe flow with variable physical properties. *Adv. Heat Transfe, 6*, 503-564.

Pitla, S., Robinson, D. M., Groll, E. A., & Ramadhyani, S. (1998). Heat transfer from supercritical carbon dioxide in tube flow: A critical review. *HVAC&R RESEARCH 4*(3), 281-301

Pitla, S. S., Groll, E. A., & Ramadhyani, S. (2002). New correlation to predict the heat transfer coefficient during in-tube cooling of turbulent supercritical CO_2. *International Journal of Refrigeration, 25*, 887-895.

Pitla, S. S., Robinson, D. M., Zingerli, A., Groll, E. A., Ramadhyani, S., & Herrick, R. W. (2000). *Heat transfer and pressure drop characteristics during in-tube gas cooling of supercritical carbon dioxide* (No. ASHRAE Research Project 913-RP): Purdue Universityo.

Prudhomme, T., & Gillet, D. (1998). *Optimisation of solar domestic hot water systems* Paper presented at the Proceedings of Eurosun 98.

Qi, S. L., Zhang, P., Wang, R. Z., & Xu, L. X. (2007). single phase pressure drop and heat transfer characteristics of turbulent liquid nitrogen flow in micro-tubes. *Heat and Mass Transfer, 50*, 1993-2001.

Rosson, H. F., & Meyers, J. A. (1965). Point values of condensing film coefficients inside a horizontal tube. *Chemical Engineering Progress Symposium Series, 61*, 190-199.

Rowland, F., & Molina, M. (1974). Stratospheric sink for chlorofluoromethanes: chlorine atom-catalysed destruction of ozone. *Nature, 249*, 810-812.

Schlager, L. M., Pate, M. B., & Bergles, A. E. (1988). Evaporation and condensation of refrigerant-oil mixtures in a smooth tube and micro-fin tube *ASHRAE Journal, 94*(1), 149-166.

Schlager, L. M., Pate, M. B., & Bergles, A. E. (1989). Heat transfer and pressure drop during evaporation and condensation of R-22 in horizontal micro-fin tubes. *International Journal of Refrigeration, 12*(1), 6-14.

Shah, M. M. (1979). A general correlation for heat transfer during film condensation inside pipes. *International Journal of Refrigeration, 22*, 547-556.
Shah, R. K., & Sekulic, D. P. (2001). *Fundamentals of heat exchanger design*. New York Wiley.
Shah, R. K., Subbarao, E. C., & Mashelkar, R. A. (1988). *Heat transfer equipment design*. New York: Hemisphere Bublishing Corporation.
Shao, D. W., & Granryd, E. (1995). Heat transfer and pressure drop of HFC134a-oil mixtures in a horizontal condensing tube. *International Journal of Refrigeration, 18*(8), 524-533.
Shikazono, N., Itoh, M., Uchida, M., Fukushima, T., & Hatada, T. (1998). Predictive equation propersal for condensation heat transfer coefficient of pure refrigerants in horizontal micro-fin tubes. *Trans. Jap. Soc. Mech. Engrs. (in Japanese), 64*, 196-203.
Shoa, W., & Granryd, E. (1995). *An investigation on flow condensation of R22 and R407C in a horizontal smooth tube* Paper presented at the 19th Int Congress of Refrig, Hague, Netherlands.
Sivashanmugam, P., Nagarajan, P. K., & Suresh, S. (2008). Experimental studies on heat transfer and friction factor characteristics of turbulent flow through a circular tube fitted with right and left helical screw-tape Inserts. *Chem. Eng. Comm, 195*, 977–987.
Sobhan, C. B., & Garimella, S. V. (2001). A comparative analysis of studies on heat transfer and fluid flow in minichannels. *Microscale Thermophysical Engineering, 5*(4), 293-311.
Soliman, H. M. (1986). Mist-annular transition during condensation and its influence on the heat transfer mechanism. *Int. J. Multiphase flow, 12*(2), 277-288.
Soliman, H. M., & Azer, N. Z. (1971). Flow patterns during condensation inside a horizontal tube. *ASHRAE Trans., 77*(Part 1), 211.
Soliman, H. M., & Azer, N. Z. (1974). Visual studies of flow patterns during condensation inside horizontal tubes. *Heat Transfer, 3*, 241-245.
Soliman, H. M., Schuster, J. R., & Berenson, P. J. (1968). A general correlation for heat transfer for annular flow condensation. *J. Heat Transfer, Trans. ASME, 90*, 267-276.
Son, C.-H., & Lee, H.-S. (2009). Condensation heat transfer characteristics of R-22, R-134a and R-410A in small diameter tubes. *Heat Mass Transfer, 45*, 1153-1166.
Son, S. H., & Park, S. J. (2006). An experimental study on heat transfer and pressure drop characteristics of carbon dioxide during gas cooling process in a horizontal tube. *International Journal of Refrigeration, 29*(4), 539-546.
Spindler, K. (2006). *A review on heat transfer correlations for supercritical carbon dioxide under cooling conditions.* Paper presented at the 7th IIR-Gustav Lorentzen Conference on Natural Working Fluids, Trondheim.
Sur, B., & Azer, N. Z. (1991). Effect of oil on heat transfer and pressure drop during condensation of refrigerant-113 inside smooth and internally finned tubes *ASHRAE Journal, 97*(1), 365-373.
Taira, S. (2008). The development of heat pump water heaters using CO_2 refrigerant: DAIKIN Industrial Ltd.
Taitel, Y., & Dukler, A. E. (1976). A model for predicting flow regime transition in horizontal and near horizontal gas-liquid flow. *AICHE J., 22*(1), 47-55.
Tanaka, N., & Kotoh, S. (2007). The current status of and future trends in heat pump technologies with natural refrigerants. *Mitsubishi Electric Advance*, 2-5.

Tandon, T. N., Varma, H. K., & Gupta, C. P. (1982). A new flow regime map for condensation inside horizontal tubes. *J. Heat Transfer, Trans. ASME, 104*, 763-768.

Tandon, T. N., Varma, H. K., & Gupta, C. P. (1995). Heat transfer during forced convection condensation inside horizontal tube. *International Journal of Refrigeration, 18*(3), 210-214.

Tichy, J. A., Macken, N. A., & Duval, W. M. B. (1985). An experimental investigation of heat transfer in forced convection condensation of oil-refrigerant mixtures *ASHRAE Journal, 91*(1A), 297-309.

Tien, C. L., Chen, S. L., & Peteron, P. F. (1988). *Condensation inside tubes* Paper presented at the EPRIO, CA.

Traviss, D. P., & Rohsenow, W. M. (1973). Flow regimes in horizontal two-phase flow with condensation. *ASHRAE Trans.*(2279), PR-63.

Traviss, D. P., Rohsenow, W. M., & Baron, A. B. (1973). Forced-convection condensation inside tubes: a heat transfer equation for condenser design. *ASHRAE Trans., 79*(1), 157-165.

Uchida, M., Itoh, M., Shikazono, N., & Kudoh, M. (1996). *Experimental study on the heat transfer performance of a zeotropic refrigerant mixture in horizontal tubes.* Paper presented at the Proceedings of 1996 international refrigerant conference, Purdue.

Urchueguia, J. F., Zacares, M., Corberan, J. M., Montero, A., Martos, J., & Witte, H. (2008). Comparison between the energy performance of a ground coupled water to water heat pump system and air to water heat pump system for heating and cooling in typical conditions of the European Mediterranean coast. *Energy Conversion and Management, 49*, 2917-2923.

Vashisth, S., Kumar, V., & Nigam, D. P. (2008). A review on the potential applications of curved geometries in process industry. *Ind. Eng. Chem. Res., 47*, 3291-3337.

Wang, C. C., Chiou, C. B., & Lu, D. C. (1996). Single-phase heat transfer and flow friction correlations for microfin tubes. *Int. J. Heat and Fluid Flow, 17* 500-508.

Wang, H. S., & Honda, H. (2003). Condensation of refrigerants in horizontal microfin tubes: comparison of prediction methods for heat transfer *International Journal of Refrigeration, 26*, 452-460.

Wang, H. S., Honda, H., & Nozu, S. (2002). Modified theoritical models of film condensation in horizontal micro-fin tubes. *J. Heat Mass Transfer, 45*, 1513-1523.

Wang, W. W., Radcliff, T. D., & Christensen, R. N. (2002). A condensation heat transfer correlation for millimeter-scale tubing with flow regime transition. *Experimental Thermal and Fluid Science, 26*, 473-485.

Webb, R. L., & Zhang, M. (1997). *Prediction of condensation and evaporation in micro-fin and micro-channel tubes.* Paper presented at the Heat Transfer Issues in Natural Refrigerants, College Park, USA.

Webb, R. L., & Zhang, M. (1998). Heat transfer and friction in small diameter channels. *Microscale Thermophysical Engineering 2*, 189-202.

Weisman, J., Duncan, D., Gibson, J., & Crawford, T. (1979). Effects of fluid properties and pipe diameter on two-phase flow patterns in horizontal lines. *Int. J. Multiphase Flow, 5*, 437-462.

Wemhoener, C., & Afjei, T. (2006). *Test Procedure and seasonal performance calculation for residential heat pumps with combined space and domestic hot water heating*. Muttenz: IEA HPP Annex 28o. Document Number)
White, A. J. (2009). Thermodynamic analysis of the reverse Joule-Brayton cycle heat pump for domestic heating. *Applied Energy, 86*, 2443-2450.
White, C. M. (1979). Fluid friction and its relation to heat transfer. *Transactions of Institution of Chemical Engineering (London), 10*, 66–86.
White, F. M. (1994). *Fluid mechanics*. New York: McGraw-Hill.
Wijaya, H., & Spatz, M. W. (1994). *Two-phase flow condensation heat transfer and pressure drop characteristics.* Paper presented at the Proceeding of international refrigerant conference Purdue.
Williamson, A. G., & Clark, S. (2001). *Domestic hot water: option and solutions*. Christchurch: University of Canterbury.
Xin, R. C., & Ebadian, M. A. (1997). The effect of Prandtl number on local and average heat transfer characteristics in helical pipes. *Journal of Heat Transfer-Transactions of The ASME, 119*(3), 467-473.
Yan, Y. Y., & Lin, T. F. (1999). Condensation heat transfer and pressure drop of refrigerant R134a in a small pipe. *J. Heat Mass Transfer, 42*, 697-708.
Yang, C. Y., & Webb, R. L. (1996). Condensation of R-12 in small hydraulic diameter extruded aluminum tubes with and without micro-fins. *International Journal of Heat and Mass Transfer, 39*(4), 789-800.
Yarrel, M. G. (1998). *Performance of a transcritical carbon dioxide heat pump for simultaneous refrigeration and water heating* Massey, Palmerston North.
Yildiz, C., Bicer, Y., & Pehlivan, D. (1995). Heat transfers and pressure drops in rotating helical pipes. *Applied Energy, 50*, 85-94.
Yoon, S. H., Kim, J. H., Hwang, Y. W., Kim, M. S., Min, K., & Kim, Y. (2003). Heat transfer and pressure drop characteristics during the in-tube cooling process of carbon dioxide in the supercritical region. *International Journal of Refrigeration, 26*, 857-864.
Yoon, S. H., Kim, J. H., Hwang, Y. W., Kim, M. S., Min, K., & Kim, Y. (2003). Heat transfer and pressure drop characteristics during the in-tube cooling process of carbon dioxide in the supercritical region *International Journal of Refrigeration, 26*, 857-864.
Yu, J., & Koyama, S. (1998). *Condensation heat transfer of pure refrigerants in micro-fin tubes.* Paper presented at the Proc. Int. Refrigerant conference, Purdue Univ., West Lafayette, USA.
Zhang, M., & Webb, R. L. (1997). *Effect of oil on R-134a condensation in parallel flow condensers.* Paper presented at the Vehicle Thermal Management System Conf.
Zhang, M., & Webb, R. L. (2001). Correlation of two-phase friction for refrigerants in small-diameter tubes. *Experimental Thermal and Fluid Science, 25*, 131-139.
Zingerli, A., & Groll, E. A. (2000). *Influence of refrigeration oil on the heat transfer and pressure drop of supercritical CO_2 during in-tube cooling.* Paper presented at the 4th IIR-Gustav Lorentzen Conference on Natural Working Fluids, USA.

NOMENCLATURE

$A_{enhance}$	heat transfer surface of enhanced tube, m^2
A_{smooth}	heat transfer surface of equivalent smooth-tube, m^2
A_{mean}^{i}	mean transfer surface area of zone *i*, m^2
$A_{wall1,in}^{i}$	inside heat transfer surface of the first wall for zone *i*, m^2
$A_{wall1,out}^{i}$	outside heat transfer surface of the first wall for zone *i*, m^2
$A_{wall2,in}^{i}$	inside heat transfer surface of the second wall for zone *i*, m^2
$A_{wall2,out}^{i}$	outside heat transfer surface of the second wall for zone *i*, m^2
A_{wall1}^{i}	mean heat transfer surface of the first wall for zone *i*, m^2
A_{wall2}^{i}	mean heat transfer surface of the second wall for zone *i*, m^2
A_{airgap}^{i}	mean heat transfer surface of the air gap for zone *i*, m^2
$B_{wall1,in}^{i}$	inside perimeter of the first wall, m
$B_{wall1,out}^{i}$	outside perimeter of the first wall, m
$B_{wall2,in}^{i}$	inside perimeter of the second wall, m
B_{r}^{i}	perimeter of refrigerant side for zone *i*, m
B_{w}^{i}	perimeter of water side for zone *i*, m
COP	coefficient of performance
$D_{h,r}$	hydraulic diameter of refrigerant flow channel, m
$D_{h,w}$	hydraulic diameter of water flow channel, m
EP	power transmitted to the water by the pump, kW
G_{r}^{i}	mass flux of refrigerant at zone *i*, kg/m^2 s
G_{w}^{i}	mass flux of water at zone *i*, kg/m^2 s
FH	heat loss factor in compressor, fraction
I	Number of zones
$\Delta L_{i\to i+1}$	the length of the heat exchanger for zone *i*, m
Nu_{r}^{i}	the Nusselt number of refrigerant side of zone *i*
Nu_{w}^{i}	the Nusselt number of water side of zone *i*
P^{i+1}	absolute pressure of refrigerant side at node *i+1*, kPa
P_{w}^{i+1}	absolute pressure of water side at node *i+1*, kPa
P^{i}	absolute pressure of refrigerant side at node *i*, kPa
P_{w}^{i}	absolute pressure of water side at node *i*, kPa
ΔP_{w}	total pressure drop of water side, kPa
P_{crit}	critical pressure of refrigerant, kPa
P_1	refrigerant pressure at the compressor suction, kPa
P_2	refrigerant pressure at the compressor discharge, kPa
P_6	inlet evaporator refrigerant pressure, kPa
P_7	outlet evaporator refrigerant pressure, kPa
ΔP_{67}	evaporator refrigerant pressure drop, kPa
ΔP_{71}	suction line pressure drop, kPa

Q^i	heat transfer rate for zone *i*, kW
Q_{45}	heating capacity of water heating heat exchanger, kW
$R^i_{convect,r}$	thermal convection resistance of refrigerant side for zone *i*, K/kW
$R^i_{convect,w}$	thermal convection resistance of water side for zone *i*, K/Kw
R^i_{wall1}	thermal conduction resistance of the first wall for zone *i*, K/kW
R^i_{wall2}	thermal conduction resistance of the second wall for zone *i*, K/kW
R^i_{airgap}	thermal conduction resistance of the air gap for zone *i*, K/kW
$R^i_{contact}$	thermal contact resistance for zone *i*, Km^2/kW
$R^i_{F,r}$	thermal fouling resistance in refrigerant flow channel for zone *i*, K/kW
$R^i_{F,w}$	thermal fouling resistance in water flow channel for zone *i*, K/kW
T^i	refrigerant temperature for node *i*, ^oC
T^{i+1}	refrigerant temperature for node *i+1*, ^oC
T^i_w	water temperature for node *i*, ^oC
T^{i+1}_w	water temperature for node *i+1*, ^oC
T^i_s	surface temperature of the inside first wall at zone *i*,^oC
T^i_{sat}	condensing temperature for zone *i*,^oC
$T_{w,in}$	inlet condenser/gascooler water temperature, ^oC
$T_{w,\text{sup}\,ply}$	supply cold water temperature, ^oC
T_6	inlet evaporator refrigerant temperature, ^oC
T_7	outlet evaporator refrigerant temperature, ^oC
T_{ai}	inlet evaporator air temperature, ^oC
T_{ao}	outlet evaporator air temperature, ^oC
ΔT^i_{LMTD}	log-mean temperature difference for zone *i*, ^oC
$\Delta T_{LM,67}$	log-mean temperature difference for evaporator, ^oC
ΔT_w	water temperature increase for each zone, ^oC
ΔT_{71}	superheated refrigerant temperature, ^oC
U^i	overall heat transfer coefficient based on the mean transfer surface area of zone *i*, kW/m^2K
$(UA)^i$	product of overall heat transfer coefficient and area of heat transfer for zone *i*, kW/K
UA_{67}	product of overall heat transfer coefficient and area of heat transfer for evaporator, kW/K
$\dot{V}_1$	compressor displacement volume, m^3/s
W_{fans}	fan power in evaporator, kW
W_{12}	compressor work rate, kW
XA_r	cross section flow area of refrigerant side, m^2
XA_w	cross section flow area of water side, m^2
c^i_{cpw}	specific heat of water at the node *i*, kJ/kgK
c^i_{pr}	specific heat of refrigerant at zone *i*, kJ/kg K

c_{plr}^{i} specific heat of saturated liquid refrigerant at zone *i*, kJ/kg K

c_{prb}^{i} specific heat at wall temperature of zone *i*, kJ/kg K

f_{r}^{i} friction factor of refrigerant at zone *i*

f_{w}^{i} friction factor of water at zone *i*

f_{LO}^{i} friction factor for only liquid phase at zone *i*

g acceleration due to gravity, m/s^2

h^{i} enthalpy of refrigerant at the node *i*,, kJ/kg

h^{i+1} enthalpy of refrigerant at the node *i+1*, kJ/kg

h_{ai} inlet evaporator air enthalpy, ^{o}C

h_{ao} outlet evaporator air enthalpy, ^{o}C

h_{f}^{i} enthalpy of saturated-liquid refrigerant at node *i*, kJ/kg

$h_{is,2}$ isentropic enthalpy at the compressor discharge, kJ/kg

h_{v}^{i} enthalpy of saturated-vapor refrigerant at node *i*, kJ/kg

h_{f}^{i+1} enthalpy of saturated-liquid refrigerant at node *i*+1, kJ/kg

h_{v}^{i+1}, h_{g}^{i+1} enthalpy of saturated-vapor refrigerant at node *i+1*, kJ/kg

h_{fg}^{i} enthalpy of vaporization of zone *i*, kJ/kg

h_1 refrigerant enthalpy at the compressor suction, kJ/kg

h_2 refrigerant enthalpy at the compressor discharge, kJ/kg

h_4 condenser/gascooler inlet refrigerant enthalpy, kJ/kg

h_5 condenser/gascooler outlet enthalpy, kJ/kg

h_6 evaporator inlet enthalpy, kJ/kg

h_7 outlet evaporator refrigerant enthalpy, kJ/kg

k_{a}^{i} thermal conductivity of air for zone *i*, kW/mK

k_{r}^{i} conductivity of refrigerant of zone *i*, kW/mK

k_{rb}^{i} conductivity of refrigerant at bulk temperature of zone *i*, kW/m K

k_{lr}^{i} conductivity of saturated liquid refrigerant at zone *i*, kW/m K

k_{rw}^{i} conductivity at wall temperature of zone *i*, kW/m K

k_{w}^{i} conductivity of water at zone *i*, kW/m K

k_{wall1} thermal conductivity of the first wall, kW/mK

k_{wall2} thermal conductivity of the second wall, kW/mK

$\dot{m}_a$ air mass flow rate, kg/s

$\dot{m}_r$ mass flow rate of refrigerant, kg/s

$\dot{m}_w$ mass flow rate of water, kg/s

x_{ave}^{i} average vapor quality for zone *i*, fraction

x^{i} vapor quality at node *i*, fraction

x^{i+1} vapor quality at node *i+1*, fraction

Δx_{wall1} thickness of the first wall, m

Δx_{wall2} thickness of the second wall, m

Δx_{airgap} thickness of the air gap, m

ρ_r^i density of refrigerant at zone *i*, kg/m^3

ρ_{rw}^i density of refrigerant at wall temperature for zone *i*, kg/m^3

ρ_{rb}^i density of refrigerant at zone *i*, kg/m^3

ρ_{vr}^i density of saturated vapor refrigerant at zone *i*, kg/m^3

ρ_w^i density of water at zone *i*, kg/m^3

ρ_1 refrigerant density at the compressor suction, kg/m^3

α_r^i heat transfer coefficient of pure refrigerant flow in or on smooth tube for zone *i*, kW/m^{2}K

α_w^i heat transfer coefficient of water flow in or on smooth tube for zone *i*, kW/m^{2}K

μ_r^i dynamic viscosity of refrigerant at zone *i*, N s m^{-2}

u_r^i velocity of refrigerant at zone *i*, m/s

u_w^i velocity of water at zone *i*, m/s

μ_{lr}^i dynamic viscosity of saturated liquid refrigerant at zone *i*, N s m^{-2}

μ_{vr}^i dynamic viscosity of saturated vapor refrigerant at zone *i*, N s m^{-2}

μ_{vr}^i dynamic viscosity of saturated vapor refrigerant at zone *i*, N s m^{-2}

μ_{rw}^i dynamic viscosity at wall temperature of zone *i*, N s m^{-2}

μ_{rb}^i dynamic viscosity at wall temperature of zone *i*, N s m^{-2}

μ_w^i dynamic viscosity of water at zone *i*, N s m^{-2}

ε heat transfer surface enhancement factor

η_v compressor volume efficiency, fraction

η_{pump} pump efficiency of water pump, fraction

APPENDIX

A1. Software Program for Condenser Design in EES

```
"************************** Condenser Model **************************"

Procedure DEHEATING(N,kwall1,kwall2,PF,P1,Pw1,Tw1,T1,Gr,di,dhw,Gw, mr,mw,Contact_%, Rcontact, TDw, Bwall1_in, Bwall1_out, Bwall2_in,
Bwall2_out, R_Fr, R_Fw, Thick_wall1, Thick_wall2, Thick_airgap, Or,Ow,Er,Ew,DH: Qdesup, Qg, Pg, Tg, Pw, Tw, PDg, PDw, PDgtotal, PDwgtotal,
Uoverall_g, yg, yw, hg, m,L12, Amean12, Twall1di, Twall2di,Twall1do, Twall2do,x,Tad, Ldesup, Ardesup, Awdesup, Amdesup, yd_average, yw_average,
Ud_average, XXrd_average, XXwd_average)

R$ = 'R410A'

Pg = P1
Pw = Pw1
Tw = Tw1
Tg = T1
Tad = (Tg + Tw)/2
m = 0
h1 = enthalpy(R$, P=P1,T=T1)
hg = h1
Ldesup = 0
Ardesup = 0
Awdesup =0
Amdesup = 0
yd = 0
ywd =0
Ud = 0
XXrd = 0
XXwd = 0
LMTD_d = 0

REPEAT

m = m +1
cpw = specheat(water, P=Pw, T=Tw)
Qg = mw*cpw*TDw
Tw = Tw - TDw
hg = hg - (Qg/mr)
Tgg = temperature(R$, P=Pg, h=hg)
TT1 = Tg - (Tw+TDw)
TT2 = Tgg - Tw
Arc = TT1/TT2
LMTD_DESUP = (TT1 - TT2)/ln(Arc)
UgAg = Qg/LMTD_DESUP
LMTD_d = LMTD_d + LMTD_DESUP
LMTD_daverage = LMTD_d/m
Tgt = (Tgg+Tg)/2
Twt = (Tw + Tw + TDw)/2
kad1 = conductivity(AirH2O, P=101.3, T=Tad, R=0.5)
```

```
kad = kad1/1000
kad = kad1/1000
D = density(R$, P=Pg, T=Tgt)
vr = viscosity(R$, P=Pg, T=Tgt)
cpr = specheat(R$, P=Pg, T=Tgt)
krr = conductivity(R$, P=Pg, T=Tgt)
kr = krr/1000
cpw = specheat(water, P=Pw, T=Twt)
kww = conductivity(water, P=Pw, T=Twt)
kw = kww/1000
Dw = density(water, P=Pw, T=Twt)
vw = viscosity(water, P=Pw, T=Twt)
Rer = Gr*di/vr
Rew = Gw*dhw/vw
fw = 1/(0.79*(ln(Rew))-1.64)^2
Prw= vw*cpw/kw
Bw = 1.07 + (900/Rew) - (0.63/(1+10*Prw))
Nuw = (fw/8)*(Rew*Prw)/(Bw + 12.7*(fw/8)^0.5*(Prw^(2/3) - 1))
yw = Nuw*kw/dhw
ywd = ywd + yw
yw_average = ywd/m
Prr = vr*cpr/kr
fr = 1/(0.79*ln(Rer) - 1.64)^2
k = 1.07 + (900/Rer) - (0.63/(1+10*Prr))
Nurb = (fr/8)*(Rer*Prr)/(k + 12.7*(fr/8)^0.5*(Prr^(2/3) - 1))
yg = (Nurb/di)*kr
yd = yd + yg
yd_average = yd/m
Rparalel = 1/(((100 - Contact_%)/100)*((Bwall1_out + Bwall2_in)/2)*(kad/Thick_airgap) + ((Contact_%/100)*((Bwall1_out+Bwall2_in)/2)/Rcontact))
L12 = UgAg*((1/(Bwall1_in*yg*Or*Er)) + R_Fr + (Thick_wall1/(((Bwall1_in + Bwall1_out)/2)*kwall1)) + Rparalel + (Thick_wall2/(((Bwall2_in +
Bwall2_out)/2)*kwall2)) + R_Fw + (1/(Bwall2_out*yw*Ow*Ew)))
Ldesup = Ldesup + L12
Ar12 = Bwall1_in*L12
Aw21 = Bwall2_out*L12
Ardesup = Ardesup + Ar12
Awdesup = Awdesup + Aw21
Amean12 = (Ar12 + Aw21)/2
Amdesup = Amdesup + Amean12
Uoverall_g = UgAg/Amean12
Ud = Ud + Uoverall_g
Ud_average = Ud/m
f = (0.316)/Rer^0.25
PDg = PF*(1/1000)*f*Gr^2*L12/(2*di*D)
Pg = Pg - PDg
Tg = temperature(R$, P=Pg, h=hg)
fw = (0.316)/Rew^0.25
PDw = PF*(1/1000)*fw*Gw^2*L12/(2*dhw*Dw)
Pw = Pw + PDw
Rconvect_r = 1/(Or*Er*yg*Ar12)
Rconvect_w = 1/(Ow*Ew*yw*Aw21)
Rwall1 = Thick_wall1/(kwall1*((Bwall1_in + Bwall1_out)/2)*L12)
```

```
Rwall_12 = ((100 - Contact_%)/100)*(Thick_airgap/(((Bwall1_out + Bwall2_in)/2)*L12*kad)) + (Contact_%/100)*(Rcontact/((Bwall1_out + Bwall2_in)/2)*L12)
Rwall2 = Thick_wall2/(kwall2*((Bwall2_in + Bwall2_out)/2)*L12)
Twall2do = Twt + (Qg*Rconvect_w)
Twall2di = Twall2do + (Qg*Rwall2)
Twall1di = Tgt - (Qg*Rconvect_r)
Twall1do = Twall1di - (Qg*Rwall1)
Tad = (Twall1do + Twall2di)/2
hv = enthalpy(R$, P=Pg, x=1)
hf = enthalpy(R$, P=Pg, x=0)
XXrd =XXrd + ((2*f)/D)
XXrd_average = XXrd/m
XXwd = XXwd + ((2*fw)/Dw)
XXwd_average = XXwd/m
x = (hg - hf)/(hv - hf)
Qdesup = mr*(h1 - hg)
PDgtotal = P1 - Pg
PDwgtotal = Pw - Pw1

UNTIL (hg<hv)

END

PROCEDURE CONDENSE(F,kwall1,kwall2,PF,Gr,Pw,Pg,L12,Tg,Tw,hg,Gw,dhw, mr, mw, Contact_%, Rcontact, TDw, x, Bwall1_in, Bwall1_out, Bwall2_in, Bwall2_out, R_Fr, R_Fw, Thick_wall1, Thick_wall2, Thick_airgap, Orc,Owc,Erc,Ewc, di,DH, Tad: Qc, Pc, Tc, Tcw, Pcw,PDc, PDcw, PDctotal, PDcwtotal, Uoverall_c, yc, ycw,Qcond, x2, Amean23, L23, mm, Twall1ci, Twall2ci,Twall1co, Twall2co,hc, Tac, Lcond, Arcond, Awcond, Amcond, yc_average, ycw_average, Uc_average, XXrc_average)

R$='R410A'

xci = x
Pc = Pg
Pcw = Pw
Grc = Gr
Tc = Tg
Tcw = Tw
hc = hg
Tac = Tad
Twall1ci = Tg - 2
mm = 0
Lcond = 0
Arcond = 0
Awcond = 0
Amcond = 0
yctotal = 0
ycwtotal = 0
Uctotal = 0
LMTD_c = 0
XXrc = 0

REPEAT
```

```
mm = mm+1
kac1 = conductivity(AirH2O, P=101, T=Tac, R=0.5)
kac = kac1/1000
cpw2 = specheat(water, P=Pw, T=Tw)
Qc =  mw*cpw2*TDw
Tcw = Tcw - TDw
hc = hc - (Qc/mr)
Tcc = temperature(R$, P=Pc, h=hc)
hcl = enthalpy(R$, T=Tc, x=0)
hcg = enthalpy(R$, T=Tc, x=1)
xcc = (hc - hcl)/(hcg-hcl)
x2 = (xci + xcc)/2
TT1 = Tc - Tcw
TT2 = Tcc - Tcw
Arc = TT1/TT2
LMTD_COND = (TT1 - TT2)/ln(Arc)
UcAc =  Qc/LMTD_COND
LMTD_c = LMTD_c + LMTD_COND
LMTD_caverage = LMTD_c/mm
Tcwt = (Tcw + Tcw +TDw)/2
Tct = (Tc + Tcc)/2
vol2 = volume(R$, T=Tct, x=x2)
Dv2 = density(R$, T=Tct, x=1)
Dl2 = density(R$, T=Tct, x=0)
vl2 = viscosity(R$, T=Tct, x=0)
vv2 = viscosity(R$, T=Tct, x=1)
hcf = enthalpy(R$, T=Tct, x=0)
hcv = enthalpy(R$, T=Tct, x=1)
Rel2 = Grc*di/vl2
Rev2 = Grc*di*(1-x2)/vv2
fl2 = (0.316)/(Rel2^0.25)
Dw2 = density(water, P=Pcw, T=Tcwt)
vw2 = viscosity(water, P=Pw, T=Tcwt)
cpw2 = specheat(water, P=Pcw, T=Tcwt)
kw22 = conductivity(water, P=Pcw, T=Tcwt)
kw2 = kw22/1000
Prw2= vw2*cpw2/kw2
Rew2 = Gw*dhw/vw2
fw2 = (0.316)/(Rew2^0.25)
cpl2 = specheat(R$, T=Tct, x=0)
kl22 = conductivity(R$, T=Tct, x=0)
kl2 = kl22/1000
y = 1/(1 + ((1-x2)/x2)*(Dv2/Dl2)^2/3)
Prl2 = vl2*cpl2/kl2
Xtt2 = (Dv2/Dl2)^0.5*(vl2/vv2)^0.1*((1-x2)/x2)^0.9
Ga = 9.81*Dl2*(Dl2 - Dv2)*(y^0.5*di^3)/vl2^2)
Jal = cpl2*(Tc - Twall1ci)/(hcv-hcf)
Angle = pi - arccos(2*y - 1)
Frl = Grc^2/(Dl2^2*9.81*di)
```

```
IF Frl > 0.7 THEN

c1 = 7.242
c2 = 1.655

ELSE

c1 = 4.172 + 5.48*Frl - 1.564*Frl^2
c2 = 1.773 - 0.169*Frl

ENDIF

PP = (1.376 + (c1/Xtt2^c2))^0.5
Nuforce = (0.0195)*(Rel2^0.8)*(Prl2^0.4)*PP
Nu2 =  (((0.23*Rev2^0.12/(1 + 1.11*Xtt2^0.58))*(Ga*Prl2/Jal)^0.25)) + (1-(Angle/pi))*Nuforce
yc = Nu2*kl2/di
yctotal = yctotal + yc
yc_average = yctotal/mm
Rew2 = Gw*dhw/vw2
Prw2= vw2*cpw2/kw2
Cfw2 = 1/(0.79*(ln(Rew2))-1.64)^2
Bwc = 1.07 + (900/Rew2) - (0.63/(1+10*Prw2))
Nuw32 = (Cfw2/8)*(Rew2*Prw2)/(Bwc + 12.7*(Cfw2/8)^0.5*(Prw2^(2/3) - 1))
ycw = Nuw32*kw2/dhw
ycwtotal = ycwtotal + ycw
ycw_average = ycwtotal/mm
Rparalel = 1/((((100 - Contact_%)/100)*((Bwall1_out + Bwall2_in)/2)*(kac/Thick_airgap) + ((Contact_%/100)*((Bwall1_out+Bwall2_in)/2)/Rcontact))
L23 = UcAc*((1/(Bwall1_in*yc*Orc*Erc)) + R_Fr + (Thick_wall1/(((Bwall1_in + Bwall1_out)/2)*kwall1)) + Rparalel + (Thick_wall2/(((Bwall2_in +
Bwall2_out)/2)*kwall2)) + R_Fw + (1/(Bwall2_out*ycw*Owc*Ewc)))
Lcond = Lcond + L23
Ar23 = Bwall1_in*L23
Aw32 = Bwall2_out*L23
Arcond = Arcond + Ar23
Awcond = Awcond + Aw32
Amean23 = (Ar23 + Aw32)/2
Amcond = Amcond + Amean23
Uoverall_c = UcAc/Amean23
Uctotal = Uctotal + Uoverall_c
Uc_average = Uctotal/mm
PDc_single_f =PF*(1/1000)* fl2*Grc^2*L23/(2*di*Dl2)
Pcrit=P_crit(R$)
Pred = Pc/Pcrit
FF = (1-x2)^2 + (2.87*(x2^2))/Pred  +  (1.68*(x2^0.8)*((1-x2)^0.25))/Pred^1.64
PDc = PF*FF*PDc_single_f
Pc = Pc - PDc
PDcw = PF*(1/1000)*fw2*Gw^2*L23/(2*dhw*Dw2)
Pcw = Pcw + PDcw
Tc = temperature(R$, P=Pc, h=hc)
hcg1 = enthalpy(R$, P=Pc, x=1)
hcf1= enthalpy(R$, P=Pc, x=0)
xci = (hc - hcf1)/(hcg1 - hcf1)
```

```
PDctotal = Pg - Pc
PDcwtotal = Pcw - Pw
Qcond = mr*(hg -hc)
Rconvect_r = 1/(Orc*Erc*yc*Ar23)
Rconvect_w = 1/(Owc*Ewc*ycw*Aw32)
Rwall1 = Thick_wall1/(kwall1*((Bwall1_in + Bwall1_out)/2)*L23)
Rwall_12 = ((100 - Contact_%)/100)*(Thick_airgap/(((Bwall1_out + Bwall2_in)/2)*L23*kac)) + (Contact_%/100)*(Rcontact/((Bwall1_out +
Bwall2_in)/2)*L23)
Rwall2 = Thick_wall2/(kwall2*((Bwall2_in + Bwall2_out)/2)*L23)
Twall1ci = Tct - (Qc*Rconvect_r)
Twall1co = Twall1ci - (Qc*Rwall1)
Twall2co = Tcwt + (Qc*Rconvect_w)
Twall2ci = Twall2co + (Qc*Rwall2)
Tac = (Twall1co + Twall2ci)/2
XXrc = XXrc + ((FF*2*fl2)/(Dl2))
XXrc_average = XXrc/mm

UNTIL (xci < 0.0001)

END
PROCEDURE SUBCOOL(K, kwall1,kwall2,PF,Pc, Tc, Tac, Pcw, Tcw, mr, mw, Gw, Gr, dhw, Contact_%, Rcontact, TDw, mm, hc, Bwall1_in,
Bwall1_out, Bwall2_in, Bwall2_out, R_Fr, R_Fw, Thick_wall1, Thick_wall2, Thick_airgap, Ors,Ows,Ers,Ews,di, Qcond, Qdesup,DH: Qs, Qsub, Ps, Ts,
Tsw, Psw, PDs, PDsw, PDstotal, PDswtotal, Uoverall_s, ys, ysw,Amean34, L34, mmm, Twall1si, Twall2si,Twall1so, Twall2so, Tas,hs, Lsub, Arsub,
Awsub, Amsub, ys_average, ysw_average, Us_average, XXrs_average)

R$ = 'R410A'
 Ps = Pc
hs = hc
Ts = Tc
Psw = Pcw
Tsw = Tcw
Tas = Tac
mmm =0
Lsub = 0
Arsub = 0
Awsub = 0
Amsub = 0
ystotal = 0
yswtotal =0
Ustotal =0
LMTD_s = 0
XXrs = 0

REPEAT

mmm = mmm + 1
kas1 = conductivity(AirH2O, P=101, T=25, R=0.5)
kas = kas1/1000
cpw4 = specheat(water, P=Psw, T=Tsw)
Qs = mw*cpw4*TDw
Tsw = Tsw - TDw
```

```
hs = hs - (Qs/mr)
Tss = temperature(R$, P=Ps, h=hs)
TT1 = Ts - (Tsw+TDw)
TT2 = Tss - Tsw
Arc = TT1/TT2
LMTD_SUB = (TT1 - TT2)/ln(Arc)
UsAs = Qs/LMTD_SUB
LMTD_s = LMTD_s + LMTD_SUB
LMTD_saverage = LMTD_s/mmm
Tst = (Tss + Ts)/2
Tswt = (Tsw + Tsw + TDw)/2
D3= density(R$, P=Ps, T=Tst)
v3 = viscosity(R$, P=Ps, T=Tst)
cp3 = specheat(R$, P=Ps, T=Tst)
k33 = conductivity(R$, P=Ps, T=Tst)
k3 = k33/1000
Dw4 = density(water, P=Psw, T=Tswt)
vw4 = viscosity(water, P=Psw, T=Tswt)
cpw4 = specheat(water, P=Psw, T=Tswt)
kw44 = conductivity(water, P=Psw, T=Tswt)
kw4 = kw44/1000
Reb3 = Gr*di/v3
Prb3 = v3*cp3/(k3)
B3=1.07 + (900/Reb3) - (0.63/(1 + 10*Prb3))
Cf3 = 1/(0.79*(ln(Reb3))-1.64)^2
Nu34 = (Cf3/8)*(Reb3*Prb3)/(B3 + 12.7*(Cf3/8)^0.5*(Prb3^(2/3)-1))
ys = Nu34*k3/di
ystotal = ystotal + ys
ys_average = ystotal/mmm
Rew4 = Gw*dhw/vw4
Cfw4 = 1/(0.79*(ln(Rew4))-1.64)^2
Prw4= vw4*cpw4/kw4
Bw3=1.07 + (900/Rew4) - (0.63/(1 + 10*Prw4))
Nuw43 = (Cfw4/8)*(Rew4*Prw4)/(Bw3 + 12.7*(Cfw4/8)^0.5*(Prw4^(2/3)-1))
ysw = Nuw43*kw4/dhw
yswtotal = yswtotal + ysw
ysw_average = yswtotal/mmm
Rparalel = 1/((((100 - Contact_%)/100)*((Bwall1_out + Bwall2_in)/2)*(kas/Thick_airgap) + ((Contact_%/100)*((Bwall1_out+Bwall2_in)/2)/Rcontact))
L34 = UsAs*((1/(Bwall1_in*ys*Ors*Ers)) + R_Fr + (Thick_wall1/(((Bwall1_in + Bwall1_out)/2)*kwall1)) + Rparalel + (Thick_wall2/(((Bwall2_in +
Bwall2_out)/2)*kwall2)) + R_Fw + (1/(Bwall2_out*ysw*Ows*Ews)))
Lsub = Lsub + L34
Ar34 = Bwall1_in*L34
Aw34 = Bwall2_out*L34
Amean34 = (Ar34 + Aw34)/2
Arsub = Arsub + Ar34
Awsub = Awsub + Aw34
Amsub = Amsub + Amean34
Uoverall_s = UsAs/Amean34
Ustotal = Ustotal + Uoverall_s
Us_average = Ustotal/mmm
f3 = (0.316)/Reb3^0.25
```

```
PDs = PF*(1/1000)*f3*Gr^2*L34/(2*di*D3)
Ps = Ps - PDs
Ts = temperature(R$, P=Ps, h=hs)
uw4 = Gw/Dw4
fw4 = (0.316)/Rew4^0.25
PDsw =PF*(1/1000)*fw4*Gw^2*L34/(2*dhw*Dw4)
Psw = Psw + PDsw
Qsub = mr*(hc - hs)
PDstotal = Pc - Ps
PDswtotal = Psw - Pcw
Rconvect_r = 1/(Ors*Ers*ys*Ar34)
Rconvect_w = 1/(Ows*Ews*ysw*Aw34)
Rwall1 = Thick_wall1/(kwall1*((Bwall1_in + Bwall1_out)/2)*L34)
Rwall_12 = ((100 - Contact_%)/100)*(Thick_airgap/(((Bwall1_out + Bwall2_in)/2)*L34*kas)) + (Contact_%/100)*(Rcontact/((Bwall1_out +
Bwall2_in)/2)*L34)
Rwall2 = Thick_wall2/(kwall2*((Bwall2_in + Bwall2_out)/2)*L34)
Twall1si = Tst - (Qs*Rconvect_r)
Twall1so = Twall1si - (Qs*Rwall1)
Twall2so = Tswt + (Qs*Rconvect_w)
Twall2si = Twall2so + (Qs*Rwall2)
Tas = (Twall1so + Twall2si)/2
Qt = Qsub +Qcond + Qdesup
XXrs = XXrs + ((2*f3)/D3)
XXrs_average = XXrs/mmm

UNTIL (Tsw<=15)

END
CALL DEHEATING(9999,kwall1,kwall2,PF,P1,Pw1,Tw1,T1,Gr,di,dhw,Gw, mr,mw,Contact_%, Rcontact, TDw, Bwall1_in, Bwall1_out, Bwall2_in,
Bwall2_out, R_Fr, R_Fw, Thick_wall1, Thick_wall2, Thick_airgap, Or,Ow,Er,Ew,DH: Qdesup, Qg, Pg, Tg, Pw, Tw, PDg, PDw, PDgtotal, PDwgtotal,
Uoverall_g, yg, yw, hg, m,L12, Amean12, Twall1di, Twall2di,Twall1do, Twall2do,x, Tad, Ldesup, Ardesup, Awdesup, Amdesup,yd_average, yw_average,
Ud_average, XXrd_average, XXwd_average)

CALL CONDENSE(999,kwall1,kwall2,PF,Gr,Pw,Pg,L12,Tg,Tw,hg,Gw,dhw, mr, mw, Contact_%, Rcontact, TDw, x, Bwall1_in, Bwall1_out, Bwall2_in,
Bwall2_out, R_Fr, R_Fw, Thick_wall1, Thick_wall2, Thick_airgap, Orc,Owc,Erc,Ewc,di,DH, Tad: Qc, Pc, Tc, Tcw, Pcw, PDc, PDcw, PDctotal,
PDcwtotal, Uoverall_c, yc, ycw,Qcond, x2, Amean23, L23, mm, Twall1ci, Twall2ci,Twall1co, Twall2co,hc, Tac, Lcond, Arcond, Awcond, Amcond,
yc_average, ycw_average, Uc_average, XXrc_average)

CALL SUBCOOL(999, kwall1,kwall2,PF,Pc, Tc, Tac,Pcw, Tcw, mr, mw, Gw, Gr, dhw, Contact_%, Rcontact, TDw, mm, hc, Bwall1_in, Bwall1_out,
Bwall2_in, Bwall2_out, R_Fr, R_Fw, Thick_wall1, Thick_wall2, Thick_airgap, Ors,Ows,Ers,Ews,di, Qcond,Qdesup,DH: Qs, Qsub, Ps, Ts, Tsw, Psw, PDs,
PDsw, PDstotal, PDswtotal, Uoverall_s, ys, ysw,Amean34, L34, mmm, Twall1si, Twall2si,Twall1so, Twall2so, Tas, hs,Lsub, Arsub, Awsub, Amsub,
ys_average, ysw_average, Us_average, XXrs_average)

R$='R410A'
Tcond = 64
Tevap = 5
TDw = 0.5
DH = 1
Pw1 = 101.3
Tw1 = 60
Twin = 15
```

" Hydralic diameter"

di = 0.006

do = di + 2*Thick_wall1

d1 - do = 0.0002

d2 = d1 + 2*Thick_wall2

Din - d2 = 0.0015

Dannulus = Din - d2

"XAw = 0.00002034"

dhw = (Din^2-d2^2)/(d2 + Din)

" % Contact"

Contact_% = 0

"Heat transfer factors"

PF = 1

Or = 1

Ow = 1

Er = 1

Ew = 1

Orc = 1

Owc = 1

Erc = 1

Ewc = 1

Ors = 1

Ows = 1

Ers = 1

Ews = 1

"Thermal resistance"

kwall1 =401/1000

kwall2 = 401/1000

R_Fr = 0

R_Fw = 0

Rcontact = (5/10000)*1000

"Configuration of HE"

Thick_wall1 = 0.0008128

Thick_wall2 = 0.0008128

Thick_airgap = (d1 - do)/2

Thick_wall3 = 0.000889

Dout = Din + 2*thick_wall3

Bwall1_in = pi*di

```
Bwall1_out = pi*do
Bwall2_in = pi*d1
Bwall2_out = pi*d2
XAr = (pi*di^2)/4
XXA = (pi*Din^2)/4
XXB = (pi*d2^2)/4
XAw = XXA - XXB
Gr = mr/XAr
Gw = mw/XAw

Qtotal = Qdesup + Qcond + Qsub
Q_desup% = (Qdesup/Qtotal)*100
Q_cond% = (Qcond/Qtotal)*100
Q_sub% = (Qsub/Qtotal)*100

PDtotal_r = PDgtotal + PDctotal + PDstotal
PDtotal_w = PDwgtotal + PDcwtotal + PDswtotal

Ltotal = Ldesup + Lcond + Lsub
Artotal = Ardesup + Arcond + Arsub
Awtotal = Awdesup + Awcond + Awsub
Amtotal = Amdesup + Amcond + Amsub

ywmean = (yw_average + ycw_average + ysw_average)/3

"Mass flow rate of water"

Q = 3
Q = cpw_aver*mw*(Tw1-Twin)
cpw_aver = specheat(water, P=101, T = 25)




"************************** Heat Pump Model **************************"
" Evaporator model "
hss = enthalpy(R$, P=Ps, T=Ts)
hei = hss
Peo = pressure(R$, T=Tevap, x=1)
heo = enthalpy(R$, T=Tevap, x=1)
Pei = Peo + PDevap
Qevap = mr*(heo - hei)
xei = (hei - hef)/(heg-hef)
hef = enthalpy(R$, P = Pei, x=0)
heg = enthalpy(R$, P = Pei, x=1)
PDevap =0

" Suction line model"
TDsuction = Tsuction - Tevap
Psuction = Peo - PDsuction
TDsuction = 0
```

```
PDsuction = 0

"Compressor model "
mr = D_s*eff_v*Vs_dot
eff_v = 0.003*PR^3 - 0.0441*PR^2 + 0.1796*PR + 0.6803
eff_s = 0.0069*PR^3 - 0.0987*PR^2 + 0.4274*PR + 0.072
PR = Pcond/Psuction
Pcond = pressure(R$, T=Tcond, x=1)
D_s = density(R$, P=Psuction, T=Tsuction)
"Vs_dot = 0.00049"
Ssub = entropy(R$, P=Psuction, T=Tsuction)
hsuction = enthalpy(R$, P=Psuction, T=Tsuction)
hdis_s = enthalpy(R$, P=Pcond, s = Ssub)
hdis_a1 = ((hdis_s - hsuction)/eff_s) + hsuction
hdis_a2 = hdis_a1 - (Qloss_comp)/mr
W_comp = mr*(hdis_a1 - hsuction)
Tdischarge = temperature(R$, P=Pcond, h=hdis_a1)
Q = mr*(hin - hsub)
hsub = enthalpy(R$, T=26, x=0)
Qloss_comp = 0.1*W_comp

" Discharge Line Model"
Qloss_discharge = mr*(hdis_a2 - hin)
P1 = Pcond - PD_dischagre
T1 = temperature(R$, P=P1, h=hin)
Qloss_discharge = 0
PD_dischagre = 0
COP = Qtotal/Wtotal
Wtotal = W_comp + (EP/1000) + 0.1
EP = 1000*(mw*PDtotal_w)/(1000*eff_pump)
eff_pump = 0.5
Weight1 = (pi*(do^2 - di^2)/4)*Ltotal*8930
Weight2 = (pi*(d2^2 - d1^2)/4)*Ltotal*8930
Weight3 = (pi*(Dout^2 - Din^2)/4)*Ltotal*8930
Weight_total = Weight1 + Weight2 + Weight3
 y_water = (ycw_average + ysw_average + ysw_average)/3

"************************** End of Model **************************"
```

A2. Software Program for Gas cooler Design in EES

```
"************************** Gas Cooler Model **************************"

PROCEDURE GasNode(N,kwall1,kwall2,P1,Pw1,Tw1,T1,Gr,di,dhw,Gw, mr,mw,Contact_%, Rcontact, TDw, Bwall1_in, Bwall1_out, Bwall2_in,
Bwall2_out, R_Fr, R_Fw, Thick_wall1, Thick_wall2, Thick_airgap, Dr,Dw,Er,Ew: Qtotal, Qg, Pg, Tg, Pw, Tw, PDg, PDw, PDgtotal, PDwtotal,
Uoverall_g, yg, yw, hg, m,L12, Amean12, Twall1di, Twall2di,Twall1do, Twall2do, Ltotal, Artotal, Awtotal, Amtotal, yg_average, yw_average,Ug_average)

R$ = 'R744'
Pg = P1
Pw = Pw1
Tw = Tw1
Tg = T1
Tad = (Tg + Tw)/2
Twall1di = T1
h1 = enthalpy(R$, P=P1, T=T1)
hg = h1
m=0
Ltotal = 0
Artotal = 0
Awtotal =0
Amtotal =0
ygtotal = 0
ywtotal =0
Ugtotal =0
LMTD = 0
Tadtotal = 0
kadtotal = 0
Twall1 = 0
Twall2 = 0

REPEAT

m=m+1
cpw = specheat(water, P=Pw, T=Tw)
hg = enthalpy(R$, P=Pg, T=Tg)
Qg = mw*cpw*TDw
Tw = Tw -TDw
hg = hg - (Qg/mr)
Tgg = temperature(R$, P=Pg, h=hg)
Tgt = (Tg + Tgg)/2
Twt = (Tw + Tw + TDw)/2
TT1 = Tg - (Tw+TDw)
TT2 = Tgg - Tw
Arc = TT1/TT2
LMTD_DESUP =   (TT1 - TT2)/(ln(Arc))
UgAg = Qg/LMTD_DESUP
LMTD = LMTD + LMTD_DESUP
LMTD_AVERAGE = LMTD/m
kad1 = conductivity(AirH2O, P=101, T=Tad, R=0.5)
```

```
kad = kad1/1000
 Drw = density(R$, P=Pg, T=Twall1di)
D = density(R$, P=Pg, T=Tgt)
vrw = viscosity(R$, P=Pg, T=Twall1di)
vr = viscosity(R$, P=Pg, T=Tgt)
cprw = specheat(R$, P=Pg, T=Twall1di)
krww = conductivity(R$, P=Pg, T=Twall1di)
krw = krww/1000
cpr = specheat(R$, P=Pg, T=Tgt)
krr = conductivity(R$, P=Pg, T=Tgt)
kr = krr/1000
Rerw = Gr*di/vrw
Rer = Gr*di/vr
frw = 1/(0.79*ln(Rerw) - 1.64)^2
Prrw = vrw*cprw/krw
Nurw = ((frw/8)*(Rerw - 1000)*Prrw)/(1.07 + 12.7*(frw/8)^0.5*(Prrw^(2/3) - 1))
Prr = vr*cpr/kr
fr = 1/(0.79*ln(Rer) - 1.64)^2
Nurb = ((fr/8)*(Rer - 1000)*Prr)/(1.07 + 12.7*(fr/8)^0.5*(Prr^(2/3) - 1))
Nur = ((Nurw + Nurb)/2)*(krw/kr)
yg = (Nur/di)*kr
ygtotal = ygtotal + yg
yg_average = ygtotal/m

kww = conductivity(water, P=Pw, T=Twt)
kw = kww/1000
Dw = density(water, P=Pw, T=Twt)
vw = viscosity(water, P=Pw, T=Twt)
Rew = Gw*dhw/vw
Cfw = 1/(0.79*(ln(Rew))-1.64)^2
Prw= vw*cpw/kw
Bw = 1.07 + (900/Rew) - (0.63/(1+10*Prw))
Nuw = (Cfw/8)*(Rew*Prw)/(Bw + 12.7*(Cfw/8)^0.5*(Prw^(2/3) - 1))
yw = Nuw*kw/dhw
ywtotal = ywtotal + yw
yw_average = ywtotal/m

Rparalel = 1/((((100 - Contact_%)/100)*((Bwall1_out + Bwall2_in)/2)*(kad/Thick_airgap) + ((Contact_%/100)*((Bwall1_out+Bwall2_in)/2)/Rcontact))
L12 = UgAg*((1/(Bwall1_in*yg*Or*Er)) + R_Fr + (Thick_wall1/(((Bwall1_in + Bwall1_out)/2)*kwall1)) + Rparalel + (Thick_wall2/(((Bwall2_in +
Bwall2_out)/2)*kwall2)) + R_Fw + (1/(Bwall2_out*yw*Ow*Ew)))

Ltotal = Ltotal + L12
Ar12 = Bwall1_in*L12
Aw21 = Bwall2_out*L12
Artotal = Artotal + Ar12
Awtotal = Awtotal + Aw21
Amean12 = (Ar12 + Aw21)/2
Amtotal = Amtotal + Amean12
Uoverall_g = UgAg/Amean12
Ugtotal = Ugtotal + Uoverall_g
Ug_average = Ugtotal/m
```

```
fr = 1/(0.79*ln(Rer) - 1.64)^2
PDg = (1/1000)*fr*Gr^2*L12/(2*D*di)
Pg = Pg - PDg
Tg = temperature(R$, P=Pg, h=hg)
fw = (0.316/Rew^0.25)
PDw = (1/1000)*fw*Gw^2*L12/(2*dhw*Dw)
Pw = Pw + PDw
Qtotal = mr*(h1 - hg)
PDgtotal = P1 - Pg
PDwtotal = Pw - Pw1
Rconvect_r = 1/(Dr*Er*yg*Ar12)
Rconvect_w = 1/(Dw*Ew*yw*Aw21)
Rwall1 = Thick_wall1/(kwall1*((Bwall1_in + Bwall1_out)/2)*L12)
Rwall_12 = ((100 - Contact_%)/100)*(Thick_airgap/(((Bwall1_out + Bwall2_in)/2)*L12*kad)) + (Contact_%/100)*(Rcontact/((Bwall1_out +
Bwall2_in)/2)*L12)
Rwall2 = Thick_wall2/(kwall2*((Bwall2_in + Bwall2_out)/2)*L12)
Twall1di = Tgt - (Qg*Rconvect_r)
Twall1do = Twall1di - (Qg*Rwall1)
Twall2do = Twt +  (Qg*Rconvect_w)
Twall2di = Twall2do + (Qg*Rwall2)
Twall1 = Twall1 + Twall1di
Twall2 = Twall2 + Twall2do
Twall1_average = Twall1/m
Twall2_average = Twall2/m
Tad = (Twall1do + Twall2di)/2
Tadtotal = Tadtotal + Tad
Tad_average = Tadtotal/m
kadtotal = kadtotal + kad
kad_average = kadtotal/m

UNTIL (Tw<=15 )

END

CALL GasNode(999,kwall1,kwall2,P1,Pw1,Tw1,T1,Gr,di,dhw,Gw, mr,mw,Contact_%, Rcontact, TDw, Bwall1_in, Bwall1_out, Bwall2_in, Bwall2_out,
R_Fr, R_Fw, Thick_wall1, Thick_wall2, Thick_airgap, Dr,Dw,Er,Ew:Qtotal, Qg, Pg, Tg, Pw, Tw, PDg, PDw, PDgtotal, PDwtotal, Uoverall_g, yg, yw, hg,
m,L12, Amean12, Twall1di, Twall2di,Twall1do, Twall2do, Ltotal, Artotal, Awtotal, Amtotal, yg_average, yw_average, Ug_average)

R$ = 'R744'
P1 = 11000
Tevap = 5
TDw = 1
DH = 0.5
Pw1 = 101.3
Tw1 = 60
Twin = 15

" Hydralic diameter"
di = 0.005
do = di + 2*Thick_wall1
d1 - do = 0.0002
```

```
d2 = d1 + 2*Thick_wall2
Din - d2 = 0.0015
Dannulus = Din - d2
"XAw = 0.00002034"
dhw = (Din^2-d2^2)/(d2 + Din)

" % Contact"
Contact_% =0

"Heat transfer factors"
PF = 1
Er = 1
Ew = 1
Dr = 1
Dw=1

 "Thermal resistance"
kwall1 =400/1000
kwall2 = 401/1000
R_Fr = 0
R_Fw = 0
Rcontact = (5/10000)*1000

"Configuration of HE"
Thick_wall1 = 0.0009
Thick_wall2 = 0.0008128
Thick_airgap = (d1 - do)/2
Thick_wall3 = 0.0008128
Dout = Din + 2*Thick_wall3
Bwall1_in = pi*di
Bwall1_out = pi*do
Bwall2_in = pi*d1
Bwall2_out = pi*d2
XAr = (pi*di^2)/4
XXA = (pi*Din^2)/4
XXB = (pi*d2^2)/4
XAw = XXA - XXB
Gr = mr/XAr
Gw = mw/XAw

"Mass flow rate of water"
Q = 3
Q = cpw_aver*mw*(Tw1-Twin)
cpw_aver = specheat(water, P=101, T = 25)



"************************** Heat Pump Model **************************"

" Evaporator model "
hss = enthalpy(R$, P=Pg, T=Tg)
hei = hss
```

```
Peo = pressure(R$, T=Tevap, x=1)
heo = enthalpy(R$, T=Tevap, x=1)
Pei = Peo + PDevap
Qevap = mr*(heo - hei)
xei = (hei - hef)/(heg-hef)
hef = enthalpy(R$, P = Pei, x=0)
heg = enthalpy(R$, P = Pei, x=1)
PDevap =0

" Suction line model"
TDsuction = Tsuction - Tevap
Psuction = Peo - PDsuction
TDsuction = 0
PDsuction = 0

"Compressor model "
mr = D_s*eff_v*Vs_dot
eff_v = 0.003*PR^3 - 0.0441*PR^2 + 0.1796*PR + 0.6803
eff_s = 0.0069*PR^3 - 0.0987*PR^2 + 0.4274*PR + 0.072
PR = P1/Psuction
D_s = density(R$, P=Psuction, x=1)
"Vs_dot = 0.00049"
Ssub = entropy(R$, P=Psuction, x=1)
hsuction = enthalpy(R$, P=Psuction, x=1)
hdis_s = enthalpy(R$, P=P1, s = Ssub)
hdis_a1 = ((hdis_s - hsuction)/eff_s) + hsuction
hdis_a2 = hdis_a1 - (Qloss_comp)/mr
W_comp = mr*(hdis_a1 - hsuction)
Tdischarge = temperature(R$, P=P1, h=hdis_a1)
Q = mr*(hin - hsub)
hsub = enthalpy(R$, T=25, P=P1)
Qloss_comp = 0.1*W_comp

" Discharge Line Model"
Qloss_discharge = mr*(hdis_a2 - hin)
T1 = temperature(R$, P=P1, h=hin)
Qloss_discharge = 0
 COP = Qtotal/Wtotal
Wtotal = W_comp + (EP/1000) + 0.1
EP = 1000*(mw*PDwtotal)/(1000*eff_pump)
eff_pump = 0.5

Weight1 = (pi*(do^2 - di^2)/4)*Ltotal*8930
Weight2 = (pi*(d2^2 - d1^2)/4)*Ltotal*8930
Weight3 = (pi*(Dout^2 - Din^2)/4)*Ltotal*8930
Weight_total = Weight1 + Weight2 + Weight3


"************************** End of Model ************************"
```